High Performance Reinforced Hemp-Lime Nanocomposite Construction Materials

Faraj Jabbar Khalaf

A thesis submitted in partial fulfilment of the requirements of

Sheffield Hallam University

for the degree of Doctor of Philosophy

May 2019

Declaration

I hereby declare that this thesis submitted for the degree of PhD is the result of my own research and that this thesis has not been submitted for a higher degree to any other university or institution.

Faraj Jabbar Khalaf

Dedication

To my family, my father and my mother who are resting in peace.

To all the great people who have taught me throughout my life,

this effort is a small gift for all of you

Faraj Jabbar Khalaf

Acknowledgment

I would like to express my appreciation and acknowledgement as follows:

My Director of Studies and supervisor Prof. Fin O'Flaherty, without the support and guidance of you, this work would not have been possible. Your patience, motivation, interest and massive knowledge has helped me throughout my research and writing of this thesis.

I gratefully acknowledge the guidance and support provided by Dr Vincenzo Starinieri through their second supervisory role in this research. Special thanks also to my family for their support, patience and understanding throughout the course of my studies.

I would also like to acknowledge the financial sponsorship provided by the Ministry of Higher Education and Scientific Research (MOHESR) in Iraq. Special thanks also, to the Iraqi Cultural Attaché in London for their support during my PhD research. Anbar University, Engineering College, Civil department are gratefully acknowledged for the continuing support during my study.

The support of staff in the Materials and Engineering Research Institute (MERI) was so vital in making life easier during my study.

I am so thankful for my PhD colleagues and friends for making life interesting during our four years together.

Abstract

The aim of the project is to develop high performance, lightweight, durable, and environmentally friendly construction materials. Construction materials should have high compressive and flexural strength, low porosity, low thermal conductivity, low shrinkage and high water vapour permeability (breathability). The following materials were selected to achieve this aim; lime was selected as the base matrix material with hemp (fibres and shives) and wood glue (Poly vinyl acetate, PVAc). Specially selected nanomaterials were used as fillers. The properties of the developed material were used to design an eco-friendly wall consisting of a central 'Core' which will be the load bearing element, highly insulative layers with low thermal conductivity 'Insulators' and outer rendering materials for enhanced aesthetics purpose and breathability 'Renders'. The research conducted in this project enabled a number of different construction materials to be developed, each exhibiting their own characteristics to enable the aims and objectives of the project to be achieved.

A summary of the findings is as follows:

A load bearing wall requires relatively high compressive and flexural strengths of about 5 MPa and 4.0 MPa, respectively or higher. The 'Core' material designed consisted of 10 wt. % hemp fibres, 12 % PVAc/L, 4 wt. % nZnO (nanozinc oxide) and lime (NHL5, which its quantity was 1 kg for each batch of 4 samples for the whole project) and prepared using air curing method. The compressive strength was 17.7 MPa and the flexural strength was greater than 7.0 MPa, which were the highest results of strength throughout the project. The same mentioned mixture (10 wt. % hemp fibres, 12 % PVAc/L, 4 wt. % nanozinc oxide of lime) was cured using 'Oven-drying', the strengths in compression and flexure were still considerable, being 10 MPa and 4 MPa respectively which were more than the minimum limit of loadbearing material. This material, therefore, due to its high compressive strength, used as the 'Core' load bearing element of the proposed wall in the absence of a timber framework.

The 'Insulator' was developed using a water removal 'Solvent exchange' technique and the mixture was 20 wt. % hemp shives, 12 % PVAc/L, 4 wt. % nanozinc oxide and lime. The thermal conductivity was 0.06 W/mK, much lower than that of pure lime which was 0.16 W/mK. The 'Insulator' will be applied in two layers, one on either side of the 'Core'.

The 'Render' was developed using lime and 4 wt. % nanozinc oxide by wt. of lime and cured via air curing. It possessed a low porosity (18 %) in comparison to that of pure lime (36.4 %) and low thermal conductivity, λ (0.13 W/mK) in comparison to pure lime 0.16 W/mK cured by solvent exchange.

Shrinkage was lowest in a Render material containing 4 % wt. nZnO, averaging 750 microstrain (μs) compared to the control sample (lime only) of 2428 μs.

Chopped fibres, PVAc and nanozinc oxide were used for the first time with lime and no other examples of this exist in the literature (in the best knowledge of the researcher). Water vapour permeability (breathability), which is a beneficial property for construction materials was generally enhanced by using nanomaterials and the optimum breathability was achieved by adding 2 wt. % nanoclay to lime.

The results achieved were used to design an eco-friendly wall in accordance with the Building Regulations. The U-value target was 0.18 W/m^{2}K and the results show that a decrease in thickness of 40 mm could be achieved by using optimum materials

developed in this project in comparison to traditional hemp shives/Lime walls, in addition to eliminating timber studding which is normally required to provide support to non-loadbearing lime based walls.

List of Abbreviations

CNF	Carbon nanotube fibres
EG	Expanded graphite
FG	Fibre glass
HF	Hemp fiber
HS	Hemp Shives
L	Lime
MIP	Mercury intrusion porosimetry for measuring porosity
nclay	Nanoclay
nFc	Nanofibrillated cellulose
$nSiO_2$	Nanosilica
nZnO	Nanozinc oxide
PVAc	Polyvinyl acetate
P %	Porosity as a percentage
ρ	Density
WVP	Water vapour permeability
λ	Thermal conductivity
U	Rate of flow of energy pass through 1 m^2 for every +1°C

List of Publications

- O'Flaherty, F.**, Khalaf, F. J.,** & Starinieri, V. (2019). Influence of Nanomaterials on Properties of Lime and Hemp/Lime Composites for Energy Efficient Wall Design. Advances in Building Energy Research, 1-21. doi:10.1080/ ISSN: 17512549.2019.1586584.

  Khalaf, F. J., O'Flaherty, F. J., Wang, H. Development of High Performance Lime Binders Using Nanomaterials, Sheffield Hallam University/ MERI Research Symposium, 6-7 Feb. 2017.

- **Khalaf, F.J.,** O'Flaherty, F. J. and Starinini, V., New kind of lightweight polymer nanocomposite buildings, Sheffield Hallam University Symposium poster 17-18 May 2016

- **Khalaf, F.J.,** O'Flaherty, F. and Wang, H., Using Nanomaterials to Develop High Performance Lightweight Construction Materials, Sheffield Hallam University Symposium Poster, 19-20 May 2015.

List of Figures

List of Tables

Table of Contents

Chapter 1 - **Introduction**

1.1 Chapter Overview

1.1.1 Background and Motivation

There is a general tendency to find new products that do not generate carbon emissions when they are manufactured or used later (Y. Liu, Kuang, Huang, Wu, & Wang, 2009). The aim is to move to green renewable energy and environmentally friendly materials (Anderzej K. B., Adam Jaskiewicz, and, & Walczak, 2012; Ariadurai, 2013; Harlin & Vikman, 2010; Laadila et al., 2017; Madhuri B. M., Prashant S. K., Aravin p. p., & S., 2012; Saba, Tahir, & Jawaid, 2014). The construction materials industry is a high emitter of carbon dioxide and, therefore, the driver behind this project is to contribute to a more eco-friendly environment by developing low carbon construction materials for use in buildings. Construction of buildings in the UK is traditionally done using common building materials such as concrete blocks, bricks and less so, timber. Although timber is a sustainable product, concrete blocks and bricks require a lot of energy input during fabrication, concrete especially being a large producer of CO_2 during its manufacture (a5verage, 0.74 kg CO_2/1 kg concrete) (Turner & Collins, 2013) in comparison to 0.77 kg CO_2/Manufactured kg lime (EuLA, 2014). The quantity of CO_2 emissions, however, will be calculated for 1 m^3 of concrete and compared to lime/hemp nanocomposite in Chapter 8 after the densities of the proposed wall layers are found in Chapter 7.

Reducing energy consumption either domestically or industrially is an important part of achieving the UK Government's legally binding commitment to reducing greenhouse gas emissions by at least 80% (relative to 1990 levels) by 2050. New, low embodied energy construction materials are urgently required to enable the construction industry to revolutionise and drastically decrease its carbon footprint. A barrier to using lime and hemp as building materials is that a large thickness of material is required to meet thermal transmission requirements (U Values) as required by the Building Regulations. A large thickness not only negatively impacts on the footprint of the building, but it also influences the drying time meaning shuttering has to remain in place for a longer period of time and, therefore, extends the construction time. Damp and cold weather periods further aggravates this issue. The research employed rapid drying of the samples as soon as was practically possible to determine if accelerated water removal is worth pursuing as a technique for on-site construction. These methods included a solvent exchange technique using isopropanol

and oven drying to hasten the water removal but with the aim of not having an adverse effect on material properties.

1.1.2 The Third Industrial Revolution

In May 2007, the European Parliament issued a formal obligatory declaration (Rifkin, 2011) for all 27 member countries in the European Union to be committed to the third industrial revolution that transforms Europe and possibly the world to a post carbon era. This revolution means transformation from reliance on the great energy stations to millions of residential units and homes which are rearranged to be minor energy stations connected by a distribution net to meet the demand for energy in residential and industrial buildings or in transportation systems. Distribution of electrical energy will be controlled by a computer program on the web according to the demand. The prices will be defined when and where the peak demand happens. These minor stations or mini-plants will be provided by all kind of energy methods and their instruments (solar, wind, bio, hydrogen and geothermal) energy with a storage of energy technologies. The prices of a unit energy will be defined according the demand level. Rifkin, 2011, reported that "The foundation of the green economy and the third industrial revolution consists of five pillars each of which only functions in combination with one another:

1 Transition from fossil to renewable energies

2 Transformation of all buildings into mini-generating plants

3 Development and build-up of energy storage technologies and capacities (e.g. hydrogen)

4 Capitalizing on internet technology for the development of a smart and bi-directional (peer-to-peer) energy-sharing-grid

5 Transformation of the transportation system to electric plug-in and fuel."

1.1.3 Redesigning Requirements of the New Clean Energy Building

The key point here is the transformation of all buildings to mini generating plants. This means a rearrangement of the present buildings and the future buildings to be fitted with green energy and built from environmentally friendly and sustainable

materials. This means high performance, durable, lightweight and high energy efficiency buildings are needed to ensure working continuity of this small energy station (house or building). This kind of building is possible by high performance lightweight nanocomposite materials, because it easier to redesign the houses and buildings in comparison to heavy concrete buildings. Hemp fibre reinforced lime nanocomposites (nanosilica, nanocellulose, nanoclay, expanded graphite, nanozinc oxide and so on), which forms the basis of the present project, is more lightweight than concrete and is a good candidate to meet this requirement.

1.1.4 Redesigning Buildings Considering Solar Roofs and Facades

New roofs can be constructed from transparent solar energy materials to achieve many tasks, one as a roof, and another as an energy generator. It may also act as energy storage for batteries in the home or transparent facades of buildings as shown in Figure 1.1 and Figure 1.2 (Ohannessian, 2015; Ulbikas, 2017). The windows and doors may act as solar energy panels Figure 1.3 (London, 2017). If the building material is from hemp fibre reinforced lime nanocomposites as in this project, these consideration should be taken into account in structural design regarding of calculating the roof loads and the facade loads of clean energy tools exerted on the hemp fibre reinforced lime nanocomposites walls.

Figure 1.1 Transparent solar roof (Ohannessian, 2015).

Figure 1.2 Building transparent façade generating solar energy (Ohannessian, 2015; Ulbikas, 2017).

Figure 1.3 Solar window (London, 2017).

1.1.5 Redesigning Buildings Considering Battery Storage and Heat Collector

According to the third industrial revolution plan, houses should be mini energy stations. The home may be redesigned for battery storage as well as saving energy to supply power for electric vehicles or to feedback energy to the buildings or grid. This means homes must be redesigned to resist the aggressive acids of the battery system or redesign a special battery storage room in the building.

As for the heat collector, the home should be redesigned as a heat collector for boilers and for the heating system, see Figure 1.4 and Figure 1.5 (Griffiths, 2015).

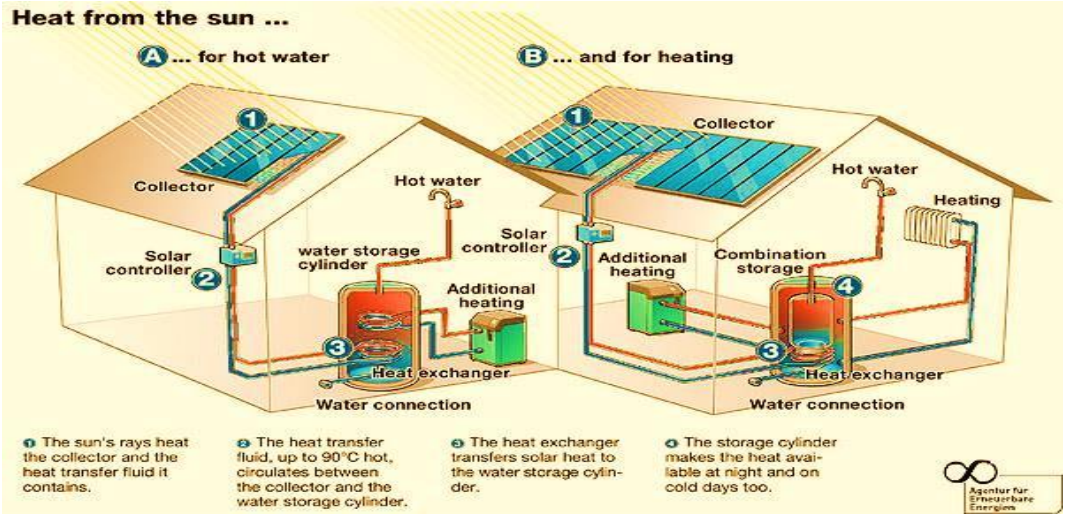

Figure 1.4 Roof heat collector for hot water and heating combined with other heat resources (like biogas) (Griffiths, 2015).

Figure 1.5 Home redesigned for roof solar energy, storage of batteries, and transparent door and window solar energy (Griffiths, 2015).

1.1.6 Redesigning Buildings Considering for Bioenergy

Furthermore, other redesigning includes a bioenergy device which could be built into the kitchen to produce biogases for cooking. However, this must be designed using fire-proof insulator walls which may be built from hemp/lime nanocomposites which were considered as good fireproof. It was reported that the internal face of a hemp lime wall was exposed to fire and it resisted for 73 minutes with respect to insulation and load bearing capacity (Gregor, 2014). Some tests were conducted to justify fire resistance for the French manufacturer Isochanvre and the various forms of material were classified as M0 and M1 "non-flammable materials" and M2 which is ‘low flammability".

1.1.7 Redesigning Buildings Considering Vertical Wind Turbines

As for wind energy, special reinforced supports must be erected on the building roofs for fixing the small vertical wind turbines; the columns and walls under these locations will be designed to carry the dead, live and dynamic loads, see Figure1.6 and Figure 1.7, both of them are from the rooftop wind turbine kinds (Nezeraud, 2012; T. Singh, 2012). These arrangements are applicable on the other methods and devices of clean energy like hydrogen production from water for vehicles fuel,

device of the geothermal energy produced from the difference of temperature degrees of heat inside and outside the earth to generate electricity or on the high heat at large depths in the ground to inject water and using the generated steam operating the electric generators. All these devices should find their way to be considered in the building construction properties which needs special composite construction materials.

Figure 1.6 Domestic roof vertical wind turbine (Nezeraud, 2012).

Figure 1.7 Group home roof vertical turbines (Nezeraud, 2012).

The recharged batteries, fuel gas and hydrogen bottles are sold to the fuel station for vehicles and cooking, energy uses and these, as it was mentioned, need to be designed into the building with special considerations, for example the storage of batteries requires durable construction materials against acids and fire (Rifkin, 2011).

1.1.8 Redesigning Buildings Considering High Heat Isolation (High Energy Efficiency)

The new building should be designed to meet a low energy requirement. High insulative materials are required for walls, roofs and floors for energy conservation along with their ability to be durable and loadbearing materials.

The aim of the present research is to investigate and achieve new forms of eco-friendly construction materials with good heat isolation, strength (loadbearing), low porosity, low shrinkage and high breathability.

1.1.9 Research Aims and Objectives

The aim of this research is to develop a fibre (hemp fibres/ or fibre glass for flexural and compressive strength improvement or hemp shives for heat insulation

improvement) reinforced lime nanocomposites. Chopped fibres to be used are measured in mm length. The material is fibre reinforced lime nanocomposite (nanoclay, nclay, nanosilica, $nSiO_2$, expanded graphite, EG, nanofibrillated cellulose, nFc and nanozinc oxide, nZnO blended with lime binder). To investigate and improve the strength, porosity, shrinkage, water vapour permeability (breathability) and thermal properties of this material by adding nanomaterials and hemp fibres or fibre glass in small proportions. Upon the best of the researcher's knowledge, limited research has been attempted to find materials that would exhibit most of the relevant properties for building construction through the addition of numerous nanomaterials and fibres (natural and industrial). The main aim is to transform the material from non-loadbearing to loadbearing mateial.

The focus of previous research studies concerned enhancing only on one or two properties such as porosity or thermal conductivity (T. Gao, Sandberg, & Jelle, 2014; Maddalena & Hamilton, 2017; Rollins, Collet, & Andres, 2018). This project is unique since it tries to design a proposed wall (Sec.1.9, Fig 1.10) by developing new building materials from hemp/lime nanocomposites with enhanced properties by adding nanomaterials (nanoclay, nclay, nanosilica, $nSiO_2$, expanded graphite, EG, nanofibrillated cellulose, nFc and nanozinc oxide, nZnO) of small proportions and fibres (glass or hemp which are not nanosize). Polyvinyl acetate or wood glue (PVAc) will be used to enhance the adhesion between fibres and lime and to increase both flexural and compressive strength. Specimens of hemp/lime nanocomposites will be tested in the lab. Ideally, the hemp/lime nanocomposite will be light-weight compared to concrete and durable. It will have sufficient flexural and compressive strengths (loadbearing material) to withstand the expected loadings, low thermal conductivity (heat isolation) to save energy, low porosity against water ingress, low shrinkage to avoid cracking and good water vapour permeability, in comparison with concrete, for a healthy environment inside the building by eliminating condensation. It should be easy to install and can either be precast or cast in-situ.

In the current project, from the point that it was mentioned above, many of the studies that discussed the methods of improving one or more properties will be highlighted. To help in choosing the right construction material and the proper nanomaterials, one must focus on the main properties of nanocomposite construction

material for building constructions which are flexural and compressive strength, porosity resistance, shrinkage to avoid the weakness of cracking and water vapour permeability (breathability). Thermal conductivity is studied to achieve heat isolation. The aim is also to establish the nanomaterials which will enhance these aforementioned properties. However, different studies that explored improving other properties will be mentioned but not in detail, such as creep, thermal stability, UV resistance and contamination resistance.

Three methods of curing will be used (Air, Solvent exchange and Oven curing) to test the effect of moisture content and drying on the properties of the materials.

1.2 Nanomaterials, Fibres and their Potential as Constituents in High Performance, Lightweight Building Materials

The emergence of nanomaterials has the potential to enhance the behaviour of lime based materials. In building and construction, one has to consider the properties of durability, flexural and compression strength, thermal conductivity resistance (heat isolation), porosity resistance (water proof) and ultra violet resistance (Saba et al., 2014). Fortunately, all these desired properties can almost be improved by using nanomaterials and fibres as it will be explained in Chapter 3. This matter has recently motivated researchers to use biomass nanocomposites in building components because it is environmentally friendly, sustainable and biodegradable (Anderzej K. B. et al., 2012; Ariadurai, 2013; Saba et al., 2014). Nanomaterials in this project will be nanosilica ($nSiO_2$), nanoclay (nclay), Expanded Graphite (EG), nanofibrillated cellulose (nFc) and nanozinc oxide (nZnO).

1.3 Hemp Shives and lime

Homes and buildings recently in the UK are made of hemp shiv and lime inside timber or steel frames; by contrast, in France they started more than 50 years ago Figure 1.8 and Figure 1.9 show example hemp lime of buildings. The shives in the stem compose of 60-80% which contains the majority of cellulose in the hemp, 34-48 %. Hemicellulose forms 21-37% and lignin 16-28% of the hemp plant (Cigasova, Stevulova, Terpakova, Sicakova, & Junak, 2013). Hemp is energy modest (no need for more energy in its life production), health friendly (non-toxic) kg CO_2/m^3 and carbon friendly (minimal pollution of CO_2 in its whole life). It is an organic material

derived from the plant Cannabis Sativa and not much fuel is needed to grow and harvest it. Hemp (Cannabis Sativa L.) is grown to get good strong fibres for multi-purposes, food oil from their seeds and core shiv for animal beds and now for insulator panels in construction. Hemp contains less than 0.3 of tetrahydrocannabinol (THC) which is the legal limit to be accepted by law – not considered as a drug like marijuana which is a plant resembling hemp (Peev, 2012).

In this project, the aim is to develop high performance materials for lightweight construction. There were three initial choices of composites to achieve the goals by using nanomaterials and fibres for improving the main properties (flexural and compressive strength, thermal conductivity and porosity). Shrinkage and water vapour permeability were also studied but they were of secondary importance. The choices were:

1 Fibre-reinforcement polymer nanocomposite (transparent polymers like polycarbonate).

2 Fibre-reinforcement geopolymer nanocomposites.

3 Fibre-reinforcement biomass lime nanocomposite.

Figure 1.8 Hemp lime home under construction (Benhaim, 2013)

Figure 1.9 Hemp lime home (Antonelli, 2015)

The third choice of fibre-reinforced biomass nanocomposites was adopted in the present project due to their key characteristics, namely environmentally friendly, sustainable and their ability to be developed.

1.4 Fibre Choices for Improving Strength

The choice adopted for this study was fibre reinforced hemp lime binder nanocomposite. The main aim was to enhance material properties to give an environmentally friendly, sustainable, biodegradable, breathable and a cost effective material for eco-friendly home and building construction.

The goal is to transform hemp lime binder composite into a load bearing material, either as cast in-situ or pre-cast as panels. To date, hemp lime binder composite is used in buildings and houses as walls, roofs and floors but supported by a timber or steel frame. Panel infills are about $1m^2$ in elevation.

As for the fibre choices, hemp fibres or fibre glass, were selected to develop the flexural and compressive strength of lime nanocomposite as load bearing materials. Fibre glass choice will be used for comparison with hemp fibres. As for nanomaterials, as a result of reviewing the literature; nanosilica, nanoclay, nanocellulose and expanded graphite were selected with different percentages to study and optimise their impact on the flexural and compressive strength. In the present project, an enhancement in strength was found by using nanomaterials but the best improvement was by using chopped fibres, 6 mm long fibre glass or 6-10 mm long hemp fibres. Based on knowledge to date, this is the first time chopped fibres from glass or hemp were mixed with lime which to give a high flexural and compressive strength. Also this is the first time the material was transformed into a load bearing material. It was reported that a load bearing material must have a compressive strength in the region 3-5 MPa, (de Bruijn, Jeppsson, Sandin, & Nilsson, 2009). According to the literature, the hemp fibres were used as multilayers of fabric or the hemp stem was crushed as shives with its bast (including fibres). They were then mixed with lime but the nanocomposite was still very weak and non-load bearing, about 0.2-0.5 MPa (Evrard, 2003) or about 0.4-1.2 MPa (Arnaud, Cerezo, & Samri, 2006).

1.5 Adhesive Enhancement for Fibres

Polyvinyl acetate was selected as an adhesive to enhance the bond between the fibres (hemp and glass) and the lime binder; as a result, the compressive strength was increased many times. Since hemp fibres are eco-friendly, biodegradable and

sustainable, the hemp fibres were the preferred choice in place of the fibre glass. Poly vinyl acetate (PVAc) is made synthetically from plastic origin, but it was made from organic origin (animal bones, hooves and hides) before discovering the plastic origin. The plastic origin of PVAc (white glue) is nontoxic and biodegrades slowly (Zara, 2016) and that means both origins are nontoxic and biodegradable.

1.6 Nanomaterials for Enhancing Strength

Nanosilica, nanoclay, nanocellulose and expanded graphite were adopted to study their impact on enhancing the strength (flexural and compressive) of lime and hemp (fibres or shives) lime composites. The choices were made according to a literature review as shown in the Chapter 2.

1.7 Nanomaterials for Thermal Conductivity

For the thermal conductivity, nanosilica, nanoclay and nanozinc oxide were used to study their effect on the thermal conductivity. Again, these nanomaterials were selected based on an extensive literature review.

1.8 Material Choices for Porosity

For porosity, nanosilica, nanoclay, expanded graphite and nanozinc oxide were selected based on a literature review. In addition, nanozinc oxide has antibacterial properties and is compatible with human body cell properties which makes it a promising material in construction (Tavassoli Hojati et al., 2013).

1.9 Summary

The addition of fibres to the lime had the greatest influence in reducing shrinkage in addition to the main impact to improve flexural and compressive strength. The breathability property of lime is important and it can be improved by nanomaterials due to their particle size which amends and organises the pore diameters (Nazari & Riahi, 2011).

The optimum design of the load bearing, thermally efficient wall was as follows see Figure 1.10: the Core of the wall will be from hemp fibres, lime binder, PVAc and nanomaterials such as nZnO which is the best for the core as it will be seen in

Chapter 4, 4, 6 and 7. The Insulator will be made from hemp shives, lime binder, PVAc and nanomaterials such as nclay, $nSiO_2$, EG and nZnO and nanozinc oxide is the best as it will be see in Chapter 5, 6 and 7. The Render will be made from the aforementioned nanomaterials (nanozinc oxide is the best as it will be seen in Chapter 5, 6 and 7) and lime, low percentages of hemp fibres (say around 5 %) to decrease the shrinkage.

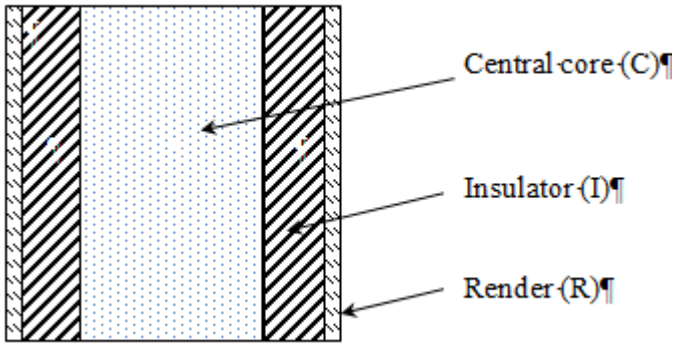

Figure 1.10 Cross section through the proposed wall.

1.10 Outline of the Thesis

The thesis is divided into eight main chapters as follows:

Chapter 1 Introduction: This introduces the research and explains why nanomaterials can be a viable solution for enhancing the properties of different construction materials such as Polymers, Cement and Biomass.

Chapter 2 Literature Review: A detailed literature review is conducted on the influence of different nanomaterials, fibres (of glass or hemp) and hemp shives in enhancing the key material properties such as flexural and compressive strength, thermal conductivity, porosity and shrinkage. A summary of the findings are presented in tabular form which demonstrates the effect of using nanomaterials on the properties of different matrices of polymer, cement, lime and biomass materials.

Chapter 3 Test Methods: A summary of the methodology of the experiments and how the lime binder properties will be enhanced is summarised in this chapter (from

the literature review given in Chapter 2) and forms the basis for choices of the materials in the project. An explanation of the characteristics of the different nanomaterials is also presented.

Chapter 4 Results and discussion of compressive and flexural strength: A detailed analysis of the experimental results for the tests of strength (flexural and compressive) using nanomaterials (nanosilica, nanoclay, nanocellulose and expanded graphite), fibres (glass and hemp) and hemp shives. The chapter also includes analysis and discussion of the results.

Chapter 5 Results and discussion of porosity and water absorption tests: a detailed analysis of the experiments for porosity and water absorption tests, followed by a discussion of results is presented.

Chapter 6 Results and discussion of shrinkage and water vapour permeability: a detailed analysis of the results using nanomaterials (nanosilica, nanoclay, nanozinc oxide and expanded graphite), fibres (glass and hemp) and hemp shives is given. A discussion of the results completes the chapter.

Chapter 7 Results and discussion of thermal conductivity: a detailed analysis of thermal conductivity using nanomaterials (nanosilica, nanoclay, nanozinc oxide and expanded graphite), fibres (glass and hemp) and hemp shives is given. Analysis and discussion of the results is also given.

Chapter 8 Conclusions and future work: Conclusions are given in addition to highlighting the future work that could be conducted to enhance the findings from that project.

Chapter 2 - **Literature Review**

2.1 Introduction

In this chapter, an introduction about composites in general, building construction materials and nanocomposites is presented. Furthermore, a brief summary about nanomaterials and their synthesis routes will be given. The beginning of this project consisted of studying the literature in order to identify required properties for construction materials and fillers used to enhance those properties.

Due to a limited number of publications in the field of transforming lime to a loadbearing construction material, it was decided to complementary conduct a literature review of research on other materials, such as cement and polymers. Important properties for Loadbearing construction materials are high compressive and flexural strength, low porosity, low thermal conductivity and low shrinkage. The approach in this work was to follow studies on polymers and other materials and the additives used to enhance the above mentioned properties. However, as at the present moment there is no distinct correlation between additives used to improve the properties of polymeric, cement, other construction materials and additives usable for lime matrices, through tests will have to be performed.

2.2 Composite materials

Composite materials are composed of two or more components; the main material is called the matrix and the others are fillers. It is a combination of two or more materials that results in better properties than those of the individual components used alone (Campbell, 2010; Jeon & Baek, 2010a; Zaman, Gutub, & Wafa, 2013). Figure 2.1 and Figure 2.2 show polymer composite panels for walls, floors and roofs made from polyurethane and additives.

The composite gains new chemical and physical characteristics when its components are combined together. If the fillers are nanomaterials and biomass like hemp and the matrix is a lime binder, it is known as biomass lime nanocomposites (Constantinides, 2013; Harlin & Vikman, 2010).

Figure 2.1 Polymer composite panels of floors and walls of houses (Inovatecsystem, 2006-2016)

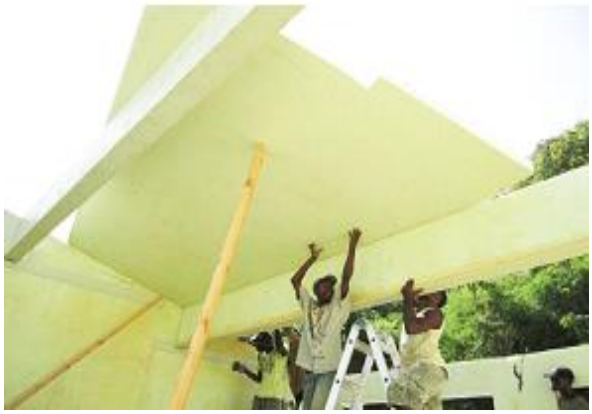

Figure 2.2 Polymer composite roof panels for roofs working (Inovatecsystem, 2006-2016)

A composite dome was built in Libya in 1968; it was manufactured in the UK as a sandwich polymer composite with an aluminium skeleton. Also, a polymer composite roof (umbrella form) was made in the UK and built in Dubai in 1972. As mentioned earlier, in 1970-1980, this kind of building structure became well-known; it depends on different skeletal frames. After 1985, structures were completely erected from polymer composite materials as modular units (Hollaway, 2003).

A bio-composite is a new technique with low cost and is environmentally friendly. It is different from all the conventional materials and possesses the required properties of traditional materials, but still there is a gap in properties and economic considerations between the high competitors of the conventional industrial and biocomposites materials (Ariadurai, 2013).

2.3 Nanocomposites

Nanocomposites are polymer, cement or any other material or bio-material matrices mixed with fillers. These fillers are nanoscale (Burgueno, Mohanty, & Quagliata, 2007). Richard P. Feynman in 1959 (published in 1960) pointed out in his famous lecture that "there's plenty of room at the bottom" (Feynman, 1960).

This initiated a significant development in all sciences; physics, chemistry and biology. This indicates the serious roles at the level of molecules and atoms which is now called nanoscale. This scale is less than 100 nanometres and the material within this scale have properties different from those in the original materials.

2.3.1 Nanoscale

The scale of nanomaterials is near to the atom dimensions. It is a billionth part of meter, 10^{-9} m (Jain & Singh, 2007). In the Greek language, the word "nano" means dwarfs and it has become a term pointing to a billionth. "Nano" is a matter or a thing on the nano-size level (Feldman, 2014) It starts from 0.1-100 nm. (Bandyopadhyay-Ghosh, Ghosh, & Sain, 2015b). Figure 2.3 shows a comparison between nano, micro and ordinary metric size.

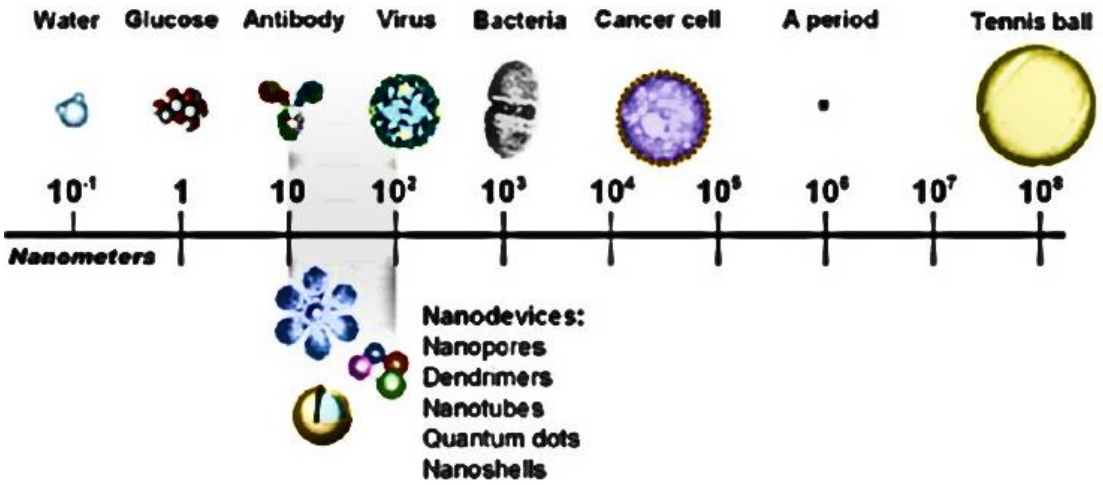

Figure 2.3 Comparison of different nanoscales (Nikalje, 2015)

2.3.2 Methods for Manufacturing Nanomaterials

There are two methods for manufacturing nanomaterials. They are top-down: the nanomaterial is prepared by reducing and decomposing the original material into nanoscale size and the bottom-up which is an assembly process of molecular or atomic scale components applied to construct the materials, see Figure 2.4 (Sanchez & Sobolev, 2010).

2.3.3 Shapes of Nanomaterials

Depending on the size levels of nanomaterials, they can be classified into three kinds: 1-Nanoparticles: which have three dimensions that are in the nanomaterial scale. 2-Nanofibres: which have one of three dimensions in the micro-dimensions and the other two are located in the nanoscale. 3-Nanolayers: found in a film or a sheet form that has 1-2 nm thickness and lengths of about hundreds to thousands nanometres such as clay layers. Figure 2.5 shows the kinds of nanomaterials according their nanoscale dimensions. 4- Nanotubes are described into two dimensions; one of them is a diameter in nanoscale which is a hollow core and the second dimension which is the length, is in microscale.

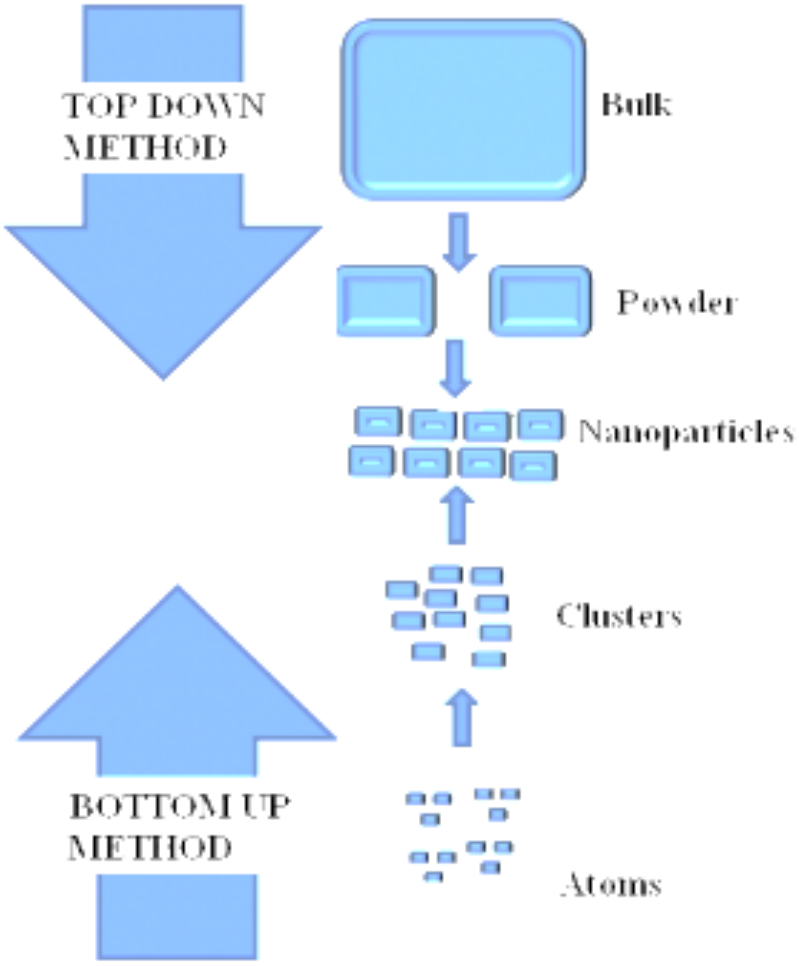

Figure 2.4 Top down and bottom up methods to synthesise nanomaterials (Bose, 2016).

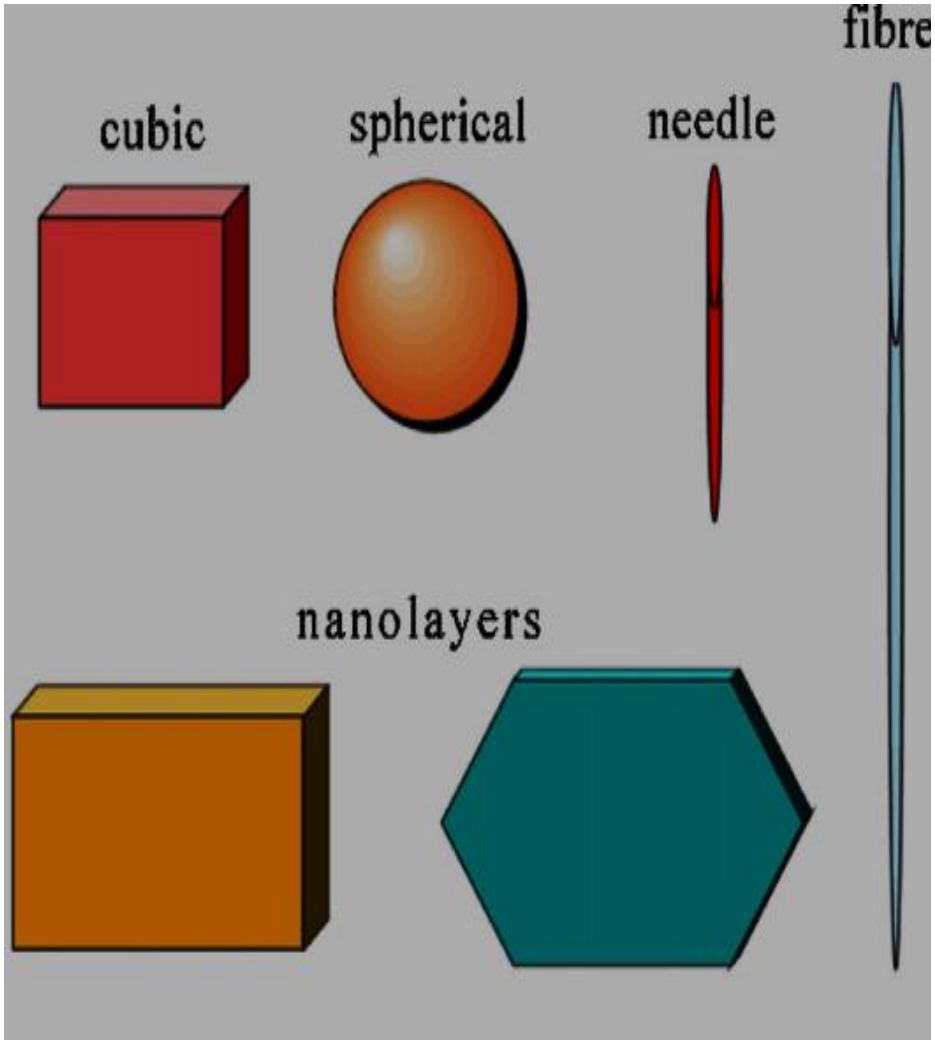

Figure 2.5 Various types of nanoscale materials (Chrissafis & Bikiaris, 2011)

2.3.4 Nanomaterial Applications

Nanomaterials have emerged as a big revolution due to their capability to improve the properties of polymers when added, such as the mechanical properties, which include tensile, flexural and compressive strength, modulus of elasticity and impact resistance amongst others. They decrease porosity which is also a decrease of permeability to water and gases, improve thermal conductivity resistance and heat isolation, enhance stability against heat, enhance flame retardancy, decrease smoke release, improve chemical resistance, surface appearance, electrical and thermal conductivity and the optical clarity for transparency polymers in contrast to the ordinary fillers (Chrissafis and Bikiaris, 2011).

2.3.5 Nanomaterials and Fibres Selection

The key to a successful outcome is to establish which nanomaterials enhance certain properties. Ultimately, the properties to be enhanced herein are flexural and compressive strength of materials, porosity resistance (low porosity), thermal conductivity (low), shrinkage (low) and maintain or increase water vapour permeability.

In this project the matrix to be considered is lime paste. The fillers are biomass which are hemp shiv, hemp fibres or fibre glass (for comparison with hemp fibres), PVAc (Polyvinyl acetate) to increase adhesion between fibres, lime and nanomaterials such as expanded graphite (EG), nanofibrillated cellulose (nFC), nanosilica ($nSiO_2$), nanoclay (nClay) and nanozinc oxide (nZnO).

2.4 Development of the Main Properties of Building Materials

As stated before, the methods of enhancing and improving one or more properties of matrices or polymer nanocomposites for different uses have been discussed and investigated in these studies. Some studies discussed improving one or more physical properties like Young's modulus, tensile strength and the impact resistance and provided information on the nanomaterials and synthesis and natural fibres that were used to improve these properties (Bhattacharya, 2016). Other research studied the methods of improving the thermal activity of matrices or polymer nanocomposites in both directions for heat isolation (low thermal conductivity) and heat conduction (high thermal conductivity). Others addressed the methods that decrease or increase the thermal conductivity of the polymer nanocomposites (Chrissafis & Bikiaris, 2011; Liao et al., 2012; Zhu, Cai, Zhou, & Shi, 2008). Some researchers focused on the porosity from both decreasing and increasing the porosity or permeability of polymer nanocomposites depending on whether they intended to develop porous or nonporous materials (Constantinides, 2013). Some studies examined the weather effects on the polymer nanocomposites such as ultra violet resistance, which means the resistance to sun light and the heat of sunlight (Biplab K Deka & Maji, 2012; Biplab K Deka, Mandal, & Maji, 2012; Devi & Maji, 2012; Feldman, 2014).

Other studies were involved in enhancing chemical resistance and some discussed the methods of improving the properties of building construction materials. They intended to improve traditional materials like cement, concrete or steel bars used for concrete reinforcement. To the best of the researcher's knowledge, there is no study that discussed or examined the main properties of nanocomposite construction material as a whole package that is needed for building construction, especially materials needed for residential buildings and houses.

2.4.1 Development of Mechanical Properties (Flexural and Compressive Strength)

For brittle materials like cement, gypsum, rock and lime; flexural and compressive strengths are very important for civil engineering and building construction. Due to the importance of both compressive and flexural strengths, they will be considered the dominant factors that define which of the nanocomposites and fibres will be selected and adopted to conduct the other tests that are required for building construction. The effects on mechanical strength in the literature studies in general will be followed to help in this project because there was little or no research on lime (binder) matrix biomass nanocomposites to guide the research.

2.4.1.1 Nano Carbontubes Fibres (CNTs) and Nanocarbon fibres (CNF)

CNTs have been studied in a lot of papers. It was reported that CNTs represent a significant improvement in flexural strength, the modulus of elasticity, toughness and compressive strength. The flexural strength, flexural toughness and compressive strength were increased by 85 %, 205 % and 22% respectively using 0.5% carbon nanotubes in cement by weight (P. W. Chen & Chung, 1993).

Adding 0.2 wt. % CNTs (carbon nanotubes) and 0.2 wt.% CNFs (carbon nanofibers) using w/c ratio of 0.35 at 28 days to cement gave both high strength at 7 days in comparison to 0.1 % composites. The results of compressive strength gave 54.5 % and 67.5 % increase respectively in comparison to pure cement. The results of flexural strength gave 14.06 % and 8.7 % increase. Adding of CNF also enhanced electrical conductivity and thermal conductivity. These materials, CNT and CNF are sometimes used but they were not beneficial in building construction materials because thermal and electrical isolation is required in civil structures (Sinha Ray, 2013).

2.4.1.2 Nanocellulose

As for nanocellulose, a study reported that a polycarbonate polymer matrix with 10 wt. % loading of microfibrillated cellulose (MFC) was developed by solving MFC and making a film of MFC using the hot press device for making layer upon layer of polycarbonate enhanced the tensile strength about 24% in comparison to the pure polycarbonate. This film was made from bleached wood pulp nanofibrillated cellulose 2 wt. % suspension of water passing through vacuum membrane filter to produce 50 microns film and polycarbonate film (Panthapulakkal & Sain, 2012b). Melamine formaldehyde and microfibrillated cellulose nanocomposites exhibited a high tensile strength of about 142 MPa by adding 5 wt.% of microfibrillated cellulose to melamine formaldehyde in comparison to tensile strength of pure polymer (104 MPa) (Henriksson, 2007). Another study pointed out that micro-fibrillated cellulose passed 30 times through the refiner and 5 wt. % to wood pulp made a jump in tensile strength of wood pulp compared to a 16 time pass through the refiner; it was raised from 200 to 300 MPa (Bandyopadhyay-Ghosh, Ghosh, & Sain, 2015a).

A bacterial cellulose ribbon was saturated with phenolic resin and it showed a higher strength than micro-fibrillated cellulose; Young's Modulus increased from 19 to 28 GPa and the bending strength increased from 370 to 425 MPa (A. N. Nakagaito, Iwamoto, & Yano, 2004; A.N. Nakagaito & Yano, 2004). Nanocellulose was used as a suspension 7 % concentration helped to increase the compressive strength of the cement with changing the density of the cement slurry, due to its specific weight of 1.06 and high water content, water can be replaced by nanocellulose to a small extent. Compressive strength was increased from 16.9 MPa of pure cement to 26.72 MPa using 5 % nanocellulose and 0.4 w/c (Shenoy, Joshi, & Dange, 2019). It is reported that adding 0.15 % by weight of nanocellulose fibres leads to a 15 % and 20 % increase in the flexural and compressive strengths of cement paste respectively due to the high degree of hydration and to the increase in the density of cement paste microstructure (Jiao et al., 2016).

2.4.1.3 Nanosilica

Nanosilica is another material used to enhance many properties in matrices like cement, lime, biomass, biopolymer and polymer nanocomposites, these applications will be explained in the next paragraphs from the literature review. Among these

properties is flexural, compressive and tensile strength. One of these studies mentioned that 4 vol. % of nanosilica ($nSiO_2$) was added to polycarbonate (PC). The composite gave maximum tensile strength and fracture toughness by adding 4 vol. % nanofillers. The improvement in fracture toughness of PC was 43%. Tensile and fracture properties decrease if the nanosilica loading increase more than the mentioned percent (Zhou & Burkhart, 2009). Impact resistance of the polycarbonate 2 vol. % nanosilica ($nSiO_2$) composites significantly improved from 521 N maximum failure load for neat PC to 1330 N due to the positive effect of the nanofillers (Luyt et al., 2010). Nanosilica was also added to polyvinyl alcohol (PVA) of 60 vol. % $nSiO_2$/PVA and the tensile strength went up from 89.9 MPa for neat polymer to 122.2 MPa for polymer nanocomposite. For epoxy, the tensile strength increased from 127 MPa to 141 MPa for the same percentage (Oja & Nanosiliko, 2013). Nanosilica was mixed with a melt mix method using a Brabender mixer with polycarbonate. The ultimate tensile strength was performed at 4 vol. %. It increased from 63.41 MPa for neat PC to 66.13 MPa for the nanosilica influenced mix (R.-J. Zhou & T. Burkhart, 2010).

Nanoparticles of SiO2 (nanosilica) can fill the spaces between particles of gel of C–S–H in cement, acting as a nano-filler. The pozzolanic reaction with calcium hydroxide led to increase the amount of C–S–H (Calcium-Silicate-Hydrate which are the main products of the of cement) which produced higher density, increase the compressive and flexural strengths and improve durability of the cement mortar. This was achieved by adding nanosilca to synthesied cement slurry which was used for oil wells. Quantity of 70 g $Na_2SiO_3.9H_2O$ (Merck) was added to 450 g of distilled water and 54.66 g of surfactant factor, N-cetyl-N,N,N-trimethyl ammonium bromide g (CTAB) were blended with 400 g of water and stirring 15 minutes. The solution was added to the solution of silicate The compressive strength was increased 5.54 MPa to 27.59 MPa at 120 hrs and 87.7°C (Choolaei, Rashidi, Ardjmand, Yadegari, & Soltanian, 2012). It was reported that adding 1 wt. % of $nSiO_2$ to cement, compressive strength was increased 37 % in respect with the pure cement (Rai & Tiwari, 2018). In another study, nanosilica was added (1,3, 5, 7 and 10 %) to cement sand, 1: 2.75 and w/c, 0.485 at 28 days, the highest compressive and flexural strengths were 36.76 MPa and 5.72 MPa respectively compared to pure cement 23.6 MPa and 3.57 MPa (Yehia, A Khattab, S Khalil, & El-Baky, 2013).

2.4.1.4 Nanoclay

Nanoclay has attracted the attention of researchers due to its potential to enhance the mechanical properties of many matrices and polymers. Tensile strength of 4 wt. % nanoclay (montmorillonite MMT)/ poly vinyl alcohol (PVA) was increased by 62 % of neat PVA (Soundararajah, Karunaratne, & Rajapakse, 2009). In another study, PVA blended with 5 wt. % of graphene oxide (GO) and MMT 1:3 GO/ MMT by wt., increased the tensile strength from 27 MPa for neat PVA to 80.7 MPa for nanocomposite (Raheel et al., 2015). The flexural strength of glass fibre reinforced epoxy blending with nanoclay (Cloisite 15 A) silane treated was increased from 155 MPa for 10% of silane treated nanoclay to 278 MPa for 200 % silane treated nanoclay. The tensile strength of the mixture was increased from 261 MPa to 390 MPa for silane treated nanoclay and from 50% - 200% silane/nanoclay (Sharma, Chhibber, & Mehta, 2016).

It was found that adding 8 wt. % of nano-metakaolin to cement at 0.5 water/cement (water to cement ratio), the tensile and compressive strengths were improved 49 % and 7 % respectively (M. Morsy, Alsayed, & Aqel, 2010). Other study was reported that cement mixed with 1 wt. % of calcined nanoclay (CNC) decreased the porosity and increased compressive strength. Calcined nanoclay is produced by heating nanoclay (Cloisite 30B) at 900° C for 2h. The study outcome was the compressive strength increased from 53.1 to 74.2 MPa or 40% increase by adding 1 wt. % CNC and the compressive strength improved to 69.8 MPa by mixing the cement of 1 wt. % nanoclay (NC) (A. Hakamy, F. Shaikh, & I. M. Low, 2015). Furthermore, cement added to sand 1: 2.75, 0.485 w/c at 28 days and they were mixed with many percentages of nanoclay (1,3, 5, 7 and 10 %). The highest compressive and flexural strengths were 37.73 MPa and 5.91 MPa respectively by adding 10 wt. % nanoclay in comparison to pure cement 23.6 MPa and 3.57 MPa respectively (Yehia et al., 2013).

2.4.1.5 Expanded Graphite (EG)

EG was used in some studies to enhance mechanical properties, but it was used to improve electrical and thermal conductivity properties of the composites which must be low in construction materials. For example, it was added to polymethyl methacrylate (PMMA) after it was slowly oxidised and became surface modified by many processes. Firstly, expanded graphite was chemically changed by adding sulphuric acid (H_2SO_4) and hydrogen peroxide (H_2O_2), and then it was surface

modified by mixing them with potassium permanganate ($KMnO_4$) and H_2SO_4. Adding modified surface of EG improved the mechanical properties of the PMMA composite; the modulus of elasticity was enhanced 3 times compared to the pure polymer. In contrast, the electrical conductivity was highly increased for the composites (> 1700 S/m or Siemens/meter) (P. Wang et al., 2017).

Epoxy was mixed with graphite nano-platelets (GNP), which the expanded graphite is derived from, after improving interfacial adhesion of GNP/ epoxy by ultra violet ozone treatment (UV/O). This composite showed flexural strength improvement. It was about 50 MPa for neat epoxy and 65 MPa for UV/Oz treatment GNP/ epoxy (Li, Kim, & Lung Sham, 2005). Expanded graphite was grafted with acrylamide and blended with epoxy showing a remarkable increase of flexural strength and modulus of elasticity; they were about 84.5 MPa, 2.77 GPa for pure epoxy and about 95 MPa, 3.55 GPa for 3 vol. % nano-graphite epoxy composite respectively. For grafted nano-platelets, the flexural strength was increased to about 112 MPa and the flexural modulus was about 3.94 GPa (Lowrence & Fukushina, 2009).

Blending graphite powder (electric discharge machining EDM) with lime from 0 %-50 %, which is the origin of expanded graphite to hydraulic lime NHL5, increased the compressive strength three times to pure lime and 80% thermal conductivity, reducing the porosity and water absorption too (Barbero-Barrera, Medina, & Guardia-Martin, 2017). The steps of manufacturing EDM are pulverising the coke, kneading, again pulverizing, isostatic pressing, baking to 1000 °C, impregnation or fertilizing, graphitising upto 3000 °C, moulding to graphite block, machining, purifying, roughing and milling (Flores Medina, Barbero-Barrera, & Bustamante, 2016). Expanded graphite was synthesised by preparing expanded graphite/paraffin gypsum composite (EGPG) modified by 1 wt. % carbon fibres, EGPG or gypsum blended with 10 wt. % EG/P (paraffin) and 1 wt. % CF (carbon fibres). The flexural and compressive strength of EGPG were increased by 65.6 % and 6.4 %, respectively. Unfortunately, the thermal conductivity increased 36.0 % which is not beneficial in construction materials (B. Zhang, Tian, Jin, Lo, & Cui, 2018). Mixing of cement with expanded graphite treated with ozone led to increase in the bonding between cement paste and the carbon of EG depending on the effect of gaseous ozone on modification of EG surfaces. Oxygen groups (carbonyl, phenol and carboxyl) were composed leading to this bonding

effect and improving the resistance to bending load in the pre-cracking zone (Slosarczyk & Krawczyk, 2016).

Hydraulic lime (NHL5) was mixed with graphite which is considered as compatible with lime paste and the compressive strength was increased three times compared to the neat graphite. Moreover, the porosity and water absorption were decreased. Unfortunately, the thermal conductivity was increased up to 80% as a result of this addition (Barbero-Barrera, Medina, & Guardia-Martin, 2017).

2.4.1.6 Fibres (Synthetic and Natural).

Fibres are used to improve the mechanical properties of matrices (polymer, cement gypsum and lime). There are many kinds of industrial fibres like steel, cuprum, polypropylene and carbon fibres. The most common industry fibres in the composites are glass fibre. In general, there is no mention in the literature of fibres being used to reinforce lime binder except when the lime or gypsum render and ceiling were reinforced by fabric hessian and chopped animal hairs (Bowley, 1994). Recently, hemp fabric was used as layers with lime/cement but still nonloadbearing material. The crushed hemp stem as shives with their fibres (not separated from shives) (de Bruijn et al., 2009) and this method didn't help to raise the material from nonloadbearing to loadbearing material (de Bruijn et al., 2009). All these examples will be discussed in the next sections.

2.4.1.6.1 Fibre Glass

Fibre glass is relatively low cost and has a good chemical resistance to acids and solvents. It is used to reinforce polymers, lead and cement. 84 wt. % of molten lead mixed with 16 wt. % of fibre glass improved tensile strength of the composite from average 200 MPa up to 315 MPa (Goddard & Kendall, 1977). Flexural strength for cement mixed with 5 wt. % fibre glass was increased from the traditional value of cement which is around 4 MPa (Aho & Ndububa, 2015; M.-h. Zhang, Jiang, & Chen, 2008) for cement mortar to 35 MPa for the composite (Thomas, 1972).

Fibre glass in 50 mm lengths was mixed with 4 wt. % to water resistant gypsum (its compressive strength was 35 MPa from the supplier), the flexural strength significantly improved for 28 days from 4.96 MPa for gypsum to 22 MPa for the

composite and the tensile strength from 2.75 to 18 MPa respectively. The water resistance gypsum mentioned above is industrially made by mixing ground granulated slag with ordinary Portland cement and calcined phosphogypsum. Lastly, a retarder is added in a ball mill (M. Singh & Garg, 1992). There was no study, to the best knowledge of the researcher, about using fibre glass with lime.

In contrast, fibre glass was used as a reinforcing in cement, 10-40 mm length of fibre glass mixed with cement 2-8 vol. %. The optimum properties of the composite at 28 days were by adding 6 vol. % of fibre glass, flexural strength was increased 4-5 times, the tensile strength was improved 3-4 times, the impact strength was highly improved 15-20 times compared with cement (Ali, Majumdar, & Singh, 1975).

2.4.1.6.2 Hemp Fibres

Hemp is a plant described as a quickly renewable construction material, biodegradable, sustainable and eco-friendly. Hemp is a fast growing, annually harvested plant and its stem can be 4 m high or more. The stem of the hemp is enveloped by the bark and the bundles of fibres are inside the bark which has a high tensile strength see Figure 2.6.

Natural fibres like flex, hemp shiv, with or without its fibres, were used to reinforce the variety of matrices (cement, polymers lime, etc...). The components are mainly used in industrial objects; food oil, fabric and clothes, nutrition, bakery and medicines (de Bruijn et al., 2009). This is with the exception of 5 % of hemp which is used in construction materials, most of them as insulations (N Stevulova & Schwarzova, 2014).

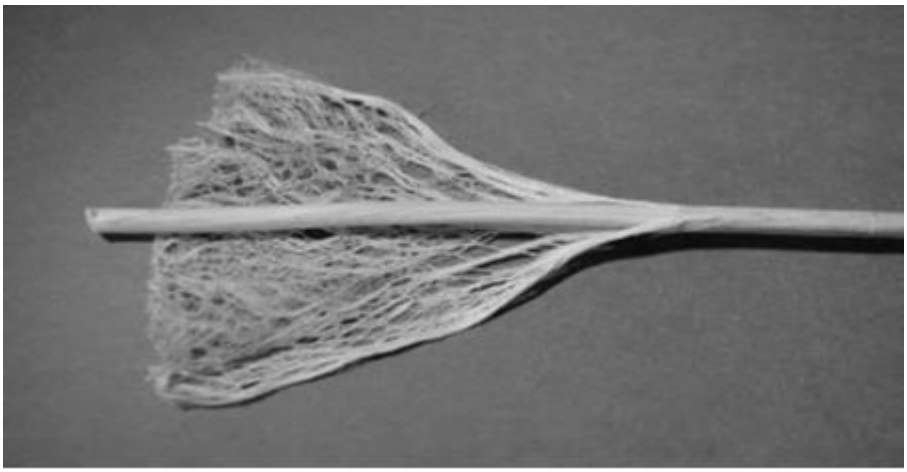

Figure 2.6 Stem part of hemp plant showing the fibres in outer envelope (bast) and the woody core which is crushed as hemp shiv (Marczyk, Jul 12, 2013)

A study reported using 40 wt. % of hemp shiv and 31 % water/binder with different percentages such that all binders in each sample were equal to 29 wt.% of the binder for the different samples: (1) 24 wt.% lime and 5 wt.% of cement; (2) 24, 2.5, 2.5 wt.% lime of (lime, cement, zeolite); (3) 24, 5 wt.% (lime and zeolite); (4) 29 wt.% of (C) ; and using 40 wt. % Hemp Flux with (5) 24, 5 wt.% of (lime: cement); (6) 29 wt.% (MgO and C). It was reported that the compressive strength results were very low (0.3, 0.27, 0.23, 2.73, 0.73 and 1.86 MPa respectively) but the thermal conductivity results were reasonable in comparison to those of the insulators (which will be considered in Chapter 7). The thermal conductivity results ranged between 0.069 to 0.111 W/mK (Nadezda Stevulova et al., 2013).

A research reported that the compression strength from 10 different labs, of samples composed of hemp shiv and cement with citric acid were between 0.32-0.45 MPa (Niyigena et al., 2015). As shown from the minimum compressive strength of load bearing materials, lime/shives or cement/shiv composites could only be used as insulators because their insignificant compressive strength.

Lime mixed with hemp shiv/flax straw was studied and it showed that the lime hemp flax composite was low in strength, density and thermal conductivity but it has absorptivity. Compressive strength was between 0.41-0.85 MPa and flexural strength

was between 0.05-0.24 MPa (Brzyski, Barnat-Hunek, Suchorab, & Łagód, 2017). It was reported that load bearing lightweight expanded clay has a compressive strength of 3-5 MPa (de Bruijn et al., 2009) and that means any material to be loadbearing must be higher than this value. It is obvious from that all compressive strength in literature studies were < 1 MPa or a little more and no study could transform the material to load bearing material in compressive strength to the value which was mentioned in the last section (3-5 MPa) and the flexural strengths also were very low < 1 MPa or a little more which is not match with flexural strength of cement mortar around 4 MPa or concrete around 7 MPa.

2.4.1.7 Adhesive Material

An adhesive material was included as a way of increasing bond between fibres and the lime matrix. Polyvinyl acetate (PVAc) was selected as a suitable option. Polyvinyl acetate is made synthetically from plastic origin, but can be made from organic origin (animal bones, hooves and hides). The plastic origin of PVAc (white glue) is nontoxic and biodegrades slowly (Zara, 2016). It was reported that the adhesion strength of two wood pieces at dry, wet and elevated temperatures was raised with the increased loading percentages (1, 2, and 4 wt. %) of nanoclay to PVAc (Kaboorani & Riedl, 2011).It was reported that the lap shear joint strength for pine wood was increased from 4.8 to 11.53 MPa by adding PVAc blended with 4 wt. % of nanoclay (Aydemir, Gündüz, Aşık, & Wang, 2016)

From the above studies, the best option for developing the mechanical strength is hemp fibre reinforced lime and lime singularly blended with nanosilica, nanoclay, nanocellulose or expanded graphite. Fibre glass was used for comparison to the result of hemp fibres. The PVAc was selected to improve the adhesion between lime and hemp fibres and hemp shives. The nanocarbon tubes were excluded from this study because it was expensive and it increased, as in the literature research, the thermal conductivity which contradicts with the heat isolation concept of construction materials. Strength will be critical the render layers (R) and the core layer (C) of the proposed wall mentioned in Chapter 1, but for insulation layers (I), the focus will be on developing thermal insulation.

2.4.2 Development of Thermal Conductivity

It is very important in building construction to use materials which have high heat isolation i.e. low thermal conductivity. A thermal conductivity test includes isolating and conducting materials. In some industries, high thermal activity materials are advantageous, like radiator bodies or the covers of the motors of the machine, vehicles or industry motors to transform or spread the heat to the surrounding spaces and to decrease the heat of the motor. In building construction, heat isolation is required to keep the building away from climatic heat to conserve conditioning energy (Energy, 2008; Laustsen, 2008). The desired construction material should have high heat insulation to keep the inside of the building at a comfortable temperature for humans even if the outside temperature is high or low, so it is preferred to use low thermal conductivity construction materials. In general, lower than 0.3 W/mK, the thermal conductivity is very good, but for highly effective thermal insulation materials values are preferred to be under 0.1 W/mK (Sičáková, 2015; Nadezda Stevulova, Cigasova, Schwarzova, Sicakova, & Junak, 2018).

2.4.2.1 Nanoclay

Nanoclay was used for decreasing thermal conductivity and increasing stability in different kinds of matrices. From literature studies it was found that thermal conductivity of nanocomposite polymethyl methacrylate PMMA was increased with the increase of the percentages of nanoclay of 0.5, 1 and 2 wt. % (A Hakamy, F. U. A. Shaikh, & I. M. Low, 2014).

Ordinary cement was blended with nanoclay and calcined nanoclay (produced by heating the nanoclay at 800, 850 and 900 ºC for 2 h using an electric furnace with increase of heat by 10º C/min. The percentages of nanoclay and calcined nanoclay were 1, 2 and 3 wt. % of cement. It was found that the thermal stability (resistance ability of the material to the deformation and decomposition under temperature effect) was improved by 3.3 % compared to the neat cement paste (A Hakamy et al., 2015). Therefore, nanoclay can be considered as a good filler for thermal stability of cement matrix. Hemp fabric (HF)/cement blended with 1, 2 and 3 wt. % nanoclay (Cloisite 30B) of cement were used as an improvement for the cement composites. The hemp fabric was included as two layers inside of the cement paste and the layers were about 2.5 wt. % of the cement. The morphology of calcium silicate hydrate gel

(C–S–H) was improved due to the presence of nanoclay and good dispersion of nanoclay in the matrix. A percentage of 1 wt. % of nanoclay decreases the intensities of calcium hydroxide more than 3 wt. % because of the agglomeration of nanoclay at high percentages. The thermal stability of hemp fibres nanocomposite was slightly better than cement paste due to the resistance of nanoclay against the decomposition (Tahereh Ghaffari, Ali Barzegar, Fahimeh Hamedi Rad, & Moslehifard, 2016).

It was reported that the thermal conductivity was reduced about 61.8 % - 61.4 % with the increase of temperature (25-1000°C) by adding 0.1% - 0.2% nanoclay by wt. in replace with cement at 200°C. The compressive strength and thermal conductivity of concrete was decreased about 58.1 % - 61.4 % at 800 °C but the thermal conductivity was increased by adding 0.3-0.5 % nanoclay (W. C. Wang, 2017). This means the optimum percent of nanoclay for decreasing thermal conductivity is within the range 0.1%- 0.2%.

2.4.2.2 Nanosilica

Nanosilica was mentioned in the research as having an effect on thermal conductivity. It was reported that the thermal conductivity of nano-silica sand 50-1000 nano-meters decreased 70% when the size was decreased from micro to nanoscale (Chari, Sharma, Prasad, & Murthy, 2013). Nanosilica was used as a filler 1-5 % from 12, 50 and 150 nm scale on cement, 4-5 wt. % of 50 nm scale of nano-silica had the best effect and gave high compressive strength and low thermal conductivity. The thermal conductivity was reduced 38 % compared with pure cement at 900ºC. The thermal conductivity was in the range 0.42-0.57 W/mK after the composite was heated to 900ºC (Jittabut, 2015). Thermal conductivity of cement decreased by mixing waste glass (replacing the river sand by waste milled glass) and nanosilica (1 and 3 wt. %). It was reported that, thermal conductivity was decreased depending on the use of waste glass, in contrast the adding of nanosilica at high percentages (3 wt. %) caused more decrease in thermal conductivity compared to using only river sand and glass waste samples (0 wt. % nanosilica). Thermal conductivity of river sand sample (0 wt. % nanosilica) was about 1.65 W/mK, waste glass sample of (0 wt. % nanosilica) was 1.45 W/mK and waste glass sample 3 wt. % nanosilica was 0.45 (Sikora, Horszczaruk, Skoczylas, & Rucińska, 2017).

2.4.2.3 Nanozinc Oxide

As for nanozinc oxide the literature mainly mentioned its impact on thermal conductivity and at the same time has some improvement for strength, anti-bacteria and resistance to ultra violet. An alkali solution of zinc oxide which was made from zinc nitrate $Zn(NO_3)_2.6H_2O$ and NaOH 0.5/1 by vol in 100 ml water and for mixing with the polymer matrix. The solution was stirred at 75ºC and heated. Polyvinyl pyrrolidone with starch 1/0.5 wt. % was added 0.5, 1.0 vol. % to the mixture. It was reported that zinc oxide solution is as an effective nanofiller to decrease thermal conductivity in respect to its heat absorption capacity property but the study didn't mention any value about thermal conductivity. The heat absorption capacity of the matrix became very high, 30-40 % more at nZnO loading 0.5, 0.1 and 1 vol. % of 5 vol. % PVP or 1 vol. % of polyvinyl alcohol (PVA) in comparison to the original matrix without nanozinc oxide. The nanozinc oxide fluid decreased the diffusion of temperature which was generated by sonication (Bhagat & Khanna, 2015).

Curing the specimens of concrete, which were blended with a replacement of 2 wt. % percentage of ZnO_2 in lime water, enhances the permeability and the strength. The nanoscale zinc oxide improved the pore structure by decreasing the harmful pores. The pores in concrete can be considered as: (1)- Harmless pores < 20 nm (2)- Few-harmful pores 20-50 nm (3)- Harmful pores 50-200 nm (4)- Multi-harmful pores > 200 nm. Nano ZnO_2 could develop the mechanical and physical properties (Nazari & Riahi, 2011).

Using ZnO as an additive to Al matrix in micro and nanoscale and nano-micro (two phases) self-assembled composites resulted in the thermal conductivity of micro-composites reducing only 15 % for loading (ZnO- 4 % Al) such that $Zn_{(1-x)}Al_xO$ ($0 \leq x \geq 0.03$). The large reduction achieved using nanocomposites in thermal conductivity was 3 times that of the micro-composites due to the uniform distribution of nano $ZnAl_2O_4$ (precipitation). The thermal conductivity was higher than the micro-composites were used with the increase of the percentage of Al; in contrast, the nanocomposites gave the lowest thermal conductivity at decreasing Al to 2 wt. %. The thermal conductivity was 7.5 W/ mK at room temperature for ZnO-2 % Al but this value was decreased to 3.7 W/ mK at 600ºC which was lower than pure ZnO by 73 % at room temperature and 40 % at 600ºC. The control role at low

temperature to perform low thermal conductivity is for two reasons which are phonon-boundary and phonon impurity scattering because 90 % of thermal conductivity is related to the thermal conductivity of phonon and the phonon scattering takes the main contribution (Y. Zhao et al., 2012).

Phonon is the quantum of acoustic or vibrational energy, considered as a particle and used especially in mathematical models to calculate thermal and vibrational properties of solids (Harcourt, 2016).

Nanozinc oxide blended at 2 wt. % and 4 wt. % with asphalt, to avoid moisture damage, led to a better aggregate coat with asphalt binder and improving adhesion between the asphalt and acidic aggregate due to decrease the acidity of the aggregate which led to decrease the active surface free energy of the modified asphalt binder (Hamedi, Nejad, & Oveisi, 2016).

2.4.2.4 Summary of Selected Materials

2.4.2.4.1 Nanomaterials

In the present work, nanomaterials $nSiO_2$ and nZnO were chosen to study their effect on thermal conductivity of NHL5 lime binder (render). Furthermore, 2% loading by wt. nClay was identified as the nanomaterial to improve the mechanical strength but concerns existed as to its influence on thermal conductivity. The nanomaterial ($nSiO_2$) not only enhances the mechanical strength but also decreases porosity and shrinkage, loading 2% by weight of lime was suggested. Adding nZnO at 4% wt. lime is expected to decrease thermal conductivity with additional benefits such as stability and protection against UV effects.

Hemp shiv and hemp fibre mixed with lime binder was the choice of organic materials to give a nanocomposite material. Lime plus selected nanomaterials was chosen as the render. The aim is to develop high performing wall layers as shown in Figure 1.10. The tests conducted were dependant of the requirements on the various layers shown in Figure 1.10 and consisted of a mixture of thermal conductivity, porosity/density and compressive strength.

2.4.2.5 Decrease in Porosity

Porosity resistance is also an important property in building construction materials. It is determined by many methods: by water pressure which can enter the material and calculate the depth of penetration with time, or by mercury pressure obliged to enter the pores while the increments of volume pores are calculated. Some nanomaterials were reported in the literature studies as sealed materials, porosity resistant or permeability resistant (decrease or close pore size). It was reported that sealing additives were used for the purpose of sealing off porous matrix like bentonite slurry to seal the wells during drilling operation (Foley, VanderHooven, & Hull, 1981)

2.4.2.6 Nanosilica

Nanosilica was mixed with cement; these silica particles penetrate the micro-pores and line the pores decreasing porosity; they might seal and close these pores (Aggarwal, Singh, & Aggarwal, 2015; Ershadi, Ebadi, Rabani, Ershadi, & Soltanian, 2011; Yusak et al., 2014). A study confirmed that nanosilica mixed with oil well cement slurry led to low permeability and porosity and high compressive strength; for example, 3 wt. % of nanosilica. The porosity test was 45 % for neat slurry cement and 28.5 % for slurry-cement/nanosilica (Ershadi et al., 2011). Another study added sintered nanosilica which became porous because it was exposed to 300°C. The polymer of the matrix, which was designed for dentist medicine, penetrated the porous silica to become nonporous and a high modulus polymer nanocomposite (Atai, Pahlavan, & Moin, 2012).

2.4.2.7 Nanoclay

Nanoclay was studied as a porosity resistant or a barrier. It is reported that 50-500 times the permeability of gas through polymer was decreased by a small loading of nanoclay; it enhanced the barrier properties of the polymer (Choudalakis & Gotsis, 2009; H. Kim, Miura, & Macosko, 2010; Z. Duan, and, & Huang, 2013). Adding 1 wt. % of nanoclay to the cement decreased porosity 20.6 % compared to neat cement (Low, Hakamy, & Shaikh, 2017). Actually, nanoclay research studies explained that nanoclay was a barrier more than porosity resistance.

The research demonstrated that the nanoparticles, which have more effect on porosity resistance, are excellent when added to the polymer as a barrier polymer nanocomposite. Nanoclay; in addition to its role as a barrier and porosity resistance, it enhances the physical properties like tensile strength. In the present project, nanoclay will be used to decrease porosity in the nanocomposite materials for building construction.

2.4.2.8 Graphene and Expanded Graphite

Graphene and expanded graphite are unique materials which were also used in the literature studies as a barrier against water (Du & Pang, 2015; Potts, Dreyer, Bielawski, & Ruoff, 2011). Mixing small quantities of graphene oxide with cement (0.05 wt. %), the compressive strength of the cement was enhanced 15-33 % and the flexural strength was improved by 41-59 % (Babak, Abolfazl, Alimorad, & Parviz, 2014; Chuah, Pan, Sanjayan, Wang, & Duan, 2014; Zhu Pan, Wenhui, Li, & Collins, 2013). Porosity of cement was decreased from 32.8 % to 28.2 % using graphene oxide 0.03 wt. % (Gong et al., 2014).

2.4.2.9 Nanozinc Oxide

Nanozinc oxide was mentioned as a material for decreasing porosity, Alginate hydrogel 3 % of water, 1% chitosan hydrogel dissolved in 1 % acetic acid and precipitated by 1 wt. % NaOH solution was mixed with zinc oxide for making wound bandage. 60 %–80 % porosity of the total bandage volume was of alginate control bandages, in contrast to 60 % - 70 % porosity of the nZnO blended composite bandages. The interaction of alginate with nZnO has an impact on porosity reduction which was about 12% (Mohandas, Pt, Raja, Lakshmanan, & Jayakumar, 2015) and this encourages the idea that there is a probability if nanozinc oxide decreasing the porosity of lime regardless of the research subject was irrelevant to the present project. Nano-zinc oxide was blended with cement (Portland Pozzolana) by 0, 0.5, 1 and 1.5 wt. % and the water cement ratio was 0.35. The study showed that nanozinc oxide improved the mechanical properties and the porosity was decreased for the cement paste. 1.5 wt. % nanozinc oxide improved the compressive strength of mortar 1:2 cement to sand by 17.27 % and the porosity of solid mortar was highly decreased (A. P. a. Singh & Tiwari, 2017). Asphalt binder was mixed with 2 and 4 % nZnO to study the humidity damage of the asphalt. The

asphalt binder acidity was decreased which increased the adhesion of asphalt with acidic aggregate in dry and wet conditions and the acid surface free energy (SFE) of the asphalt was significantly decreased. This led to an increased adhesion between asphalt and aggregate and decreased the voids as a result porosity. (Hamedi et al., 2016). From reviewing the literature, it seems that nZnO has multi-effects. One of these effects is decreasing porosity; the nanozinc oxide decreased the humidity damage on asphalt by decreasing the pores between the aggregate and asphalt binder and lowered the porosity.

Specimens of concrete mixed with 1 wt. % percentage of $nZnO_2$ in limewater, reduced the porosity by 8 %. The nanoscale zinc oxide improved the pore structure by decreasing the harmful pores within 20-50 nano-meter or less. The pores in concrete can be considered and classified as stated in Section 2.3.2.3, nZnO2 could develop the mechanical and physical properties (Nazari & Riahi, 2011). It has two contradicting roles: it enhances the strength of the matrix and decreases the porosity, which is reasonable due to increasing density and making different links with many kinds of chemical roots such as hydroxyl and carboxyl. At the same time it has another role, it lowers the thermal conductivity of many matrices, which seems opposite of the first role but the studies explained this property due its potential to absorb heat by slowly releasing it and due to its capability to absorb a broad spectrum of solar radiation see Section 2.3.2.3 The collection properties of nZnO are very interesting in construction and it opens the doors for promising uses in the construction industry.

2.5 Conclusion

From the literature review conducted in the chapter, the choice of materials and nanomaterials to improve the properties of lime binder and lime biomass lime nanocomposite and to optimise these improvements are given in the following sections.

2.5.1 Materials Identified to Improve Strength (Flexural and Compressive) of the Lime Matrix

1- Nanosilica

2- Nanoclay

3- Nano-cellulose

3- Expanded graphite

4- Polyvinyl acetate adhesive

5- Fibre glass

6- Hemp shiv

7- Hemp fibres

2.5.2 Materials Identified to Decrease Thermal Conductivity of Lime Matrix

1- Nanozinc oxide

2- Nanosilica

3- Nanoclay

2.5.3 Materials Identified to Decrease Porosity of Lime Matrix

1- Nanozinc oxide

2- Nanosilica

3- Nanoclay

4- Expanded graphite

2.5.4 Materials Identified to Reduce Shrinkage of Pure Lime

1- Nano-silica

2- Nano-clay

3- Expanded graphite

4- Fibre glass

2.5.5 Materials Identified to Enhance Water Vapour Permeability (Breathability) of Pure Lime

1- Nano-silica

2- Nano-clay

3- Expanded graphite

Nano-carbon tubes were not considered because they are expensive and give an increase thermal conductivity due to the conductive property of carbon for heat.

Instead expanded graphite was used in spite of its high thermal conductivity because it is cheaper than nanocarbon tubes and works on both increasing strength and decreasing porosity.

Table 9.1 in Chapter 9 Appendix is a summary of the different matrices (polymers, cement, lime, geopolymer and biomass) and the possible nanomaterials that can be used to form a nanocomposite. The influence on the matrix nanocomposite properties as a result of combining the matrix with the nanomaterial is also given in addition to the process which was used. This project concentrated on using biomass as the matrix for the development of eco-friendly construction materials.

Chapter 3 - **Materials and Test Methodology**

3.1 Introduction

In the present project, the target is to use nanomaterials to develop a new, durable light-weight building material in comparison to concrete from biomass nanocomposites. Biomass materials such as lime/ hemp shives may not have the strength characteristics of ordinary construction materials but it can be strengthened and used in conjunction with other materials such as hemp fibres mixed with lime binder to become a structural material (loadbearing for walls, roofs and floors). Furthermore, the lime binder can be improved to have both a low porosity and be a low thermally conductive render. Also, insulator materials made from hemp shives and lime binder can be improved to be low in thermal conductivity and porosity too. The addition of nanomaterials to biomass materials can enhance durability and improve its flexural and compressive strengths, thermal conductivity (heat isolation) and porosity. This chapter discusses the materials and processes required to develop the biomass lime nanocomposite from lime/ hemp (fibres or shives) for loadbearing walls, insulator panels for thermal insulation or lime nanocomposite for rendering. Also, included is information on the main tests to demonstrate their performance. Selection of materials is based on the extensive literature reviewed and summarised in Table A.1 in Appendix A, for the enhanced properties of different matrices from polymers, cement, gypsum, lime and biomass (although biomass was only considered in this project).

Four property enhancements are proposed (flexural and compressive strength, porosity and thermal conductivity) through the addition of nanofillers to varying quantities (nanocellulose, nanosilica, nanoclay, expanded graphite, nanozinc oxide) in addition to using natural fibres like hemp fibres and industrial such as fibre glass for increasing the flexural and compressive strength. Fibre glass and hemp fibres will also help reduce material costs as it can partially or totally replace the more expensive nanofibres like halocarbon tubes (chlorofloro-carbon which the hydrogen replaced by halogen) or nanocellulose. Appendix A, Table A.1 provides an overview of the different matrices and associated properties which can be enhanced by nanomaterials.

3.2 Material Selection

A detailed review was conducted to identify a number of materials that could be used in the research. The nanofillers and fibres were also identified and selected based on the property improvement which can be achieved by using these fillers.

3.2.1 Matrix Materials

Singleton Birch Secil Natural Hydraulic Lime NHL 5 was purchased from Lincolnshire Lime in the UK. Nanomaterials used to decrease the thermal conductivity (nClay, $nSiO_2$ and nZnO) were purchased from Sigma Aldrich in the UK. Hemp shiv was procured from East Yorkshire Hemp, Driffield, UK (average size: 15mm x 5mm). The hemp fibre was sourced from Wild Colours, Birmingham, UK. Polyvinyl acetate (PVAc) adhesive was purchased locally (Evo-Stik Super Evo-bond Waterproof PVA), an environmentally friendly hazard-free wood glue.

3.2.2 Lime Matrix

Lime binder NHL5 was purchased locally in UK market as explained in Section 3.2.1. It was chosen as the main matrix for this project, as it is an environmentally friendly material because it belongs to the earth, it was made from natural rocks (Calcium carbonate, $CaCO_3$) which is heated (calcined) around 900-1200ºC. It is then transformed to calcium oxide, CaO. The last product can be dissolved in water and transformed to calcium hydroxide in contrast the calcium carbonate which doesn't dissolve in water as in Eq's 3.1 and 3.2.

$CaCO_3$ heated $\longrightarrow$ $CaO + CO_2$ Equation 3.1

$CaO + H_2O \longrightarrow Ca(OH)_2$ Equation 3.2

Calcium hydroxide reacts with carbon dioxide to become calcium carbonate. This process is called carbonation which occurs throughout the lifetime of the building structure from which it is erected as lime. In lime production process, the emission that resources of CO_2 are three fold (1) process emission is 0.751 kg CO_2/kg of lime but this is offset due to the CO_2 emissions will be adsorbed (2) combustion emission is 0.322 CO_2/kg of lime (neglected, it will be absorbed by lime to become calcium carbonate) (3) electricity emissions are 0.019 CO_2/kg of lime. The total emissions are, threfore, 0.77 CO_2/kg of lime (Turner & Collins, 2013). The emissions will be

calculated later for 1 m^3 and compared to the emission of the same concrete volume. The density of Core, Insulation and Render layers (see Sec 1.9, Figure 1.10) are lower than the density of concrete and the weight of 1 m^3 from the proposed wall in this project is lower than the weight of concrete. Concrete carbon emissions are about 2.5 times more than those of lime of the same volume (1 m^3) according to their densities. As a result, the emission from lime are lower than concrete production emissions from all components and resources; fuel and electricity (average 0.74 kg CO_2/kg of concrete) (EuLA, 2014). Lime is cheap and widely used in different aspects. It is lightweight as a construction binder material in comparison to cement concrete mix. It is compatible with the biomass from hemp shives and hemp fibres which will be used with the present project. The definition of lime in British and Europe standard is "calcium oxide and/or hydroxide, and calcium-magnesium oxide and/or hydroxide produced by the thermal decomposition (calcination) of naturally occurring calcium carbonate (for example limestone, chalk, shells) or naturally occurring calcium magnesium carbonate (for example dolomitic limestone, dolomite)" (459-1, 2015). It was reported that the compressive strength of cement: lime: sand (C:L:S) decreases with the increase of lime content (Arandigoyen & Alvarez, 2007), Figure 3.1.

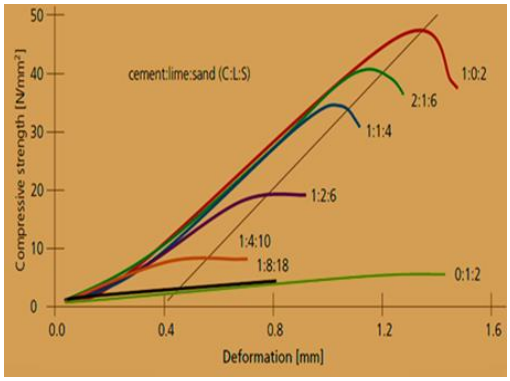

Figure 3.1 Correlation between compressive strength and deformation of cement: lime sand mixture (Arandigoyen & Alvarez, 2007).

The compressive strength becomes slightly higher when it is added at a ratio up to 40% of cement to lime-based mortars. The compressive strength highly decreases in cement mortars when a minor quantity of lime is added (from Figure 3.1, the ratios

of cement/ lime are 1/0, 2/1, 1/1, 1/2, 1/4, 1/8 and 0/1 in contrast, the compressive strengths are 49, 40, 35, 20, 9, 4 and 5 MPa respectively). It was reported that the high percent of lime to cement mortars show a plastic behaviour under load that is not noticed in the other mixed mortars. Therefore, a big extent of deformation can be absorbed by lime-rich mortars before the failure. So that, the rich lime mortars can be a material for reformation work or crack fillers (Arandigoyen & Alvarez, 2007). That means lime is a weak strength material but its plastic behaviour is one of their advantages to absorb vibration and earthquake in building construction. Furthermore, its availability as a sustainable material and its eco-friendly property qualifies this material to be developed as a main material in building construction. Therefore, this present work is to transform its properties from nonloadbearing strength (flexural and compressive), to a loadbearing construction material with low thermal conductivity, porosity and shrinkage.

3.2.3 Hemp

Hemp is a rapidly growing plant, about 3-5 m within three months, intensively cultivating 200-250 plants per square meter and pollinated by wind. The dioecious kind the male plants are 10-15 % taller and lower strength than fibres in female plants which are preferred for use in construction. Hemp which its scientific name is Cannabis Sativa L. contains low quantity of tetrahydrocannabinol (THC) = about 0.2 % < 0.3% (non-psychoactive limit) (Peev, 2012) which is considered non-psychoactive material and different from the Indian Cannabis that has high percentage of marijuana (THC) 3-10% of the active components (Heisters, 2008). Hemp gives 5 tonnes biomass per each hectare within four months and this is the biggest biomass plant product in the world. The outer bark of stem has the strongest fibres. In comparison to cotton, hemp fibres are longer, 8 times higher in tensile strength and higher mildew resistance. Fibres, shives and seeds are the important product of hemp plants. Figure 3.2 and Figure 3.3 show the hemp plant and the hemp fibres. Figure 3.4 and Figure 3.5 show hemp shives and a cross section of hemp stem. Hemp is durable, reusable, low energy lifetime, carbon friendly or carbon negative, healthy to human use (it is not toxic) and broad extent of application (Peev, 2012). Hemp fibres start in thermal degradation above 150ºC which is a relatively high degree (Shahzad, 2013). Tensile strength of hemp fibres is about 550-

900 MPa (Anderzej K. B. et al., 2012) and the average diameter is 22 micron (Hurter & Eng, 2001).

Accordingly, hemp fibres are proposed to reinforce the lime binder in this project. The aim is to reduce energy consumed during building use and to use construction materials with lower embodied carbon which can also be recycled. Furthermore, there is a tendency to transform to zero carbon housing. Buildings take around 40 % share of the CO_2 emissions (BEIS, 2018) and this means reducing CO_2 emissions in building construction is environmentally very important. About 40-60 % of the Cannabis Sativa L. plant is hemp shives from the crushed woody core of the plant stalk (Edward AJ Hirst, Peter Walker, Kevin A Paine, & Yates, 2010). The natural fibres in comparison with industrial fibres are cheaper, lighter, renewable and biodegradable (A. Hakamy, F. U. A. Shaikh, & I. M. Low, 2014).

Figure 3.2 Hemp plant (Heisters, 2008).

Figure 3.3 Hemp fibres (Heisters, 2008).

For these reasons, hemp fibres were an important choice in the present project and it was adopted to be a part of the proposed wall and it was preferred to be used more than fibre glass.

Figure 3.4 Hemp shives (Wikimedia, 2017)

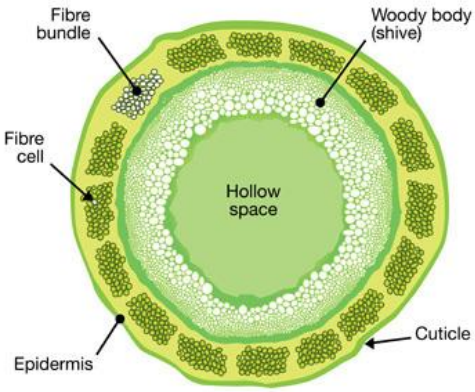

Figure 3.5 Cross-section of a hemp stem (Canada, 2009)

3.2.4 Fibre Glass

Fibre glass (FG) is added to improve the physical properties of the binder, especially flexural and compressive strength (Raju, Ramji, & Prasad, 2015). It is sold as tissues, rod bars, threads and chops (Bagherpour, 2012). It has been chosen in this project to decrease the cost because the nanomaterials are expensive. It may be linked to the other nanomaterials in the matrix to strengthen the nanocomposite. Furthermore, it is used in comparison to hemp fibres and to conduct optimisation in their properties. As it appeared from lab experiment the strength results of hemp fibres/ lime were also very near to fibre glass/lime but hemp fibres were adopted for use in the proposed wall (see Figure 1.10). FG was bought from Sea Coast Company in UK (chopped, 6mm long and 13 microns in diameter) and white in colour with a density 2.5-2.65 g/cm^3 as shown in Figure 3.6.

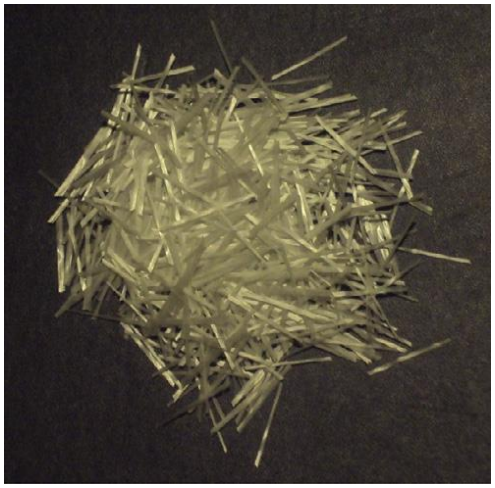

Figure 3.6 Chopped fibre glass (Tassew & Lubell, 2014).

3.2.5 Polyvinyl Acetate (PVAc)

This is a traditional adhesive which is used for wood connection in the furniture industry for example. It has good strength characteristics. It was selected to get more enhancements for bonding between fibres and lime binder. The flexural strength results were doubled by using this adhesive as will be seen in Chapter 4. The hemp fibres or fibre glass were blended with PVAc and then mixed with the lime binder. PVAc adhesive was purchased from the UK local market (Evo-Stick Super Evo-bond waterproof PVA) which is an environmentally hazard-free glue and it is a resin. Polyvinyl acetate resin is a chain of monomers $(C_4H_6O_2)_n$ and its density is about 1.03-1.13 g/cm^3 (as in the safety data sheet of Evo-Stick Company). The average density is 1.08 which closes to the density of water. PVAc can be mixed with water. If the percent of PVAc is 30 % of water and the water is 0.4 W/L of a 1 kg of lime, that means the water is 400 g from 1000 g lime and the weight of PVAc is (0.3 x 400 = 120 gm or cm^3). This PVAc quantity 120 divided by 1000 gm lime and will be 12 wt. % of lime. For more precision, if the density of PVAc is taken into consideration; 120 cm^3 of PVAc multiply by its density 1.08 g/cm^3 =129.6 gm. Then PVAc percent will be 129.6 g/ 1000 g of lime = 12.96 or about 13 wt. % of lime. This difference of percent is not large in building construction. It is easier for practical work to use volumetric percent of PVAc of water added to water lime ratio in the same

measuring cylinder in cm^3. The percentages 20, 30, 50, 100 and 200 vol. or wt. % of water can be written 8, 12, 20, 40 and 80 wt. % of lime respectively.

3.2.6 Nanomaterials

Nanomaterial particles are in nanoscale dimension (1-100 nm), the specific area is a very large and active surface which interacts with polymers if they are processed very well to give good dispersion. In this research, many materials were selected to improve the lime matrix in order to achieve the desired properties for building construction, such as nanocellulose to improve tensile or flexural strength of the matrices like lime binder which is cheaper than carbon nanotubes. Besides, it is more preferential for heat isolation than CNT's. Nano-silica is very good for sealing against water ingress in different matrices like cement, lime or polymers as it decreases porosity or blocks pores. In addition to this behaviour, it was found that it enhances other physical properties such as flexural, compressive, tensile strength or impact resistance. Nano-clay is the choice to achieve low thermal stability. It is also fire retardant.

3.2.7 Nanocellulose

Nanocellulose was purchased from the laboratories of Maine University, process Development Centre in the USA. It is called cellulose nanofibres (CNF). The chemical formula of polysaccharides is $C_x(H_2O)_y$ and the monosaccharides have a formula $(CH_2O)_n$. Cellulolose is a kind of polysaccharide (Klemm, Heublein, Fink, & Bohn, 2005). CNF in this project was supplied as a solid white powder, its pH at 2 % suspension in water is 5-7 and its thermal decomposition is 175ºC. It enhances the mechanical strength of the (lime, cement, polymer …etc.) nanocomposite. To ensure good dispersion in a matrix (paper paste and polyvinyl alcohol), it has to be stirred on a magnetic plate in water (Fiberlean; Siró & Plackett, 2010; Tanpichai, Sampson, & Eichhorn, 2013). Nanocellulose was one of many choices in this project due to its ability from the literature review to enhance mechanical properties like flexural and compressive strength.

3.2.8 Nanosilica

Nanosilica (nSiO2) is an inorganic filler. It was bought from Sigma Aldrich in the UK as white powder; its molecular weight is 60.08 g/mol. It is used to enhance water

proofing of silica calcium carbonate (SiO_2:$CaCO_3$) by decreasing porosity but it also enhances the physical properties like tensile strength, impact resistance and hardness. It must be suspended in solvent by magnetic stirring, mixed with polymer and stirred again to achieve good dispersion (F. A. Morsy, El-Sheikh, & Barhoum; M. Morsy et al., 2010; Qijie Xu1, Fangfei Chen1, Xiaohong Li1, & Zhang1, 2013; Quercia Bianchi & J H Brouwers, 0002).

3.2.9 Nanoclay

Nano-clay was also purchased from Sigma Aldrich in formula $H_2Al_2O_6Si$. It is 180.1 g/ mol. with light tan to brown in colour. Its bulk density is 600-1100 kg/m^3. It is mixed with matrices like cement, gypsum and polymer for thermal stability and heat isolation or for decreasing thermal activity. In general it enhances chemical resistance, as fire retardant and thermally stable but sometimes it enhances the mechanical properties of polymer, cement and biomass composites. Besides, it could be suspended in solvent like water and stirred to be added and blended very well in starch matrix (Cyras, Manfredi, Ton-That, & Vázquez, 2008; Q. K. Meng, Hetzer, & De Kee, 2011; Olad, 2011; Scarfato, Di Maio, Fariello, Russo, & Incarnato, 2012).

3.2.10 Nanozinc Oxide

Nano-zinc oxide (nZnO) is an inorganic material reported as Ultra Violet resistant (Feldman, 2014; Gomez-Ortiz et al., 2013; Raju et al., 2015; Souza Aguiar, Tanomaru, Faria, Leonardo, & Tanomaru-Filho, 2015) but sometimes it enhances heat isolation, especially when it is used as a paint coating. It was reported that it improves the tensile strength and the modulus of the elasticity of polycarbonate at 1wt% by melting and at 0.5 wt. % it improves hardness and wear resistance (Carrion, Sanes, & Bermudez, 2007; Raju et al., 2015). It was also purchased from Sigma Aldrich as white powder; its density is 5.61 g/cm^3. It is suspended by stirring, in solvent like water, mixed and stirred with solution of dissolved polymer or after stirring, added to cement paste using a mixer to ensure good dispersion (Bhagat & Khanna, 2015; A. Hazarika & Maji, 2014).

3.2.11 Expanded Graphite

Expanded graphite is made by exposing natural flake graphite in a bath of chromic acid, and then adding concentrated sulfuric acid, which separates the crystal lattice

planes, thus the graphite is expanded. It is a black powder in appearance. It can be used as a barrier, as insulation between molten metal and the hot top to decrease heat loss, fire stops around a fire door and used as gasket or valve for high temperature use (Jungbluth, 2008).

3.3 Processing, Blending and Test Specimens

A food mixer was used to mix lime binder (NHL5) with nanofillers and water for 5 minutes at low speed and 15 minutes at quick speed. For dispersion, the nanofillers were stirred by magnetic plate with deionized water then added to the mixer. In the case of hemp fibres or shives, the mixing became very hard (the workability of the mix was very low) and three mixers were broken within many months, before a cement mixer was successfully used. The hemp fibres or shives were blended with dry lime and then the dispersed nanomaterials in water lime ratio (W/L) were added to the mixture of lime and hemp (shives or hemp fibres). The mix was then placed in the mould of the required test. The specimens remained in storage (60 % relative humidity and temperature of 20ºC) for five days in polyethylene bags before demoulding. The specimens remained in storage for 28 days, they are dried by many methods, Air-Cured drying, Solvent exchange using Isopropanol, the specimens are immersed in for seven days after 5 days demoulding and Oven-cured drying in an oven at 50ºC (oven cured samples) 2 days before the testing.

The water lime ratio was 0.4 since the nanofillers absorb water, this was accounted for by adding water to achieve a similar flow (150 mm) on a flow table compared to the control sample. The nanomaterials were magnetically stirred for complete nanomaterial dispersion in the water for two hours prior to adding to the mixture. As for nclay, it needed more stirring time for better dispersion so this continued overnight. The lime and hemp (shives or fibres) were dry mixed for five minutes. The PVAc was mixed with the water/nanomaterial mixture and stirred for 15 minutes before gradually adding into the dry mix of lime hemp (shives or fibres). Slow speed mixing continued for 5 minutes on and 10 minutes quick speed. The mixed composite was compacted into a mould and via tamping with a mallet of dimensions similar to the surface area of the specimen for compaction. A mould size of 180 x 130 x 20 mm was used.

At 5 days after casting, samples were carefully demoulded and immersed in isopropanol for 7 days. Following this, they were dried in an oven for two days at 60°C. At 14 days, samples were removed from the oven and either tested or transferred to a temperature control room (60% RH and 20°C).

The optimum water lime binder ratio was conducted by a flow rate device as shown in Figure 3.7. The mortar was placed in a conical mould and allowed to free fall after 15 raising/dropping cycles. The spread of mortar diameter had to be 160mm for the optimum water lime ratio (when it was demoulded on the flow table, its demoulded shape was spherical). The percentage of water binder ratio firstly was 0.5 W/L (water lime ratio but if additives are used it means water solid ratio) and the paste spread was within the standard limit. The water lime ratio was then decreased to 0.4 W/L which too, was within the limit. The mix is not very workable tamping was used for placing the mix. In practice, hemp is placed by a timber rod and tamping head for full compaction.

Figure 3.7 Flow rate device determining optimum lime water ratio

3.3.1 Dispersion

The methods of dispersion, as mentioned in Chapter 2, is the stirring method on a magnetic plate and sonication. In addition to that, using a surfactant factor (soluble compound that reduces the surface tension of liquids, or interfacial tension between two liquids or a liquid and solid) (Nawla, 2004 (vol. 1-10) and 2011 (10-25)), for inorganic nanofillers (expanded graphite, nanosilica and nanozinc oxide) to make an envelope around the particles, help disperse the particles and prevent the

composition of conglomerates. The tendency to make conglomerates results from the interior attraction between the active surfaces of the nanomaterial particles (or attractive forces, called Van der Waals). In this present project, stirring nanomaterial in deionised water by magnetic plate was used for nanoclay and nanocellulose but for inorganic nanomaterials like expanded graphite, sonication for one hour after stirring on a magnetic plate was used. Nanomaterials were stirred in a beaker with deionized water on magnetic plate for 1 hour and then added to the lime in the mixer. With regard to the PVAc, it was added after 1 hour to the nanomaterial in the beaker and stirred with the nanomaterial before adding to the lime matrix in the mixer.

3.3.2 Moulding Method

The moulding methods depend upon the methods of mixing and the matrix. In this project, the matrix was lime binder with or without hemp (shives or fibres). As mentioned before, a food mixer was used in the present project and the resulting paste was placed in the mould according to the required test. The demoulding time for all moulds of lime is five days for all test specimens as specified in the British Standard BS EN 459-1:2015 Building lime Part 1.

3.3.2.1 Flexural and Compressive Strength

The mould size is 160 x 40 x 40 mm with three cavities being available in each mould. The flexural specimens were tested by a three point load method and the two portions of the broken specimen were used for compressive strength. For compression test, each portion is placed between two 40x40 mm plates in accordance with the British Standard (BSEN1015, 2000).

3.3.2.2 Thermal Conductivity Test

The mould size was 180 x 130 x 20 mm, it was made from "Wisaform" timber in accordance with the procedures explained in British Standard (BSEN12664, 2001). Two methods are recommended in this standard, one of them was adopted to perform the tests conducted in this research using the heat flow meter single specimen method.

3.3.2.3 Water Vapour Permeability

A circular mould is made of corrosion resistant material with an open upper side with an area of about 0.02 m^2 as given in the standard (BSEN1015-19, 1999). That means:

$A=0.02\ m^2=\pi x R^2$ Equation 3.3

$R^2=0.02/\pi = 0.006366\ m^2$ Equation 3.4

R= 0.07978 m x 1000 =79.78 ≈ 80 mm or D = 160 mm

A: area, R: radius, D: diameter

The thickness of the specimen is 20 mm with 160 mm diameter.

3.3.3 Shrinkage and Water Absorption

The mould as used for flexural strength was also used for shrinkage and water absorption samples (160 x 40 x 40 mm). Two demecs were centrally fixed by glue on the longitudinal centre line of the specimen, 100 mm distance between them to measure the contraction (shrinkage) of the materials.

3.3.3.1 Porosity

The fragments which were cut by a knife from the crushed flexural and compressive test specimens were used for porosity testing, 1.5 x 1.0 cm approximately to fit inside the mercury intrusion porosimetry device.

3.4 Experiments

The main experiments being conducted are outlined in the following sections. The most important experiments are the strength, flexural and compressive strengths are usually determined in accordance with BS EN 1015-11:1999 and BS EN 196-1:2005, with size of 40x40x160 mm. The three point load method is used to test the specimens. The compressive strength is conducted on the broken halves of the flexural specimens using two square plates of dimensions 40x40 mm top and bottom of these halves (BSEN1015, 1999; BSI, 2005)

3.4.1 Flexural Strength Test

The procedures of flexural and compression strength followed BS EN 1015-11-1999. As mentioned previously, the specimen sizes are 160 x 40 x 40 mm. Three point load method was used and the "Instron device" was used as shown Figure 3.8. Flexural strength is an indirect expression for the tensile strength of the material. Deflection rate was 1 mm/sec. The flexural test results of lime or any solid mortar are expressed as modulus of rupture which is denoted as MR or R in MPa or psi. The equation for calculation of flexural strength is:

$R= 3PL/2b^3$ Equation 3.5

P: the exerted load (N)

L: span of the prism (mm)

b: dimension of the square cross section of the specimen

R: flexural strength, MPa

Figure 3.8. Instron device (3367) for three point load flexural strength test

3.4.2 Compressive Strength Test

As mentioned before, it was conducted on the two portions of the broken prism in flexural strength. Two plates 40x40 were placed on the upper and lower faces to define the area under the exerted load. The test was achieved using the same device (Instron 3367), see Figure 3.9. The calculation was conducted in accordance with the basic equation:

Compressive strength= P/A (MPa), Equation 3.6

P= load (N), A= cross section area of the specimen prism

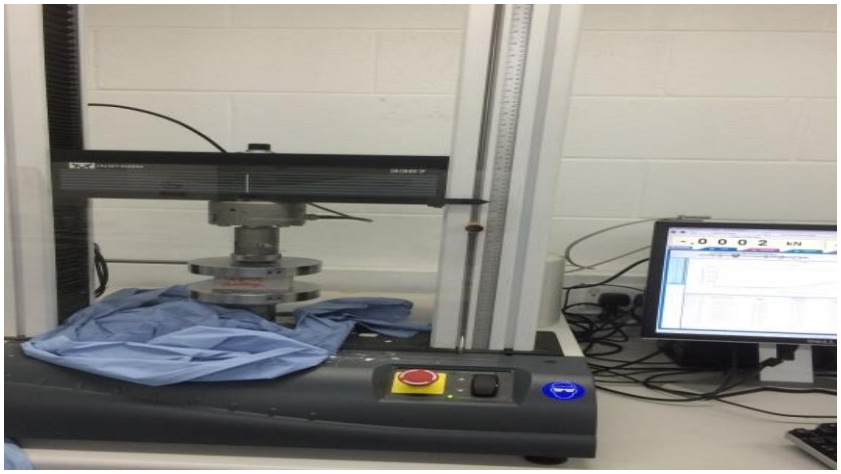

Figure 3.9 Instron (3367) device with specimen under compressive strength test.

3.4.3 Thermal Conductivity Test

The thermal conductivity test was conducted following the procedures of BS EN 12664 (ENNF, 2001). Two methods are recommended in this standard, one of them is the heat flow meter single specimen (180 x130 x 20 mm) method which was adopted in this project. The Instrument comprises a cold plate under the specimen to decrease the temperature to 2ºC. The specimen is placed on the cold plate and it is surrounded by polystyrene insulation. The upper face of the specimen is exposed to the room temp which is constant at around 16ºC. Four thermocouples are attached to the upper and lower faces of the specimen. On the upper face of the specimen, two heat flux sensors (Hukseflux HFP01, 80mm diameter and 5 mm thick) were placed for measuring the heat flux through the thickness (20 mm) of the specimen. The mixing of the materials is described in Section 3.3 and the timber (Wisaform) mould which was made in the lab was explained in Section 3.3.2. The thermocouples and the heat flow meter sensors are connected to data logger to record the data, see Figure 3.10 and Figure 3.11.

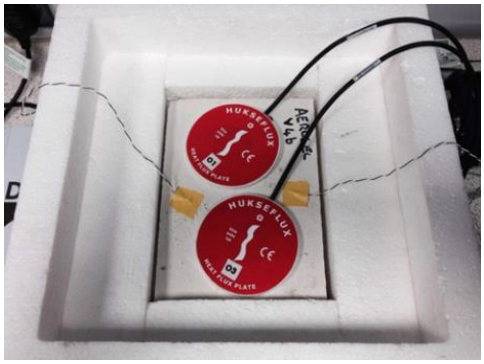

Figure 3.10 Heat flow sensor and thermocouple

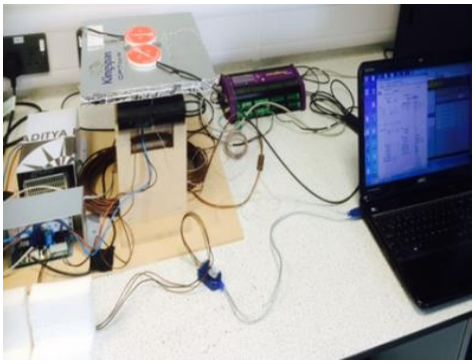

Figure 3.11 Heat flow meter device and data logging equipment

3.4.3.1.1Theory

Fourier's Law in a simplified form was used to determine the one directional thermal conductivity of the samples as follows in Equation 3.7:

$$q_x = -\lambda\,(dT/dx) \qquad \text{Equation 3.7}$$

where

q_x is the heat flux in direction x (W/m^2)

λ is the thermal conductivity of the material (W/mK)

dT/dx is the thermal gradient in the direction of the flow (K/m)

From the measured heat flux at steady state conditions and the temperature difference between the hot and cold sides, the thermal conductivity of the samples was determined.

In order to evaluate the accuracy of the apparatus, expanded polystyrene of a 25 mm thick sample (180 mm×130 mm) of known thermal conductivity (0.033 W/mK) was used. Thermal conductivity was found 0.032 W/mK of the reference polystyrene sample. Therefore, the apparatus can measure thermal conductivity of materials even with very low λ with reasonable accuracy (O'Flaherty & Alam, 2018)

3.4.3.2 Apparatus Accuracy

Accuracy of the apparatus has been investigated by measuring the thermal conductivity of a sample of expanded polystyrene (180mm × 130mm x 25 mm) of thermal conductivity (33 mW/mK). The reference sample was measured in the laboratory and the thermal conductivity was found to be 32 (mW/mK) and this means that the apparatus can measure even very low thermal conductivities of materials with good accuracy.

3.4.4 Porosity Test

Porosity can be measured to determine the resistance of the movement of water or humidity through the material (biomass nanocomposite) building construction material. It is as a result of the pore size through the material which controls the quantity of discharge from one face of the material to the other side across its thickness. Porosity test is conducted in one of two ways: Pore size calculated by mercury pressure i.e. Mercury intrusion porosimetry (MIP). Further details are given in the following section.

3.4.4.1 Mercury Intrusion Porosimetry (MIP)

The relationship between the pore diameter and the pressure is the basis of this method for measuring porosity. The mercury is pushed into the specimen under gradual pressure to enter the pores inside the nanocomposite. The mercury which touches the solid materials in the pores is non-wetted; angle $\theta > 90°$ will be between the solid material and the surface of the non-wetted mercury because of the cohesion which is developed between the mercury and the solid material. The increments of pore volume are measured at each change in pressure. The behaviour of the non-wetted mercury with materials is repeated, for that the pressure for small pores must be high to define the value of the increment (intrusion) of pore volume. The device has two parts; one is 140 Pascal and the specimen is about 1.5 x 1.0 cm, and the second part is 240 Pascal. The specimen is moved to the second part to complete the test, see Figure 3.12 and Figure 3.13.

Figure 3.12 Mercury intrusion porosimetry (MIP) 140 Pascal

Figure 3.13 Mercury intrusion porosimetry (MIP) 240 Pascal.

3.4.4.1.1Porosity Calculations

The Washburn equation below is used to find the pore radius:

$$r_w = \frac{-2*cos\theta*\gamma_{s-l}}{P_w} \qquad \text{Equation 3.8}$$

Where

r_w: Pore radius (Washburn equation), m;

γ_{s-l}: Surface tension solid liquid, N/m;

θ: Contact angle between the liquid and the pore wall, degrees;

Pw: Pressure applied on mercury to intrude the pore, N/m^2.

To find the bulk density of the sample equation 3.8; it is supposed that there is no intrusion by the pressure exerted by mercury on the sample at 0.033 MPa.

$$\frac{W_{pt}}{\rho_{Hg}} = \frac{W_{ps-W_s}}{\rho_{Hg}} + \frac{W_s}{\rho_{bulk}} \qquad \text{Equation 3.9}$$

Where

Wpt: Weight of penetrometer sample cell filled with mercury, g;

Ws: Weight of dry sample, g

Wps: Weight of penetrometer with the sample and mercury until 0.033 MPa the volume, g;

ρHg:Density of mercury, 13.5 g/ cm^3;

ρbulk: Bulk density of sample; g/ cm^3;

To calculate the volume of pores, the equation 3.9 is used:

$$V_p = V_{Hg} \frac{\rho_{bulk}}{W_s}$$ Equation 3.10

Where

V_p: Volume fraction of pores, cm^3

V_{Hg}: Volume of mercury intruded, cm^3

3.4.5 Water Absorption Test

This test is to determine the water absorption of the specimen; it is done in accordance with the standard EN BS 772 Part 21, 2001. The specimen size was the same as that for the flexural strength test (160 x 40 x 40 mm). The specimens were placed in a plastic case and then glass tubes (10 mm diameter) were placed under the specimens. Deionized water was poured inside the plastic case to just touch the lower face of the specimens at time t=0. Before starting the test, the specimen must have a stable weight by oven drying and reweighing many times. Then, after the weight has stabilized, the test starts. The water will be absorbed and the specimen weight increases with time.

1-The first stage of the test during the first half an hour, the specimen weight must be registered every five minutes

2- The second stage during the second half hour, the specimen weight must be taken every 15 minutes

3- At the third stage, during the second and third hours, the specimen weight must be taken every 30 minutes

4- At the fourth stage, four hours and beyond, the specimen weight is taken every 60 minutes

5- The last stage is when the sample reaches its limit of water absorption, the sample is left 24 hours before taking the last weight.

3.4.5.1 Water Absorption Calculations

% Open porosity= Volume of water absorbed/Vol. of specimen, OP%= V_{op}/V_{sp}*100

V_{sp}=4x4x16= 256 cm^3, V_{op}= volume of open pores= U_O= Wmax-Wdry

Weight of absorbed water, U_t= (wet - dry) weight

Max absorbed water=Max. weight - dry weight, U_o= Wmax-Wdry

Imbibition capacity, IC= U_o/ W_d, U_o= Total water content

Absorption or (apparent porosity), ABS= IC X 100, IC= Imbibition capacity

Capillary porosity= total water absorbed/ capillary area, M_i= Ut/ 64 cm^3.

3.4.6 Water Vapour Permeability Test

The water vapour permeability was applied to study the impact of nanomaterial on the breathability of lime which has good breathability even without fillers. The goal is to keep or increase the water vapour permeability of lime. It was conducted according to BS EN 1015-19 1999. It is defined in this standard as the water vapour permeance multiplied by the thickness of the specimen. The water vapour permeance is the water vapour flux passing through a unit area under equilibrium conditions per unit difference in water vapour pressure between the two sides of the material. The apparatus is a circular container or cup, it must be made of material resistant to corrosion with area about 0.02 m^2 and diameter of 160 mm as shown in Figure 3.14 and Figure 3.15, demoulded specimen is shown in Figure 3.16 and Figure 3.17.

The specimen curing conditions are 20°C, 60 % humidity, demoulded after 5 days and then stored for 23 days at 20°C and 60 % humidity.

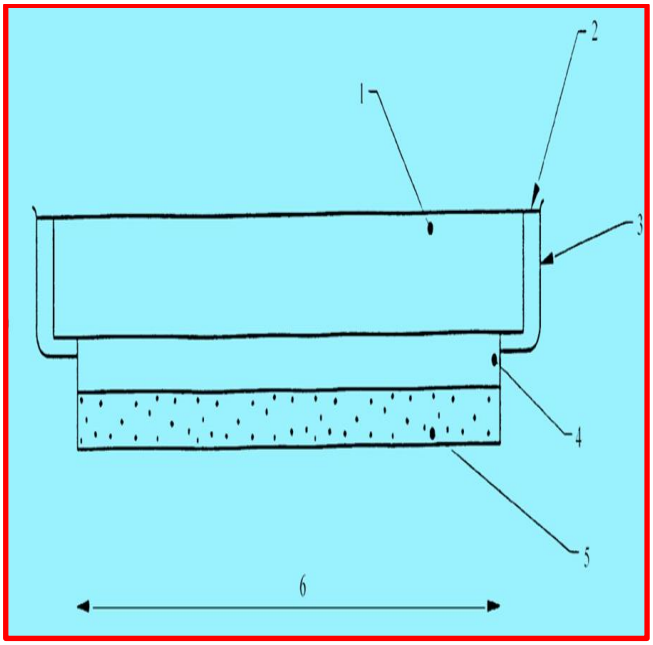

Figure 3.14 Sketch of water vapour cup BS EN 1015-19 1999.

Key to Figure 3.14.

1. Specimen

2. Sealant

3. Circular test cup

4. Air gap ≈ 10 mm

5. Saturated salt solution

6. Area ≈ 0.02 m^2

Saturated solution of potassium nitrate (KNO_3) was poured under the specimen in the bottom of the cup with a gap between the solution and the lower face of the specimen of about 10 mm to provide 20ºC and relative humidity 93.2 %.

To prepare the specimen for the test, the dry specimen was put on the mouth of the cup and impermeable mass sealant was used to seal the clearance between the cup and the specimen.

Note: the humidity according to BS EN 1015-19 1999 in the storage chamber is 95 % to promote hydration but at the time of testing becomes 50 % as in the mentioned standard to let the water vapour going out from inside the cup (high humidity, 93.2 %) to outside the cup or to the chamber (low humidity, 50 %). In this project, the

humidity was 60 % for the 23 days of storage in order to match the curing of all the experiments (strength, porosity, shrinkage and thermal conductivity).

Figure 3.15 Water vapour cups.

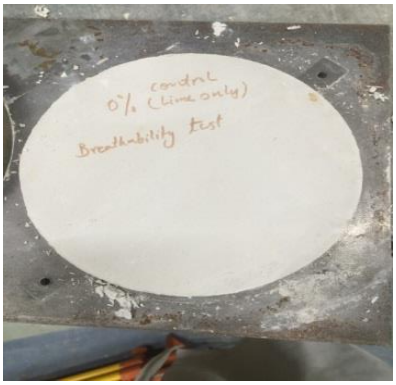

Figure 3.16 Lime specimen (demoulded)

Then, the specimen and the apparatus were kept in a storage chamber at 20ºC and humidity 50 % as shown in Figure 3.17, Figure 3.18 and Figure 3.19.

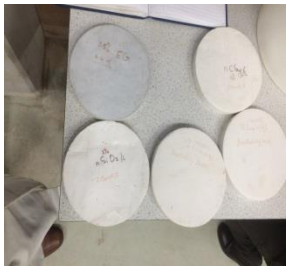

Figure 3.17 Specimens of different fillers/ lime.

Figure 3.18 Climatic chamber with specimens.

Figure 3.19 Climatic chamber used in the study.

3.4.6.1 Theory and Calculation of Water Vapour Permeability (WVP)

Water vapour flux = $\Delta G/\Delta t$ from the graph. Equation 3.11

V = water vapour permeance Kg/ m^2 x S x Pa. Equation 3.12

$\Delta G/\Delta t$ = water vapour flax (kg/s)

ΔP = the difference in water vapour pressure between the ambient air and the salt solution and is taken from appropriate tables, Pa.

R_A = water vapour resistance of the air gap between salt solution and the specimen.

$R_A = 0.048 \times 10^9$ Pa m^2 s/ Kg per 10 mm air gap.

t = is the specimen thickness (m).

W_{vp} = water vapour permeability = V x t. Equation 3.13

V water vapour permeance = $1/ (A \Delta P/ (\Delta G/\Delta t))$- R_A in Kg/ m^2. Equation 3.14

3.4.7 Shrinkage Test

Shrinkage test followed BS ISO (BS-ISO-1920-8, 2009). The mould and the specimens were the same for flexural strength test 40 x 40 x 160 mm. Strain demecs (two) were centrally glued on the centre line of the specimen, spaced 100 mm apart. The demec gauge is shown in Figure 3.20 and Figure 3.21 and the test specimens with demec points is shown in Figure 3.22.

Figure 3.20 Demec device, side view

Figure 3.21 Demec device, top view

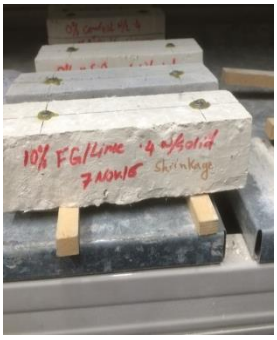

Figure 3.22 Specimens with demec points

3.4.7.1 Theory and Calculation of Shrinkage

The strain gauge factor is 1.608×10^{-5}

If the measurement of first reading is = x

Any reading measurement at any day = x_i

The strain at this day for a material is = $(x-x_i) \times 1.608 \times 10^{-5}$ µm Equation 3.15

Then the curve is drawn from strain versus time.

3.5 Curing Methods

Three drying methods were adopted in this project; Air dry curing, Solvent exchange curing and Oven dry curing. Air curing means the specimens are left in the storage (20°C and 60 % RH) for 23 days after demoulding at 5 days (Part A-Air). In the solvent exchange method, the specimens were demoulded after 5 days and immersed 7 days in isopropanol then are left in the storage under the same aforementioned conditions (Part B-Solvent Exchange). The last method is Oven drying, the specimens are left for 26 days in the same storage and conditions before being put 2 days in an oven 50°C (Part C-Oven drying).

Chapter 4 - **Compressive and Flexural Strength of Lime Nanocomposites**

4.1 Introduction

The main project objective is to change the lime from a non-loadbearing to a loadbearing material. The flexural strength should be similar to the flexural strength of cement mortar (4.0 MPa) and the compressive strength must be more than the minimum value of a loadbearing construction material (5 MPa) as shown in the literature (de Bruijn et al., 2009). It must be lightweight in comparison to concrete as this is a beneficial property to optimise design by reducing section sizes and material used. Table 4.1 shows the objectives and their description. Error bars based on standard deviation as a comparison will be exhibited within the mean of strength tables and charts for each method of curing throughout Chapter 4.

Table 4.1 The aims and objectives of Chapter 4

No	Objectives	Description
1	Lightweight	Lime nanocomposite density is less than that of concrete or brick < 2.5 g/cm^3. Densities are in Chapter 8
2	Load bearing construction material	Able to withstand self-weight and live loads such as wind loading
2.1	Improve compressive strength to be more than minimum limit of load bearing materials	Compressive strength > 5 MPa
2.2	Improve flexural strength to be around that of cement mortar	Flexural strength ≈ 4 MPa

Many series of experiments were conducted to determine the impact of different nanomaterials such as nanosilica ($nSiO_2$), nanoclay (nclay), nanofibrillated cellulose (nFc), and expanded graphite (EG) on the mechanical strength (flexural and compressive) of lime composite properties. Furthermore, hemp shives (HS), polyvinyl acetate (PVAc), hemp fibres (HF) and fibre glass (FG) were also used to determine their effects on the mechanical strength properties. The impact of these

components on other properties such as thermal conductivity, porosity, shrinkage, water absorption and water vapour permeability of lime was studied and will be presented in the following chapters. SEM images were taken of many specimens to obtain a better understanding of the composition of the fibres and lime matrix. In Chapter 4, the focus is on the mechanical properties (flexural and compressive strength) due to their importance in construction materials.

For the flexural and compressive strength tests, the specimens were divided into groups, with each group focusing on a different nanomaterial such as nanosilica (nSiO2), nanoclay (nclay), nanofibrillated cellulose (nFc), and expanded graphite (EG) which were added to lime matrix. The percentage of nanomaterial was varied to find the optimum percentage which gave the highest flexural and compressive results. Further testing then followed to verify the optimum results from the initial tests. Fibre glass, hemp fibres and PVAc were also added to the lime nanocomposites to determine their influence on strength. Initially, the water lime binder ratio was 0.6 W/L but most of the specimens failed before testing during the storage time or transportation so later the ratio was decreased to 0.5 to determine its improvement and influence on strength.

Finally, a ratio of 0.4 W/L was used which gave optimum strength results, but workability became an issue. To overcome this, the on-site placing method was followed where a 'mortar-board' type tamping tool was used to compact the material. This technique worked quite well. The moulds were 40 x 40 x 160 mm as shown in Figure 4.1. Three groups (each group includes different percentages of nanofillers) of specimens were cured by three different methods of curing (Air, Solvent exchange and Oven dry curing) and were cast yielding a total of 200 specimens in total. Three different curing regimes were adopted and these are described in Section 4.2. Drying times of hemp/lime composites on site is an issue hence accelerated methods were also investigated to determine if other curing techniques could be used.

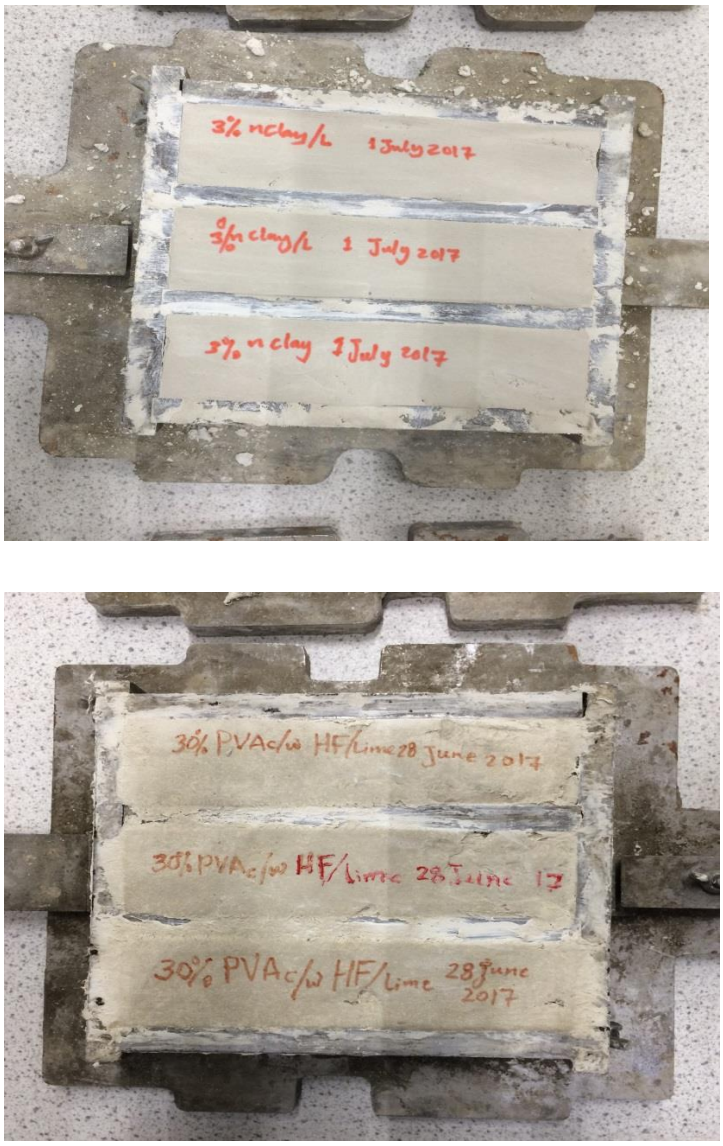

Figure 4.1 Moulds of 40x40x160 mm with nanocomposite specimens

Fig.4.2 is an example of different series of mechanical (flexural and compressive) strength specimens.

Figure 4.2 Different series of mechanical strength (flexural and compressive) specimens

4.2 Classification of test specimens according to their curing regime

Three different curing methods were adopted to study the different effects of curing on the properties (compressive and flexural strength in Chapter 4, thermal conductivity Chapter 7, porosity Chapter5 and shrinkage 6 later) of the composite. The Air curing was conducted to allow the reaction to complete as the water was slowly evaporated. It will be shown that air cured samples yielded the largest strength (Section 4.3). Solvent exchange (Section 4.4) is most likely to be beneficial for heat isolation since the reaction stops early as the free water is evaporated with the solvent evaporation. This is as a result of the density remaining low. Oven curing may give higher strength result than Solvent exchange but some free water of this method is evaporated. More tests in the future are important to define the best number of days for oven curing which give optimum properties (strength, heat isolation, porosity and shrinkage). A summary of the curing methods and nanofillers/ additives used are given in Table 4.2. Referring to Table 4.2, Part A, Air curing is adopted. This method better replicates the in-situ conditions.

In addition, a solvent exchange method (Section 4.4 and Section 4.5) which was applied as soon as practically possible (five days after casting when the materials were sufficiently hardened, immersed 7 days in isopropanol and then 2 days in an oven 50ºC) was used to determine its influence on longer term strength, called Part B-Solvent exchange method. Finally, a drying method where the specimens were put 2 days in an oven at 50ºC at days 26 and 27 then tested at 28 day was adopted, named Part C- Oven drying method (Section 4.6 and Table 4.2.).

Table 4.2 Summary of tests

Curing Method	**Part A Air drying** • Stored throughout at • 20°C/60% RH • Demoulded at 5 days • Cured for +23 days	**Part B Solvent exchange** • Demoulded at 5 days • Immersed in isopropanol • for +7 days • 20°C/60% RH for +14 days • Oven for +2 days (26-27) (50°C)	**Part C_1 Oven drying** • Demoulded at 5 days • 20°C/60% RH for +21 days • Oven for +2 days (50°C) **Part C_2 Oven drying** • Demoulded at 5 days • Shrinkage test days (5-28) test • Oven for +2 days (29-30) (50°C) • Water absorption test days (31-32) • 20°C/60% RH for +51 days

Strength (N/mm^2)								
		Table	**W/L**		**Table**	**W/L**	**Table**	**W/L**
	Part A			**Part B**			**Part C_1**	
	Control	4.3	0.5	Control	4.10	0.4	Control 4.11	0.4
	2.0%$nSiO_2$	4.4	0.5	0.5% EG	4.10	0.4	0.5% nclay 4.11	0.4
	4.0% $nSiO_2$	4.4	0.5	1.0% EG	4.10	0.4	1.0% nclay 4.11	0.4
	0.5% nclay	4.5	0.5	2.0% EG	4.10	0.4	2.0% nclay 4.11	0.4
	1.0% nclay	4.5	0.5	2.0% nclay	4.10	0.4	3.0% nclay 4.11	0.4
	2.0% nclay	4.5	0.5	2.0% $nSiO_2$	4.10	0.4	1.0% $nSiO_2$ 4.11	0.4
	5.0% nFC	4.6	0.5	10% FG	4.10	0.4	2.0% $nSiO_2$ 4.11	0.4
	7.0% nFC	4.6	0.5	80% PVAc	4.10	0.4	3.0% $nSiO_2$ 4.11	0.4
	5.0% FG	4.7	0.5	40% PVAc	4.10	0.4	1.0% EG 4.11	0.4
	10% FG	4.7	0.5	20% PVAc	4.10	0.4	2.0% EG 4.11	0.4
	15% FG	4.7	0.5	8% PVAc	4.10	0.4	5.0% nFC 4.11	0.4
	10% HF 4 % nZnO and 12% PVAc	4.8	0.4	10% HF	4.10	0.4	10% nFC 4.11	0.4
Nanofiller Additive							5.0% HF 4.11	0.4
							7.0% HF 4.11	0.4
							10% HF 4.11	0.4
							20% HS 4.11	0.4
							12% PVAc, 20% HS 4.11	0.4

Curing Method	**Part A Air drying** • Stored throughout at • 20°C/60% RH • Demoulded at 5 days • Cured for +23 days	**Part B Solvent exchange** • Demoulded at 5 days • Immersed in isopropanol • for +7 days • 20°C/60% RH for +14 days • Oven for +2 days (26-27) (50°C)	**Part C_1 Oven drying** • Demoulded at 5 days • 20°C/60% RH for +21 days • Oven for +2 days (50°C) **Part C_2 Oven drying** • Demoulded at 5 days • Shrinkage test days (5-28) test • Oven for +2 days (29-30) (50°C) • Water absorption test days (31-32) • 20°C/60% RH for +51 days		
			8% PVAc, 10% FG	4.11	0.4
			12% PVAc, 10% FG	4.11	0.4
			8 % PVAc, 10% HF	4.11	0.4
			12% PVAc, 10% HF	4.11	0.4
Nanofiller additives			**Part C_2**		
			Control	4.13	0.4
			2.0% nclay	4.13	0.4
			2.0% EG	4.13	0.4
			2.0% $nSiO_2$	4.13	0.4

Key: $nSiO_2$= nanosilica; nclay= nanoclay; nFc= nanofibrillated cellulose; FG= fibre glass; PVAc= Polyvinyl acetate; HF= hemp fibres; EG=expanded graphite.

Furthermore, the range of nanomaterials and additives for Parts B and C were adopted based on the results of the preceding part i.e. the better performing nanocomposites in the previous tests of Part A-Air curing. New additives were also added as appropriate to establish influence on strength characteristics.

For Part C-Oven drying method, it was adopted due to its accelerated drying which gave a quick hydration reaction, because the hydration takes many years. Anyway, the main strength propagates at the first 28 days. This method dries the W/L gradually within two days which gives quick hydration at 50 ºC but still allows strength development. More work is required to investigate the influence of drying on strength.

Part C was divided into two parts (Part C_1 and Part C_2). Part C_2 was the same as Part C_1 except curing was up to 60 days as opposed to 28 days at Part C_1. Part C_2 specimens were also used for shrinkage testing from the age of 5 days to 28 days. At 29-30 days was dried in oven using 50°C. At 31-32 days, a water absorption test was conducted after shrinkage test for 2 days and will explain in Chapter 5. Then at the day 60, strength tests were conducted. It is likely that the specimens were affected by the changes of water content due to the water absorption test because the strength decreased. The low strengths were not evident at 60 days age (Part C_2).

Table 4.3 is the mean of the results of compressive and flexural strengths (Control, nSiO_2, nclay, nFc, HF and PVAc with nZnO) as given in Table 9.2 to Table 9.7 (Chapter 9, Appendix). Referring to Table 9.2 (Chapter 9, Appendix), the test part is given in Column 1, "A" being the designated letter for the curing method. The specimen number is given in Column 2. The percentage and type of nanofiller is given in Column 3. The water/lime ratio (W/L) is given in Column 4. The age at testing is given in Column 5. The storage conditions are given in Columns 6 and 7. This labelling system was repeated for all tables of results. The samples were stored in a controlled environment for the first five days after casting (60 % RH; 20ºC) before demoulding, Column 6. Following demoulding, they were stored at 60% RH; 20ºC up to 28 days which were similar to the controlled environment (Column 7). The compressive strength results are given in Column 8, the flexural strength results are given in Column.9.

4.3 Flexural and compressive strength test results Part A-Air cured.

The flexural and compression test results for all groups of specimens of Part A-Air cured are presented in Section 4.3.1 to 4.3.7, Tables 9.2 to 9.7 (Chapter 9, Appendix) and their mean is in Table 4.9.

4.3.1 Control Specimens (Pure Lime) of Part A-Air cured

The flexural and compressive strength results for the control specimens are given in Table 9.2 (Chapter 9, Appendix). A total of eight specimens were tested in flexure and 10 halves, using the broken flexural specimens, were tested in compression (some of the compression samples were damaged prior to testing so were not included). Referring to Table 9.2, the average compressive strength of the control samples was 2.9 MPa (range 1.80 - 4.2 MPa) whereas the average flexural strength was 1.4 MPa (range 0.2-3.0 MPa). The individual values are presented graphically in Figure 4.3 and Figure 4.4.

The average compressive and flexural strength of the control specimens (as shown in Table 9.2) was 2.9 MPa and 1.4 MPa respectively. These results were achieved at 0.5 W/L. They are clearly weak in flexure in comparison to the flexural strength of cement mortar which is about 3.0 MPa for moderate strength mortars and about 4.0 MPa for high strength mortars (Swan & and Bonora, 2017).

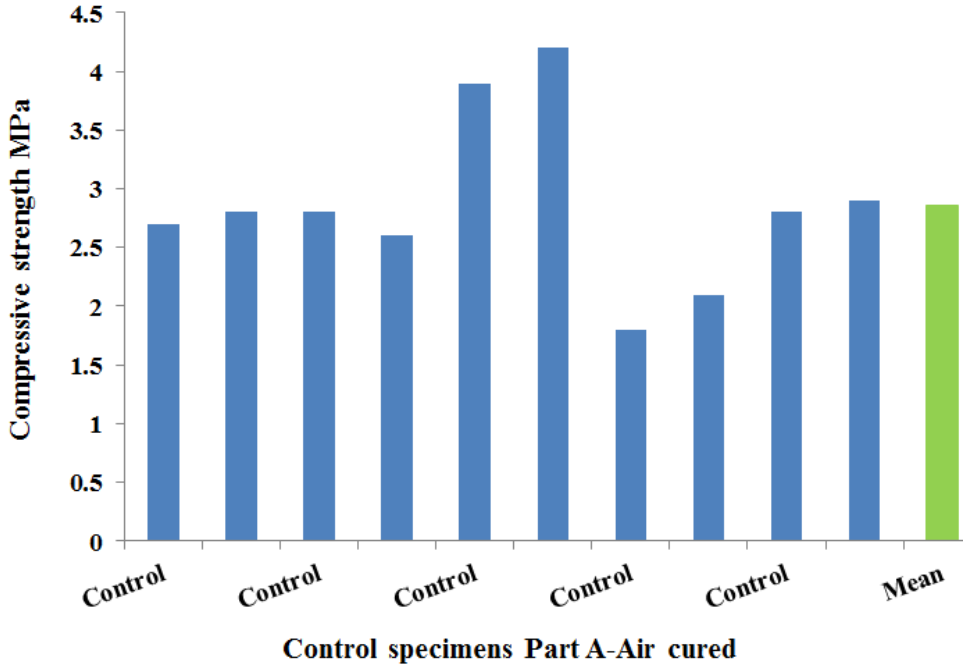

Figure 4.3 Compressive strength specimens and their mean, Part A-Control

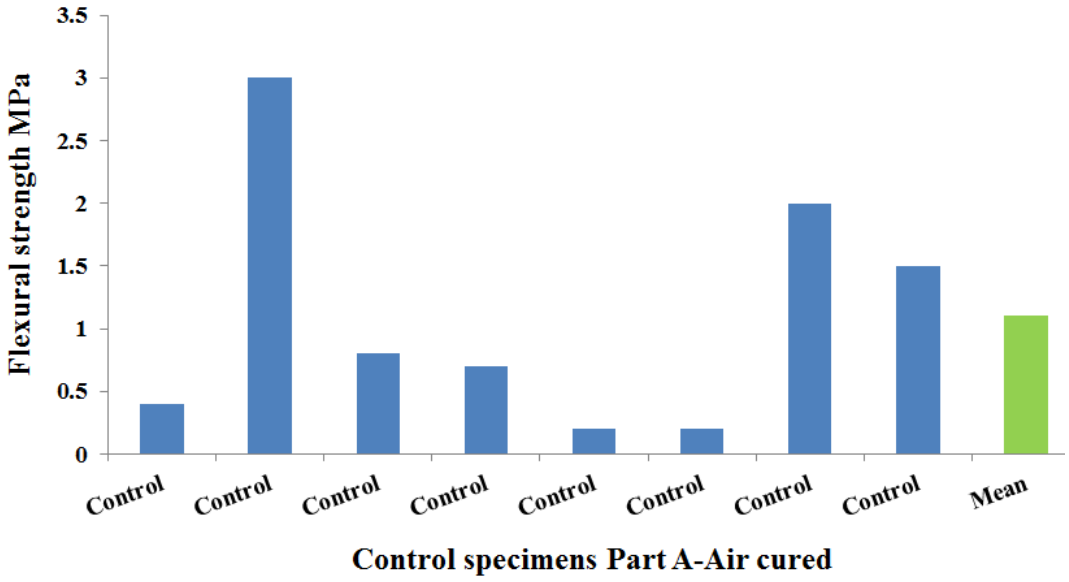

Figure 4.4 Flexural strength specimens and their mean, Part A-Control

The mean compressive strength of 2.9 MPa is slightly lower than the minimum limit of load bearing materials 3-5 MPa (de Bruijn et al., 2009). Aho and Ndububa (2015) reported a flexural strength of 4.0 MPa for 1:2 cement: sand mix (Aho & Ndububa, 2015) which is higher than mean flexural strength of Control specimens in this project (1.4 MPa) The specimens had cracking due to shrinkage and it may be that these cracks contributed to low failure loads, especially when the cracking was near the mid-span of the prisms.

4.3.2 Nanosilica (nSiO2)/lime nanocomposite specimens, Part A-Air cured

The compressive and flexural strength results for the nanosilica/lime nanocomposite specimens are given in Table 9.3 (Chapter 9, Appendix) and shown graphically in Figure 4.5 and Figure 4.6. Referring to Table 9.3 (Chapter 9, Appendix), two groups of specimens are presented, one group has 2 wt. % of nanosilica added as a nanofiller whereas the other has 4 wt. %. Referring to Samples 1-4 with 2 wt. % nanosilica in this table, the average compressive strength was 2.8 MPa but when the quantity of nanosilica increased to 4 wt. %, the average compressive strength decreased a little to 2.7 MPa. With regards to the flexural strength results, the 2 wt. % $nSiO_2$ exhibited strength of 0.4 MPa whereas the 4 wt. % specimens averaged 0.8 MPa. However, this was influenced by an unusually large flexural strength for Specimen A3, which yielded a flexural strength of 2.13 MPa. This value is suspect and if omitted, the average flexural strength would broadly be in line with the 2 wt. % samples. From the test results, it can be concluded that the $nSiO_2$/lime nanocomposite specimens with 2 wt. % $nSiO_2$ nanofiller yield the slightly better compressive strength (2.8 MPa). However, 2 wt. % $nSiO_2$ decreases the cost compared to 4 wt. (2.7 MPa) with no big difference between both compressive results (2 and 4 %). Flexural strength of both the 2 and 4 wt. % was very low (0.4 and 0.8 MPa respectively) which is much lower than the flexural strength of cement mortar (around 4 MPa).

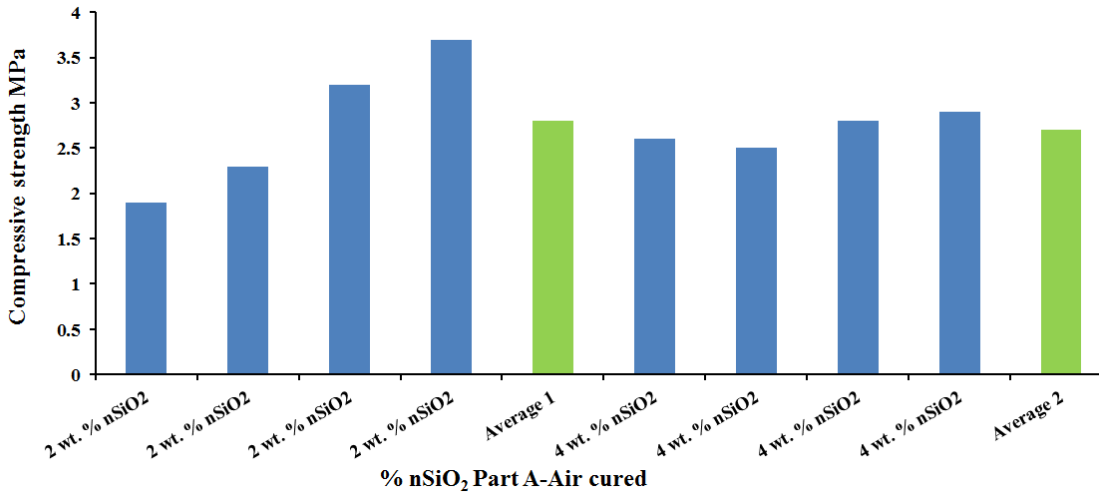

Figure 4.5 Compressive strength of $nSiO_2$/lime nanocomposites and their mean, Part A-Air cured

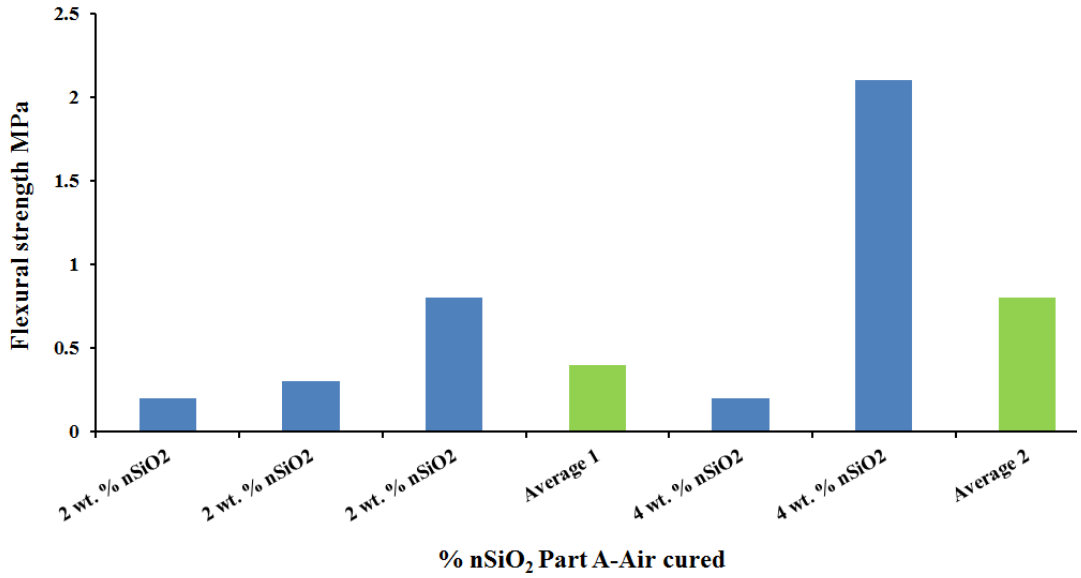

Figure 4.6 Flexural strength of $nSiO_2$/ lime nanocomposites and their mean, Part A-Air cured

A possible reason for the low flexural strength of $nSiO_2$/lime nanocomposites was due to cracking as a result of drying shrinkage as shown in Figure 4.7 (shrinkage data will be presented in Chapter 6).

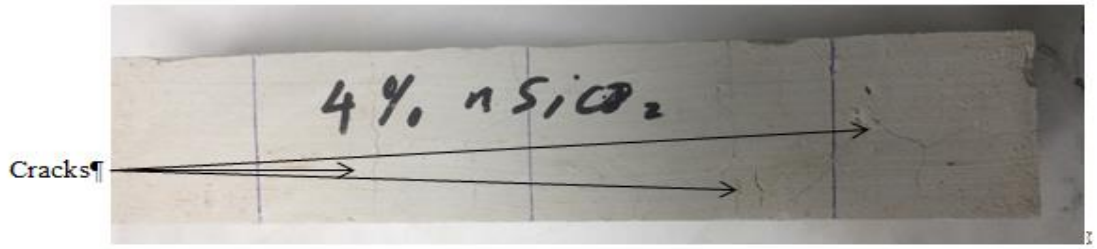

Figure 4.7 Shrinkage cracking of the nanosilica specimen

4.3.3 Nclay/Lime Nanocomposite Specimens, Part A-Air cured.

The flexural and compressive strength test results are given in Table 9.4 (Chapter 9, Appendix) for the nanoclay/lime nanocomposites. Samples dosage of 0.5 wt. % and 1 wt. % nclay exhibited an average compressive strength of 3.0 and 2.9 MPa respectively. When the percentage increased to 4 wt. % nclay, the compressive strength increased to 3.6 MPa. The corresponding flexural strengths were 0.3, 0.6 and 0.7 MPa respectively. Figure 4.8 and Figure 4.9 show these test results in graphical form. The 2 wt. % nclay gave the highest flexural strength (0.7 MPa) compared to flexural strength of 1 wt. % nclay 0.6 MPa (Probably, it is due to the effect of cracks which likely appears under flexural loads more than compressive loads because of the tension is at the lower half side and the compression is on the upper half side of the specimen cross section around the neutral axis which is seprates between compression and tension zone) and the compressive strength (3.6 MPa) higher than the flexural strength of 1 wt. % nclay was 2.9 MPa. Probably, this 2 wt. % nclay can be optimised if it was dispersed completely in the lime matrix, as it seemed that the particles precipitated at the bottom of the beaker.

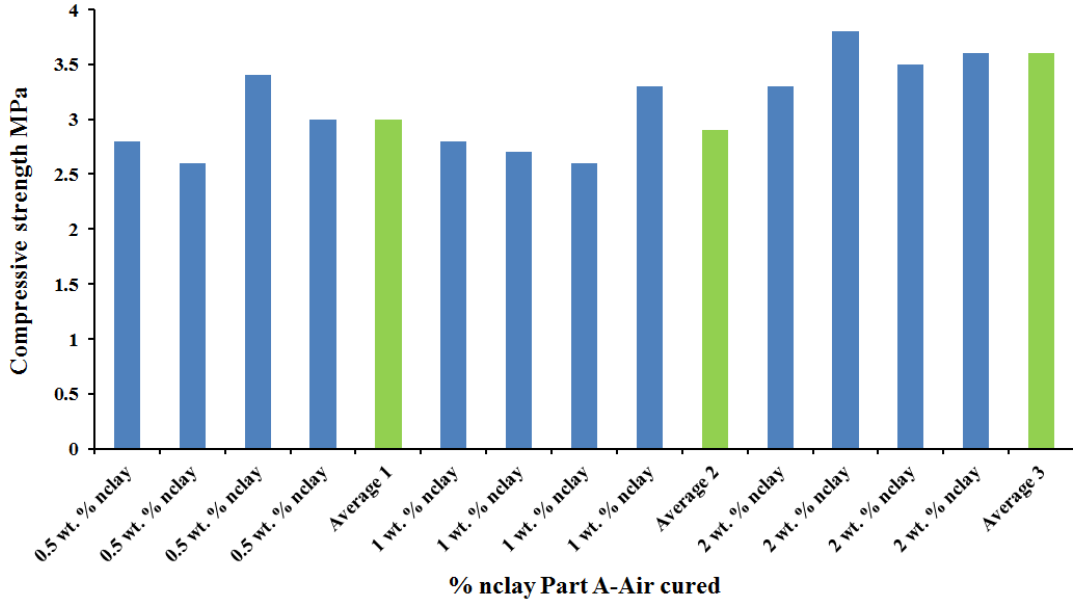

Figure 4.8 Compressive strength of nclay/lime nanocomposites and their mean, Part A-Air cured

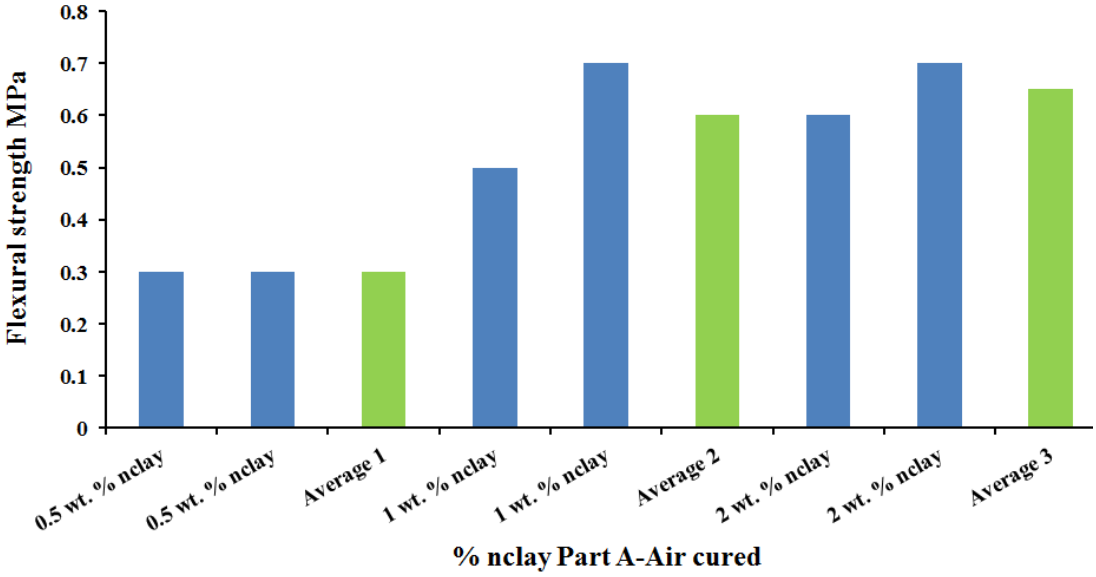

Figure 4.9 Flexural strength of nclay/ lime nanocomposites and their mean, Part A- Air cured

4.3.4 Nanofibrillated cellulose nFc/lime nanocomposites, Part A-Air cured

A total of seven specimens containing nanofibrillated cellulose were tested for compressive and flexural strength as shown in Table 9.5 (Chapter 9, Appendix). Four specimens were dosed with 5 wt. % nFc giving an average compressive strength of 2.3 MPa and flexural strength of 0.35 brought up to 0.4 MPa. The remaining three samples had an nFc content of 7 wt. % and yielded a higher compressive strength of 2.3 MPa. The flexural strength increased to 0.8 MPa. These test results are shown graphically in Figure 4.10 and Figure 4.11.

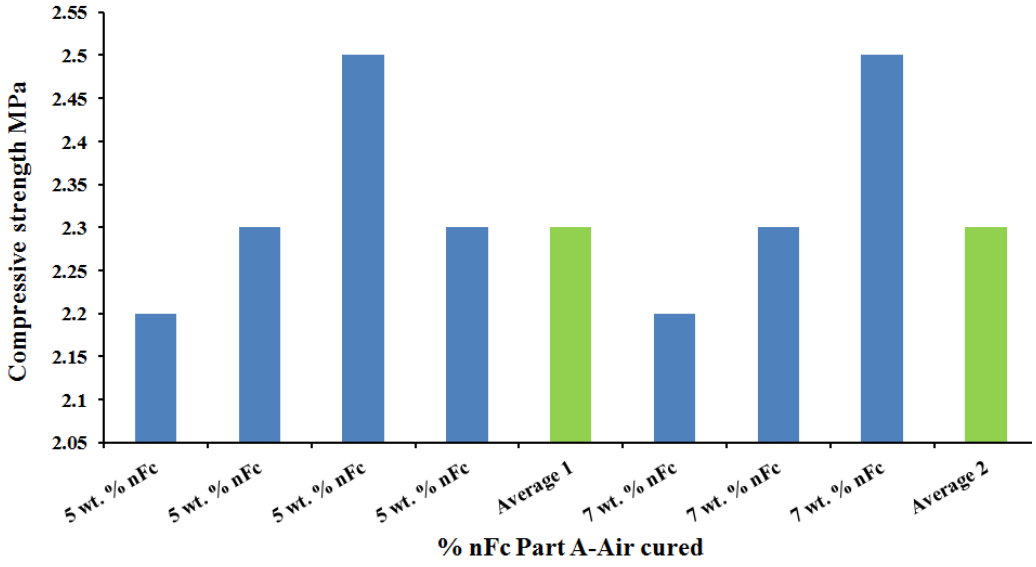

Figure 4.10 Compression strength of nFc and their mean, Part A-Air cured

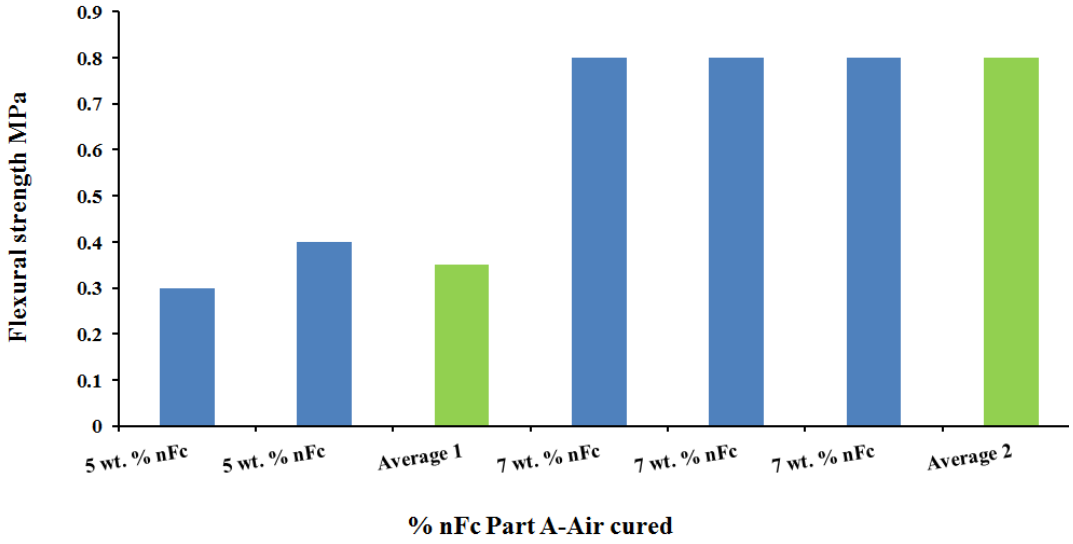

Figure 4.11 Flexural strength of nFc and their mean, Part A-Air cured

4.3.5 Fibre Glass/Lime Nanocomposites

Table 9.6 (Chapter 9, Appendix) shows the compressive and flexural strength results for the fibre glass FG/lime composite specimens. The data shown graphically in Figure 4.12 and Figure 4.13 shows that 10 wt. % FG/L had the highest results in compressive strength, 10.7 MPa, and the highest result in flexural strength, 3.9 MPa. The 5 wt. % FG sample had an average compressive strength of 3.4 MPa and an average flexural strength of 2.2 MPa. For 15 wt. % FG, their compressive and flexural strength values were 6.7 MPa and 1.9 MPa respectively.

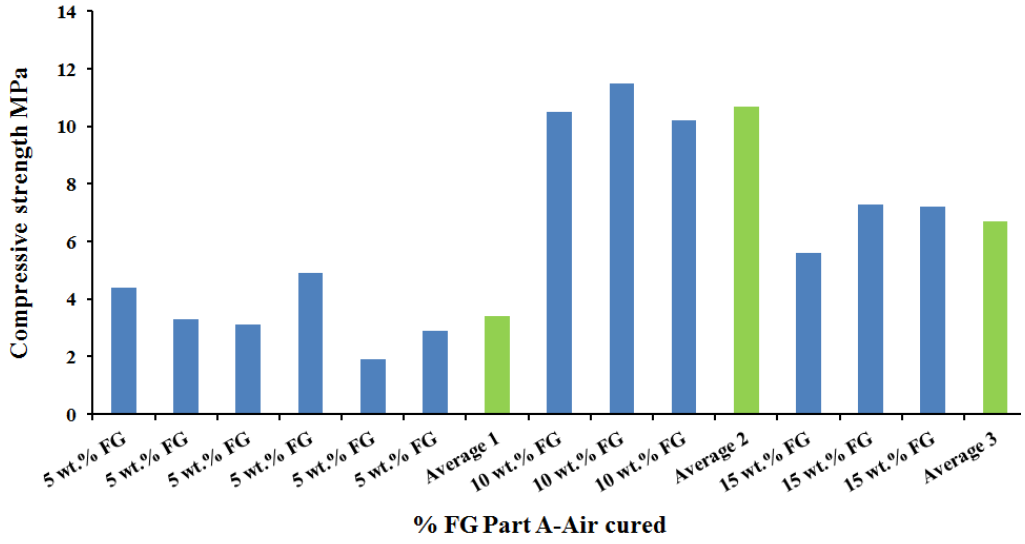

Figure 4.12 Compressive strength of Fibre glass composites and their mean, Part A- Air cured

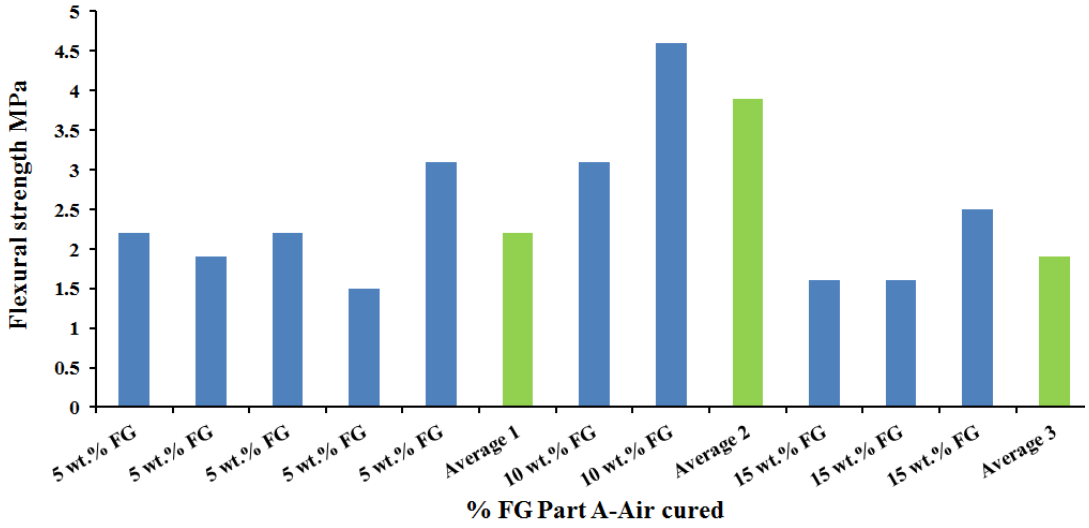

Figure 4.13 Flexural strength Fibre glass composites and their mean, Part A-Air cured

4.3.6 Hemp Fibres/PVAc nZnO/Lime Nanocomposites

Mix of 10 wt. % HF, 12 wt. % PVAc, 4 wt. % nZnO/L nanocomposite were tested using Part A-Air cured method with W/L decreased from 0.5 W/L to 0.4 W/L using three specimens which is important to use in the Core of the proposed wall. Two

specimens of 4 wt. % nZnO/L were placed using 0.4 W/L which can be used in the Render of the proposed wall was also tested using Part A-Air cured method and 0.4 W/L. Table 9.7 (Chapter 9, Appendix) shows the results of compressive and flexural strength of these tests.

Referring to Table 9.7 (Chapter 9, Appendix) and Table 4.3, the highest result of compressive strength of 10 wt. % HF, 4 wt. % nZnO, 12 % wt. PVAc/L and 0.4 W/L following Part A-Air cured method was 19.7 MPa and the mean of 6 specimens was 17.7 MPa which was about 4 times of the minimum limit of the load bearing material. The highest flexural strength was 7.7 MPa and the mean was 7.3 MPa which was more than cement mortar (4.0 MPa) and the same as the flexural strength of concrete (about 7 MPa). As for 4 wt. % nZnO/L, the strength was very low, the highest compressive strength was 0.9 MPa and the mean was 0.7 MPa. The highest flexural strength of 4 wt. % nZnO/L was 0.7 MPa and the mean was 0.6 MPa. Figure 4.14 and Figure 4.15 show these results graphically.

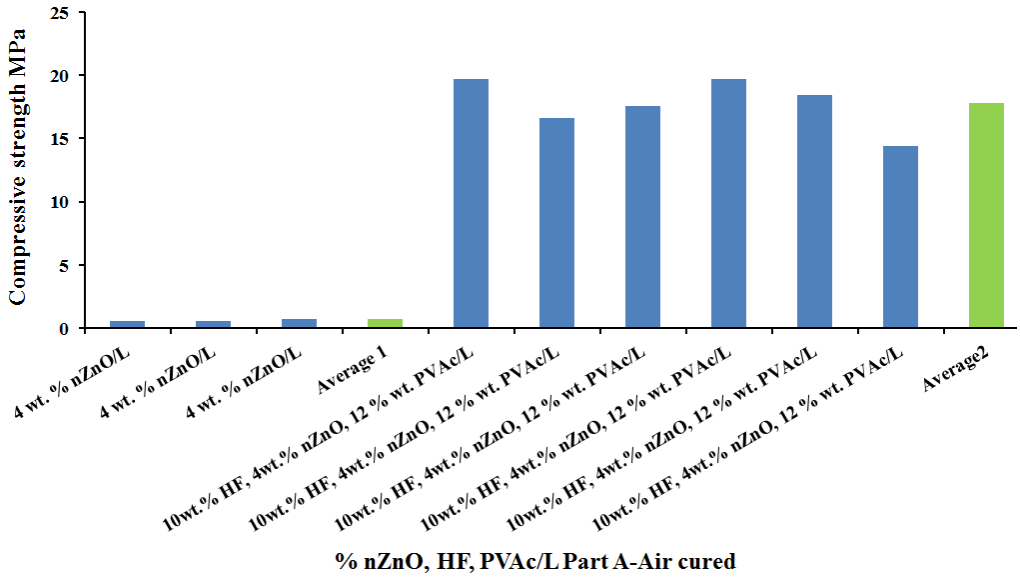

Figure 4.14 Compressive strength of HF, nZnO and PVAc composites of 0.4 W/L and their mean, Part A- Air cured

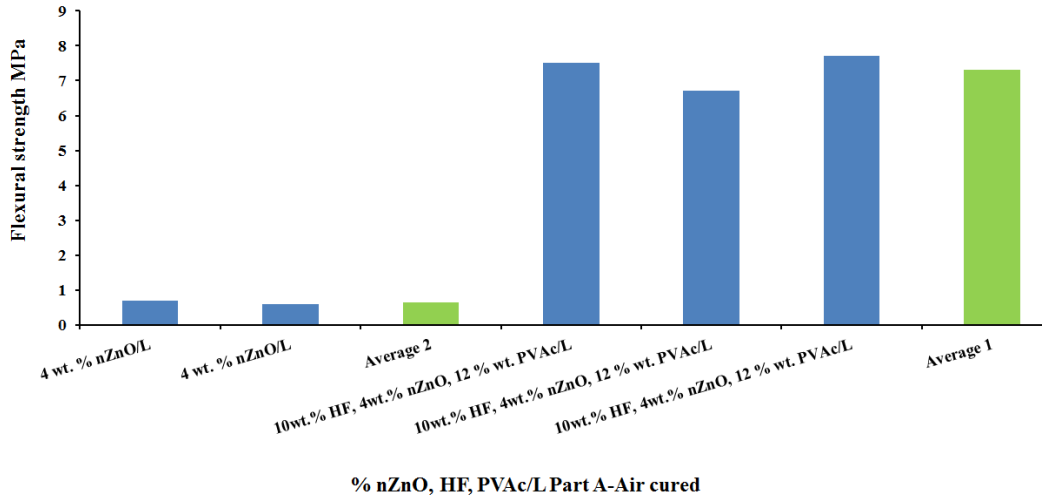

Figure 4.15 Flexural strength HF, nZnO and PVAc composites of 0.4 W/L and their mean, Part A- Air cured

4.3.7 Summary of the Test Results of Part A-Air Cured

Table 4.3 provides a summary of the average compressive and flexural strength tests of all the specimens from Part A-Air cured. It shows that all the materials were low in flexural strength except fibre glass at 10 wt. % loading to lime which gave a flexural strength of 3.9 MPa. The sample with 5 and 7 wt. % nFc didn't enhance the compressive and flexural strength in comparison to pure lime. The effective increase in compressive strength was by adding FG. The compressive strengths increased to 10.7 and 6.7 MPa by adding 10 and 15 wt. % FG respectively. The optimum percent of FG was 10 wt. % to lime. Figure 4.12 and Figure 4.13, show graphically the compressive and flexural strengths for Part A for nanofiller/lime nanocomposites. The highest strengths (compressive and flexural) were by mixing 10 wt. % HF, 4 wt. % nZnO, 30 % wt. PVAc/L and 0.4 W/L (which is a different water lime ratio from the W/L of the remainder of the Part A-Air cured specimens 0.5 W/L) and the results were 17.7 MPa and 7.3 MPa respectively.

Referring to Figure 4.12, Figure 4.13 and Table 9.3, FG at loading of 10 wt. % gave the second highest results in both flexural and compression strength tests of all the tests (10 and 15 wt. %) of Part A-Air cured.

In compressive strength, it can be summarised that the mean value of compressive strength for pure lime (control) 0.5 W/L was about 2.9 MPa. The highest result of nanosilica was at the 2 wt. % in compressive strength, which was 2.8 MPa, and it was slightly more than the result of 4 wt. % $nSiO_2$ to lime (2.7 MPa). Probably, 4 wt.% needs more dispersion to increase compressive strength and work as nanomaterial in the matrix because the probability of dispersion decreases with the dose quantity of the nanofiller. Figure 4.8 and Figure 4.9 show that the percentage of 2 wt. % nanoclay to lime has a compressive strength of 3.5 MPa, more than the result of 0.5 wt. % (3.0 MPa) and 1 wt. (3.0 MPa) to lime. For nFc, the percentage of 7 wt. % to lime gave a higher result in compressive strength than 5 wt. %, it was 4.7 MPa compared to 2.3 MPa for the 5 wt. %. Figure 4.10 and Figure 4.11 show the relationship between percent of nFc and their compressive and flexural strengths respectively.

It was noticed that the failure of fibre glass was by the fibre pulling out under flexural load, which may mean that the flexural strength can be increased if the adhesion between fibre glass and lime increases. For the next series of tests, polyvinyl acetate (PVAc) was added at 8 and 12 wt. % as a percentage of the W/L ratio of the mixture (calculation of PVAc percent was explained in Section 3.2.5). The aim is to increase the adhesion and subsequently the strength. Figure 4.16 and Figure 4.17 show graphically a comparison between the mean results of compressive and flexural strengths of all the fillers of Part A-Air cured. Figure 4.18 and Figure 4.19 show the compressive and flexural strengths for different filler of Part A-Air cured as a curve. Error bars on these two curves show that there are no high contrasts between the compressive and flexural strength results (which means repeatable results). For FG, the contrasts of the results are higher than the other filler specimen results. More details about Error bars based on standard deviation will be discussed in the Section 4.8 (Discussion of Chapter 4).

Table 4.3 Summary of Part A-Air cured for compressive and flexural strength

No	% filler	Mean Compressive strength MPa	STD	Mean flexural strength MPa	STD
1	0 % pure lime	2.9	0.72	1.1	2.48
2	2 wt. % $nSiO_2$	2.8	0.82	0.4	0.32
3	4 wt. % nSiO2	2.7	0.18	0.8	0.89
4	0.5 wt.% nclay	2.9	0.34	0.3	0.4
5	1 wt.% nclay	2.9	0.31	0.6	0.31
6	2 wt.% nclay	3.6	0.21	0.7	0.89
7	5 wt.% nFc	2.3	0.12	0.3	0.07
8	7 wt.% nFc	2.3	0.15	0.8	0
9	5 wt. % FG	3.4	1.1	2.2	0.58
10	10 wt. % FG	10.7	0.68	3.9	1.0
11	15 wt. % FG	6.7	0.95	1.9	0.52
12	Core composite	17.7	2.03	7.3	0.53
13	4 wt. % nZnO/L	0.7	0.14	0.6	0.07

The highlighted results are the highest results of Part A-Air cured. Table A is the summary of the optimum results and it is expressed by the letter A referring to Part A, STD is standard deviation and Core composite is 10wt.% HF, 4wt.% nZnO, 12% wt. PVAc/L

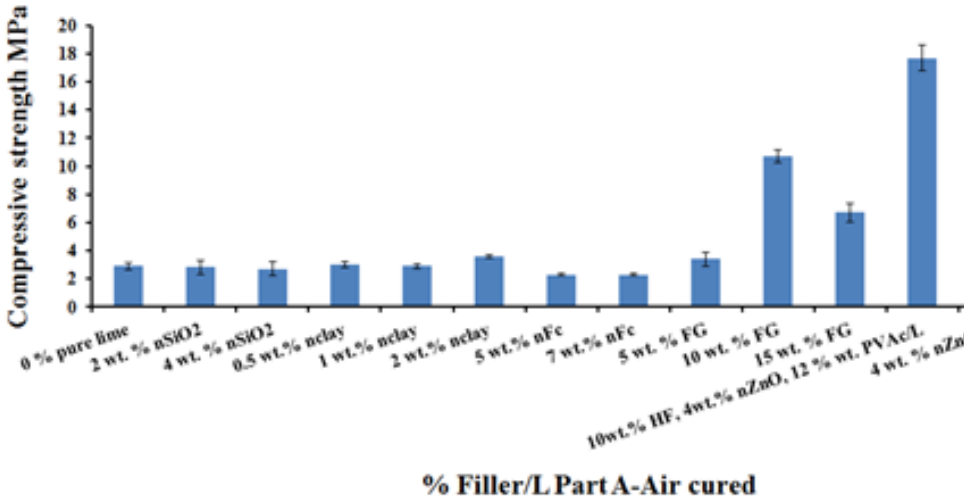

Figure 4.16 Average compressive strength of Part A-Air cured, Error bar ± < 1.

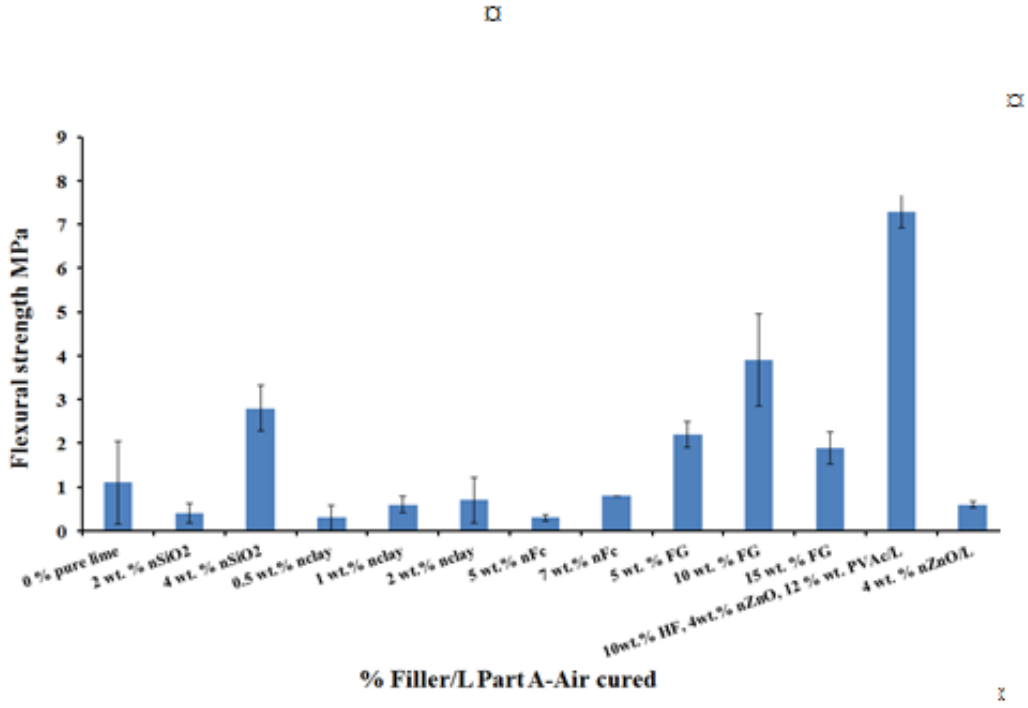

Figure 4.17 Average flexural strength of Part A-Air cured Error bar ± < 1.

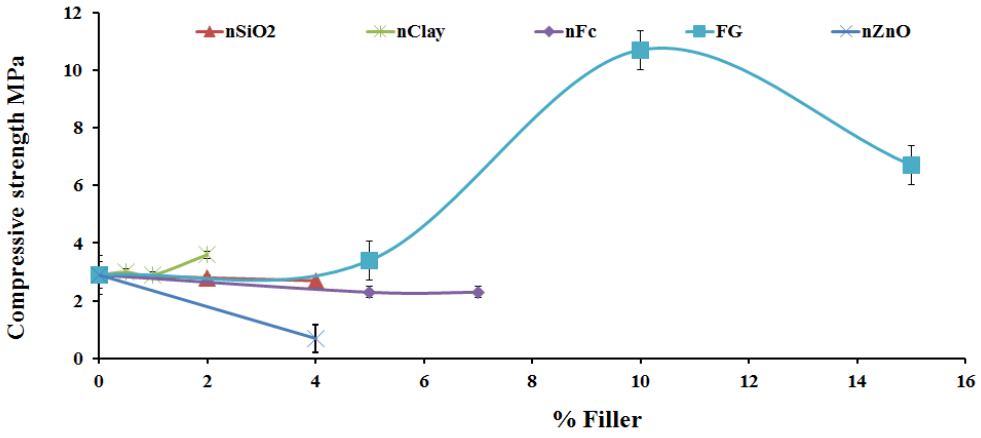

Figure 4.18 Compressive strength of filler/ lime at 0.5 W/L Part A-Air cured, Error bar ± < 1.

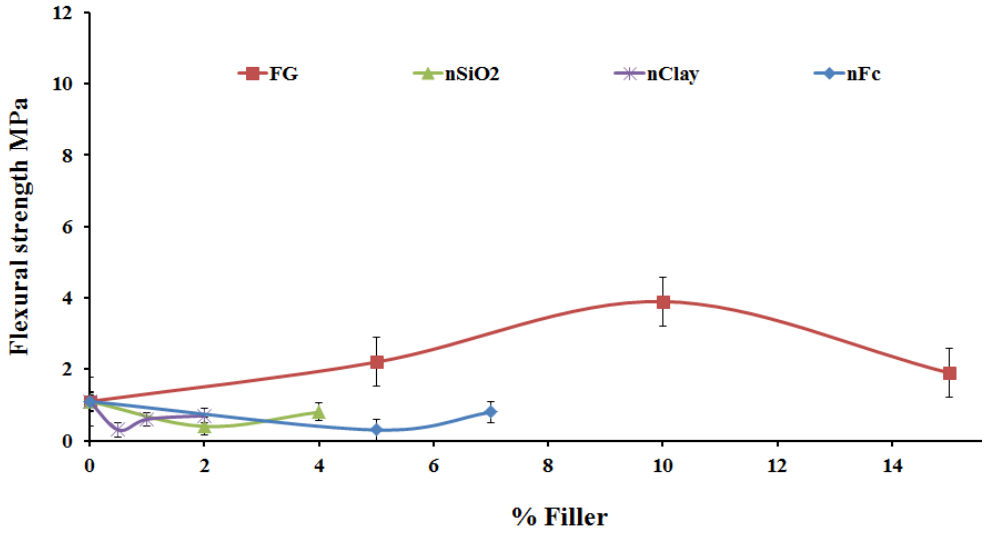

Figure 4.19 Flexural strength of filler/ lime at 0.5 W/L Part A-Air cured, Error bar ± < 1.

Table 4.3.A is the important means of compressive and flexural strength results of Part A-Air cured.

Table 4.3.A Summary of the highest results of Part A-Air cured of Part A-Air cured

No	% filler	Compressive strength MPa	Flexural strength MPa
1	**Control**	**2.9**	**1.0**
2	2 wt. % $nSiO_2$	**2.8**	**0.4**
3	2 wt.% nclay	**3.6**	**0.7**
4	7 wt.% nFc	**2.3**	**0.8**
5	10 wt. % FG	**10.7**	**3.9**
6	10wt.% HF, 4wt.% nZnO, 12 % wt. PVAc/L	**17.7**	**7.3**

4.4 Flexural and Compressive Strength Test for Part B-Solvent Exchange

In the solvent exchange method, Part B, the water lime ratio was decreased from 0.5 to 0.4 to minimise the water binder ratio but was still sufficient to produce chemical reactions from the hydration of the calcium silicates and calcium aluminates. Previous research found that the water (due to evaporation throughout drying) leaves micro-pores in the paste which leads to a weak mortar (Lawrence & & Walker, 2008), hence the method adopted in this part of the project (Solvent exchange) is to determine by this method the influence against conventionally cured specimens in air (Part A-Air cured) method.

The specimens (Part B) were demoulded after 5 days curing at 20ºC and 60% relative humidity. Specimens were then put in plastic cases immersed in isopropanol for 7 days and then by two days in an oven at 50ºC at 26-27 days as shown in Table 4.2. Tests were conducted at 28 days. The basis for using this curing method was based on previous work (Alvarez, Fernández, Navarro-Blasco, Duran, & Sirera, 2013).

It was reported by Alvarez et al., 2013 that the results of compressive strength of nanosilica/lime nanocomposites at 7, 28 and 91 days was increased by using the solvent exchange method (excess water removal). The results in this project were compared to test results from ordinary air curing. The compressive strength of the

control specimen of pure lime at 28 days using ordinary curing (60 % RH, 20 ºC) was 4.3 MPa whereas the result of solvent water removal for 7 days nanosilica/lime was 0.9 MPa. It was reported that the weight loss percentage of cement paste immersed 1 hour in isopropanol was 82 % after 9 hours and that mean decrease in water is 18 % from 0.4 water/cement ratio. The rest of the water is (40 % -18 % = 22 %) which is about more than half of the water cement ratio (Canut, 2011). For hydration percent, it was 65 % hydration for the samples after 48 hours took out of a case which were 1 hour immersed in isopropanol (Maciel, Soares, de Oliveira Romano, & Cincotto, 2019). These studies explained the loss in water by using isopropanol.

The results of the compressive and flexural strength results for Part B-Solvent exchange are given in Table 4.10. They were different w/c and different drying than Part A and the results also were different. The test specimens of Part A consist of the better performing nanocomposites from Part B in compressive strength and slightly lower in flexural strength (except Control was decrease in flexural from 1.1 to 0.7 MPa). Part A were Control (2.9, 1.1 MPa), 2 % $nSiO_2$ (2.8, 0.4 MPa), 2 % nclay (3.6, 0.7 MPa) and 10 % FG (10.7, 3.9 MPa) respectively whereas Part B were Control (2.2, 0.7 MPa), 2 % $nSiO_2$ (2.2, 0.8 MPa), nclay (3.8, 1.6 MPa) and 10 %FG (4.3, 4.1). In spite of the water/lime ratio was reduced to 0.4. The remaining samples in Part A and B introduced new additives such as polyvinyl acetate (PVAc) and hemp fibres (HF) to further investigate if the addition of new nanomaterials or fibrous additives could increase the strength properties of the lime based materials.

Referring to Table 4.4, the Control specimens had an average compressive strength of 2.2 MPa and flexural strength of 0.7 MPa. The control compressive strength from Part A (Air cured, 0.5 W/L) was 2.9 MPa, hence the solvent exchange method has led to a reduced compressive strength in general except 2 % nclay which slightly was increased. Flexural strengths were also a little decreased from 1.1 to 0.7 MPa but in general were higher than Part A. The highest performing specimen in the nanofillers in Part B was 2 wt. % nclay at 3.8 MPa in compression. However, the compressive strength was similar, 3.5 MPa for air cured, Part A. Again flexural strengths were increased from 0.7 MPa for Part A, Air cured to 1.0 MPa for Part B solvent exchange. Regards to the fibrous additives tested under Part B, the fibre glass (FG)

and the hemp fibres (HF) exhibited compressive strengths of 4.3 MPa and 4.9 MPa respectively. Flexural strength was also high as would be expected for fibre additives, strengths tested under Part B of 4.1 MPa and 6.2 MPa being recorded.

Table 4.4 Compressive and flexural strength specimen test results, Part B-Solvent exchange

1 Part	2 No	3 % wt. nano-filler/ lime	4 W/L	5 Storage condition 5 days % RH/ºC	6 Curing up to 28 days % RH/ºC	7 Compressive strength MPa	8 Flexural strength MPa
B	1	0 % Control	0.4	60/20	60/20	2.3	0.9
B	2	0 % Control	0.4	60/20	60/20	2.2	0.3
B	3	0 % Control	0.4	60/20	60/20	2.2	1.0
Av.						2.2	0.7
B	1	0.5 wt. % EG	0.4	60/20	60/20	2.8	1.7
B	2	0.5 wt. % EG	0.4	60/20	60/20	2.4	1.3
B	3	0.5 wt. % EG	0.4	60/20	60/20	2.3	-
Av.						2.5	1.5
B	1	1 wt. % EG	0.4	60/20	60/20	3.6	1.1
B	2	1 wt. % EG	0.4	60/20	60/20	3.8	1.2
B	3	1 wt. % EG	0.4	60/20	60/20	3.5	1.2
B	4	1 wt. % EG	0.4	60/20	60/20	3.1	-
B	5	1 wt. % EG	0.4	60/20	60/20	3.3	-
Av.						3.5	1.2
B	1	2 wt. % EG	0.4	60/20	60/20	3.3	1.4
B	2	2 wt. % EG	0.4	60/20	60/20	3.5	1.2
B	3	2 wt. % EG	0.4	60/20	60/20	2.8	1.3
B	4	2 wt. % EG	0.4	60/20	60/20	2.8	1.3
B	5	2 wt. % EG	0.4	60/20	60/20	3.0	1.2
Av.						3.1	1.1
B	1	2 wt. % nclay	0.4	60/20	60/20	4.9	1.5
B	2	2 wt. % nclay	0.4	60/20	60/20	2.9	1.6
B	3	2 wt. % nclay	0.4	60/20	60/20	3.5	
B	4	2 wt. % nclay	0.4	60/20	60/20	3.9	

Table 4.4 (Contiued) compressive and flexural strength specimen test results, Part B-Solvent exchange

1	2	3	4	5	6	7	8
Part	**No**	**% wt. nano-filler/ lime**	**W/L**	**Storage condition 5 days % RH/ºC**	**Curing up to 28 days % RH/ºC**	**Compressive strength MPa**	**Flexural strength MPa**
Av.						3.8	1.5
B	1	2 wt. % $nSiO_2$	0.4	60/20	60/20	2.21	0.7
B	2	2 wt. % $nSiO_2$	0.4	60/20	60/20	1.98	0.9
B	3	2 wt. % $nSiO_2$	0.4	60/20	60/20	2.37	-
B	4	2 wt. % $nSiO_2$	0.4	60/20	60/20	2.03	-
Av.						2.2	0.8
B	1	10 wt. % FG	0.4	60/20	60/20	4.92	3.8
B	2	10 wt. % FG	0.4	60/20	60/20	4.06	4.3
B	3	10 wt. % FG	0.4	60/20	60/20	4.02	-
B	4	10 wt. % FG	0.4	60/20	60/20	4.42	-
B	5	10 wt. % FG	0.4	60/20	60/20	4.21	-
Av.						4.3	4.1
B	1	80 wt. % PVAc	0.4	60/20	60/20	2.17	0.8
B	2	80 wt. % PVAc	0.4	60/20	60/20	2.16	-
Av.						2.2	0.8
B	1	40 wt. % PVAc	0.4	60/20	60/20	3.89	1.7
B	2	40 wt. % PVAc	0.4	60/20	60/20	2.88	
Av.						3.4	1.7
B	2	20 wt. % PVAc	0.4	60/20	60/20	3.86	1.3
B	3	20 wt. % PVAc	0.4	60/20	60/20	4.61	
Av.						4.2	1.3
B	1	8 wt. % PVAc	0.4	60/20	60/20	4.92	2.4
B	2	8 wt. % PVAc	0.4	60/20	60/20	4.92	
Av.						4.9	2.4

Table 4.4 (Contiued) Compressive and flexural strength specimen test results, Part B-Solvent exchange

1	2	3	4	5	6	7	8
Part	**No**	**% wt. nano-filler/ lime**	**W/L**	**Storage condition 5 days % RH/ºC**	**Curing up to 28 days % RH/ºC**	**Compressive strength MPa**	**Flexural strength MPa**
B	1	10 wt. % HF/L	0.4	60/20	60/20	4.9	6.2
Av.						4.9	6.2

The failure of the 10 wt. % FG/lime and 10 wt. % HF specimens in flexure mode appeared to be pulling out of the fibres. The failure wasn't by hemp fibre breakage as shown in Figure 4.20 and Figure 4.21. That means if the adhesion is increased between the hemp fibres and the lime binder, the flexural strength in particular will be increased. Therefore, in Part B, polyvinyl acetate (PVAc) adhesive was added at different percentages of water lime binder to determine the optimum percentage. The addition of PVAc generally showed that a lower quantity, 8 % - 12 % of lime, had a higher influence on compressive strength (4.9 MPa) and tensile strength (2.4 MPa). The next aim is to use PVAc with fibres to improve their bond. The optimum results of all fillers from Part A-Air cured were tested again in Part B using 0.4 W/L (as opposed to 0.5 W/L) and the solvent exchange method to evaluate their strength.

In addition, a new nanofiller called expanded graphite to improve the strength was also added in Part B. Mean compressive strength of 1 wt. % EG (3.5 MPa) was the highest results a mong 0.5 and 2 wt. % EG (2.5 and 3.1 MPa respectively).

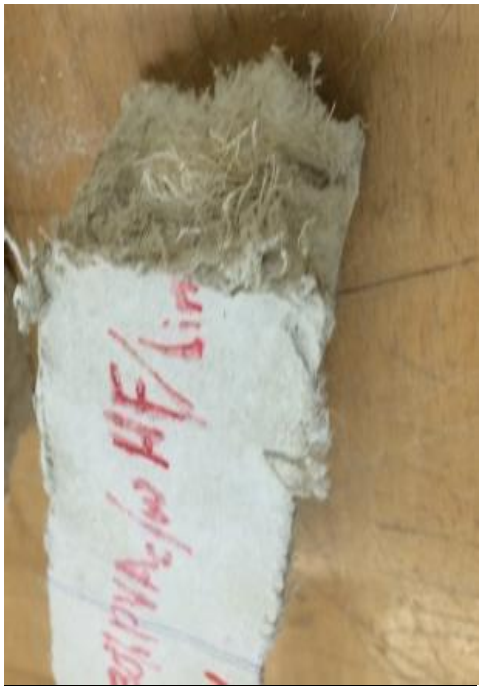

Figure 4.20 Hemp fibres with fibres pull-out failure mode

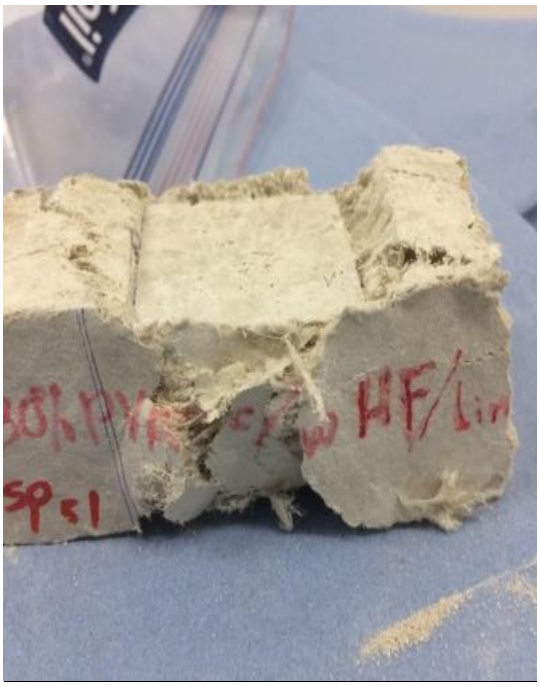

Figure 4.21 Hemp fibres lime composite ductility failure mode

4.5 Comparison of Part A-Air cured and Part B-Solvent exchange

From Table 9.2 (Chapter 9, Appendix), Table 4.3 and Figure 4.3, Section 4.3.1, it can be concluded that the compressive strength of Control specimens decreased by 24 % from Part A, 0.5 W/L, Air-curing to Part B solvent exchange drying, 0.4 W/L (2.9 MPa to 2.2 MPa). As for the flexural strength of the Control specimens, it decreased by approximately 36% from Part A to Part B (1.1 MPa-0.7 MPa). With regards to expanded graphite which wasn't used in Part A, adding 1 wt. % EG/L gave the optimum result, but it may be that if the dispersion of EG in lime at 2 wt. % was improved, the compressive and flexural strength will also be improved. Therefore, the specimens of 2 wt. % EG need further research. The EG particles can be seen in the bottom of the beaker when stopping the stirring which means the dispersion is not complete. As shown in Figure 4.22 and Figure 4.23, the compressive strength of EG/L was optimised at 1 wt. % but the flexural strength decreased with the further increase of EG percentages.

The compressive strength of 2 wt. % $nSiO_2$ slightly decreased from Part A to Part B from 2.8 MPa to 2.2 MPa. Regarding FG/L percentage (10 wt. %), compressive strength decreased from Part A to Part B from 10.7 MPa to 4.3 MPa, which means stopping the hydration affected the lime matrix but the adhesion between the FG and lime matrix became better probably by using the solvent exchange method since the flexural strength increased from 3.5 MPa to 4.1 MPa. It is shown that all results of compressive strength, except nanoclay, decreased from Part A ordinary curing, to Part B, solvent exchange. The flexural strength wasn't highly affected, but the compressive results were probably decreased due to stopping of hydration by the effect of solvent removing the free water. These effects were as a result of the change between the effect of changing the W/L from 0.5 to 0.4 and / or the effect of Solvent-exchange method.

The best percentage of PVAc was 8 wt. % of lime binder as shown in Figure 4.24 and Figure 4.25. However, based on the shape of the curve given in Figure 4.24 the optimum percentage is likely to be between 8 and 12 %. Hence both of these percentages will be considered and tested in future designs e.g. Part C_1 Oven drying, where fibres (hemp) will be added to the mix and these percentages (8 and 12 wt. % PVAc/L) will be tested as it was tested (12 %) in Part A-Air cured. Regarding the

adhesion property of PVAc, it was reported that polyvinyl acetate latex is good adhesives for paper, plastics, metal foil, leather, and cloth (Ebnesajjad, 2012). Adding 30 wt. PVAc (replacement) to melamine formaldehyde increased the bonding from 0 for PVAc pure to 2.5 MPa for composite (S. Kim & Kim, 2005). Adding 30% of fibre glass (E-glass) to PVAc, the product was many layers of fibreglass mat and polyvinyl acetate were combined on a mould. The material is flexible, translucent, and strong (Roth, 2014). These studies showed the capability of PVAc to increase bonding for many material other than wood, one of them is FG.

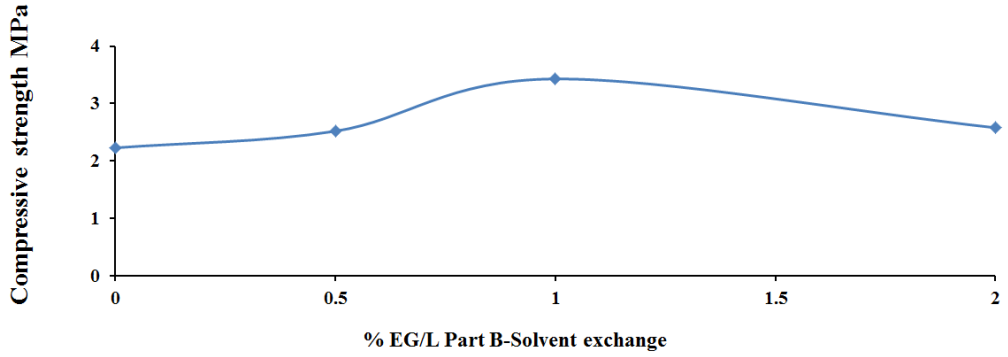

Figure 4.22 Compressive strength for different % wt. EG/L, Part B-Solvent exchange

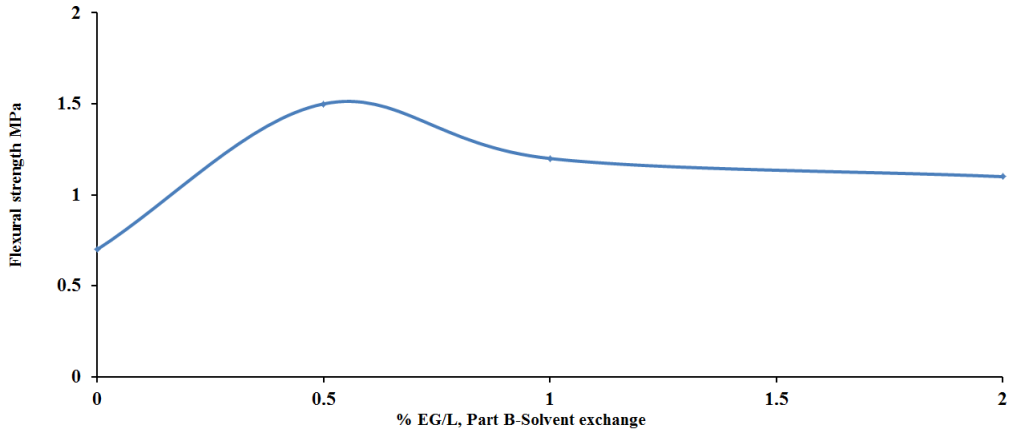

Figure 4.23 Flexural strength for different % wt. EG/L, Part B-Solvent exchange

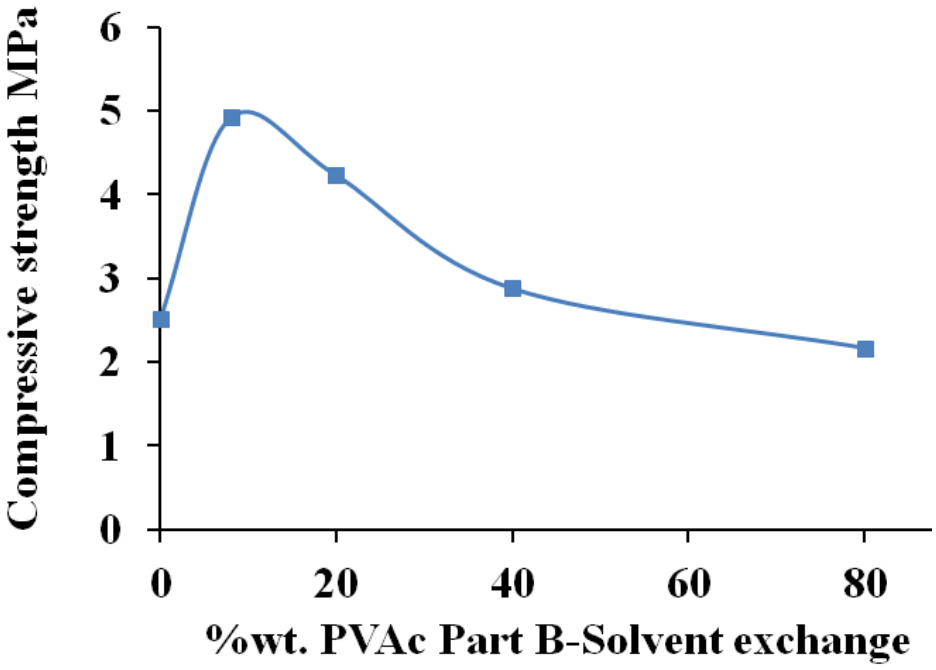

Figure 4.24 Compressive strength for different % PVAc/L Part B-Solvent exchange

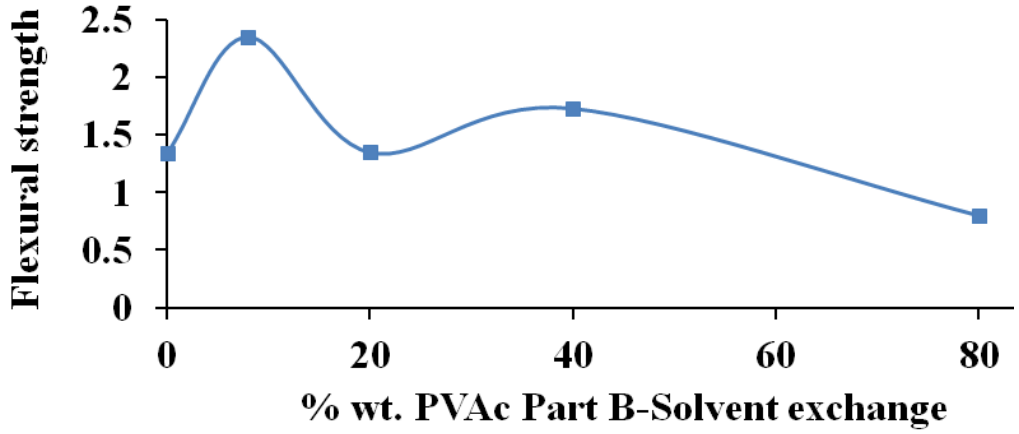

Figure 4.25 Flexural strength for different % PVAc/L, Part B-Solvent exchange

Table 4.5 provides a summary of mean values of compressive and flexural strength of Part B-Solvent exchange tests. The results are also shown graphically in Figure 4.26 and Figure 4.27. Table 4.5 B, shows the important results of Part B.

Table 4.5 Mean value of compressive and flexural strength, Part B Solvent exchange.

No	% wt. of filler	Mean Compressive strength MPa	STD	Mean Flexural strength MPa	STD
1	0 wt. % control	2.2	0.06	1.0	0.37
2	0.5 wt. % EG	2.5	0.30	1.5	0.28
3	1 wt. % EG	3.5	0.30	1.2	0.06
4	2 wt. % EG	3.1	0.31	1.1	0.08
5	2 wt. % nclay	3.8	0.84	1.6	0.07
6	2 wt.% $nSiO_2$	2.1	0.20	0.8	0.14
7	10 wt. % FG	4.3	0.36	4.1	0.35
8	80 wt. % PVAc/L	2.2	0.01	0.8	0
9	40 wt. % PVAc/L	3.4	0.71	1.7	0
10	20 wt. % PVAc/L	4.2	0.53	1.4	0
11	8 wt. % PVAc/L	4.9	0	2.4	0
12	10 wt.% HF/L	4.9	0	6.2	0

STD: standard deviation

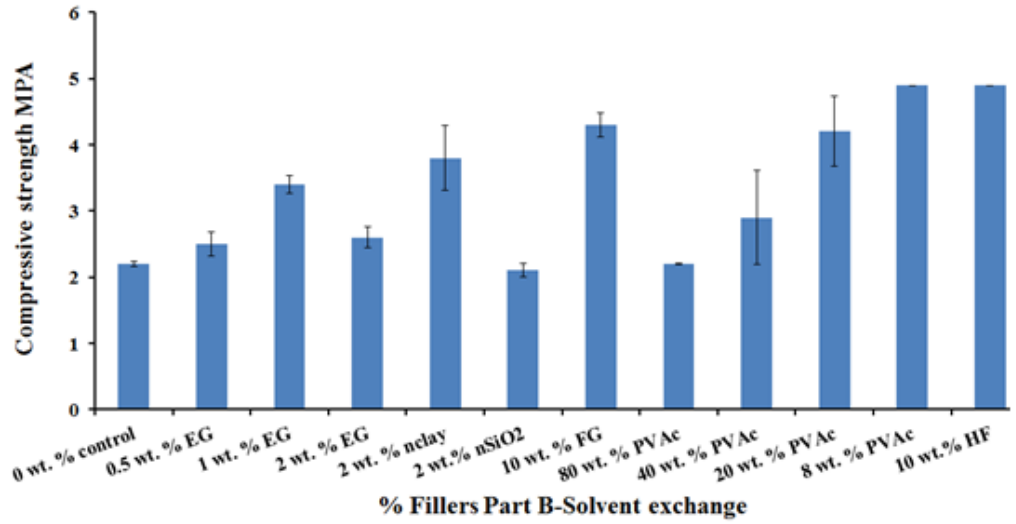

Figure 4.26 Mean compressive strength specimen results for Part B-Solvent exchange, Error bar ± < 1.

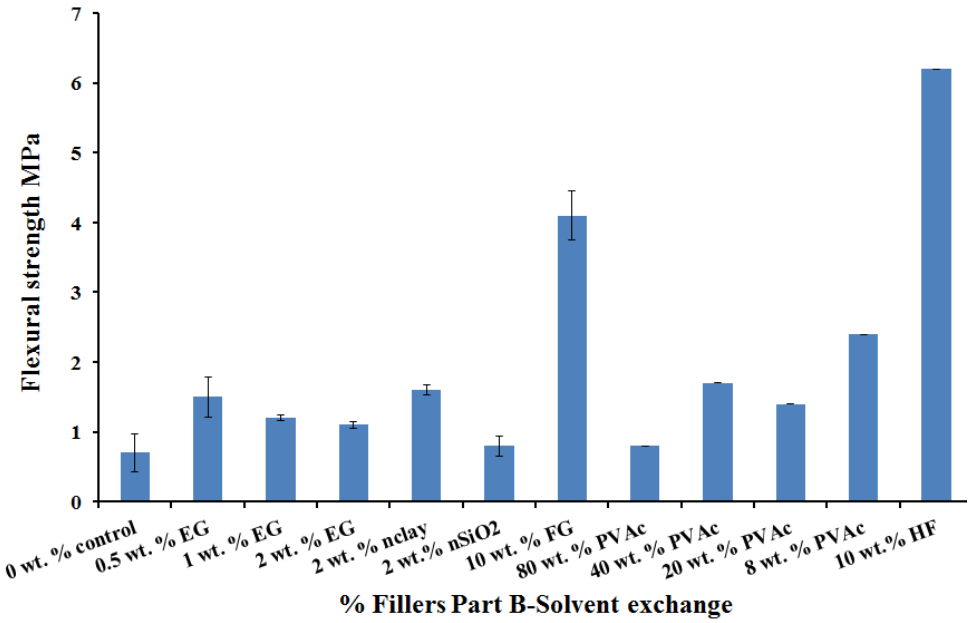

Figure 4.27 Mean flexural strength specimen results for Part B-Solvent exchange, Error bar ± < 1.

Table 4.5 B Summary of the optimum results of Part B-Solvent exchange

No	% Filler	Compressive strength MPa	Flexural strength MPa
1	1 wt. % EG	3.5	1.2
2	10 wt. % FG	4.3	4.1
3	8 wt. % PVAc/L	4.9	2.4
4	10 wt.% HF/L	4.9	6.2

4.6 Compressive and flexural strength specimen results for Part C-Oven dry cured.

In Part C, the compressive and flexural strength tests were conducted for the optimum results from Part A and Part B and new specimens of hemp fibres (HF), and hemp shives (HS), mixed with PVAc, were added to study their strength and the effect of the PVAc adhesive on their bonding. All tests in Part C_1 and C_2 were oven cured after demoulding at 5 days, 60 % humidity, 20 ºC until 26 days and 2 days 50°C in an oven. The water of mixture was 0.4 W/L. The difference between Parts C_1 and C_2 was the age of the specimens. The total age was 28 days in Part C_1 and 60 days in Part C_2, all stored under similar curing conditions (60 %RH, 20 ºC).

It was found that 86 % weight loss of cement paste (0.4 w/c) was completed at 9 hours using the Oven drying method for 1 day in an oven at 105°C (Canut, 2011). According to this loss (100 - 86= 14 %) and (water/cement (0.4 in this project) or 40 % - 14 % = 26 %) of the water cement ratio which is slightly lower than half of the water cement ratio by using Oven drying method remains.

4.6.1 Part C_1 Compressive and Flexural Strength Results

This part many tests were conducted for some specimens with fillers in previous Part B and new fillers for other specimens. The following is a summary of the tests:

1- Nclay/L (0.5, 1, and 2 wt. %).

2- FG/L (5 and 10 wt. %).

3- New tests for HF/L (5, 7 and 10) wt. %.

4- Repeat for nFc/L (5 wt. %) and new test for nFc (10 wt. %).

5- New tests for PVAc/L (8 and 12 wt. %) with 10 wt. % FG, PVAc /L.

6- New tests for 8 and 12 wt. % PVAc/L with 10 wt. % HF/L.

This part was done with many aims, to verify the nclay percentages (0.5, 1 and 2 wt. %) and its optimum percentage result which was found in the previous Parts A and B. Furthermore, nFc (5 and 10 wt. %) of lime, HF/L (5, 7 and 10 wt. %), 10 wt. % FG/L with 8 and 12 wt. % PVAc/L which was added to the mixture and 10 wt. HF %

/L with 8 and 12 wt. % PVAc/L were tested to find their optimum results of each material. PVAc was added here to enhance the adhesion between the fibres (hemp or glass).

In Part C_1 (Table 4.6) the compressive strength was increased in 1 wt. % and 3 wt. % nclay specimens (6.8 and 6.7 MPa) compared to 2 wt. % (5.2 MPa), 5 wt. % nFc (6.4 MPa) and 1 and 2 wt. % $nSiO_2$ (8.5 and 9.7 respectively) in comparison to neat lime (5.6 MPa). In contrast, the compressive strength decreased by adding 0.5 wt. % nclay (2.2 MPa), 3 wt. % $nSiO_2$ (4.5 MPa) compared to 2 wt. % (9.7 MPa), 1 and 2 wt. % EG (3.5 and 1.4 MPa respectively) and 10 wt. % nFc (4 MPa). The flexural strengths were still very low for all nanomaterial specimens. As for compressive strength with 10 wt. % FG, both 8 and 12 wt. % PVAc, FG, was 9.9 and 11.7 MPa respectively. For 10 wt. % HF mixed with both 8 and 12 wt. % PVAc 10 wt. % HF compressive strengths were 4.11 and 10.3 MPa respectively. The compressive strengths, therefore were highly improved along with the flexural strength (4.9, 4.7, 3.0 and 4.4 MPa respectively whereas neat lime was 0.9 MPa). Figure 4.28 and Figure 4.29 show the flexural loads vs deflection, the failure was graduated not sudden and this is highly wanted property in construction as it is safer. Figure 4.30 and Figure 4.31 show the effect of HF, FG and PVAc improvement in strength under the mean compressive and flexural loads in comparison to nanoclay, nanocellulose and pure lime.

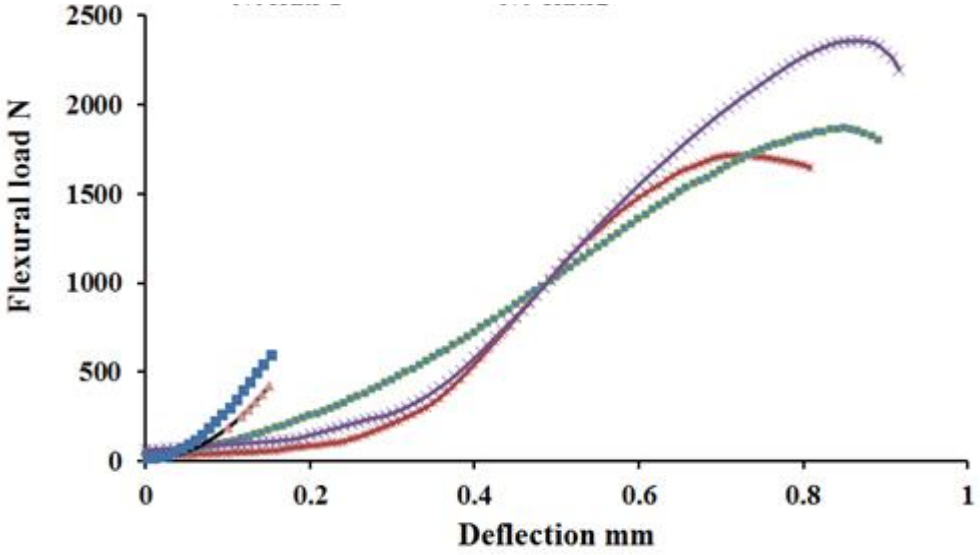

Figure 4.28 Comparison of flexural loads versus deflection of different percentages of FG/L with 12 wt. % PVAc/L (30 vol. % PVAc 0f water) and control specimens, Part C_1-Oven cured

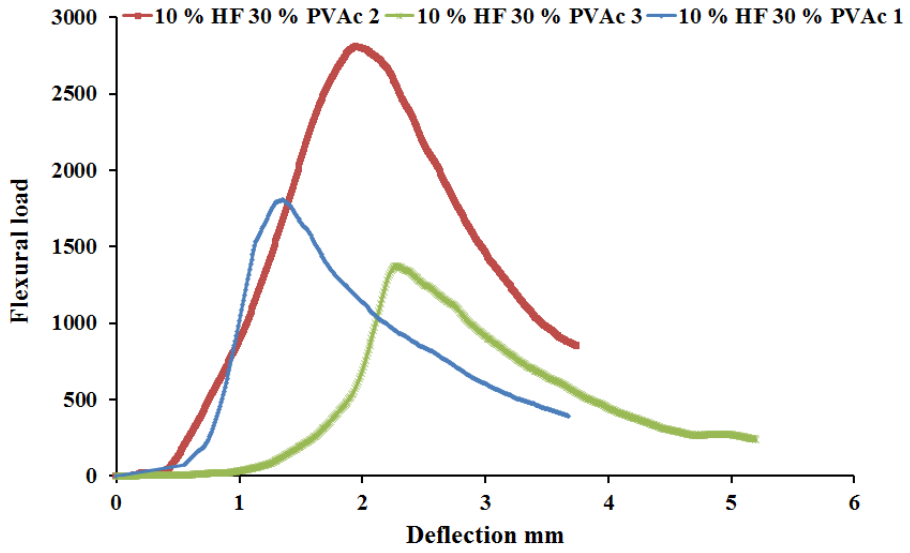

Figure 4.29 Comparison of flexural loads versus deflection of different percentages of HF/L with 12 wt. % of PVAc/L (30 vol. % PVAc of water) to control specimens, Part C_1-Oven cured

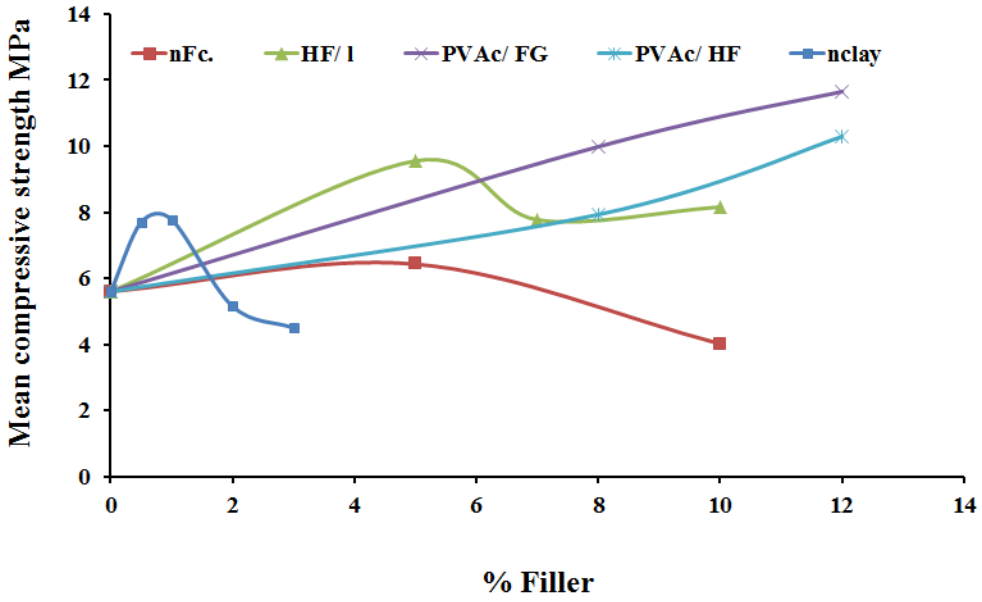

Figure 4.30 Mean compressive strength of Part C_1-Oven cured test specimens

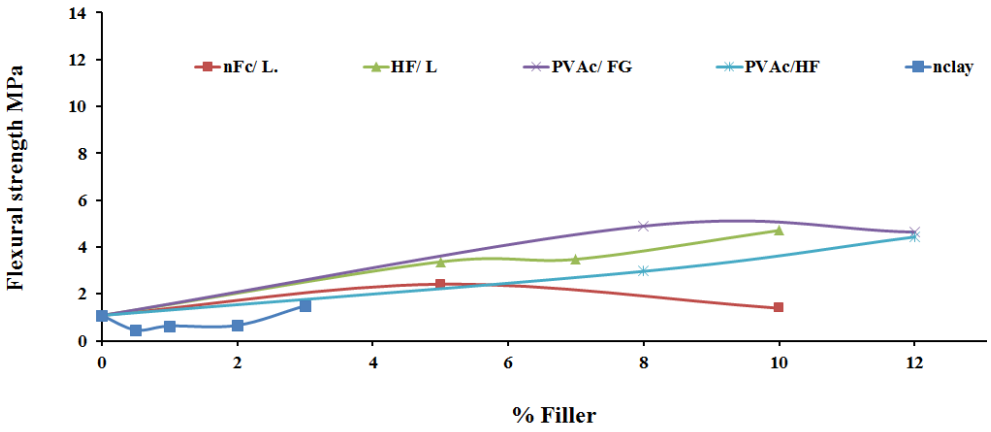

Figure 4.31 Mean flexural strength of Part C_1-Oven cured test specimens

Table 4.6 shows that the flexural strength of nanoclay was a little enhanced (0.4, 0.6, 0.7 and 1.5 MPa) with the increase of nanoclay percentages of 0.5, 1, 2 and 3 wt. %. With regard the low loading of nFc, 5 wt. %, the flexural strength was 2.4 MPa, higher than the 10 wt. % nFc (1.4 MPa)

In contrast, both compressive and flexural strengths were greatly improved by using fibres (HF and FG). Referring to Table 4.6, there is an increase in flexural strength with the use of 12 wt. % PVAc in comparison to using only HF. Compressive strengths at 5, 7 and 10 wt. % of HF/ L were 9.6, 7.4 and 8.7 MPa respectively and flexural strengths were 3.4, 3.5 and 4.7 MPa respectively. Figure 4.30 and Figure 4.31 show the mean compressive strengths of all specimen results of Part C_1-Oven cured. Figure 4.32, Figure 4.33 confirm the mean results of flexural and compressive strength for Part C_1-Oven cured. Figure 4.34 Figure 4.35 show not only the mean compressive strength and flexural strength but all specimen results with their means.

It can be said that the optimum results for both compressive and flexural strength of 12 wt. % PVAc as percentage of the mixture's water with 10 wt. % of FG or HF, were 11.7 and 10.3 MPa in compression, 4.7 and 4.4 MPa in flexure respectively. The 10 wt. % HF was consider better because although it has results very close to FG, it is compatible with the environment and is available as a renewable organic material from hemp plant.

Table 4.6 Compressive and flexural results, Part C_1-Oven cured

Part	No	% wt. nano-filler/ lime	W/L	Age at test days	Storage to 5 days %RH/ºC	Curing up to 28 days %RH/ºC	Compressive strength MPa	Flexural strength MPa
1	2	3	4	5	6	7	8	9
C_1	1	Control	0.4	28	60/20	60/20	5.4	1.3
C_1	2	Control	0.4	28	60/20	60/20	5.6	0.8
C_1	3	Control	0.4	28	60/20	60/20	5.9	1.2
C_1	4	Control	0.4	28	60/20	60/20	5.5	0.2
Av.							5.6	0.9
C_1	1	1wt. % nSiO2/L	0.4	28	60/20	60/20	7.9	2.6
C_1	2	1wt. % nSiO2/L	0.4	28	60/20	60/20	8.2	2.4
C_1	3	1wt. % nSiO2/L	0.4	28	60/20	60/20	8.5	2.3
C_1	4	1 wt. % nSiO2/L	0.4	28	60/20	60/20	9.1	-
C_1	5	1 wt. % nSiO2/L	0.4	28	60/20	60/20	8.9	-
C_1	6	1 wt. % nSiO2/L	0.4	28	60/20	60/20	8.3	-
Av.							8.5	2.4
C_1	1	2 wt.% nSiO2/L	0.4	28	60/20	60/20	10.2	0.2
C_1	2	2 wt. % nSiO2/L	0.4	28	60/20	60/20	9.5	0.3
C_1	3	2 wt. % nSiO2/L	0.4	28	60/20	60/20	9.1	0.2
C_1	4	2 wt. % nSiO2/L	0.4	28	60/20	60/20	9.1	0.2
C_1	5	2 wt. % nSiO2/L	0.4	28	60/20	60/20	10.7	
C_1	6	2 wt. % nSiO2/L	0.4	28	60/20	60/20	9.4	
Av.							9.7	0.2
C_1	1	3 wt. % nSiO2/L	0.4	28	60/20	60/20	4.5	0.1
C_1	2	3 wt. % nSiO2/L	0.4	28	60/20	60/20	4.7	0.4
C_1	3	3 wt. % nSiO2/L	0.4	28	60/20	60/20	4.6	0.4
C_1	4	3 wt. % nSiO2/L	0.4	28	60/20	60/20	4.1	-
C_1	5	3 wt. % nSiO2/L	0.4	28	60/20	60/20	4.6	-
C_1	6	3 wt. % nSiO2/L	0.4	28	60/20	60/20	4.35	-
Av.							4.5	0.3

Table 4.6 Compressive and flexural results, Part C_1-Oven cured

Part	No	% wt. nano-filler/ lime	W/L	Age at test days	Storage to 5 days %RH/ºC	Curing up to 28 days %RH/ºC	Compressive strength MPa	Flexural strength MPa
1	2	3	4	5	6	7	8	9
C_1	1	0.5 wt.% nclay/L	0.4	28	60/20	60/20	2.1	0.4
C_1	2	0.5 wt.% nclay/L	0.4	28	60/20	60/20	2.5	0.3
C_1	3	0.5 wt.% nclay/L	0.4	28	60/20	60/20	2.1	-
Av.							2.2	0.4
C_1	1	1 wt.% nclay/L	0.4	28	60/20	60/20	6.5	0.5
C_1	2	1 wt.% nclay/L	0.4	28	60/20	60/20	6.8	0.7
Av.							6.7	0.6
C_1	1	2 wt. % nclay/L	0.4	28	60/20	60/20	5.5	0.6
C_1	2	2 wt. % nclay/L	0.4	28	60/20	60/20	5.9	0.7
C_1	3	2 wt. % nclay/L	0.4	28	60/20	60/20	4.7	-
C_1	4	2 wt. % nclay/L	0.4	28	60/20	60/20	4.9	-
C_1	5	2 wt. % nclay/L	0.4	28	60/20	60/20	5.2	-
C_1	6	2 wt. % nclay/L	0.4	28	60/20	60/20	4.6	-
Av.							5.1	0.7
C_1	1	3 wt.% nclay/L	0.4	28	60/20	60/20	6.5	1.5
C_1	2	3 wt. % nclay/L	0.4	28	60/20	60/20	6.7	1.7
C_1	3	3 wt. % nclay/L	0.4	28	60/20	60/20	6.7	1.3
C_1	4	3 wt. % nclay/L	0.4	28	60/20	60/20	6.8	-
Av.							6.7	1.5
C_1	1	1 wt. % EG/L	0.4	28	60/20	60/20	3.6	1.9
C_1	2	1 wt. % EG/L	0.4	28	60/20	60/20	3.8	1.9
C_1	3	1 wt. % EG/L	0.4	28	60/20	60/20	3.5	1.1
C_1	4	1 wt. % EG/L	0.4	28	60/20	60/20	3.1	1.4
Av.							3.5	1.6
C_1	1	2 wt. % EG/L	0.4	28	60/20	60/20	1.4	1.6
C_1	2	2 wt. % EG/L	0.4	28	60/20	60/20	1.2	1.9
C_1	3	2 wt. % EG/L	0.4	28	60/20	60/20	1.3	1.6

Table 4.6 Compressive and flexural results, Part C_1-Oven cured

Part	No	% wt. nano-filler/ lime	W/L	Age at test days	Storage to 5 days %RH/ºC	Curing up to 28 days %RH/ºC	Compressive strength MPa	Flexural strength MPa
1	2	3	4	5	6	7	8	9
Av.							1.3	1.7
C_1	1	5 wt. % nFc/L	0.4	28	60/20	60/20	6.4	2.4
C_1	2	5 wt. % nFc/L	0.4	28	60/20	60/20	5.7	2.5
C_1	3	5 wt. % nFc/L	0.4	28	60/20	60/20	7.2	2.3
C_1	4	5 wt. % nFc/L	0.4	28	60/20	60/20	6.4	
C_1	5	5 wt. % nFc/L	0.4	28	60/20	60/20	6.4	
Av.							6.4	2.4
C_1	1	10 wt. % nFc/L	0.4	28	60/20	60/20	4.4	1.3
C_1	2	10 wt. % nFc/L	0.4	28	60/20	60/20	4.1	1.8
C_1	3	10 wt. % nFc/	0.4	28	60/20	60/20	4.3	1.1
C_1	4	10 wt. % nFc/L	0.4	28	60/20	60/20	3.8	
C_1	5	10 wt. % nFc/L	0.4	28	60/20	60/20	3.5	
C_1	6	10 wt. % nFc/L	0.4	28	60/20	60/20	3.9	
Av.							4.0	1.4
C_1	1	5 wt. % HF/L	0.4	28	60/20	60/20	9.5	3.2
C_1	2	5 wt. % HF/L	0.4	28	60/20	60/20	9.3	3.6
C_1	3	5 wt. % HF/L	0.4	28	60/20	60/20	9.7	3.4
C_1	4	5 wt. % HF/L	0.4	28	60/20	60/20	9.9	
C_1	5	5 wt. % HF/L	0.4	28	60/20	60/20	9.8	
C_1	6	5 wt. % HF/L	0.4	28	60/20	60/20	9.2	
Av.							9.6	3.4
C_1	1	7 wt. % HF/L	0.4	28	60/20	60/20	7.5	3.6
C_1	2	7 wt. % HF/L	0.4	28	60/20	60/20	6.7	3.3
C_1	3	7 wt. % HF/L	0.4	28	60/20	60/20	7.4	3.5
C_1	4	7 wt. % HF/L	0.4	28	60/20	60/20	7.8	-
C_1	5	7 wt. % HF/L	0.4	28	60/20	60/20	7.1	-
C_1	6	7 wt. % HF/L	0.4	28	60/20	60/20	7.7	-

Table 4.6 Compressive and flexural results, Part C_1-Oven cured

Part	No	% wt. nano-filler/ lime	W/L	Age at test days	Storage to 5 days %RH/ºC	Curing up to 28 days %RH/ºC	Compressive strength MPa	Flexural strength MPa
1	2	3	4	5	6	7	8	9
Av.							7.4	3.5
C_1	1	10 wt. % HF/L	0.4	28	60/20	60/20	8.7	4.7
C_1	2	10 wt. % HF/L	0.4	28	60/20	60/20	9.1	4.9
C_1	3	10 wt. % HF/L	0.4	28	60/20	60/20	8.0	4.5
C_1	4	10 wt. % HF/L	0.4	28	60/20	60/20	8.8	-
C_1	5	10 wt. % HF/L	0.4	28	60/20	60/20	8.9	-
Av.							8.7	4.7
C_1	1	8 wt. % PVAc,10 wt. % FG/L	0.4	28	60/20	60/20	9.1	5.3
C_1	2	8 wt. % PVAc,10 wt. % FG/L	0.4	28	60/20	60/20	10.9	4.4
C_1	3	8 wt. % PVAc,10 wt. % FG/L	0.4	28	60/20	60/20	10.1	5.0
C_1	4	8 wt. % PVAc,10 wt. % FG/L	0.4	28	60/20	60/20	9.9	-
C_1	5	8 wt. % PVAc,10 wt. % FG/L	0.4	28	60/20	60/20	9.5	-
C_1	6	8 wt. % PVAc,10 wt. % FG/L	0.4	28	60/20	60/20	10.4	-
Av.	.						9.9	4.9
C_1	1	12 wt. % PVAc,10 wt. % FG/L	0.4	28	60/20	60/20	12.1	4.0
C_1	2	12 wt. % PVAc,10 wt. % FG/L	0.4	28	60/20	60/20	11.1	4.4
C_1	3	12 wt. % PVAc,10 wt. % FG/L	0.4	28	60/20	60/20	10.1	5.5
C_1	4	12 wt. % PVAc,10 wt. %	0.4	28	60/20	60/20	12.3	-

Table 4.6 Compressive and flexural results, Part C_1-Oven cured

Part	No	% wt. nano-filler/ lime	W/L	Age at test days	Storage to 5 days %RH/ºC	Curing up to 28 days %RH/ºC	Compressive strength MPa	Flexural strength MPa
1	2	3	4	5	6	7	8	9
C_1	5	FG/L 12 wt. % PVAc,10 wt. % FG/L	0.4	28	60/20	60/20	12.7	-
Av.							11.7	4.6
C_1	1	8 wt. % PVAc,10 wt. % HF/L	0.4	28	60/20	60/20	8.1	2.6
C_1	2	8 wt. % PVAc,10 wt. % HF/L	0.4	28	60/20	60/20	8.7	2.6
C_1	3	8 wt. % PVAc,10 wt. % HF/L	0.4	28	60/20	60/20	7.4	3.7

Table 4.12 (Continued) Compressive and flexural results, Part C_1-Oven cured

Part	No	% wt. nano-filler/ lime	W/L	Age at test day	Storage to 5 days %RH/ºC	Curing up to 28 days %RH/ºC	Compressive strength MPa	Flexural strength MPa
1	2	3	4	5	6	7	8	9
C_1	4	8 wt. % PVAc,10 wt. % HF/L	0.4	28	60/20	60/20	7.4	-
C_1	5	8 wt. % PVAc,10 wt. % HF/L	0.4	28	60/20	60/20	8.3	-
C_1	6	8 wt. % PVAc,10 wt. % HF/L	0.4	28	60/20	60/20	7.6	-
Av.							7.9	3.0
C_1	1	12 wt. % PVAc,10 wt. % HF/L	0.4	28	60/20	60/20	8.2	4.2
C_1	2	12 wt. % PVAc,10 wt. % HF/L	0.4	28	60/20	60/20	8.8	6.6
C_1	3	12 wt. % PVAc,10 wt. % HF/L	0.4	28	60/20	60/20	11.3	3.2
C_1	4	12 wt. % PVAc,10 wt. % HF/L	0.4	28	60/20	60/20	12.2	3.7
C_1	5	12 wt. % PVAc,10 wt. % HF/L	0.4	28	60/20	60/20	10.4	-
C_1	6	12 wt. % PVAc,10 wt. % HF/L	0.4	28	60/20	60/20	12.8	-
C_1	7	12 wt. % PVAc,10 wt. % HF/L	0.4	28	60/20	60/20	9.4	-
C_1	8	12 wt. % PVAc,10 wt. % HF/L	0.4	28	60/20	60/20	9.2	-

Table 4.6 Compressive and flexural results, Part C_1-Oven cured

Part	No	% wt. nano-filler/ lime	W/L	Age at test days	Storage to 5 days %RH/ºC	Curing up to 28 days %RH/ºC	Compressive strength MPa	Flexural strength MPa	
1	2	3	4	5	6	7	8	9	
Av.								10.3	4.4
C_1	1	20 wt. % HS/L		0.4	28	60/20	60/20	0.6	0.2
C_1	2	20 wt. % HS/L		0.4	28	60/20	60/20	0.6	0.2
C_1	3	20 wt. % HS/L		0.4	28	60/20	60/20	0.5	
C_1	4	20 wt. % HS/L		0.4	28	60/20	60/20	0.5	
C_1	5	20 wt. % HS/L		0.4	28	60/20	60/20	0.4	
C_1	6	20 wt. % HS/L		0.4	28	60/20	60/20	0.8	
Av.								0.6	0.2
C_1	1	12 wt. % PVAc 20 wt. % HS/L		0.4	28	60/20	60/20	0.9	0.9
C_1	2	12 wt. % PVAc 20 wt. % HS/L		0.4	28	60/20	60/20	0.9	0.9
C_1	3	12 wt. % PVAc 20 wt. % HS/L		0.4	28	60/20	60/20	0.8	0.8
C_1	4	12 wt. % PVAc 20 wt. % HS/L		0.4	28	60/20	60/20	0.8	0.8
C_1	5	12 wt. % PVAc 20 wt. % HS/L		0.4	28	60/20	60/20	0.8	0.8
C_1	6	12 wt. % PVAc 20 wt. % HS/L		0.4	28	60/20	60/20	0.9	0.9
Av.								0.9	0.9

Referring to Table 4.6, the optimum result in compressive strength of nanoclay/L was 6.7 MPa at 1 wt. % in comparison to 2.2 MPa of 0.5 wt. %. The highest flexural strength result was 0.6 MPa at 1 wt. % nclay. It can be said the 2 wt. % nclay, which gave a lower compressive strength (5.2 MPa), wasn't dispersed very well.

The compressive strength for 5 wt. % nFc was 6.4 MPa, which was higher than 10 wt. % which gave 4.0 MPa. 5 wt. %, therefore, was the optimum percent of nFc in this research.

The optimum result of HF/L was 10 wt. %, giving the highest compressive and flexural strength, 8.7 MPa and 4.7 MPa respectively. In contrast, flexural strength of 5 and 7 wt. % HF/L were lower, relatively, being 3.4 and 3.5 MPa respectively, in spite of them having relatively high compressive strengths (9.5 and 7.4 MPa respectively).

Adding PVAc to the mixture was done to increase the adhesion between the fibres and the lime matrix, 12 wt. % of PVAc to the weight of water was the optimum ratio which improved the compressive strength from 10.0 MPa at 8 wt. % PVAc to W/L to 11.7 MPa at 12 wt. % PVAc to W/L. The flexural strengths were almost equal (4.9 and 4.7 MPa respectively). In contrast, flexural strength of 5 and 7 wt. % HF/L were lower than 10 wt. % HF/L, they were 3.4 and 3.5 MPa respectively, compared to 9.5 and 7.4 MPa respectively.

When the HF was used in place of FG, the optimum percentage was 12 wt. % of PVAc/L, which improved both flexural and compressive strength by more than 8 %. The compressive strength increased from 7.9 to 10.3 MPa and the flexural strength increased from 3.0 to 4.4 MPa.

The flexural strength of cement mortar is about 4.0 MPa for cement: sand at a ratio of 1:2 (Aho & Ndububa, 2015). Using the flexural strength of cement mortar as a guide, it was shown that the flexural strength of 10 wt. % HF/L mixed with 12 wt. % PVAc to the weight of water of the mixture was very good (4.4 MPa). The compressive strength of 10.3 MPa was well more than the load bearing material limit (3-5 MPa) as mentioned before (de Bruijn et al., 2009).

This percentage of HF, PVAc/L to lime (10 wt. % HF/L and 12 wt. % PVAc/L and 0.4 W/L) is the optimum result. It is environmentally friendly in comparison to FG. The sustainability of HF cannot be compared with industrial fibres like fibre glass.

Figure 4.28 and Figure 4.29 show a graphical display of flexural loads (N) versus deflection (mm). They show the enhanced performance by adding nanomaterials (nclay, EG, $nSiO_2$), a good improvement using FG and an even better performance by using FG or HF mixed with PVAc (8 and 12 %)/L. The highest result was by adding 12 wt. % PVAc/L to the HF/L or to the FG/L as it mentioned previously.

Referring to Table 4.7, Figure 4.32 and Figure 4.33 show a comparison between the mean compressive and flexural strength specimen results of all percentage nanofillers of Part C_1-Oven cured. Figure 4.34 and Figure 4.35 show graphically the compressive and flexural strength for each specimen and for Part C_1-Oven cured which includes 20 % hemp shives blended with or without 12 % PVAc of water to lime binder. They were very weak in both compressive and flexural strength, for 20 wt. % HS/L the mean were 0.6 and 0.2 MPa respectively and for 20 wt. % HS/L blended with 12 wt. % PVAc of water, the compressive and flexural strength were 0.9 and 0.5 MPa respectively. This low results because HS which have large volume aren't distributed as HF which are very thin chopped and more strong than HS.

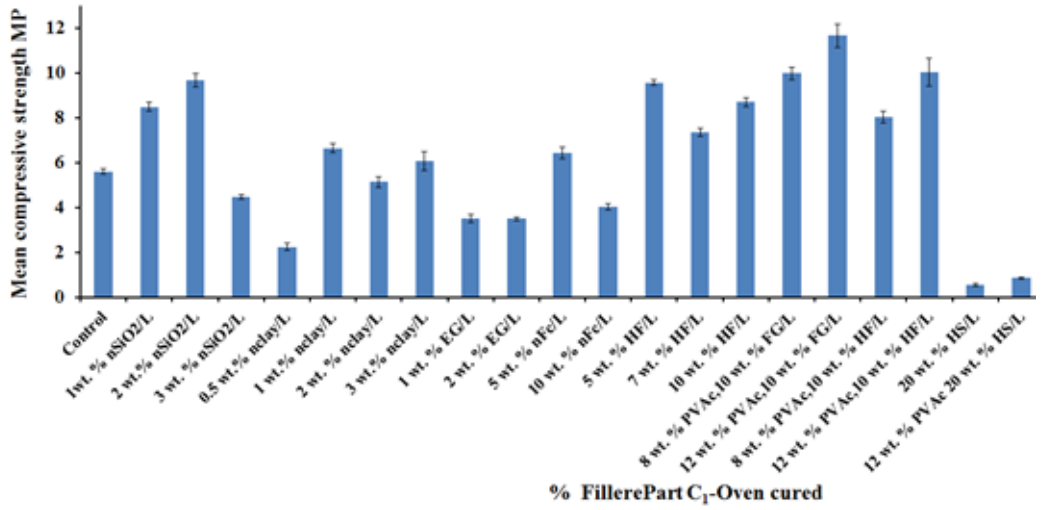

Figure 4.32 Mean compressive strength of Part C_1- Oven cured specimens, Error bar ± < 1.

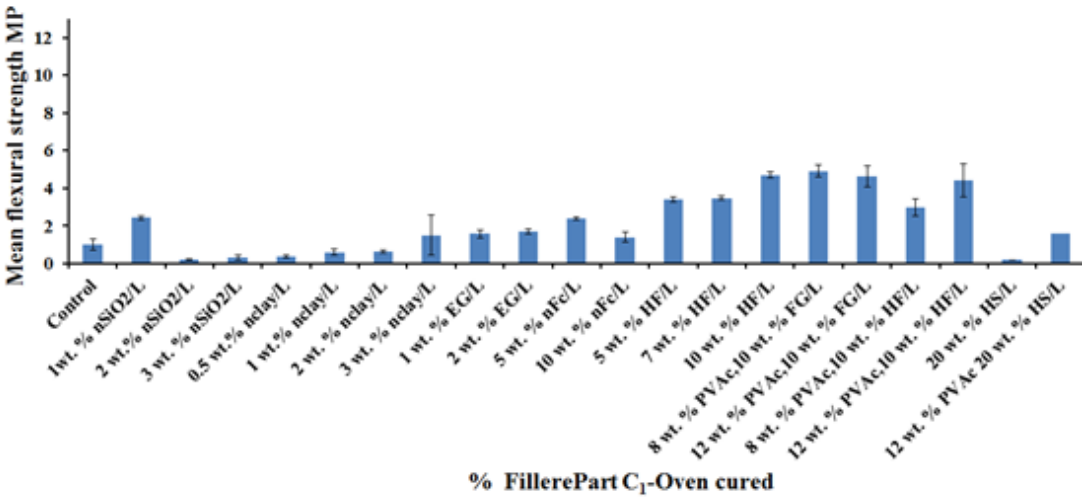

Figure 4.33 Mean flexural strength of Part C_1- Oven cured specimens, Error bar ± < 1.

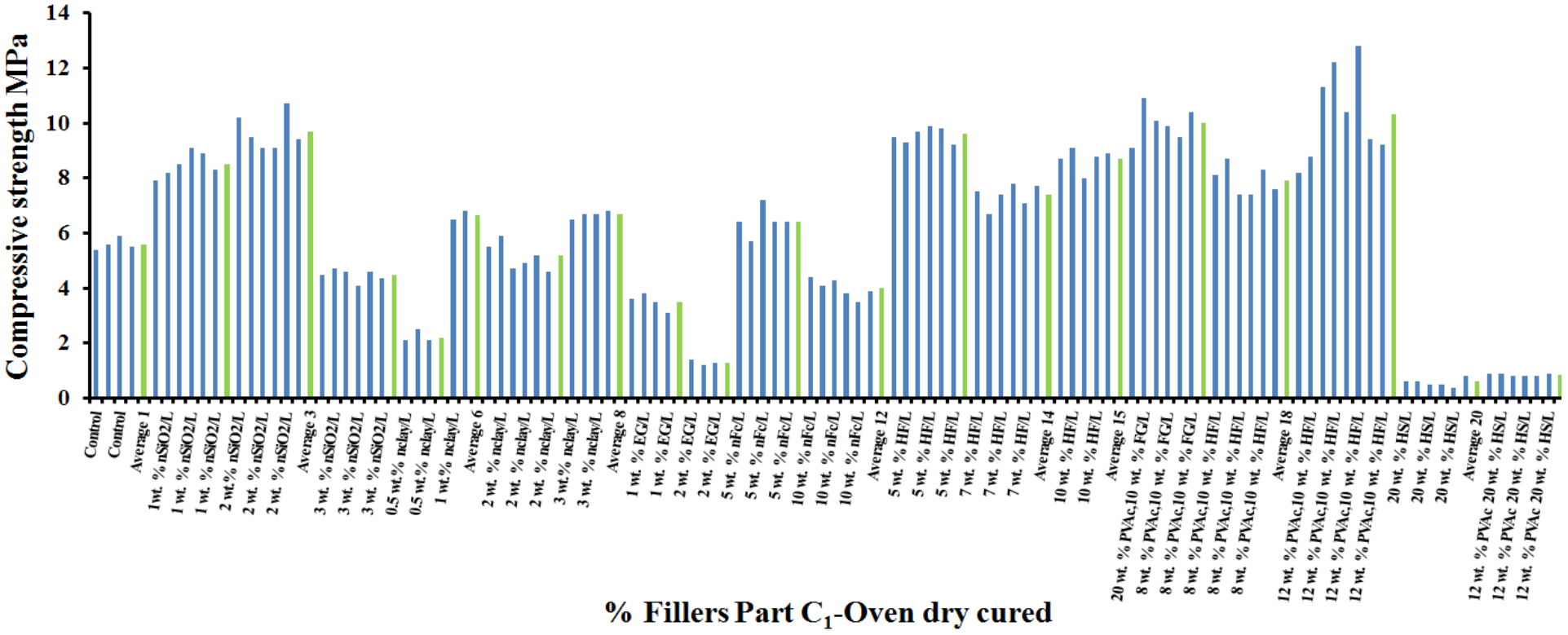

Figure 4.34 Compressive strength of specimens and their means Part C_1- Oven cured

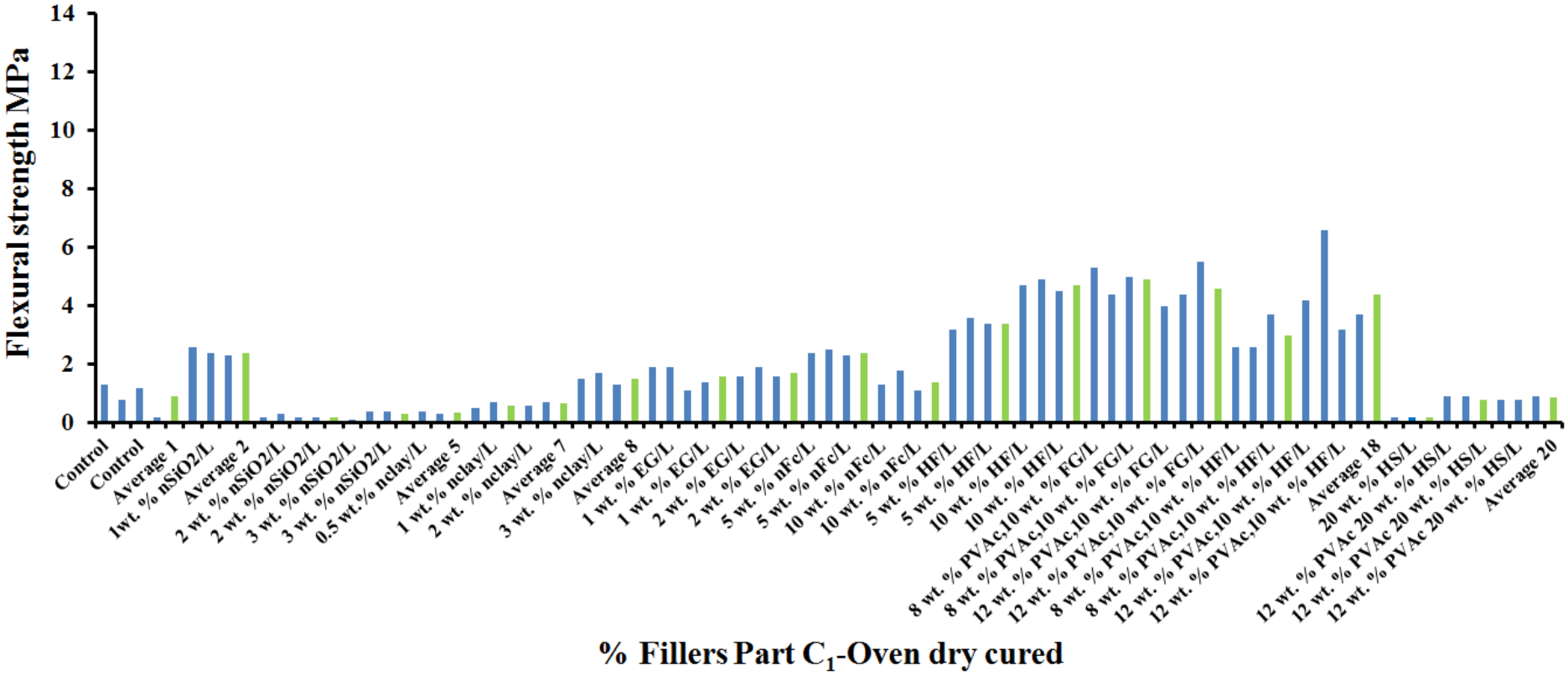

Figure 4.35 Flexural strength of specimens and their means Part C_1-Oven dry cured

Table 4.7 Mean compressive and flexural strength specimen results, Part C_1- Oven cured

No	% wt. filler	Mean compressive strength MPa	STD	Mean flexural strength MPa	STD
1	Control	5.6	0.22	0.9	0.54
2	1wt. % $nSiO_2$	8.5	0.45	2.4	0.15
3	2 wt. % $nSiO_2$	9.7	0.65	0.2	0.05
4	3 wt. % $nSiO_3$	4.5	0.21	0.3	0.17
5	0.5 wt. % nclay	2.2	0.23	0.4	0.07
6	1 wt. % nclay	6.7	0.21	0.6	0.14
7	2 wt. % nclay	5.1	0.50	0.7	0.07
8	3 wt. % nclay	6.7	0.94	1.5	1.5
9	1 wt. % EG	3.5	0.29	1.6	0.39
10	2 wt. % EG	1.4	0.10	1.7	0.17
11	5 wt. % nFc	6.4	0.53	2.4	0.10
12	10 wt. % nFc	4.0	0.33	1.4	0.36
13	5 wt. % HF/ L	9.6	0.28	3.4	0.20
14	7 wt. %HF/ L	7.4	0.41	3.5	0.15
15	10 wt. % HF/ L	8.7	0.42	4.7	0.20
16	8 wt. % PVAc + 10 wt. % FG/L	9.9	0.64	4.9	0.46
17	12 wt. % PVAc + 10 wt. % FG/L	11.7	1.00	4.6	0.77
18	8 wt. % PVAc + 10 wt. % HF/L	7.9	0.53	3.0	0.64
19	12 wt. % PVAc + 10 wt. %HF/L	10.3	1.67	4.4	1.51
20	20 wt. %HS/L	0.6	0.14	0.2	0
21	20 wt. % HS/L + 12 wt. %PVAc	0.9	0.05	0.9	0.055161,

The important results in Part C1were summarised in Table 4.7 C as outcome of this part in developing strength.

Table 4.7 C Summary of the optimum results of Part B-Solvent exchange

No	% Filler	Compressive strength MPa	Flexural strength MPa
1	1wt. % $nSiO_2$	8.5	2.4
2	3 wt. % nclay	6.7	1.5
3	1 wt. % EG	3.5	1.6
4	5 wt. % nFc	6.4	2.4
5	10 wt. % HF/ L	8.7	4.7
6	20 wt. % HS/L + 12 wt. %PVAc	0.9	0.9
7	12 wt. % PVAc + 10 wt. % FG/L	11.7	4.6
8	12 wt. % PVAc + 10 wt. %HF/L	10.3	4.4

4.6.2 Compressive and Flexural Strength Part C_2-Oven cured

Part C_2-Oven cured also used the oven dry method, similar to Part C_1, but the curing time was 60 days as opposed to 28 days. The specimens were Control, 2 wt. % nclay and 2 wt. $nSiO_2$ and 2 wt. % EG specimens. Part C_2 was conducted to reconfirm the optimum percentage of nanofiller obtained from previous tests Part C_1-Oven cured. These specimens were also used for studying shrinkage after demoulding at 5 days and drying 2 days in an oven at 28 days. Following shrinkage tests, their compressive and flexural strength were tested, after 5 days demoulding, put in storage at 60 % RH, 20ºC curing and 0.4 W/ L and tested for shrinkage up 28 days, then tested for strength (compressive and flexural) at 60 days. The results are shown in Table 4.8 and presented graphically in Figure 4.36 and Figure 4.37.

The compressive strength results from Part A and Part C_2 were almost equal or increased slightly. For example, compressive strength of control specimens was 3.1 MPa in Part A but increased to 4.9 MPa in Part C_2. The difference is likely to have come from the decrease in the water lime ratio which affected the pore sizes (decreased) and from the age of the specimens (60 days) as the strength has probably increased with time. The flexural strength increase, for example, at 0 wt. % it was 1.1 MPa in Part A and 3.1 MPa in Part C_2 for the same reason, but here, the effect of water decrease was higher due to the flexural strength being very sensitive to pore sizes which decreased by decreasing the water.

There was a slight increase in compressive strength of 2 wt. % nclay from 3.5 MPa in Part A to 3.9 MPa in Part C_2. The flexural strength increased from 0.7 MPa in Part A to 1.8 MPa in Part C_2. There was also an increase in compressive strength for 2 wt. % nSiO_2 between Part A and Part C_2. It increased from 2.8 to 4.0 MPa. There was also a slight increase in flexural strength from 0.3 to 0.9 MPa.

Table 4.8 Part C_2-Oven cured compressive and flexural strength

Part	No	% wt. nano-filler/ lime	W/L	Age at test days	Storage condition to 5 days %RH/ ºC	Curing up to 60 days %RH/ ºC	Mean Compressive strength MPa	Mean flexural strength MPa
C_2	1	0 wt. % control	0.4	60	60/20	60/20	4.9	3.1
C_2	2	2 wt. % nclay	0.4	60	60/20	60/20	3.9	1.8
C_2	3	2 wt. % EG	0.4	60	60/20	60/20	2.9	3.7
C_2	4	2 wt. % $nSiO_2$	0.4	60	60/20	60/20	4.0	0.9

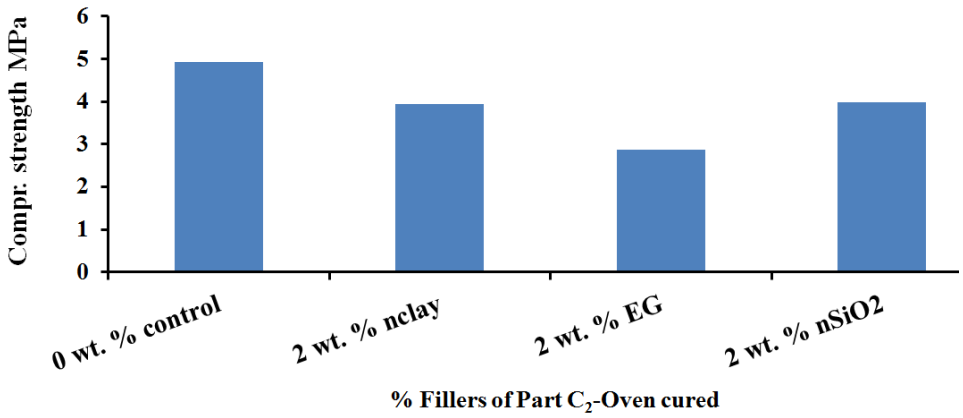

Figure 4.36 Mean compressive strength of Part C_2-Oven cured

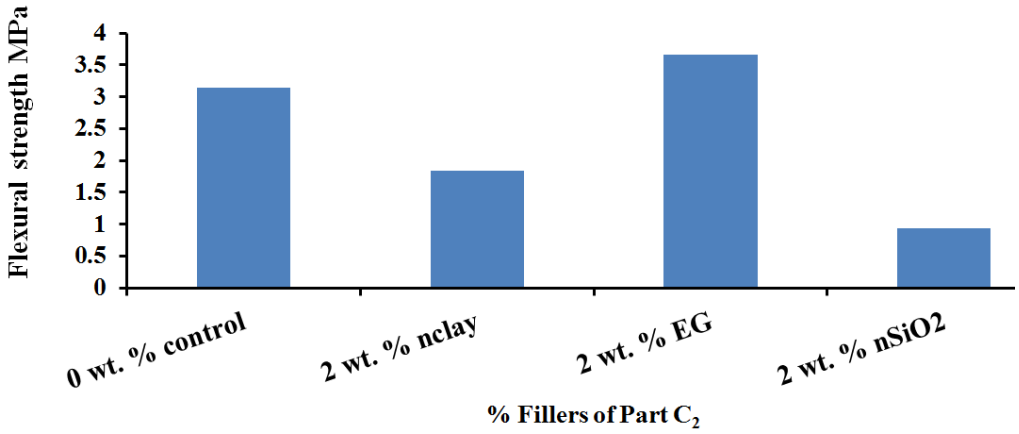

Figure 4.37 Mean flexural strength of Part C_2-Oven cured

4.7 Summary of Results

A summary of the mean compressive and flexural strengths from Chapter 4 for all parts (Part A-Air curing, Part B-Solvent exchange, and Part C-Oven drying) are shown in T 4.9,

4.7.1 Part A-Air Cured

Referring to Table 4.9, **Part A-Air cured**, it can be seen that:

- Flexural strengths of nanomaterials Control, 2.0% nSiO2, 4.0% nSiO2, 0.5 % nClay, 1.0% nClay, 2.0% nClay, 5.0% nFC and 7.0% nFC were 0.3, 0.9, 0.3, 0.6, 0.7, 0.3 and 0.9 MPa respectively and were all lower than pure lime (1.1 MPa) except FG at 5, 15 and 10 wt. % which gave 2.2, 1.9 and 3.6 MPa respectively. The optimum percentage of FG was 10 wt. % giving 3.6 MPa in flexural strength and it was the highest result of all added fillers in Part A.

- The compressive strength results range of all materials except HF and PVAc with nZnO in Part A (4.3-4.5 MPa) is slightly enhanced but still around the value of the control specimens (4.2 MPa). This weakness was possibly due to the W/L ratio which was 0.5.

- The highest result was 17.7 MPa and 7.3 MPA of compressive and flexural strength respectively which was 4 wt.% nZnO, 10 wt. HF and 12 wt. % PVAc of water. This results was the highest result of the whole project of all parts (A-Air cured, B-Solvent exchange and C_1 and C_2 - Oven cured).

- There was a small increase in compressive strength by adding nanomaterials such as 1 wt. % EG and 2 wt. % nclay (3.4 and 3.8 MPa) but was still lower than pure lime in Part A (4.3 MPa)
- However, 10 wt. % FG and 10 wt. % HF gave the highest results in both compressive and flexural strength (4.3, 4.9 MPa in compressive strength repectively and 4.1, 6.2 MPa in flexural strength respectively)

- The hemp fibre lime composite HF/L was cosidered the best composite, it gave the second highest results after the fibre glass in compressive and flexural strength of all fillers.

4.7.2 Part B-Solvent Exchange

Referring to Table 4.9, Part B-Solvent exchange, the water binder ratio was reduced to 0.4 W/ L.

The average compressive strength of control specimens was 2.2 MPa which was about half of its value in Part A control specimens (4.3 MPa). The compressive strength for 7 days by solvent water removal as reported and 28 days test therefore was higher than 28 days under ordinary air curing by 0.2 MPa. Also, for 91 days of ordinary air curing, compressive strength was 1.1 MPa lower than 28 days by using solvent exchange at 1.8 MPa (Alvarez et al., 2013).

Table 4.9 Summary of test results

Curing Method	**Part A Air drying** • Stored throughout at 20°C/60% RH • Demoulded at 5 days Cured for +23 days	**Part B Solvent exchange** • Demoulded at 5 days • Immersed in isopropanol for +7 days • 20°C/60% RH for +14 days • Oven for +2 days (26-27) (50°C)	**Part C_1 Oven drying** • Demoulded at 5 days • 20°C/60% RH for +21 days • Oven for +2 days 50°C **Part C_2 Oven drying** • Shrinkage test days (5-28) test • Oven for +2 days (29-30) (50°C) • Water absorption test days (31-32) • 20°C/60% RH for +51 days

Strength (N/mm^2)				**C**	**F**				**C**	**F**				**C**	**F**
		Table	**W/L**				**Table**	**W/L**				**Table**	**W/L**		
	Part A					**Part B**					**Part C_1**				
	Control	4.3	0.5	2.9	1.1	Control	4.9	0.4	2.2	0.7	Control	4.11	0.4	5.6	0.9
	2.0% $nSiO_2$	4.4	0.5	2.8	0.4	0.5% EG	4.9	0.4	2.5	1.5	0.5% nClay	4.11	0.4	2.2	0.4
	4.0% $nSiO_2$	4.4	0.5	2.7	0.8	1.0% EG	4.9	0.4	3.4	1.2	1.0% nClay	4.11	0.4	6.8	0.6
	0.5% nClay	4.5	0.5	2.9	0.3	2.0% EG	4.9	0.4	2.6	1.1	2.0% nClay	4.11	0.4	5.2	0.7
	1.0% nClay	4.5	0.5	2.9	0.6	2.0% nClay	4.9	0.4	3.8	1.6	3.0% nClay	4.11	0.4	6.7	1.5
	2.0% nClay	4.5	0.5	3.6	0.7	2.0% $nSiO_2$	4.9	0.4	2.2	0.8	1.0% $nSiO_2$	4.11	0.4	8.5	2.4
	5.0% nFC	4.6	0.5	2.3	0.3	10% FG	4.9	0.4	4.3	4.1	2.0% $nSiO_2$	4.11	0.4	9.7	0.2
	7.0% nFC	4.6	0.5	2.3	0.8	80% PVAc	4.9	0.4	2.2	0.8	3.0% $nSiO_2$	4.11	0.4	4.5	0.3
	5.0% FG	4.7	0.5	3.4	2.2	40% PVAc	4.9	0.4	2.9	1.7	1.0% EG	4.11	0.4	3.5	1.6
	10% FG	4.7	0.5	10.7	3.6	20% PVAc	4.9	0.4	4.2	1.3	2.0% EG	4.11	0.4	1.4	1.7
	15% FG	4.7	0.5	6.7	1.9	8% PVAc	4.9	0.4	4.9	2.4	5.0% nFC	4.11	0.4	6.4	2.4
	(4% nZnO)	4.8	0.4	0.7	0.6	10% HF	4.9	0.4	4.9	6.2	10% nFC	4.11	0.4	4.0	1.4
Nanofiller/L	12%PVAc, 10% HF, 4% nZnO)	4.8	0.4	17.7	7.3						5.0% HF	4.11	0.4	9.6	3.4
											7.0% HF	4.11	0.4	7.4	3.5

Table 4.9 Summary of test results

Curing Method	Part A Air drying • Stored throughout at 20°C/60% RH • Demoulded at 5 days Cured for +23 days	Part B Solvent exchange • Demoulded at 5 days • Immersed in isopropanol for +7 days • 20°C/60% RH for +14 days • Oven for +2 days (26-27) (50°C)	Part C_1 Oven drying • Demoulded at 5 days • 20°C/60% RH for +21 days • Oven for +2 days 50°C Part C_2 Oven drying • Shrinkage test days (5-28) test • Oven for +2 days (29-30) (50°C) • Water absorption test days (31-32) • 20°C/60% RH for +51 days

Strength (N/mm^2)			C	F			C	F				C	F
	Table	W/L			Table	W/L				Table	W/L		
									10% HF	4.11	0.4	8.7	4.7
									20% HS	4.11	0.4	0.6	0.2
									12% PVAc,20% HS	4.11	0.4	0.9	0.5
									8% PVAc / 10% FG	4.11	0.4	9.9	4.9
									12% PVAc / 10% FG	4.11	0.4	11.7	4.7
									8% PVAc / 10% HF	4.11	0.4	4.11	3.0
									12% PVAc / 10% HF	4.11	0.4	10.3	4.4
									Part C_2				
Nanofille									Control	4.13	0.4	4.9	3.1
									2.0% nClay	4.13	0.4	3.9	1.8
									2.0% EG	4.13	0.4	2.9	3.7
									2.0% $nSiO_2$	4.13	0.4	4.0	0.9

4.7.3 Part C-Oven Drying

The last method, Part C-Oven dried results were adopted for strength improvement because it was different from Part B-Solvent exchange. The hydration doesn't stop but the water dries slowly at 50ºC for two days in the oven which is a period long enough for hydration and quick maturing. It gave higher results than both Part A and Part B except 4 wt. % nZnO and 12 wt. % PVAc of water with 10 wt. % HF in Part A which gave 17.7 and 7.3 MPA (compressive and flexural strength respectively). Part C_2 results were lower than the results in Part C_1. This has probably come from the effect of water content changes from the water absorption (the specimens were firstly tested for water absorption). The water was under the surface of the specimens (in touch with the lower side). The water level was gradually raised by capillary action within two days. The water absorption specimens were dried to prepare the specimens for the strength tests. The gradually saturation and drying might cause some reactions and components dissolved.

- The flexural strength in Part C_1-Oven dried curing compared with the cement mortar strength, was lower than the flexural strength of cement mortar which was about 4 MPa for cement: sand at a 0.5 water cement ratio (Aho & Ndububa, 2015), The values of flexural strength from Part C_1 were in the range 0.2-0.9 MPa for nanomaterials $nSiO_2$, nclay and HS and from 1.4-2.4 MPa for nanomaterials EG and nFc. All nanomaterial flexural strengths were lower than the flexural strength of cement mortar.

- The FG and HF raised to the value of cement mortar in flexural strength. They were 4.7 and 4.4 MPa respectively

- The compressive strengths ranged from 3.5-11.7 MPa which were greater than the minimum strength for load bearing materials (3-5 MPa) (de Bruijn et al., 2009)

4.7.4 Optimised results

- The optimum results in compressive strength for all project specimens were 12 wt. % PVAc of water, 10 wt. % HF in Part A-Air cured which were 17.7 MPa and 7.3 MPa compressive and flexural strength respectively. They also

gave the highest flexural strength 7.3 MPa, highest than the value obtained in literature of cement mortar around 4.0 MPa and very close to flexural strength of concrete at around 7.0 MPa.

- Hemp fibres (HF) with the PVAc adhesive was selected as the preferred choice compared to FG because it is renewable, available, environmentally friendly, lightweight, and compatible with lime and human circumstances. It will form the central core (C) of the proposed wall panel as shown in Figure 4.38. The insulator (I) of the same wall panel will be selected based on thermal conductivity values as described in Chapter 7. The render (R) lime/nanocomposite will be chosen in Chapter 6 and will be based on porosity characteristics.

Table 4.9 D was a brief for the important result of strength in all parts.

Table 4.9 D Summary of the optimum results of all parts

No	Part	% Filler	Compressive strength MPa	Flexural strength MPa
1	**A**	12%PVAc, 10% HF, 4% nZnO	**17.7**	**7.3**
2	B	8 wt. % PVAc	4.9	2.4
3	**B**	10 wt. % FG	**4.3**	**4.1**
4	**B**	10 wt. % HF	**4.9**	**6.2**
5	**C1**	3 wt. % Nclay	**6.7**	**1.5**
6	**C1**	1 wt. % $nSiO_2$	**8.5**	**2.4**
7	**C1**	5 wt.% nFc	**6.4**	**2.4**
8	**C1**	10 wt. % HF	**8.7**	**4.7**
9	**C1**	12% PVAc / 10% FG	**11.7**	**4.7**
10	**C1**	12% PVAc / 10% HF	**10.4**	**4.4**

Figure 4.38, The Core (C) of the proposed wall in this research will be designed from (12%PVAc, 10% HF, 4% nZnO) Part A-Air cured which gave 17.7 and 7.3 MPa compressive and flexural strength respectively.

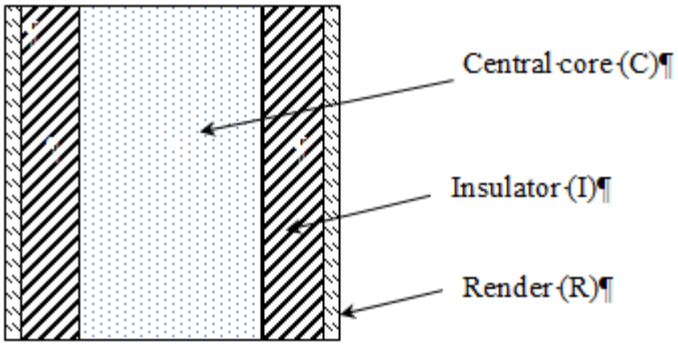

Figure 4.38 Cross section through the proposed wall.

Figure 4.39 and Figure 4.40 show a comparison between compressive and flexural strength results of filler percentages of Part A, Part B and Part C. Error bar exhibits low spread around the mean of points and there are no high variation between the results.

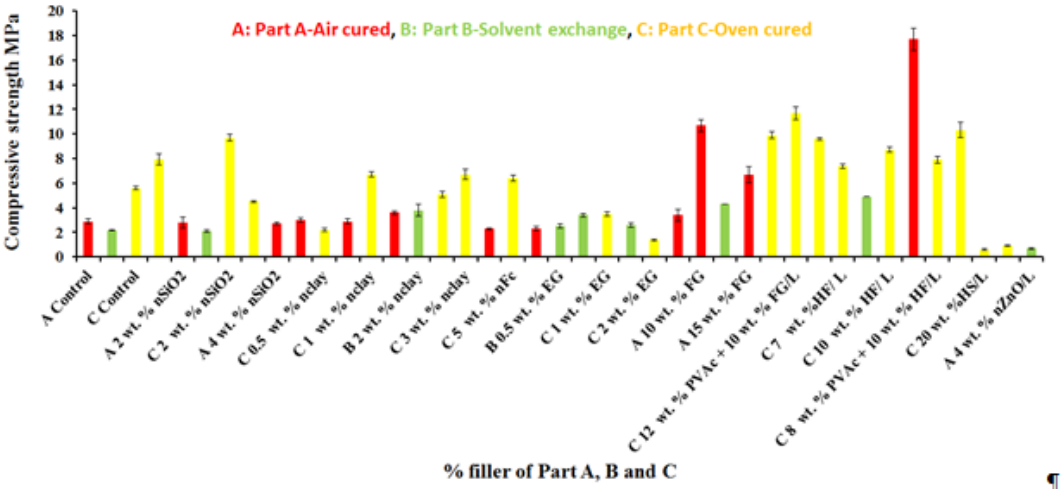

Figure 4.39 Comparison between compressive strength results of Part A-Air cured, Part B-Solvent exchange and Part C1-Oven cured, Error bar ± < 1

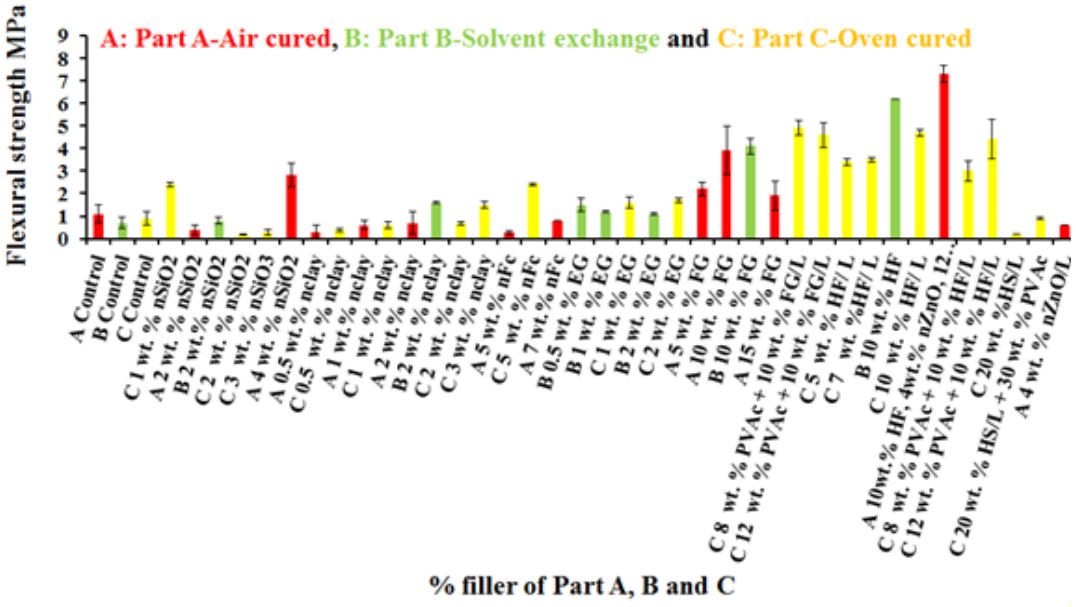

Figure 4.39 Comparison between flexural strength results of Part A-Air cured, Part B-Solvent exchange and Part C1-Oven cured, Error bar ± < 1.

4.8 Discussion

It can be seen in Table 4.9 that flexural strengths were generally low in Part A and Part C (excluding the fibres, glass and hemp) but they were a little higher in Part B. It may be that the enhancement was due to stopping the hydration in Part B and from permitting evaporation of the water from the mixture by using the isopropanol solvent. When the moisture content becomes low, the pores decrease too (Collier, Sharp, Milestone, Hill, & Godfrey, 2008; Konecny & Naqvi, 1993), which leads to enhanced flexural strength because the flexural area of the specimens is very sensitive to the pore volume more so than the compressive area due the type of stress applied. The hydration in this project was stopped by using the solvent exchange method and this was probably why the compressive strength decreased in Part B. In the present project, decreasing water lime ratio helped in developing the strength in both compression and flexure. Water lime ratio was originally 0.6 but the strength results were very poor and, therefore, it would be difficult to achieve high strengths

as a result. W/L decreased to 0.5 and the results improved but not remarkably. At 0.4 W/L, the highest results were achieved, especially when using 12 wt. % PVAc, 10 wt. % HF and 4 wt. % nZnO as was shown in Table 4.9 A.

There were two variables between Part A-Air cured and Part C-Oven cured, they were the water cement ratio, which was decreased from 0.5 to 0.4 W/L and, of course, the method of curing. Clearly, the W/L ratio has an effect on the compressive strength of the solid specimens, it was reported elsewhere that the compressive strength of cement and lime mixture increased as the water cement ratio decreased, the w/c ratios for 14 groups decreased from 0.55-0.27 w/c and the compressive strength were increased from 39.9-66.6 MPa (Sarika, Rao S., Sekhar, & Apparao.G, 2013). The lime and cement require a minimum quantity of water to produce the chemical compounds from hydration (Lawrence & & Walker, 2008).

Part A-Air cured was used to replicate the typical way of placing the materials. Referring to Table 4.9 Part A, the optimum percentages of the nano and natural materials for the highest compressive strength was 2 wt. % $nSiO_2$/L, 2 wt. % nclay/L, 5 wt. % nFc/L and 10 wt. % FG/L. For flexural strength, all the results of nanomaterials ($nSiO_2$, nclay and nFc were in the range, 0.3-0.9 MPa lower than the pure lime specimens (1.1 MPa). Compressive and flexural strength for 10 wt. % FG/L were the highest value of both compressive and flexural strength of all specimen results (11.7, 4.7 MPa respectively) except 10 wt. HF, 12 wt. % PVAc of water with 4 wt. % nZnO which were both compressive and flexural strength (17.8 and 7.4 MPa respectively at 0.4 W/L) the highest results among all results of the project..

Part B-solvent exchange was used in the literature for many reasons; it was the best way for measuring the development of porosity at certain ages by stopping the hydration process by evaporating the excess water using solvent exchange. It was used in the project as an accelerated method for curing the materials since drying on site is an issue. The method had an influence on the quantity of pores (reduced). Further work is required to optimise the technique which could have wide ranging benefits for on-site placing. The results at 14 days curing by solvent exchange in Part B tests are compared with 28 days of ordinary air curing. Also, it was reported that the solvent exchange method is the best method to keep pores in the finest pore size

range (Alvarez et al., 2013). Referring to the literature, the solvent exchange method was found to be the best method to examine and evaluate the properties of shrinkage, permeability and strength which have a relation to pore size distribution, Shrinkage is related to finer pore size range whereas permeability and strength are related to larger pore size range (Konecny & Naqvi, 1993). The solvent exchange method cannot remove all the free water (it is non reacted and found free in the pores of the specimen) so the combined water content (it is reacted and linked with the materials of the specimen), which is considered as the indicator of the extent of hydration, is the highest water removal in comparison to the other methods (Saraya, 2010). From this literature, it can be summarised, the effect of larger pore size on strength was decreased by removing the free water using a solvent exchange method. This is not without limits, it depends on the hydration and if there is enough water for reaction. The balance between removing free water and having enough water for the hydration process needs more studying to find the optimum case. On the other hand, it was reported the percentage increase in compressive strength from 7 days testing to 28 days for air cured specimens was 86 %, the percentage increase for the same period by solvent exchange was 112 % (Alvarez et al., 2013).

This means the increase from 7 days to 28 days is almost the same, but the difference from 86% to 112% came from the adding of nanosilica and not due to the solvent exchange technique. Pores and shrinkage are important to be discussed within compressive and flexural strength results because they are related to decreasing strength and studying the factors affecting on decreasing them is important.

In addition,

- The results of the compressive strength specimens in Part B decreased by about 50 % in comparison to Part A. The mean compressive strength decreased for control specimens (4.3 to 2.9 MPa), 2 wt. $nSiO_2$ (4.9 to 2.8 MPa), 10 wt. % FG (7.3 to 4.3 MPa). The compressive strength of nanoclay decreased slightly from 4.0 to 3.8 MPa.

- New materials that were tested in Part B which differed from Part A (EG, HF and PVAc/L) were studied to determine the optimum percentage of each. The

optimum percentage of EG was 1 wt. % to lime. Its compressive strength was 3.4 MPa, higher than 0.5 wt. % EG (2.5 MPa) and 2 wt. % EG (2.6 MPa).

- The compressive strength of 80, 40, 20 and 8 wt. % of PVAc/L were 2.2, 2.9, 4.2 and 4.9 MPa respectively. For EG, 1 wt. % was the optimum percent of EG for compressive strength.

- 10 wt. % HF/L was tested in Part B, and gave 4.9 and 6.2 MPa compressive and flexural strengths respectively which were the highest values in all Part B tests.

- The optimum PVAc was 8 wt. % of water/Lime without fibres, it gave 4.9 and 2.4 MPa of compressive and flexural strength respectively and they were higher than the results of the percentages 80, 40 and 20 wt. % of lime which gave compressive strengths of 2.2, 2.9 and 4.2 MPa respectively and flexural strengths of 0.8, 1.7 ad 1.3 MPa respectively.

- This optimum result (8 wt. % PVAc/L both flexural and compressive strengths for PVAc/L blended with 10 wt. % HF/ L) was tested with another ratio of PVAc/L of 12 wt. % in Part C_1-Oven cured to determine the optimum ratio when PVAc is mixed with HF or FG. It was found that the optimum ratio of PVAc for blending with 10 wt. % of (FG or HF) was 12 wt. % PVAc/L.

It has been found from Part A-Air cured and Part B-Solvent exchange that there was commondity between the optimum performance of materials in both parts e.g.

- For nanomaterials, 2 wt. % $nSiO_2$/ L, 2 wt. % nclay/ L, 5 wt. % nFc/ L, 8 wt. % PVAc to the W/ L, 1 wt. % EG/ L

- For fibres, 10 wt. % FG/ L and the percent of 10 wt. HF/L was very close to 10 wt. % FG/ L by using Part C-Oven dry cured

- The optimum percentage of HF blended with PVAc was later investigated in Part C_1 and the optimum was found 10 wt. % HF/L with 12 wt. % PVAc/l which gave compressive and flexural strength 10.3 and 4.4 MPa respectively,

and by using Part A-Air cured method 17.8 MPa and 7.3 MPa respectively which is the highest results amongst all parts

Regard to Part C_1, research elsewhere reported the substantial effects on compressive strength of lime concrete specimens due to the capillary of the degree of water saturation. When the degree of saturation of specimens increased from 0 % to 100%, the bond between soil and lime completely disappeared, and the compressive strength of the lime concrete decreased to zero. Moreover, it was remarked that the bond between soil and lime became weakened when the capillary water absorbed. It was increased by up to 20 % or more; the strength was substantially reduced (Saberian, Jahandari, Li, & Zivari, 2017) This means oven drying is necessary to decrease the capillary water which is produced from excess water in the matrix and may help to enhance the strength.

The results of the strength tests in Part C_2 were:

- For compressive strength, it was 4.9 MPa for the Control (pure lime), 3.9 MPa for 2 wt. % nclay/L, 2.9 MPa for 2 wt. % EG/L and 4.0 MPa for 2 wt. % $nSiO_2$/L.

- For flexural strength, it was 3.1, 1.8, 3.7 and 0.9 MPa respectively.

Part C_1-Oven dry cured was the same curing procedure of Part C_2 except the age of the test specimens were 28 days not 60 days. It used the optimum percentages of the specimens from Parts A and B

- The mean compressive strength was 5.6 MPa for the Control, more than its value in Part A (4.3 MPa)

- The optimum percentage result for nanoclay for compressive strength (6.8MPa) was 2 wt. % nanoclay/ L, better than 0.5 wt. % (2.2 MPa), 1 wt. % (6.7 MPa) and 3 wt. % (6.7 MPa), which were in general higher than the compressive strengths of Part A-Air cured, Part B-Solvent exchange and Part C_2

- The optimum percentage result of compressive strengths for $nSiO_2$ (9.7 MPa) were 2 wt. %, better than 1 wt. % (8.5 MPa) and 3 wt. % (4.5 MPa)

- The optimum percentage result of compressive strength for EG (3.5 MPa) was 1 wt. %, more than the 2 wt. % (1.4 MPa)

- The optimum percentage result specimen for compressive strength of nFc (6.4 MPa) was 5 wt. % nFc, more than the of 10 wt. % (4.0 MPa).

- The optimum percentage result in terms of compressive strength for HF was both 10 wt. % and 5 wt. %, both gives 9.6 MPa. The 10 wt. % had a higher flexural strength of 4.7 MPa compared to the 5 wt. % (3.4 MPa). In addition, increasing the HF percent led to difficult mixing and distribution which probably affected its compressive strength

- The highest percentage result in terms of compressive strength was 10 wt. % FG mixed with 12 wt. % PVAc of the mixing water (11.7 MPa)

- The optimum percentage result for compressive strength in Part C was 10 wt. % HF mixed with 12 wt. % PVAc of the mixing water (10.3 MPa)

- These two optimum results of FG and HF were the highest compressive strength results among the parts (Part A-Air cured, Part B-Solvent exchange, Part C_1 and C_2 - Oven dry cured) and they had highest results in flexural strength too. The result of these two optimum results were 11.7 and 4.7 MPa compressive and flexural strength respectively using Part A-Air cured and 10.3 and 4.0 MPa respectively using Part C_1-Oven cured for 10 wt. % HF and 4 wt. % nZnO with 12 wt. % PVAc

- The 10 wt. % HF, 4 wt. % nZnO and 12 wt. % PVAc was considered the best material because it was environmentally friendly and similar in performance to the FG. Hemp is sustainable, available, environmentally friendly and compatible with lime paste. Furthermore, it is lightweight in comparison to concrete construction as will be calculated in Chapter 8 when the densities of materials are determined from the porosity test. This material was chosen as the core (C) of the proposed wall in this project as explained in Section 4.7 and Figure 4.38 and the compressive strength (10.3 MPa) was significantly more than the minimum limit of a load bearing material (3-5 MPa)

- The compressive and flexural strengths for 20 wt. % HS/L were 0.6 and 0.2 MPa respectively but when mixed with 12 wt. % PVAc they were 0.9 and 0.5 MPa respectively. These compressive strengths were very weak and is non-load bearing, but because of the relative high percentage of shives, it has high heat isolation due to low thermal conductivity. It was adopted to be the insulation layers either side of the core, see Figure 4.38

- Chopped fibres (FG and HF) were used for the first time with lime and the compressive and flexural strengths were very encouraging. Hemp fibres were better than fibre glass because they are environmentally friendly and are available as a renewable agricultural plant which can grow quickly to 4-6 m within 3 months

- In addition, PVAc (or wood glue) was used for the first time with lime and fibres as an adhesive to increase the bond between the fibres (FG and HF) and the results showed that the strength obtained were comparable to those required for load bearing materials

- Referring to load deflection curves Figure 4.28 and Figure 4.29, the shape of the curves for the nanomaterial specimens was linear and the failure was sudden i.e. brittle whereas with the FG and HF mixed with PVAc, the failure was gradual. This property, called ductility, is beneficial in construction materials

- In the literature it was reported that hemp/lime composite had a ductile behaviour in its stress/strain profile which started as a linear increase but changed to ductile behaviour due to the transfer of stresses to the interface of lime/hemp (Muphy, Pavia, & Walker, 2010).

- As for ductility, it can be seen in Figure 4.40 under compressive loadings; the specimen was compressed up to failure without cracking except the thickness reduced. Hemp fibre lime composites exhibited higher ductility. Ductility emerged at the compressive strength failure tests. Also in flexural strength (Figure 4.28 and Figure 4.29), the mode of failure curve is not sudden but from the maximum point is gradually decreased which is a behaviour of a

ductile, not brittle material. Ductility is an important factor for human safety and durability of the material which makes the lime a good candidate under vibration loads.

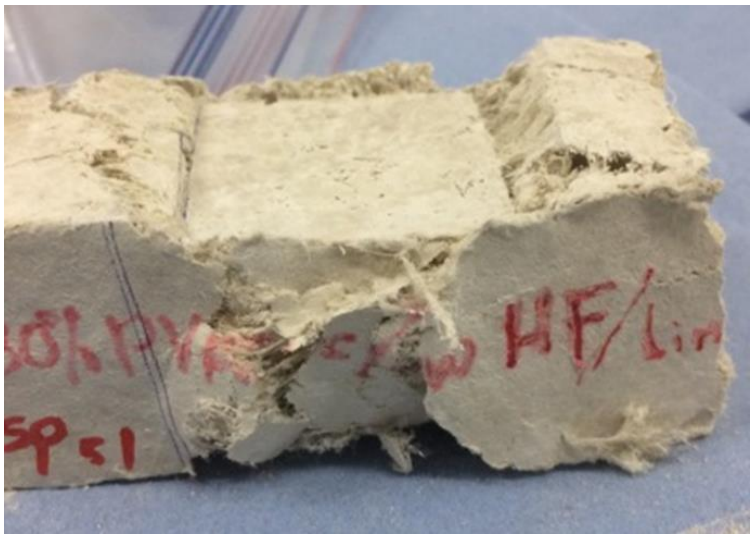

Figure 4.40 Compressed specimen of 12 %PVAc 10 % HF/ L without complete crushing

In another study, many percentages of hemp to concrete were studied in a mix, the flexural strength increased and provided a ductility case for a post cracking situation of the fibre reinforced concrete mix and this was similar to the compression test. It just added 1% HF and the outcome was 20 % reduction in coarse aggregates (Awwad, Hamad, Mabsout, & Khatib, 2010). In the present project, the specimens reinforced by hemp fibres were void of cracks and no cracks. Under load the specimens compressed but without showing signs of cracking.

4.9 Summary of Findings and the Relationship to project Objectives

Table 4.1 in the Introduction highlighted the project objectives and their description. This table has been updated with the project findings and summarised in Table 4.10.

The research in this project showed that although the procedure adopted a solvent exchange or a water removal technique which stops the hydration process from the age of 26 days, the tested materials still possessed the required characteristics of strength and thermal performance. More research is required to assess the influence of accelerated drying on the durability of renders and to investigate the best drying method for site use and the optimum time for implementation due to thickness of the material and possible adverse weather conditions.

Part A-Air cured was adopted for the central Core of the proposed wall (12%PVAc, 10% HF, 4% nZnO). The latter two curing regimes were adopted according their high improvement of strength in Part C and decreasing thermal conductivity in Part B. Part B-Solvent exchange led to stopping hydration which meant no more reaction, no more generated materials like calcium hydroxide gel, and there are enough pores to increase the heat isolation (decrease thermal conductivity). Part B was adopted for decreasing thermal conductivity. It can be used in the application of isolator panels of the proposed wall in this project (Figure 4.38, Section 4.7).

Table 4.10 Summary of findings and achieved objectives

No	Objectives	Objectives Description	Outcomes
A	1.Environmentally friendly 2. Sustainable	Compatible with the: 1. Environment (human, animals and plants) 2. Available and renewable	1. Environmentally friendly was achieved by 1.1. Choosing biomass materials such as fibres and shives of hemp and lime for the matrix. 2. Sustainable property was achieved by selecting sustainable materials. 2.1. Hemp which grows quickly is considered due to its low CO_2 footprint in its life cycle. Note: a comparison between the quantity of CO_2 emission for $1m^3$ from proposed wall in this project and $1m^3$ concrete wall depending on the densities (to calculate the weights) of material from porosity test will be conducted in Chapter 8
B	Lightweight	1. Density of proposed wall layers is less than concrete density of concrete < 2500 kg/m^3	1- For lightweight goal by using: hemp fibres or hemp/Lime nanocomposite which is lighter than concrete, their bulk densities: 1.1. Lime density= 1500 kg/m^3 1.2. 10 % HF/L+12 % PVAc/L=1260 kg/m^3 1.3. 10 % HS/L+12 % PVAc/L=540 kg/m^3 Densities above will be found by porosity testing in Chapter 7
C	1. Load bearing construction material, ability to withstand 1.1. Wind load and 1.2. Eccentricity of its load Increase compressive strength 2. Flexural strength must be increased 3. The resulted composite must be: Safe against Sudden collapse Durable material	1. Its compressive strength could be > 5 MPa, which is the minimum limit of load bearing material. 2. To bear flexural loads, It must be around the flexural strength of cement mortar ≈ 4 MPa to increase flexural strength 3. For safety and durability must be behaved as gradual failure in both flexural and compressive strength	1.Compressive strength (MPa) achieved by: 1.1. 10 % HF/L + 12 % PVAc/L= 17.7 MPa Part A-Air cured 1.2. 10 % FGL+12 % PVAc/L= 11.7 MPa Part C_1. Oven dry cured 1.3. By adding 2 % $nSiO_2$= 8.5 > 3-5 1.4. By adding 3 % $nSiO_2$= 9.7 > 3-5 2-Flexural strength (MPa) achieved by: 2.1. 10 % HF/L+12 %PVAc/L= 7.3 > 4 MPa Part A-Air cured 2.2. 10 % FG/L+12 % PVAc/L= 4.4 > 4 MPa Part C 3. For ductility the mixture of 10 % HF/L+ 12 %PVAc/L showed high ductility in compression and tension according to failure mode: It was noticed from: 3.1. Failed specimens 3.2. From the Load-deflection curve 3.3. From Load-compression curve 3.4 Ductility is important factor of durability in construction

Chapter 5 - **Porosity and Water Absorption**

5.1 Introduction

Porosity is an important property in building construction materials. Low porosity is required to protect the building materials from water ingress. Porosity is perhaps the third most significant property for construction materials after strength and thermal conductivity and can be more important than strength in certain cases such as plaster. Both of these properties were discussed in Chapter 4 and Chapter 7, respectively.

The aim is reducing porosity whilst still maintaining breathability. It is beneficial to have porosity as low as possible, perhaps in the range of concrete porosity which is about 12-21 % as shown in the literature (Y. Y. Kim, Lee, Bang, & Kwon, 2014; H. Zhao, Xiao, Huang, & Zhang, 2014) to keep and conserve the breathability (water vapour permeability WVP) of lime, which increases and decreases as porosity increases or decreases.

As shown in the literature (Demo, 2017; IAQ, 2013), moisture content has a negative effect on construction building materials. Differing moisture content leads to expansion and contraction at dry state when the moisture content evaporates and this causes cracks and weakness in flexural and compressive strength of the lime. Moisture content increases thermal conductivity and has a negative effect on the heat insulation property of the material. Porosity therefore, is a very important indicator for the influence of moisture content. Reduced porosity means reduced moisture content.

Tests were conducted to check the porosity of lime with nanofillers (expanded graphite, nanoclay, nanosilica, nanozinc oxide) and also with fibre glass and/or polyvinyl acetate as a percentage of water.

The porosity tests were generally conducted for the optimum percentage of fillers which were adopted in strength tests in Chapter 4 and gave the best mechanical properties. A comparison was made between porosity for each kind of filler to that of pure lime. The first group of tests was for the render of the proposed wall in this study (Figure 5.1). The group focused on using nanomaterials with lime; however fibre glass was added to the mixtures to help in reducing shrinkage and provide

additional strength. Nanozinc oxide was included in the tests because it was good for decreasing thermal conductivity and this is important in the study. Other tests related to the Core of the proposed wall and the Insulator panels of the wall (Figure 5.1). These were hemp fibres (HF) with polyvinyl acetate and HF with PVAc. Air curing was used for all samples. The samples were cut by a knife from the specimens which were tested for strength (compressive and flexural strength). These specimens were demoulded after 5 days and then stored for 23 days in a temperature and humidity control room (20°C and RH, 60 %). Porosity samples were cut from the tested strength specimens and they were put in an oven 24 hours at 50°C.

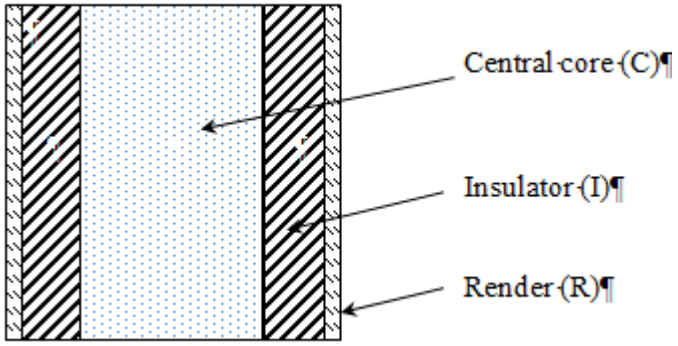

Figure 5.1 Cross section through wall: (R) Lime nanocomposite render; (I) lime/hemp shiv nanocomposite insulator (C); lime/hemp fibres nanocomposite.

5.2 Porosity Results and Pore Size Distribution

Two groups P_1 and P_2 of specimens were tested for Render (R) and Core (C) respectively as shown in Figure 5.1.

5.2.1 Porosity Tests for Render (R) Materials P_1

The Render (R) materials were tested for porosity (2 wt. % $nSiO_2$, 2 wt. % nClay, 0.5 wt. % EG, 2 wt. % EG, 4 wt. % nZnO) compared to the pure lime porosity. The results are given in Table 5.1.

Referring to Table 5.1, the Group ID is given in column 1, P_1 standing for 'Porosity' and 'Group 1'. The specimen number is given in column 2. The filler used are in column 3 and include control, $nSiO_2$, nanoclay, expanded graphite (EG) and nZnO.

For example, P_1 2 wt. % $nSiO_2$ means; porosity test of Group1, specimen of nanosilica of 2 % by weight of lime binder.

The water/lime ratio in the porosity tests was 0.4 for all these tests. The porosity as a percentage is given in column 4, Table 5.1. Referring to Table 5.1 and Figure 5.2, EG at 0.5 wt. % of lime exhibited the highest porosity (40.9 %).

Table 5.1 Porosity test results for Render (R) materials (P_1)

Group 1	No 2	Filler 3	% Porosity 4
P_1	1.	Control	36.4
P_1	2.	2 wt. % $nSiO_2$	34.3
P_1	3.	0.5 wt. % EG	40.9
P_1	4.	2 wt. % EG	28.4
P_1	5.	2 wt. % nclay	31.5
P_1	6.	4 wt. % nZnO	18.1

The porosity of the Control was 36.4 %. Nanosilica added to lime at 2 wt. % gave a porosity of 34.3 %. The lowest porosity result was 18.1 % by mixing 4 wt. % nZnO with lime. Surprisingly, the nZnO to lime decreased the porosity from 36.4 % to 18.1 % and this is the best result for render. The nanozinc oxide was lastly included in the tests because it showed high effect (decrease) on the thermal conductivity. This nanofiller, nZnO can be used in render, core and insulator of the proposed wall of this study. That means, it is very important and its effect on porosity must be studied and for that it was included in this group P_1. The second lowest porosity was 28.4 % by mixing 2 wt. % EG with lime. This can also be used as a filler for the lime nanocomposite render or fibre reinforced lime nanocomposite. Unfortunately, the black colour of EG gave a dark appearance to the render which can be aesthetically unpleasing. The MIP device normally measures pore sizes at a pressure up to (200 MPa) within the range (0.01- 100 μm). Due a fault of the instrument the pressure of MIP did not reach 200 MPa, therefore the smaller pore size were not measured for 2

wt. % EG (0.01- 0.4 ± 0.03 µm). So that, the results were not precised but the error is not high because the cumulative intrusion volume was very low at these pore sizes (less than 0.4 µm). That means this error in the percentage of porosity is not significant.

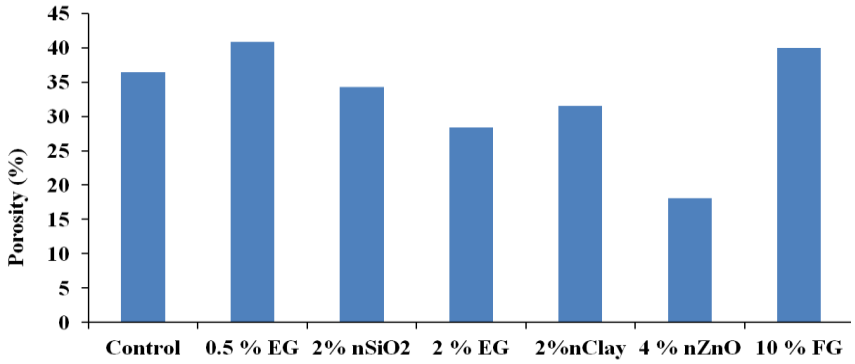

Figure 5.2 Porosity of P_1 specimens

These results were for the materials which can be used in the Render (R) of proposed wall in this project (Figure 5.1) and then, the materials which can be used for the core of the proposed wall must also be checked in P_2 group. These materials are FG/L, hemp fibres HF and PVAc which was added to HF to increase its bond with lime which gave higher strength (flexural and compressive) than HF lime composites. The insulator (I) panel materials of the proposed wall as shown in Figure 5.1 were not tested because they contain an effective percentage of hemp shives (20 wt. %) and their pore size are outside (larger) the measuring range of MIP.

5.2.2 Porosity Tests for Core (C) Materials P_2

The materials which were tested for porosity in group P_2 were 10 wt. % HF with 30 wt. % PVAc and 4 wt. % nZnO, 10 wt. % HF with 30 wt. % PVAc and FG/L. The results are given in Table 5.2 and Figure 5.3. This table is formulated in a similar way to Table 5.1. Table 5.1, see Section 5.2.1 for a description of its content.

Table 5.2 Group P_2 porosity tests for core materials

Group	No	Filler	% Porosity
P_2	1	10 % HF+30 % PVAc + 4 % nZnO	20.7
P_2	2	10 % HF + 30 % PVAc	16.6
P_2	3	10 wt. % FG	40.0

Table 5.2 shows the porosity results of Group P_2 which is the Core (C) and Figure 5.3 shows a comparison between P_1 and P_2 groups; nanozinc oxide is significantly decreased the porosity from 36.4 % for pure lime to 18.1 %. This is very good to use in the (R) render and in the core of proposed wall as well. Furthermore, the nanozinc oxide can be used for decreasing thermal conductivity and porosity which is cheap and readily available on the market. Nanozinc oxide has a potential to absorb the heat and slowly release it. Nanozinc oxide decreases the pore size diameters by lining the pores (Handoko et al., 2018) as a nanomaterial which is small particles and has hexagonal structure close to sphere shape (Bouzourâa et al., 2016; Mala et al., 2016). Hemp fibres of 10 wt. % with 30 wt. % PVAc of water gave the high decrease in porosity, 16.6 %, but when mixed with nZnO, the porosity increased marginally to (20.7 %). The last porosity 20.7 % can be used for the Core (C) due to the presence of nZnO which works as anti-bacteria and anti-fungus which is preferred more than HF with just PVAc. The porosity of hemp fibres with PVAc was 16.6 %. Porosity became a little higher (20.7 %) by using hemp fibres with PVAc and nZnO due to the nanozinc oxide. In the lab usually when the nZnO is added at the mixing time, the workability was decreased and extra water was added (0.4 wt. % of 4 wt. % nZnO or the total water of mixture became 0.4 water to solid content). Possibly, the additional water increases the pore size volume a little more than just PVAc and this leads the hemp fibres to absorb more water by capillary action which evaporates and leaves pores of higher size which increases porosity as well.

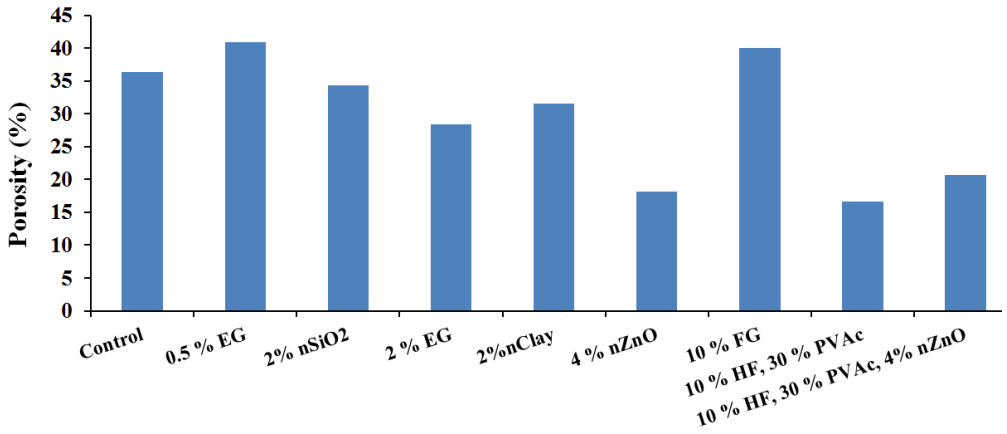

Figure 5.3 Comparison % porosity of all materials of groups P_1 and P_2

5.2.3 Pore Size Distribution

The pore size distribution for nine specimens are given in Figure 5.4 to Figure **5.12**,

Figure 5.4 control, Figure 5.5, 0.5 wt.% EG/L; Figure 5.6, 2 wt. % EG/L; Figure 5.7, 2 wt. % $nSiO_2$/L; Figure 5.8, 2 wt. % nclay/L, Figure 5.9, 10 wt. % FG/L with 20 wt. % PVAc to water; Figure 5.10, 10 wt. HF/L and 30 wt. % PVAc of water and Figure 5.11, 10 wt. HF/L and 30 wt. % PVAc of water with 4 wt. % nanozinc oxide/L and Figure 5.12; 4 wt. % nZnO/L. The pressure of MIP device for the specimens; 2 wt. % EG, 10 wt. HF and 30 % PVAc of water, 10 wt. % HF and 30 % PVAc of water with 4 wt. % nZnO wasn't reached the maximum value (200 MPa). Therefore, the small pore sizes are not shown in the charts

Referring to Figure 5.4 to Figure 5.12, the modal pore size diameter (critical radius) for Control Figure 5.4, 0.5 wt. % EG Figure 5.5, 2 wt. % EG Figure 5.6, 2 wt. $nSiO_2$ Figure 5.7 and Figure 5.8, 2 wt. nclay were (1.2, 1.1, 1.8, 0.9 and 1 µm), they were around 1.0 µm but their range of pore sizes are different, for Control, it was between 0.01- 1.8 µm and cumulative intrusion volume was 0.27 cm^3/g, its porosity was 36.35 %, but for $nSiO_2$ Figure 5.7, it was a little less in the range 0.01-1.1 µm. Its cumulative intrusion volume was 0.26 cm^3/g, the porosity was a little lower at 34.34 %.

Specimens of 20 and 30 wt. % HS/L were not tested because porosity of this kind of mixtures (as reported) is very high and more than that of pure lime (36.4 %). It was found that the porosity of 16 wt. % hemp, 32 wt. % of lime and 0.5 W/L was 75 % (Glé, Gourdon, & Arnaud, 2011). This porosity is much higher than the normal porosity of concrete (12-20 %) (Y. Y. Kim et al., 2014; H. Zhao et al., 2014). The main usage of hemp shives (which has high porosity and porous structure) is to increase efficiency of envelopes and reduces production cost as a best heat insulator (Balčiūnas, Vėjelis, Vaitkus, & Kairyte, 2013). More tests should be conducted on controlling the porosity of shives.

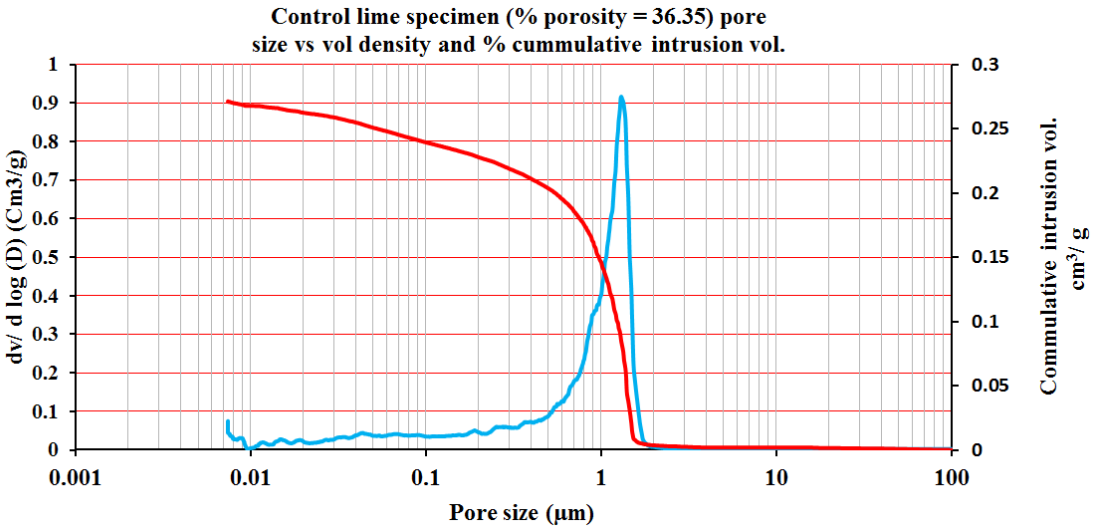

Figure 5.4 Pore size distribution for control specimen

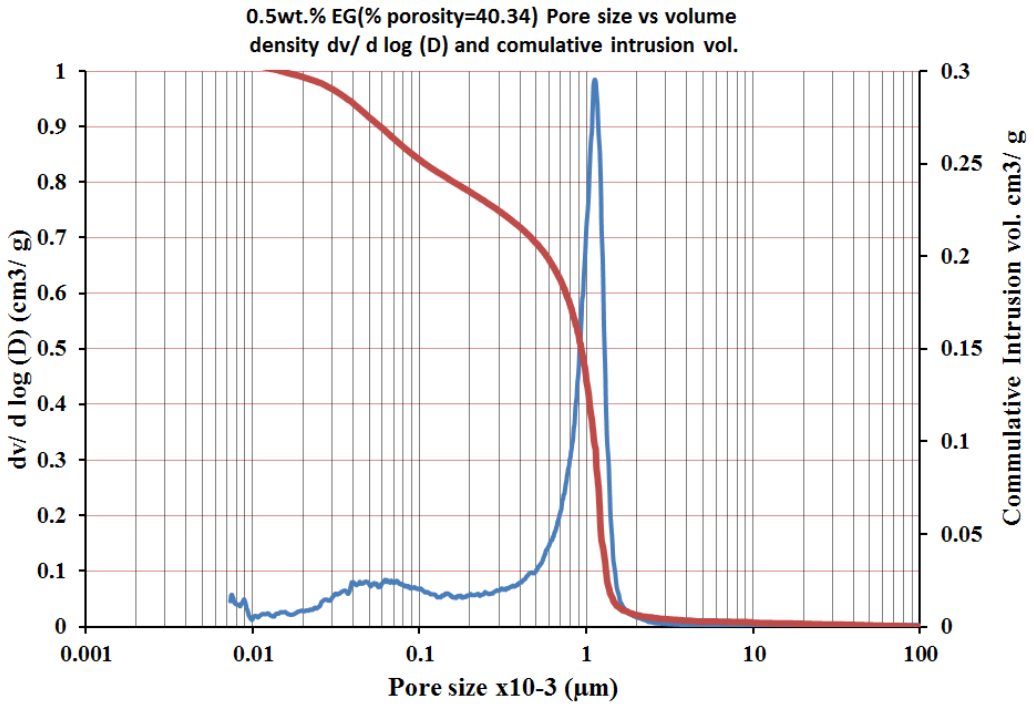

Figure 5.5 Pore size distribution for 0.5 wt. % EG specimen

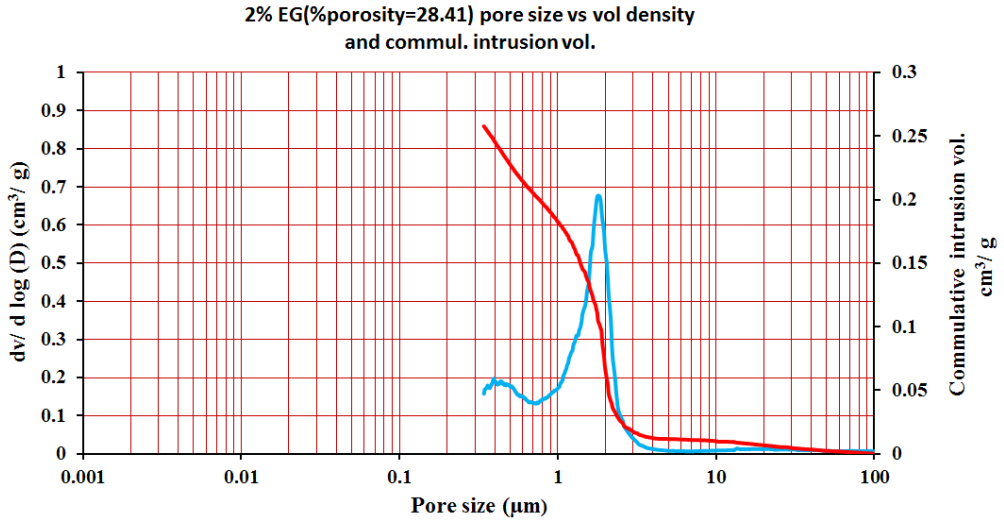

Figure 5.6 Pore size distribution for 2 wt.% EG specimen

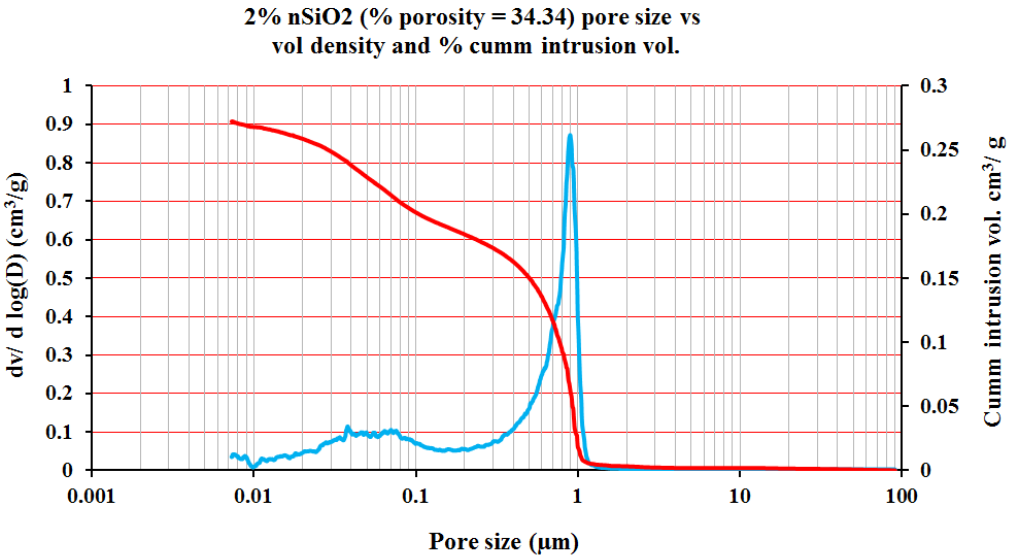

Figure 5.7 Pore size distribution for nSiO2 specimen

As for nanoclay Figure 5.8, the pore size range was 0.01-2 µm, similar to the control specimen (0.01-1.8 µm) but the cumulative intrusion volume was about 0.14 cm^3/g lower than for control (0.27 cm^3/g), The porosity of nanoclay (31.5 %) was less than the control specimen porosity (36.4 %).

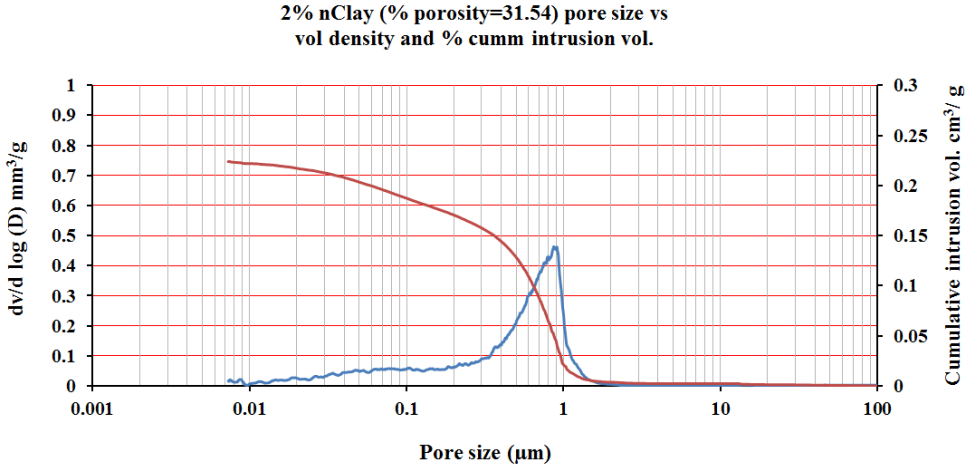

Figure 5.8 Pore size distribution for nclay specimen

The specimens of 10 wt. % FG had a critical pore diameter of 1.0 µm but their intrusion volume was 0.09 cm^3/g lower than control (0.27 cm^3/g) but the range of pores was 0.01-100 µm and gave higher porosity for higher range of pore size diameter. As for $nSiO_2$ Figure 5.7 and nclay Figure 5.8 decreased the critical size radius for both is around 0.9 (less than 1 µm) in comparison to the critical size diameter of control (1.2 µm) Figure 5.4.

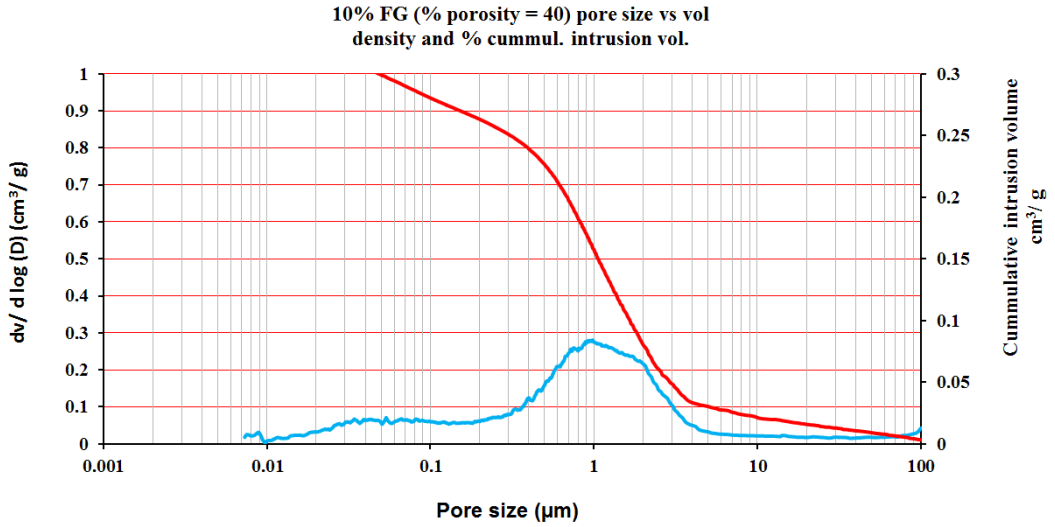

Figure 5.9 Pore size distribution for FG specimen

For HF with PVAc Figure 5.10, HF with PVAc + nZnO Figure 5.11 and nZnO, Figure 5.12, the pore size range was 0.1-100 µm, 0.4-100 µm and 0.45-50 µm respectively. Their critical pore radius were 0.35 and 15 µm for HF with PVAc, two critical diameters. Also, there are two critical diameters 0.7 and 15 µm for HF with PVAc blended with nZnO. As for nZnO/L (nanozinc oxide to lime) was 1.1 µm, but the cumulative intrusion volume of these pore sizes was about 0.02 0.04 and 0.09 cm^3/g respectively. It can be said that the pore size ranges were larger than of the group mentioned above but the cumulative intrusion volumes were lower, they were 0.02-0.09 cm^3/g which was the lowest and yielded the lowest porosity. The lowest cumulative intrusion volume was 0.02cm^3/g for (HF with PVAc) and yielded the lowest porosity (16.6 %), The second highest cumulative intrusion volume was 0.09 cm^3/g for % (nZnO/L) which gave a second lowest porosity 18.1% and cumulative intrusion volume 0.04 cm^3/g for (HF with PVAc + nZnO) which gave a porosity of 20.7 %. Figure 5.10, 5.11 and 5.12; show the range of pore size is not completed for the same reason of Figure 5.6; the pressure of the MIP device didn't reach 200 MPa due to a fault. The mistake in the percentage of their porosity is low because the cumulative intrusion volume versus the non-accessed pore size is low.

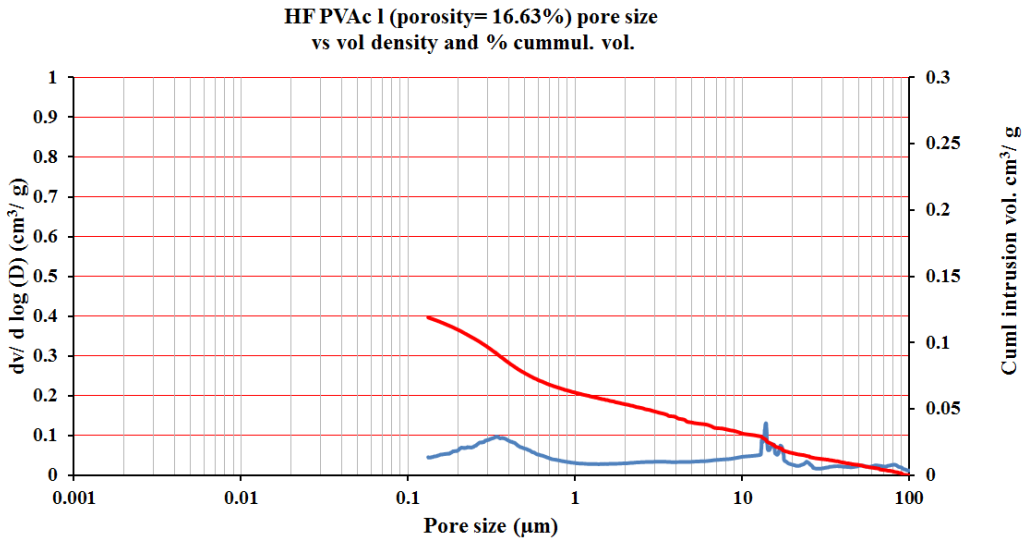

Figure 5.10 Pore size distribution for HF PVAc/w specimen.

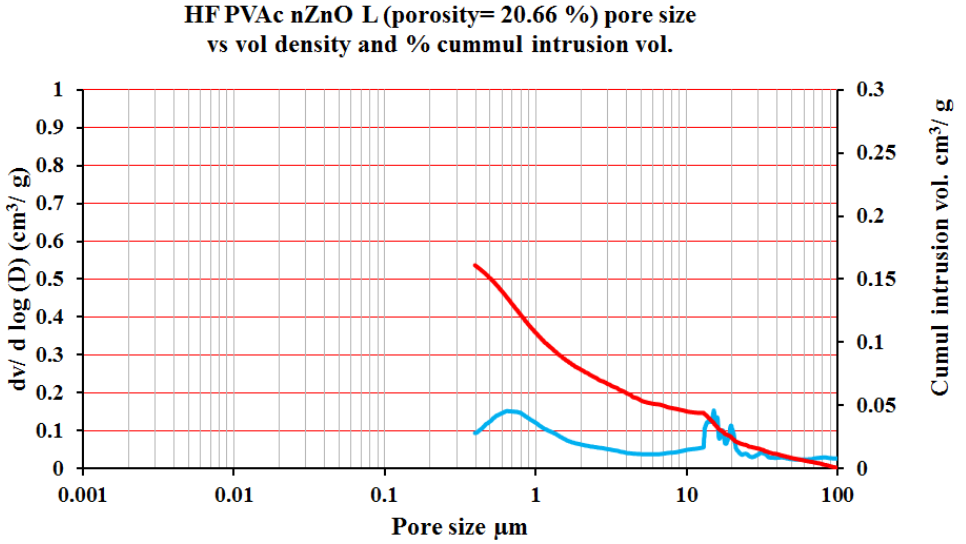

Figure 5.11 Pore size distribution for 10 wt.% HF 30 wt. %PVAc/w 4 wt. % nZnO specimen

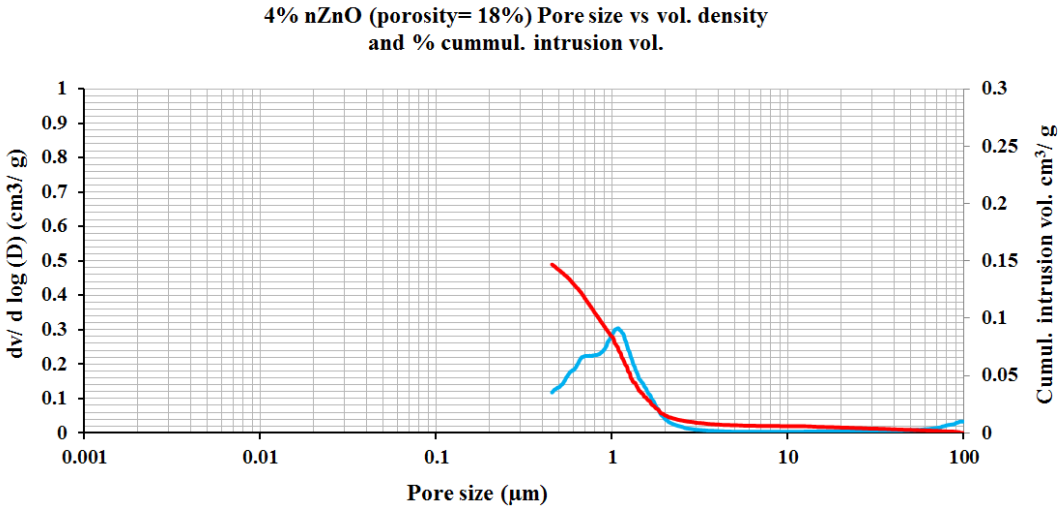

Figure 5.12 Pore size distribution for 4 wt. % nZnO specimen

In the literature, it was shown that is impossible in concrete to have a total porosity of less than 10 %. The porosity of concrete for a young age is about 20-25 % and 10-15 % at a mature age (Aligizaki, 2014). This is a good guide for porosity since the main material in this project is lime which is porous material and as in group P_1 tests, its porosity was 36.4 % (Control specimen). It will be beneficial to decrease the porosity of these materials to ideally a little higher than 10-15 % of a mature concrete porosity. Or it can be decreased to the highest side of the range 12-21 % which is the range of concrete porosity as reported (Y. Y. Kim et al., 2014; H. Zhao et al., 2014). Some studies mentioned other range for example; porosity of hardened cement paste range is 25-50 %. (Jennings, Thomas, Rothstein, & Chen, 2008). It means the porosity of lime is preferred to be slightly higher than the lower limit of cement porosity range. The required porosity in lime is to be a little higher than cement porosity range (10-15 %) or a little less than the higher side of concrete porosity range (12-21 %) in order to keep the required breathability (WVP) of lime higher than cement or from the higher side porosity range of concrete breathability. The breathability of concrete is lower than lime due to its lower porosity. Porosity of lime in this project was decreased from 36.4 % to 16.6 by using 10 wt. % HF and 12 wt. % PVAc/L, 18.1 % using 4 wt. % nZnO to lime and 20.7 % using 10 wt.% HF 12 wt. % PVAc + 4 wt. % nZnO.

All these porosity result values 16.6, 18.1 and 20.7 % were an exceptional achievement because they were at least half that of the pure lime porosity and at the higher side range of concrete porosity. This is the first time, according to the available knowledge that nZnO is added to lime and the first time PVAc, HF and nZnO were added to lime to decrease porosity. Nanozinc oxide was beneficial in decreasing both thermal conductivity and porosity meaning it will have a double benefit in term of decreasing thermal conductivity and porosity.

5.2.4 Critical Pore Size

Critical radius or modal pore size is the most frequent pore radius, and an explanation is given in Figure 5.13. It relates to the transmissivity of the material, it is used to examine the effects of the factors such as water content ratio, material temperature etc.., and it is corresponding to the steepest portion of the cumulative porosity curve (Aligizaki, 2014).

That means the critical pore radius of the Control specimen; it was about 1.00 µm which is in the change point of the steep slope. For $nSiO_2$ specimen, was about 0.9 µm and 1.0 µm, for nanoclay. For 0.5 and 2 wt. % EG, they were 1.1 and 1.8 µm respectively. For FG, it was 1.00 µm, and there were two critical pore dimeters 0.35 and 14 µm for HF with PVAc , 0.7 and 15 µm for HF with PVAc and nZnO and 1.1 µm for nZnO/L. The critical pore diameter for the materials which included PVAc is high but their porosity is low (16.6 and 20.7 % respectively) due to the lowering of their cumulative intrusion volume as shown in Figure 5.4 to Figure 5.12.

Threshold radius is the limit between majority and minority of intrusion pore volume, or it is the diameter of which the mercury intrusion, if it is above the threshold size, is little, and if it is below of its size, is great portion of intrusion. The threshold diameter can be defined that is the largest pore diameter at which great intruded pore volume is happened (Aligizaki, 2014).

Threshold diameter decreases with the decrease of water binder ratio and with an increase of age. It starts from the change point of the curve, see Figure **5.13** Definition of critical and threshold pore radius (X. Chen, Wu, & Zhou, 2014)**.** Threshold diameter is a good guide for permeability because it is related to the connective pores which has a high effect on permeability (Aligizaki, 2014).

For pure lime (Figure 5.4), the threshold diameter is about 1.7 µm, for $nSiO_2$ (Figure 5.7), it is 1.10 µm, nclay is 1.5 µm (Figure 5.8), 1.7 and 2.5 µm for 0.5 and 2 wt. % EG respectively (Figure 5.5 and Figure 5.6), 90.0 µm for FG (Figure 5.9), 60.0 µm for HF with PVAc (Figure 5.10), 60.0 for HF with PVAc and nZnO (Figure 5.11), 2.0 µm (Figure 5.12) for nanozinc oxide.

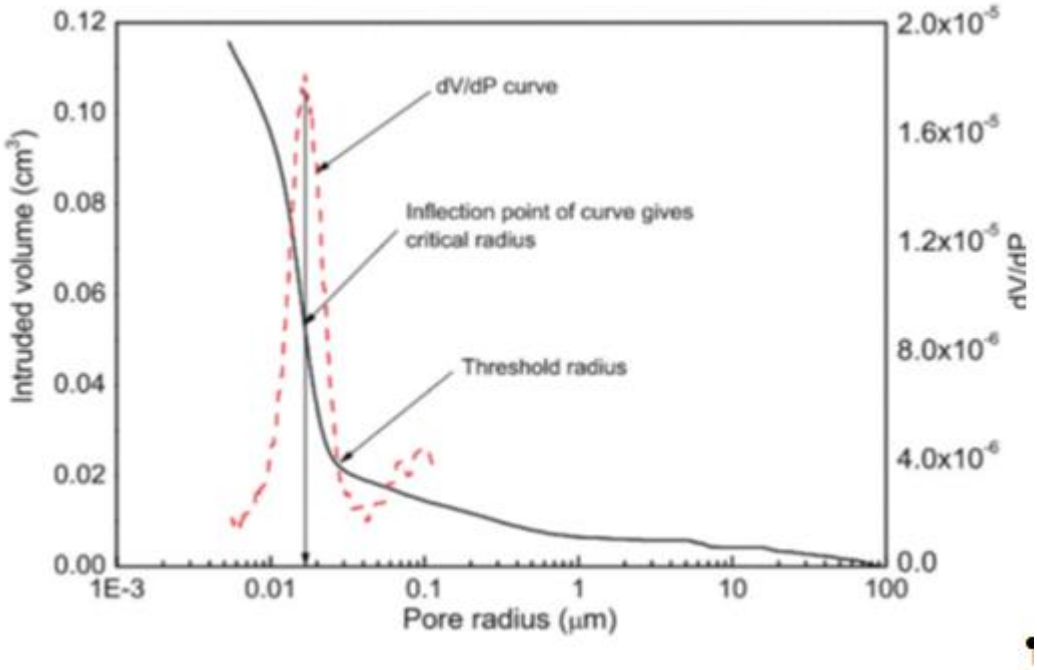

Figure 5.13 Definition of critical and threshold pore radius (X. Chen, Wu, & Zhou, 2014)

5.2.5 Comparison of Pore Size Distribution vs Volume Density for Specimen Groups P_1 and P_2

It was mentioned previously that the pore size ranges and critical pore size for all specimens of groups P_1 and P_2 varied and the critical pore sizes are different too but they were very close to each other's in P_1 and their porosity as well. Group specimens P_2 results were different from group p1, but their critical pore sizes and

their ranges of pore sizes in group P_2 were also close to each other and they gave porosities close to each other too.

A balance between the cumulative intrusion volume and the critical pore size is required. The porosity cannot be assessed solely on one of them; both must be taken in consideration. Figure 5.14 shows the critical pore size for all specimens of groups P_1 and P_2 and the pore size ranges. The critical pore size and the range of pore size as appears in the graph below are not enough indicators for porosity, it also depends on the cumulative intrusion volume of the pores in cm^3/g (Volume Density) which was discussed in advanced in this Section 5.2.4. The cumulative volume represents the whole volume in one gram and this is more accurate. Figure 5.14 shows that adding $nSiO_2$ and nclay to lime was decreased pore diameter of lime nanocomposites.

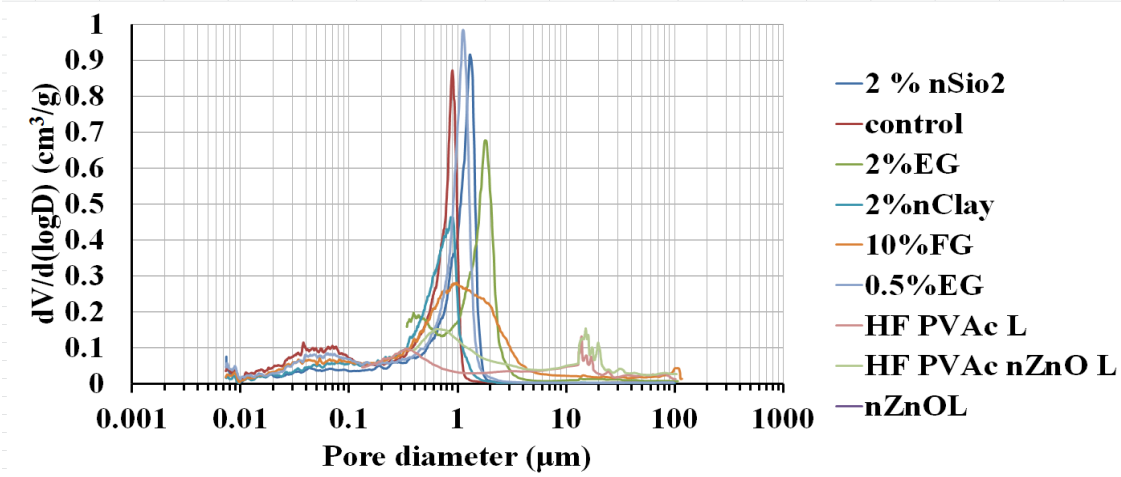

Figure 5.14 Comparison chart of pore diameter versus volume density for all specimens of different fillers

5.2.6 Porosity and Compressive Strength

Usually, higher compressive strength means lower porosity, but this is not always a constant rule (Bu & Tian, 2016; Erniati, Tjaronge, Zulharnah, & Irfan, 2015). For example, in porous composite materials which were reinforced by lightweight fibres (natural, like hemp fibres, or industrial, like fibre glass), higher porosity may not necessarily mean lower strength due to fibres effect which increases the compressive

strength in spite of them having a high porosity as it was appeared from the results of the porosity and strength of this project.

The effect of fibres is to increase the strength of the material and hold the porous materials by the friction between the fibres and lime matrix under loads such as the lime mixed with hemp fibres or fibre glass in this project.

Table 5.3 shows the results of porosity for Control, 0.5 wt. % EG, 2 wt. % EG, 2wt. % nclay, 2 wt. % $nSiO_2$and 4 wt. % nZnO and their compressive strength.

Table 5.3 Porosity and compressive strength for Render materials

No	% Filler	% Porosity	Compressive strength MPa
1	Control	36.4	4.2
2	0.5 wt. % EG	40.9	2.5
3	2 wt. % EG	28.4	3.4
4	2 wt. % nclay	31.5	4.5
5	2 wt. % $nSiO_2$	34.3	6.3
6	4 wt. % nZnO	18.1	0.7

Referring to Table 5.3, the highest compression strength (6.3 MPa) was obtained from material 5 2wt. % $nSiO_2$, conversely, when 4 wt. % nZnO was added, the compressive strength was only 0.7 MPa. The porosity for these specimens was 34.3 % and 18.1 % respectively. This result is unusual, the compressive strength decreases compared to pure lime (from 4.2 to 0.7 MPa) with the decrease of porosity (from 36.4 to 18.1 %). The effect of nanozinc oxide as small particles in lining and decreasing the pore diameters and as a result was led to decreasing porosity. Table 5.4 shows the porosity versus compressive strength of the Core (C) materials which include fibres (HF and FG).

Table 5.4 Porosity and compressive strength for Core (C) materials

No	% Filler	% Porosity	Compressive strength MPa
1	10 wt. % HF 30 wt. % PVAc	16.6	10.3
2	10 wt. % FG	40	7.2

Referring to Table 5.4, material 1 with a compressive strength of 10.3 MPa yielded a porosity of 16.6 %, whereas material 2 had a lower compressive strength of 7.2 MPa but higher porosity of 40 %. These two materials followed standard convention where a lower porosity led to a higher compressive strength despite the use of fibrous additives.

In Summary, by using Air-cured drying method the best core was 10 wt. % HF/L with 12 wt. % PVAc/L and 4 wt. % nZnO gave 17.8 and 7.3 MPa compressive and flexural strength respectively which can be used in Core material. In contrast, by using Oven-cured drying method and the same mixture of 10 wt. % HF/L with 12 wt. % PVAc and nZnO was considered the second best Core material in the proposed wall of this project because it has a high compressive and flexural strength (10.3 MPa and 4.4 MPa respectively) in comparison to pure lime (3.4 and 2.1 MPa respectively), and has low porosity (16.6 %) much lower than that of pure lime (36.3 %), and it is low porosity in comparison to concrete walls.

5.3 SEM Images

The samples for SEM were cut by a sharp knife from tested specimens for strength and prepared to be tested by SEM. Due to the samples were from lime and they were considered as porous material, the images of porous material usually are not obvious in spite of they were coated by carbon or by gold layer.

Nanosilica (SEM image) in Figure 5.15 (50 µm and magnification 4000, the image deforms when it magnificates more because the lime is porous material) shows that most of the nanosilica particles were assembled in clusters or microscale groups which propably the dispersion was low and their effect as nanomaterial was low too. The maximum pores as it was measured by the device of SEM and were about 7-8 µm and the most of pores were very small size as it was obtained by MIP pore size distribution which the critical diameter of pores of nanosilica was around 1 µm Figure 5.7 Figure 5.14. That means the porosity must be lower than its value of neat lime which was decreased from 36.4 to 34.3 % or the difference was about 2.1 % lower due the effect of nanosilica on decreasing the pore diameters. The white agglomerates are $nSiO_2$ (lime matrix is dark) and nanosilica agglomerates are larger or around the size of the measured pores in the image (7-8 µm) and it can be said that they are in micro not in nanosize.

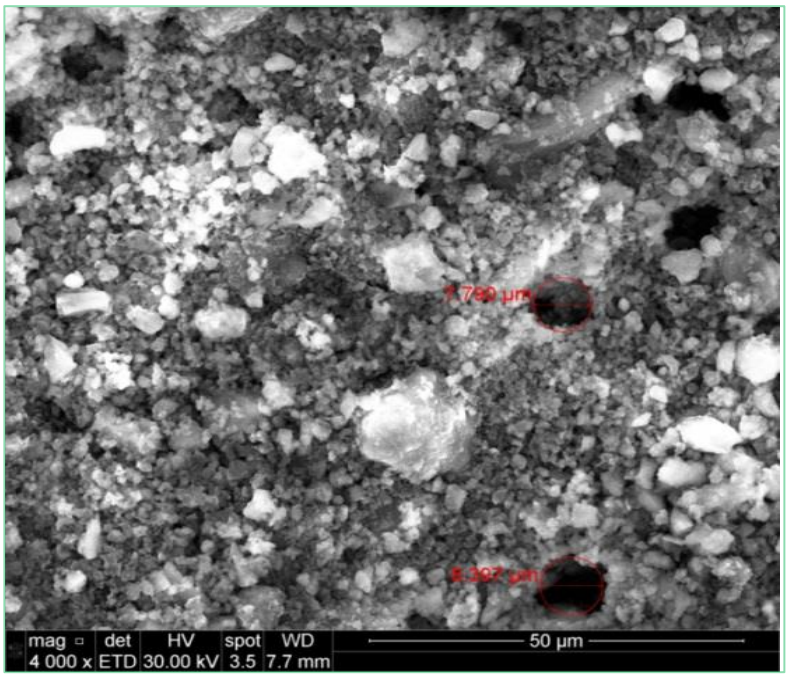

Figure 5.15 SEM image of 2 wt. % $nSiO_2$/L

Referring to Figure 5.16 nanoclay/L, the surface of the image appears as it is covered by nanoclay agglomerates and covered all the particles of lime which means the porosity was decreased and this was confirmed by MIP test. The porosity of the lime nanoclay composite by MIP test was 31.54 % which was decreased about 4.8 % to the neat lime. But the dispersion wasn't good as in the image a little of nanoclay agglomerates seems in singular case, the majority were in micro-groups not as nanoscale. The pores can be seen but they were very small compared to nanosilca image, the image of nclay/L is 2 µm scale and magnificated to 100000.

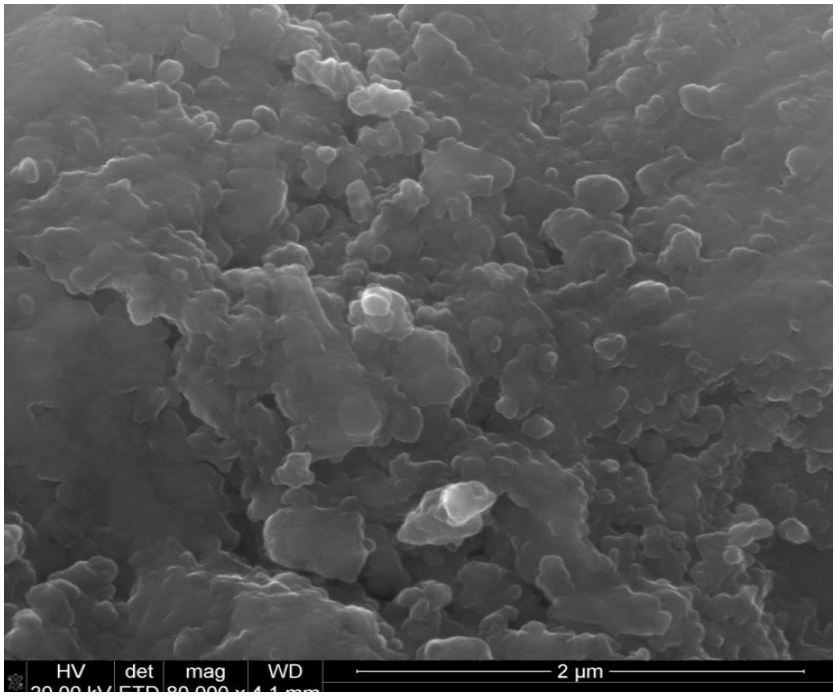

Figure 5.16 SEM image of 2 wt. % nclay/ L

Fibre glass as it appears in Figure 5.17 there are cavities between the lime paste and the fibre which permit to the water to move between the fibres and the paste. This case was led to more pores where the fibres are found in the paste which increased the porosity of FG/ L more than the pure lime as it was obtained by MIP test (40 %).

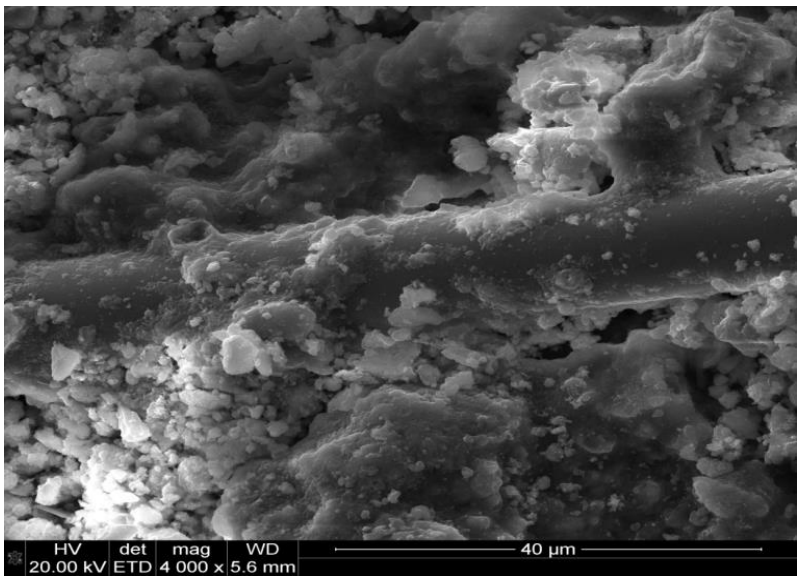

Figure 5.17 SEM image of FG/ L

Figure 5.18 represent SEM image of nZnO/L. Referring to Figure 5.18 of nZnO/ L, it can be seen a small agglomerates are dispersed in the paste cavities but it is not well dispersed. Possibly, the hexagonal structure of the shape of nZnO which is almost spherical shape disperses regularly in the pores and decreases the pore diameters; the porosity as a result was significantly decreases, its porosity was 18 %. It was reported that ZnO2 nanoparticles 2.0 weight percent could improve the strength of concrete and water permeability by curing the specimens in saturated limewater in tap water. Curing the specimens adding ZnO2 nanoparticles in saturated limewater led to form gel around nanoparticles improving permeability and giving high strength. Furthermore, ZnO2 nanoparticles are act as nanofillers recovering the pore structure of the specimens and decreasing harmful pores (Nazari & Riahi, 2011). Probably, the white structure is the gel which formed around nanozinc oxide agglomerates.

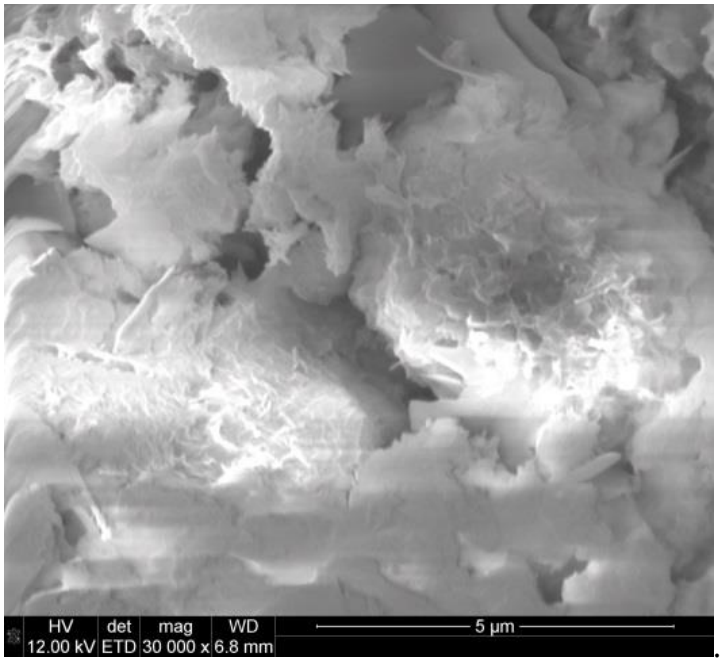

Figure 5.18 SEM image of nZnO/ L

5.4 Water Absorption Test

A water absorption test was conducted on a number of the specimens. These specimens were 2 wt. % Nanoclay, 2 wt. % $nSiO_2$, 2 wt. % EG, 10 wt. % FG and

pure lime. Table 9.8(Chapter 9, Appendix), shows the increasing weight (due to the continuing of water absorption) of the nanofillers at the times which is explained in column 2. The water absorption methodology is described in Chapter 3. Referring to Table 5.5, the specimen number is given in column 1. Column 2, identify the hour at which the reading were taken and column 3 is the time in minutes. Columns 4-8 are the wet weights which absorbed water with time for (control, 2% nclay, 10% FG, 2% nSiO2 and 2% EG). Column 9 contains the root square of time in second.

Table5.5 shows the calculation of the water absorbed according to the equations 5.3-5.6

U_t= (wet - dry) weight Equation 5.1

U_o= Wmax-Wdry Equation 5.2

IC= U_o/ W_d Equation 5.3

ABS= IC X 100 Equation 5.4

OP%= V_{op}/V_{sp}*100 Equation 5.5

Such that: V_{sp}= 4x4x16= 64 cm^3, V_{op}= volume of open pores= Wmax- Wdry.

M_i= Ut/ 64 cm^3 Equation 5.6

Table 5.5 Comparison between water absorption and porosity shows that as percentages, all porosity results of MIP test for Group P_1 were higher than the absorption test. The porosity by absorption and MIP tests for Control, nclay, $nSiO_2$ don't have a big difference and they were close to each others.

In contrast, the porosity by these two methods in the FG and EG samples yielded a higher difference. It may be the mercury, which was exerted by the MIP between the cavities of fibre glass and lime lead to an apparently higher porosity as a result.

For EG may the carbon origin was not encourage the absorption through absorption test. Probably, the Mercury under MIP method could enter between the EG platelets. So, for these reasons the porosity by MIP of EG was higher. MIP test may be more accurate because a standard device, standard steps were used. The water absorption

mainly depends on the practical case and on the human which is lower accuracy than standard devices.

In both the MIP and water absorption methods, the lowest porosity was for EG/ L at 2 wt. % was 18.9 % for water absorb and 28.4% for MIP. The other results were: 10 wt. % FG gave a water absorption porosity of 25.3%, 40 % for MIP, 2 wt. % nclay 25.9% water absorption, 31.5 MIP, 2 wt. % $nSiO_2$ 28.7% water absorption, 34.3 % MIP and control, 33.68% water absorption, 36.4 MIP. 4% wt. nZnO to lime gave the lowest porosity (18 % by using MIP) but it wasn't measured by using water absorption test. The rate of absorption is important because the capillary absorption represents the main and normal way of water and water vapour transport in a matrix (lime). The capillary water absorption defines the rate of change of matrix structure (J. Zhang et al., 2019). A number of water absorption characteristics are calculated in Table 9.8 (Chapter 9, Appendix). The data of this test relatively were relatively accurate, the test was conducted twice (repeatable).

The capillary porosity calculated and compared to MIP porosity in the table below is a comparison between capillary and MIP porosity results which they are higher in MIP than capillary porosity. The Table 5.5 below is a comparison between capillary and MIP porosity results.

Table 5.5 Comparison between water absorption and porosity

No	% Filler	% Capillary porosity from water absorption test	% Porosity by MIP group P_1
1	control	33.9	36.4
2	2 wt. % nclay	25.9	31.5
3	10 wt. %FG	25.3	40.0
4	2 wt. % $nSiO_2$	28.7	34.3
5	2 wt. % EG	18.9	28.4
6	4 wt. %nZnO		18.1

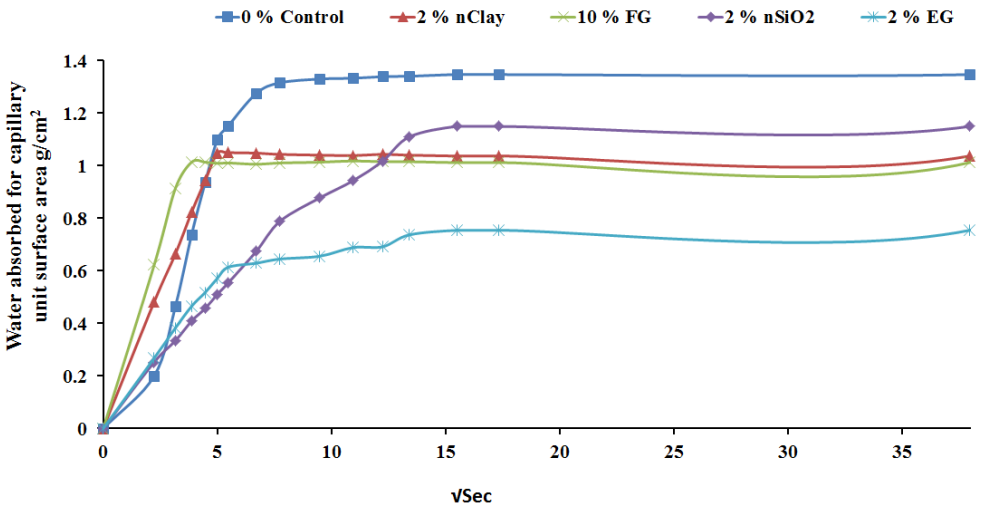

Figure 5.19 Water absorbed vs root square of time for lime with different fillers

Capillary test was conducted for group P_1 only, and didn't conduct for group P_2 which contains hemp fibres and shives because the absorption of cellulosic material is very high as mentioned for porosity (materials which contain hemp) in Sec. 5.2.3. More studies are needed about P_2 (10 wt. % HF 12 wt. % PVAc and 10 wt. % HF 12 wt. % PVAc with 4 wt. % nZnO) materials to check the effect (positive or negative) of PVAc and nZnO on water absorption of cellulose in hemp fibres.

Figure 5.19 shows also these results graphically that the lowest water absorption for capillary unit surface area g/cm^2 as a guide for porosity was ascending 2 wt.% EG, 10 wt. % FG, 2 wt.% nclay, 2 wt. % $nSiO_2$ and control and the values were (18.8, 28.7, 25.3, 25.9 and 33.6 % respectively). The capillary porosity of these fillers exhibited resemble result such as the EG (2 wt.%) was the lowest in this group as it was the lowest in MIP test. but is not the same sequence (Table 5.5) such that FG/L is higher than pure lime in MIP porosity (40 %) but it came the second lowest capillary porosity (25.3).

The lowest specimen results of porosity were obtained by MIP test in P_2 which didn't replicate by water absorption test and as they were mentioned, 10 wt. % HF/L 30 wt. % PVAc of water, 16.6 %, 4 wt. % nZnO, 18.1 % and 10 wt. % HF + 30 wt. % PVAc of water mixed with + 4 wt. % nZnO, 20.7 %. These results are near each

other and they can properly be used in the proper part of the proposed wall in this project. 4 wt. % Nanozinc oxide (18 % porosity can be used as a Render (R), 10 wt. % HF, 30 wt. % PVAc of water, 4 wt. % nZnO, 20.66 % can be used as Core (C) which is the highest compressive strength (10.3 MPa), high flexural strength (4.4 MPa) and low porosity by using oven dried method but the isolator panels can be used from 20 wt. % HS blended with 30 wt. % PVAc of the water (0.9 MPa) low compressive strength and has a high heat isolation (lowest thermal conductivity, 0.06 W/mK).

5.5 Discussion

Referring to Table 5.5, is a comparison between capillary and MIP porosity results which they were higher in MIP porosity than capillary porosity. The porosity obtained from water absorption test results were lower than porosity obtained by MIP. Possibly, by the impact of the intrusion pressure of mercury which increases the pore size and as a result increases the porosity in comparison to water absorption method. This case was agreed with the literature, which was reported, that the obtained porosity results by water absorption were lower by 2 % than by MIP (Arandigoyen & Alvarez, 2006). In this study the difference was more than 2 wt. % due to the pressure of MIP method possibly, increases the pore volume of lime and high porous materials higher than concrete for their variation in bond particles connection between concrete and lime.

The lowest porosity which was obtained by water absorption test (capillary porosity) 2 wt. % of EG (18.8 %) was different from MIP porosity but still the lowest (28.4 %) by using MIP

method). The highest result by using water absorption test was control (33.6 %) and it was different but still the highest in MIP test too (36.4 %).

The lowest specimen results of MIP porosity were that 10 wt. % HF, wt. 30 % PVAc, 16.6 %, 4 wt. % nZnO/L, 18.1 % and 10 wt. % HF/L, 12 wt. % PVAc/l and 4 wt. % nZnO, 20.7 %. These results are near each other's and they can be recommended for using in the proper layer (Lowest porosity will be in render layer, highest strength (compressive and flexural) in core layer even if it is higher porosity than render materials) of the proposed wall in this project. 4 wt. % (nZnO)/L of 18

% porosity can be used as a Render (R), 10 wt. % HF/L, 30 wt. % PVAc of water 4 wt. % nZnO, 20.66 % can be used as core which is high compressive strength (10.3 MPa), high flexural strength(4.4 MPa) and low porosity.

Referring to Table 5.3 and Table 5.4, the compressive strength was increased with the decreasing of the porosity except $nSiO_2$. Possibly, the effect of nanosilica is high on the compressive strength of lime nanocomposite which leads to increase the compressive strength regardless the porosity is high or low. For EG, the porosity was decreased by adding EG without increase in compressive strength because the particles were behaved as microscale groups not as nano-separated particle to strengthen the solid paste of lime and the particles were participated in the beaker directly after stirring was stopped and it can be seen by free eye.

In contrast, the fibres composite in Table 5.4 was different, the compressive strength significantly was increased, regardless the decreasing or increasing much or less the percentage of porosity. For example, the compressive strength of FG/L was high (7.3 MPa) in spite of its highest porosity (40 %) which was more than the neat lime but for 10 wt. % HF and 30 wt. % PVAc, the compressive strength (10.3 MPa) was higher than FG/L (7.3 MPa) and its porosity was the lowest (16.6 %) and that means the strength depends on the fibres effect out of the limit of porosity effect.

It can be said, nanozinc oxide was the first time used with lime, PVAc was the first time used with lime too and the results of porosity were the lowest results (18 and 16 % by MIP). These results were about half of the porosity value of pure lime (36 %). This is beside of the benefits of nanozinc oxide which was mentioned in literature review Chapter 2, it was antibacterial material and healthy for human.

The goal of decreasing the porosity of lime nanocomposite to be a little higher than cement mortar limit of porosity (10-15 %) was achieved it was 18.1 % for render (R) and (16.6-20.7 %) for Core (C) in comparison to the porosity of pure lime (36.4 %).

Chapter 6 - **Shrinkage and Water Vapour Permeability**

6.1 Shrinkage

Reducing shrinkage is very important for strength and durability of construction materials. Durability is affected by shrinkage due to the cracks which allow moisture an easy path into the material. This chapter investigates the shrinkage properties of a number of nanomaterials as fillers added to lime.

6.1.1 Introduction

Shrinkage, physically and chemically is a reduction of volume due to loss of water, free shrinkage is a change in size but not deterioration in the shape. Shrinkage is calculated as the change in length relative to the original length. The strain is normally given in parts per million $1.0 * 10^{-6}$, but is more frequently referred to as microstrain (µs). About 20-30 % of shrinkage happens in the first 7 days and about 80 percent occurs by water evaporation effect. The volume shrinkage is about 3.2 % for neat cement and 9.0 % for neat lime paste which leads to cracks (JOHNSON, 1926). The percentage change limit in length (shrinkage) of prism of cement was less than 0.04 at 28 days (Mokarem, Weyers, & Lane, 2005). Furthermore, another standard reported that the percentage change limit in the length of a prism of cement should be less than 0.05 % or 500 microns at 28 days of drying (ASTM, 2017; MasterKureER50, 2014). The studies on lime shrinkage are very limited. It was reported that the drying shrinkage was studied for two lime mortars, the first mortar was lime and sand 1 to 3 by weight and the second was lime and fine aggregate called Albero, 1 to 3 ratio also. The first mortar with fine aggregates, granular diameter size more than 0.08 mm, gave 1200 µs or 0.12 % shrinkage. The second mortar exhibited 12500 µs or 1.25 % shrinkage with granular diameter size less than 0.08 mm. Sanchez et. al (1997) commented in the conclusion on the first mortar shrinkage (1200 µs) that it was almost negligible shrinkage (A. Sánchez, Barrios, Barrios Padura, & De Arellano Agudo, 1997).

The goal in this research is to decrease the shrinkage in the lime binder to ensure a durable lime based construction material is produced. The aim is to get the shrinkage

of the lime based materials as low as possible to ensure the materials are strong and durable.

6.1.2 Shrinkage Specimen Curing and Results

A group of specimens were tested in the present project with dimensions 40 x 40 x 160 mm. They were demoulded after five days and stored at 60 % humidity at 20ºC. Two strain demec points, 100 mm apart, were centrally placed on the centre line of the specimen and fixed by epoxy. This was repeated on the opposite side of the specimen.

The shrinkage was measured by a demec strain gauge with a gauge constant of 1.608 $x10^{-5}$. The specimens were Control of pure lime, 2 wt. % nclay, 2 wt. % $nSiO_2$, 2 wt. % EG and 10 wt. % FG and 4 wt. % nZnO. Measuring of shrinkage continued up to 28 days after which the specimens were used for flexural and compressive strength (Chapter 4).

The shrinkage strain values are shown in Table 6.1. The days of the test are given in column 1, columns 2-6 are the calculated shrinkage values of the Control and nanocomposite samples. The results from Table 6.1 are presented graphically in Figure 6.1.

Table 6.1 Shrinkage of different specimens

	Shrinkage $x10^{-6}$					
1	**2**	**3**	**4**	**5**	**6**	**7**
Days	**Control**	**2 % EG**	**2 % nclay**	**2 % $nSiO_2$**	**10 % FG**	**4 % nZnO**
1	00.0	00.0	00.0	00.0	00.0	00.0
2	112.5	48.2	128.6	192.9	32.2	32.2
3	321.6	257.3	514.6	321.6	160.8	117.9
4	562.8	498.5	1000.8	514.6	289.4	278.7
5	836.2	739.7	1300.9	804.0	418.1	375.2
6	1125.6	996.9	1700.4	1350.7	530.6	471.7
7	1366.8	1238.2	2100.0	1527.6	659.3	525.3
8	1543.6	1447.2	2350.5	1929.6	755.8	573.5
9	1768.8	1559.7	2540.6	2219.0	836.2	605.7
10	1929.6	1688.4	2765.7	2492.4	900.5	675.4
11	2074.3	1784.9	2894.4	2669.3	980.9	728.9
12	2154.7	1833.1	3006.9	2814.0	1013.0	739.7
13	2219.0	1881.4	3087.4	2878.3	1061.3	739.7
14	2267.3	1929.6	3151.7	2942.6	1093.4	739.7
15	2299.4	1929.6	3232.1	2974.8	1109.5	734.3
16	2331.6	1945.7	3264.2	2990.9	1125.6	728.9
17	2379.8	1977.8	3296.4	2998.9	1141.7	723.6
18	2428.1	1993.9	3328.6	3006.9	1157.8	723.6
19	2428.1	2042.2	3376.8	3039.1	1173.8	745.0
20	2428.1	2042.2	3392.9	3055.2	1189.9	745.0
21	2428.1	2042.2	3392.9	3071.3	12221	745.0
22	2428.1	2042.2	3392.9	3071.3	1222.1	771.8
23	2428.1	2042.2	3392.9	3071.3	1222.1	771.8
24	2428.1	2042.2	3392.9	3071.3	1222.1	771.8
25	2428.1	2042.2	3392.9	3071.3	1222.1	771.8
26	2428.1	2042.2	3392.9	3071.3	1222.1	761.1
27	2428.1	2042.2	3392.9	3071.3	1222.1	750.4
28	2428.1	2042.2	3392.9	3071.3	1222.1	750.4

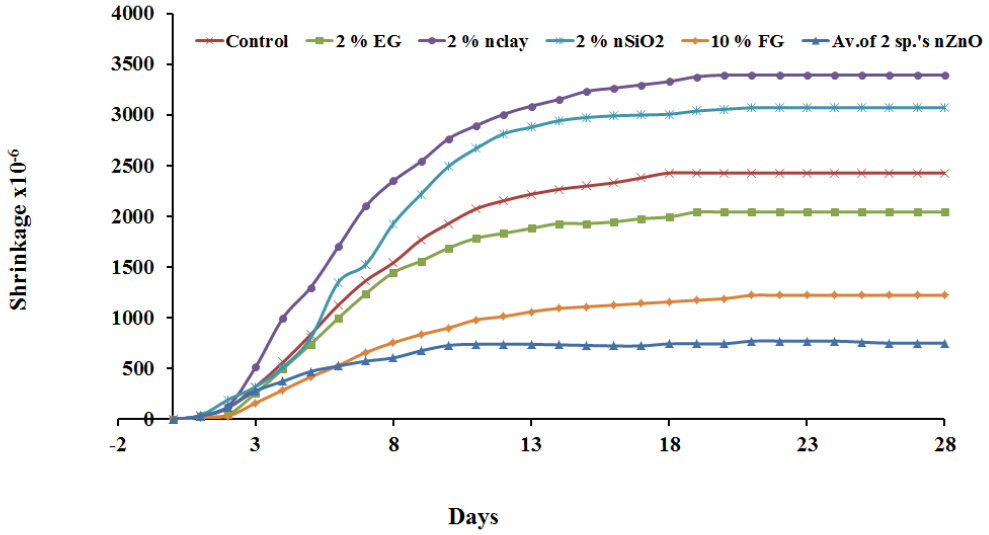

Figure 6.1 Shrinkage of lime nanocomposite and fibre glass lime composite

Table 6.1 and Figure 6.1 show that the lowest shrinkage was obtained by adding 4 wt. % nZnO/L which was about 750.4 x 10^{-6} at 28 days. The second lowest result was achieved by mixing FG/L at 10 wt. % of lime and the shrinkage was about 1222 x 10^{-6} at 28 days. The next lowest shrinkage was achieved by adding 2 wt. % EG which was 2042 x 10^{-6} at 28 days. Control specimen had the fourth lowest shrinkage of 2428 x 10^{-6} and the final two were 2 wt. % $nSiO_2$ and 2 wt. % nclay with shrinkages of 3071.3 and 3392 x 10^{-6} respectively. The lowest shrinkage was achieved by adding 4 wt. % nZnO; it was 750.8 x 10^{-6} at 28 days which is a little higher than the shrinkage of a cement mortar referred to earlier in this chapter which was 500 µs (Mokarem et al., 2005). However, comparing to the shrinkage study of lime/sand with the particle size of the sand less than 0.08 mm (the lowest shrinkage in the mentioned study=1200 µs), the addition of 4 wt. % nZnO resulted in a lower shrinkage (~750 µs) (A. Sánchez et al., 1997). Shrinkage cracks can be seen by the naked eye, this was particularly the case for the pure lime and the nanosilica lime samples. The fibre reinforced samples were completely void of cracks but for the other lime nanocomposite samples, the cracks were very small (micro-cracks). It is theoretically assessed elsewhere that contraction due to long time drying shrinkage could be

of the order of 10,000 microns, but values up to 4,000 microns have been actually observed and led to obvious cracks (Ahmad, Ibrahim, & Tahir, 2010; Passuello, Moriconi, & Shah, 2009; *Shrinkage of concrete*, 2018). In this project, the specimens which were mixed from 12 wt. % PVAc, 10 wt. % HF/L and 4 wt. % nZnO didn't show any crack. It can be concluded that the shrinkage was very low and the differential contraction was stopped by fibres.

6.2 Water Vapour Permeability (WVP)

6.2.1 Introduction

This test was conducted according to standard procedures (BSEN1015-19, 1999). Lime is a breathable material which is a healthy property; it permits humidity and gas to move through the wall of the building better than concrete which can eliminate bacteria and fungal growth, moisture trapping, surfaces breaking down, colour change, damp patches appearing and rot and beetle infestation occurring. This can be harmful to the wellbeing of the building and the residents. Sometimes, there is a misunderstanding about breathability. It is confused with air permeability but they are different things. The water vapour transmission rate or the vapour speed at which it passes through a particular construction material is the meaning of the breathability term. The uncontrolled movement of air through joints and gaps means air permeability (air leakage).

In comparison to industrial insulators (especially from plastic, it seals the wall preventing vapour movement), natural insulators are better due to their higher breathability and they are like moisture buffers, they absorb and release water as the relative humidity through the building becomes high or low (Hunt, 2018).

Water vapour permeance is considered the quantity of water vapour passed across a unit area which will pass through a unit thickness while it is under a unit vapour pressure difference, whereas the water vapour permeability is the water vapour permeance multiplied by the thickness of the specimen. In a study about lime, river sand, crushed brick (which had the same particle size as the sand), cement and sand, it was found that water vapour permeability for a 1: 3 cement : sand mix (cement mortar) was 0.98 $x10^{-11}$ kg/m s Pa, lime : sand mix (lime mortar), also with 1 : 3 was 1.76 x 10^{-11} kg/m s Pa and for lime : sand : brick dust : crushed brick grains ratios

mix 1 : 0.5 : 1 : 2 was 1.99 $x10^{-11}$ kg/m s Pa (Matias, Faria, & Torres, 2008). Water permeability means interconnected opened pores, and these pores already are opened for water vapour permeability (breathability). Higher permeability to water and water vapour are found in mortars especially with higher percentage of aggregate. The behaviour to water and water vapour as well as the drying shrinkage of mortars is affected by the differences in microstructure and pore system between mortars. Water vapour transmission rates are preferred to be higher to activate drying through the mortar. There are two drying stages of porous material surfaces, one is related to the temperature, relative humidity and ventilation, and the another is obtained by the water transfer properties of the material, which depend on the pore system (pore size and interconnection among pores) (Anna Arizzi & Cultrone, 2013; Nokken, 2003).

6.2.2 Water Vapour Permeability Specimen Curing and Results

The procedures adopted for water vapour permeability testing followed British Standard BS EN 1015-19, 1999. According to the test standard, the area of the open mouth of the cup is 0.025 m^2 which translates to a diameter of about 160 mm. The cup is designed with a lip to support the disc specimen meaning the overall diameter of the specimen is 185 mm. The thickness is about 20 mm. At 5 days after casting, the specimens were demoulded, put 2 days in an oven at 50ºC and were then stored for up to 28 days at 60 % RH and 20 ºC. Figure 6.2 shows the mould and the control specimen inside. It was cured as Part C1- Oven cured which was the preconditioning of samples before test.

After curing, one specimen at a time was placed in the cup containing saturated solution of potassium nitrate (KNO_3). A gap was maintained between the top of the KNO_3 and the bottom of the specimen. The specimen was then sealed by adhesive around the circumference to prevent water vapour escaping. The weight of the specimens and the cups which contained KNO_3 were taken daily for a week to calculate the weight loss of the whole specimen and the cup with KNO_3.

The humidity inside the cup is 93.2% and the outer humidity in the storage chamber at the start of the test is 50 % at 20°C.

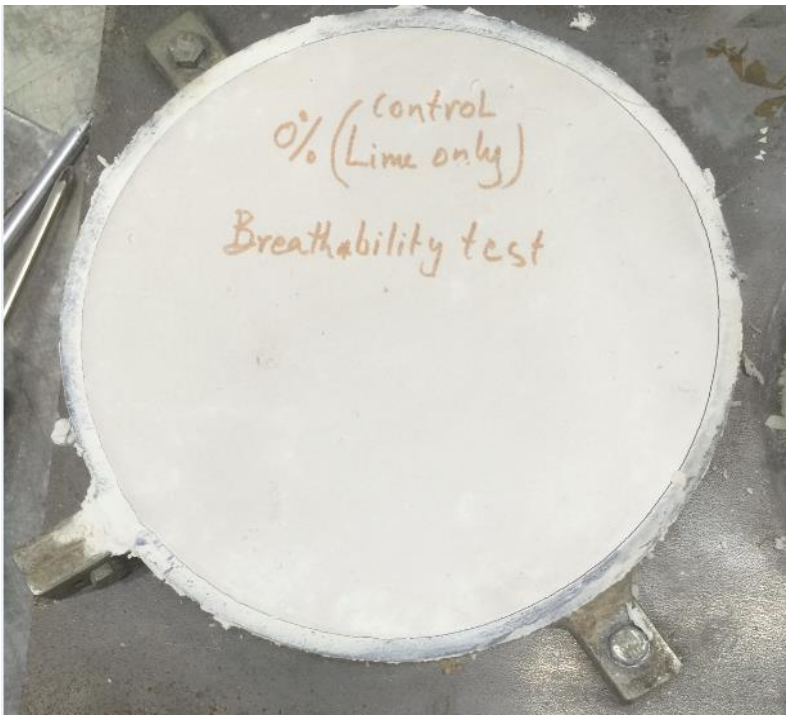

Figure 6.2 Water vapour permeability mould and specimen

6.2.3 Theory

A= Area of the open mouth of the specimen = 0.025 m^2,

Sample thickness = 0.02 m, Ra (given from standard tables) = 86400000 Pa m^2/ kg per 18 mm air gap,

P_o= 2.3393 KPa, P= (RH/ 100) P_o=50/100 (2339.3)= 1170 Pa; if RH = 50 %,

P_{salt}= (93.2/ 100) P_o= 2180 P_a; if RH= 93.2 % and then

ΔP or $D_p = P_{ambient} - P_{salt}$= -1010 P_a.

WVP (water vapour permeability) =Δ (water vapour permeance). t (thickness)

$WVP = \Delta t$ Equation 6.1

$\Delta = 1/ [A.Dp/ (\Delta g/\Delta t)-Ra]$ Equation 6.2

$\Delta g/\Delta t$ (Water vapour flux Kg/s) = the tangent of the last three weight loss vs the last three measured weights. The tangent is only calculated for the last three measured

weights at stable case of low weight loss as in the standard reference BS EN 1015-19, 1999.

Table 6.2 shows the original weight of the specimens (Control, 1.5 wt. % EG, 2 wt. % nclay and 2 wt. % $nSiO_2$) and their daily weights up to 7 days.

Referring to Table 6.2, Col 1 is the sample id number, Col 2 shows the day, time and details of the specimens (Control 1, Control 2, 1.5 % EG, 2 % nClay and 2 % $nSiO_2$), Columns 3-9 are the weights in grams at the date and time for each specimen throughout the eight day test period.

Table 6.2 Weights of fillers/ lime nanocomposite specimens with time for water absorption

1	2	3	4	5	6	7	8	9	10
	Day	**Wt.1 (g)**	**Wt.2 (g)**	**Wt.3 (g)**	**Wt.3 (g)**	**Wt.4 (g)**	**Wt.5 (g)**	**Wt.6 (g)**	**Wt.7 (g)**
No		**1**	**2**	**3**	**4**	**5**	**6**	**7**	**8**
	Time	11:30	11:30	11:30	18:37	11:30	11:45	11:50	11:30
	% nFiller								
1	**Control 1**	1472.2	1467.2	1464.4	1461.7	1460.5	1458.5	1456.9	1455.2
2	**Control 2**	1492.6	1487.9	1485.6	1482.9	1481.8	1479.9	1479.4	1476.8
3	**1.5% EG**	1351.6	1345.9	1342.4	1338.9	1337.3	1334.6	1332.5	1330.6
4	**2%nClay**	1456	1450.4	1447.3	1444.3	1442.6	1440	1437.9	1335.7
5	**2%nSiO2**	1398.6	1391.7	1388	1384.3	1382.6	1379.9	1377.7	1375.4

6.2.4 Example WVP Calculations

Calculation examples for the Control specimens are given in Table 6.3 and the details of these calculations are:

$\Delta wt/\Delta t$ (g/ hr) = mean weigh loss difference/mean time difference (for the last three stable measurements)

= [(17-15.3) + (15.3-13.7)]/2/[(168-144.33)+(144.33-120.25)]/2

= [(1.7) + (1.6)]/2/[(23.67) +(24.08)]/2=[(3.3/2)/ (47.75/2)]

= 16.5/ 23.875=0.0691 g/ hrs or =.0691/ 1000 x 3600

= 1.1944×10^{-8} Kg/ s

Dp or ΔP= -1010 Pa as calculated above

Permeance (Δ) = 1/ [A (Dp)/(Δwt. / Δt) - Ra]

Permeance (Δ) = 1/[025 (-1010)/ (-1.65./23.875) - 86400000] = -7.13325 x 10^{-10} ($kg \cdot s^{-1} \cdot Pa^{-1}$)

WVP = Δ x t or (water vapour permeance x thickness) = -7.13325E-10 x 0.002 =-1.42665 x 10^{-11} ($kg \cdot m^{-1} \cdot s^{-1} \cdot Pa^{-1}$)

Table 6.3 Weights and time of weighing two control specimens and the calculations

WVP calculations		Day and Time	Time in hours	Square root of time ($t^{1/2}$)	Wt. (g) 1	Wt. loss (g)	Wt. (g) 2	Wt. loss (g)	Av. (g)
Δwt/Δt=0.0691	**g/hr**	1			1472.2		1492.6		
=1.91944E-08	**Kg/s**	2	24.00	4.9	1467.2	-5	1487.9	-4.7	-5
0.025	**A**	3	48.00	6.9	1464.4	-7.8	1485.6	-7	-7.8
86400000	**Ra**	4	79.12	8.9	1461.7	-10.5	1482.9	-9.7	-10.5
-1010	**Dp**	5	96.00	9.8	1460.5	-11.7	1481.8	-10.8	-11.7
-7.13325E-10	**Permeance**	6	120.25	11.0	1458.5	-13.7	1479.9	-12.7	-13.7
-1.42665E-11	**WVP**	7	144.33	12.0	1456.9	-15.3	1479.4	-13.2	-15.3
		8	168.00	13.0	1455.2	-17	1476.8	-15.8	-17
-7.60176E-10	**Perm w/o Ra**								
-1.42E-11	**WVP w/o**								

6.2.5 WVP of Selected nanomaterials

Figure 6.3 shows the average weight loss in grams of the Control specimen vs time in hours. Referring to Figure 6.3, it shows a very strong correlation factor between evaporation (weight loss) and time. The average weight loss can be determined for the Control sample using the equation:

$y = -0.0691x - 5.3692$ Equation 6.3

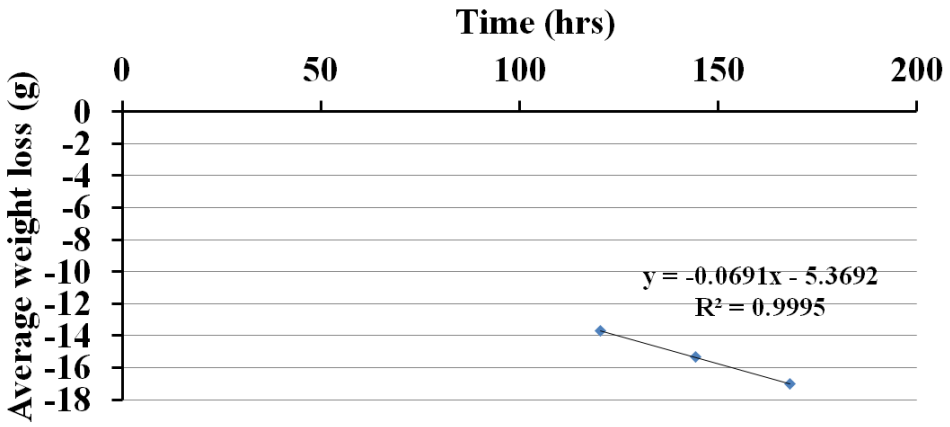

Figure 6.3 Average weight loss vs time for WVP for control specimens.

The value (-0.0691) in the Equation 6.3 is the slope of Δ wt./Δt and it is used to calculate the WVP as described in Section 6.2.4. The specimens WVP for 2 wt. % nclay/L, 2 wt. % $nSiO_2$/L and 1.5 wt. % EG/L were calculated in the same way and the results are given in Table 6.4. The results were ended by 10^{-11}, they were different from the results of shrinkage which usually ends by 10^{-6}.

Table 6.4 Results of calculation of WVP for different lime nanocomposite and control specimen

No	% Fillers	Water Vapour Permeability ($kg \cdot m^{-1} \cdot s^{-1} \cdot Pa^{-1}$)
1	Control	$1.43E^{-11}$
2	1.5% EG	$1.71E^{-11}$
3	2% nClay	$1.96E^{-11}$
4	2% $nSiO_2$	$1.90E^{-11}$

Figure 6.4 graphically shows that the breathability was enhanced for all fillers of nanomaterial in spite of the pure lime having good water vapour permeability. The

best performing material was 2 % nclay with a WVP of 1.96 E^{-11} $kg \cdot m^{-1} \cdot s^{-1} \cdot Pa^{-1}$ and this result is very close to the highest result of WVP in the study of Matias et al, 2008 which was 1.99 E^{-11} $kg \cdot m^{-1} \cdot s^{-1} \cdot Pa^{-1}$ for lime mixed with sand, crushed brick and brick dust. Overall, the addition of nanomaterials has generally enhanced the breathability of the lime nanocomposites. Nanozinc oxide was not tested due to an issue with the supply of KNO_3

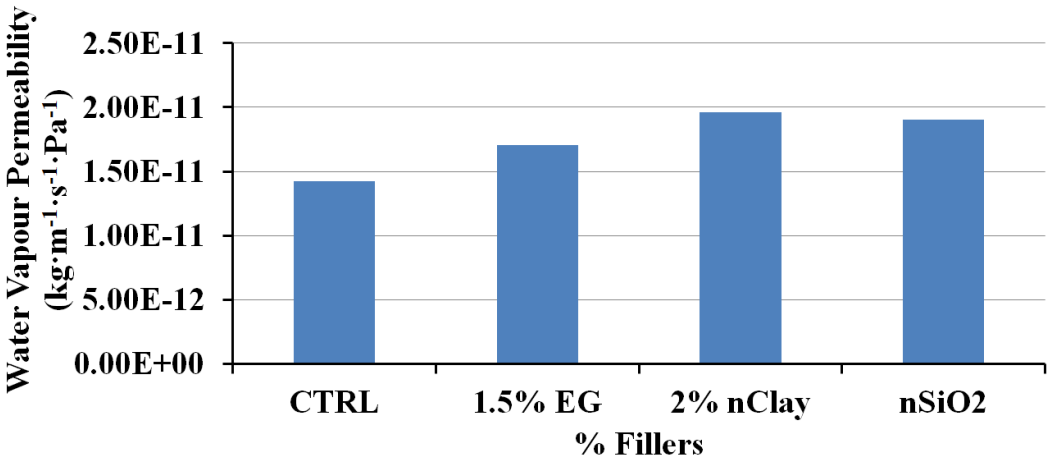

Figure 6.4 Comparison of water vapour permeability for different lime nanocomposites and pure lime

6.3 Discussion

The lowest result for shrinkage was, 4 wt. % nZnO 10wt./lime composite which was 750.4 $x10^{-6}$ The second best was 1222 $x10^{-6}$.for 10 wt. % FG and the third best was 2042 x 10^{-6} for 2 wt. % EG. The nanoclay filler was the highest value followed by nanosilica value, they were more than pure lime which was 2428 $x10^{-6}$. The platelets of EG have a high effect on shrinkage due to its structure. The chopped fibres which were dispersed in lime matrix in different directions were beneficial in decreasing the shrinkage but the shrinkage of hemp fibre wasn't tested in this project except FG was tested. The positive effect on decreasing shrinkage is agreed with the literature, for example, polyvinyl alcohol mixed with recycled tyre polymer fibres added to concrete, using three fibre diameters of 10, 20 and 30 µm and mean length of 12 mm indicating that there was a good chance of using recycled tyre polymer fibres in concrete products as the results were similar to these obtained using polypropylene fibres in preventing micro-cracking developed by shrinkage. The polypropylene

fibres at 0.5 % were added to the concrete mix, the shrinkage reduction was 31%, 40 % and 46 % at 20ºC, 35ºC and 50ºC in comparison to plain concrete (Bouziadi, Boulekbache, & Hamrat, 2016). Mix of hemp lime NHL3.5 and water at ratios 3: 5: 2.5 showed low shrinkage and the shrinkage tension was reduced to zero, low thermal conductivity and high acoustic insulating behaviour (A. Arizzi, Brummer, Martin-Sanchez, Cultrone, & Viles, 2015). The fibres are adopted to reduce shrinkage due to its availability as a sustainable material especially natural fibres, as hemp fibres are environmentally friendly, sustainable, durable, proved to improve mechanical strength and now as a way to decrease shrinkage. The shrinkage for FG was about 0.12 % as it is known that fibre glass doesn't bond well with lime, but the hemp fibres have a higher bond with lime than fibre glass and will help reduce shrinkage more so than fibre glass. Simply, the surfaces of hemp fibres are rougher than the surfaces of fibre glass. In the literature, it was reported that hemp shives mixed with lime led to low shrinkage (A. Arizzi et al., 2015). Possibly, the hemp fibres can reduce shrinkage more than hemp shives due the network of fibres inside the lime matrix. There are multiple benefits of using fibres for the "core" material (see Figure 5.1, Chapter 5). Not only does it help strengthen the lime and PVAc mixture, it is also helps to reduce shrinkage of the material. However, for the finer materials such as the lime render ("Render", Figure 5.1, Chapter 5), the shrinkage can be reduced by adding fine aggregate such as sand. The addition of fine aggregate was not considered in the project but could be investigated in future work. In the literature it was reported that an increase in the quantity of sand leads to a decrease in compressive strength and workability but using fibres helps exceed the strength decrease or a combination of the fibres and the sand (Zeng, Li, Fen-chong, & Dangla, 2012). The platelets of EG have a high effect on shrinkage due to its structure. The expanded graphite has only one dimension in nanosize and the others are in microns, hence the reason why their components are called platelets. These three dimensions probably help in confirming the lime matrix and decreasing the shrinkage.

As for water vapour permeability of pure lime, the literature reports on the breathability being better for pure lime rather than cement mixed with lime (Hatherngton, 2014; Rhydwen, 2015). Fortunately, using nanomaterials as additives enhanced the WVP of lime nanocomposites in comparison to pure lime by adding 2

wt. % nclay, 1.5 wt. % EG and 2 wt. % $nSiO_2$. Nanomaterials in general organise the pore size, decrease porosity but leave pore size open and less than 10 μm as it was seen in Chapter 5. Improving porosity and pores led to an increased WVP. Porosity was tuned by annealing the membranes at different temperatures by using nanomaterials (Marchetti, Mechelhoff, & Livingston, 2015). Cement mixed with 0.5 wt. % multiwall carbon nanotubes improved its porosity by 64 % and its pores with size more than 50 nm by 82 % in comparison to cement with microscale carbon fibres which had high porosity (Parveen, Rana, & Fangueiro, 2013). WVP increases with the decrease of porosity and pores which is a benefit of using nanomaterials. The optimum result of porosity was by adding 4 wt. % nZnO in this project Chapter 5, and is likely be the optimum in WVP but this property was not tested for nZnO which will be a future work. The mixture of lime, HF, PVAc and nZnO which represents the Core layer of the proposed wall in this project was tested for flexural and compressive strength, porosity and shrinkage. Testing for WVP of lime, HF, PVAc and nZnO was not done due to issues with the supply of KNO3 as mentioned in Section 6.2.5.

Adding nZnO to lime achieved many benefits, such as decreasing porosity to 18 %, shrinkage to 750 μs and thermal conductivity to 0.13 compared to pure lime (36.4 %, 2428 μs, 0.16 W/mK respectively). This is as a result of its many properties (high heat absorption capacity, it is hexagonal structural shape as a small spherical particles to lining pores and phonon phenomenon). The small spherical structural particles of nZnO in nanosize help in filling and lining the pores and decreasing the diameter size of the pores which leads to a decrease in porosity. High absorption capacity of nanozinc oxide helps to reduce thermal conductivity. Phonon improves heat absorption because it is the vibration of the lattice of its particle structure with heat transfer and this property improved heat isolation and reduced shrinkage by decreasing heat transfer which led to a reduction in differential drying which prevented cracking and decreased shrinkage (Bhagat & Khanna, 2015; Mohandas et al., 2015; Nazari & Riahi, 2011; Y. Zhao et al., 2012).

Chapter 7 - **Factors Affecting Thermal Properties of Lime nanocomposites**

7.1 Introduction

Factors affecting pore structure of construction materials has become very important due to their direct effect on the energy efficiency of buildings. The aim of this work, therefore, is to design an energy efficient wall for use in domestic buildings, consisting of five layers (2 Renders, 2 Insulators, 1 Core) as outlined in Chapter 1. Different percentages of nanomaterials to enhance performance ($nSiO_2$, nClay and nZnO) were added. The porosity of a number of specimens was determined (Chapter 5) and related to thermal conductivity and density properties in this Chapter. Renders were designed from materials consisted of lime nanocomposites (properties determined were thermal conductivity (λ) and porosity). Insulators used for thermal isolation (λ) consisted of lime/hemp shiv nanocomposites. A lime/hemp fibre nanocomposite, with polyvinyl acetate (PVAc) glue for strength, was developed as a load bearing material (Core, its important properties are λ and strength). A solvent exchange method for drying the specimens was applied as soon as practically possible to investigate if rapid drying could be considered without adverse effects. This chapter concludes by comparing the U value of a wall utilising these findings to those from an existing lime/hemp design.

7.1.1 Recent Statistics in Energy Consumption in the Domestic Sector

Recent statistics show that 30 per cent of all energy consumed was for domestic energy in the United Kingdom (UK) in 2017 (BEIS, 2018). Space heating accounted for 19 % of this energy. It is clear that a major contributor of greenhouse gas emissions is domestic energy use in the UK, especially carbon dioxide (CO_2), not least due to the age of properties, they are very energy inefficient (BRE, 2015). The UK Government's legally binding commitment to reducing greenhouse gas emissions was by at least 80% (relative to 1990 levels) by 2050 (CommitteeOnClimateChange, 2008; Henderson, Reinert, Dekhtyar, & Migdal, 2015; Scheer & Hoppner, 2010). The traditional construction of buildings in the UK is by 203using relevant building materials such as concrete blocks, bricks and less so, timber. Although timber is a sustainable product, fabrication of concrete blocks and bricks require a lot of energy input, a large producer of CO_2 during its manufacture especially is concrete. However, other materials of low embodied energy are being developed and used, some are new innovations, such as

alkali activated such as fly ash (Mangat & Ojedokun, 2018), others are a mixture of old and new such as lime and hemp composites (Collet & Prétot, 2014; Walker & Pavía, 2014)

With regard to the materials used in the construction of buildings, a very important property is thermal conductivity. A low value will help and keep the living environment at a comfortable temperature. Nowadays, greater effort is spent in making buildings more eco-friendly. For a long time, lime render has been used as a finish to walls, but the use of lime has gone through a renaissance due to its low embodied energy in production. It is used as a binder for hemp shiv and hemp fibres to create lime/hemp composites. Hemp stem straw contains two products for building materials: hemp fibres are strong and can be used to make lime/hemp fibre panels and hemp shiv is used as a bio aggregate in hemp composites (also known as hemp concrete) (Collet & Prétot, 2014). The lime/hemp shiv composite, in particular, has advantageous insulative characteristics as it has a low thermal conductivity, about 100 mW/mK (Bederina et al., 2007) and is lightweight, density is 200-400 kg/m^3 (Amziane & Arnaud, 2013).

7.1.2 Significance of Thermal Conductivity

Although hemp concrete has a low thermal conductivity of about 100 mW/mK as stated in Section 7.1.1, this is still much higher than current state-of-the art insulants such as vacuum insulation which has a thermal conductivity of only about 4 mW/mK (Alam & O'Flaherty, 2017). It is normally used with timber studding to enhance the structural performance because it does not possess great strength characteristics. The research will investigate ways of improving the thermal conductivity of lime render and lime/hemp composites with nanomaterials to create a high performing lime nanorender and hemp fibre/shiv nanocomposite. Since strength is an issue for lime/hemp fibre composites (it was reported elsewhere that future research could focus on the use of additives to eliminate the wooden frame as the load-bearing structure of a wall (Barnat-Hunek, Smarzewski, & Fic, 2015), the influence of adding an environmentally friendly PVAc to the nanocomposite on compressive strength will also be investigated. The newly developed nanocomposite materials will be used to design a high performance, load bearing eco-friendly wall. This will consist of a central Core, Figure 7.1, comprising lime/hemp fibre/nanomaterial/PVAc to provide the strength element, thereby reducing reliance on timber studding, two layers of lime/hemp shiv/nanomaterials for enhanced insulative purposes (Insulator on both faces of the Core, Figure 7.1) and a

lime/nanomaterial nanocomposite render to provide an aesthetically pleasing appearance inside and out (Figure 7.1).

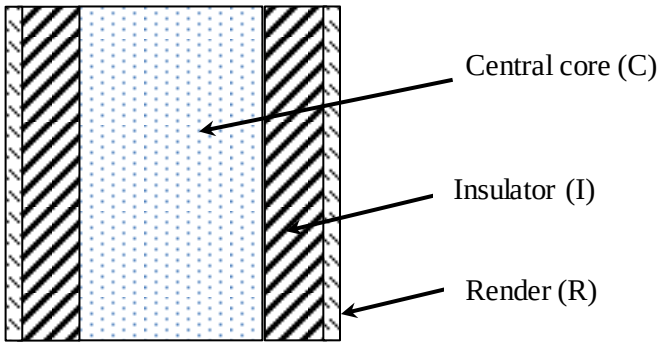

Figure 7.1 Cross section through wall: (R) Lime nanocomposite render; (I) lime/hemp shiv nanocomposite insulator (C); lime/hemp fibres nanocomposite.

An extra-obstacle to using lime and hemp as building materials is that a large thickness of wall, roof or any panel made of this material is required to meet thermal transmission requirements (U Values) as required by the Building Regulations (H.M. Government, 2010). A large thickness not only has negative impacts on the appearance of the building, but it also effects the drying time and that means shuttering has to remain in place for a longer period of time and, therefore, extends the construction time. Damp and cold weather periods increase the drying time. The research used rapid drying of the samples as soon as was practically possible to determine if accelerated water removal can be considered as a technique for on-site construction. A number of accelerated drying techniques were investigated elsewhere (Alvarez et al., 2013) and among these was a solvent exchange method and freeze-drying which performed well. Due to the size of the samples in this work, the solvent exchange method was chosen as the accelerated drying method. This was implemented five days after casting when the samples were considered strong enough for demoulding to take place.

7.1.3 Short Review of the Methods to Improve Thermal Conductivity

The following sections investigate the influence of various factors on the thermal and/or mechanical properties of lime/hemp composites in addition to the literature in Chapter 2. A summary is provided at the end giving a description of the optimised selection of nanomaterials to improve the performance of the lime/hemp composites.

7.1.3.1 Methods to Improve Thermal Conductivity

Thermal conductivity of lime/hemp composites is a property which has attracted a lot of recent interest in the literature. It is possible to use hemp in precast insulation panels (hemp fibres alone) or as a construction material (hemp bast and concrete mix) (Benfratello et al., 2013). Their research found good heat isolation characteristics (values between 0.0899 and 0.1408 W/mK were obtained). They also found that the size of hemp shiv is important, shives with a granulometry higher than 4 mm are too brittle. The maximum quantity must be no more than 30% and 40% for shiv size 2 and 4 mm respectively.

7.1.3.2 Influence of Density on Thermal Conductivity

Thermal conductivity of hemp composites is affected by its density (Collet & Prétot, 2014). It was reported that variations to the density of an industrially produced spray applied hemp shiv concrete (0.5 hemp: binder ratio) had a larger impact on thermal conductivity compared to changes in the moisture content. It was found that when the density increased by two-thirds, the thermal conductivity increased by about 54%. However, the same material showed an increase of only 15%-20% in thermal conductivity when the moisture content increased from a dry condition to 90% relative humidity (Collet & Prétot, 2014).

Lime and hemp for construction usage, as reported in another study (Elfordy, Lucas, Tancret, Scudeller, & Goudet, 2008) also used a spray applied technique to deposit the material. The mechanical properties increased as a result of better compaction, as did density, leading to a higher thermal conductivity. Densities of 417, 475, 496 and 551 kg/m^3 gave thermal conductivities of 0.179, 0.421, 0.542 and 0.485 W/mK respectively. A compromise must be found between thermal conductivity and mechanical properties for designing load bearing walls.

A direct relationship between thermal conductivity and density was also found elsewhere (Kiran, Nandanwar, Naidu, & Rajulu, 2012). The thermal conductivity of bamboo mat board was conducted at constant fixed temperatures of 30°C and 50°C and bulk densities of 0.75 to 1.65 g/cm^3. From a starting point of 0.121W/mK for bulk density of 0.765 g/cm^3, thermal conductivity increased to 0.384W/mK for a bulk density of 1.61 g/cm^3. Density and thermal conductivity showed a linear relationship between them. From the results, the thermal conductivity of bamboo mat board increased with increasing bulk density.

An increase in density was also observed due to aluminium nanoparticles comprising different bulk density pellets, the thermal conductivity increased from 0.2 W/mK up to 1 W/mK as densities increased from 1.1 to 2.3 g/cm^3 as a result of more contact between particles by consolidation (Stacy, Zhang, Pantoya, & Weeks, 2014).

In other studies, it was found that the thermal conductivity decreased for hemp-lime to give comfortable thermal indoor conditions (23-25°C and humidity ≤ 55 %) and low energy requirements (Kinnane et al., 2015; Ponni & Baskar, 2015). Adding 70 % of cork granulate to hydraulic lime with cement, the thermal conductivity decreased by 75 % for conventional cement mortar and 50 % for NHL5 compared to the reference value (Brás, Gonçalves, & Faustino, 2014). Adding cork to a cement mortar was also beneficial as it led to an elimination of temperature variation (higher thermal delay) and permeability decrease for the same starting temperature (Brás et al., 2014).

7.1.4 Influence of Nanomaterials on Thermal Conductivity from Previous Studies

Some work has been done on studying and investigating the impact of nanomaterials on properties of hemp based materials. nZnO and nClay mixed in a wood polymer composite can increase the mechanical properties, thermal stability and ultraviolet resistance of the composites due to its behaviour as an ideal UV blocker and UV inorganic absorber (Ankita Hazarika, Baishya, & Maji, 2015). The temperature transportation was largely reduced in a sono-chemically heated system by adding ZnO nanofluid. The nanofluid zinc oxide at 4% dosage increased heat absorption capacity by about 30-40% (Bhagat & Khanna, 2015).

Furthermore, it was reported that the 28 day, the cement paste mixed with 1-5% wt. $nSiO_2$, thermal conductivity reduced by 38% (range: 0.42 - 0.57 W/mK) after a cement paste was heated to 350ºC and 900ºC for six hours and then after heating to 900 °C compared to the paste at ambient temperature (Jittabut, 2015). The results after heating to 350ºC were very close to those obtained at ambient temperature.

It was found that an aerogel based plaster (nanotechnology coating) has a higher capability of heat isolation. That means the required thickness of plaster can be reduced to yield the same thermal performance (Barbero, Dutto, Ferrua, & Pereno, 2014). Research reported that replacing ordinary Portland cement by 1 wt.% of nClay increased thermal stability, decreased porosity and water absorption as it increased

density, flexural strength, fracture toughness and impact strength of the hemp fabric-reinforced cement nanocomposite (A. Hakamy et al., 2014). However, adding more than 1 wt. % adversely affected thermal, physical and mechanical properties.

7.2 Thermal Conductivity Test Scenarios

A summary of the test scenarios is given in Table 7.1. Referring to Table 7.1and Figure 7.1, the samples investigated in the first series of tests (Render) consist of lime as the base material with different nanomaterials added to determine their influence on thermal conductivity, λ. Nanofillers used were None (i.e. control), nSiO2, nZnO and nClay. The 'R' series of tests were conducted first and the findings were used to formulate test series 'I' (Insulator) and 'C' (Core). The second series (Table 7.1) investigated the influence of selected nanomaterials on the thermal conductivity of lime/hemp shiv, with and without PVAc since hemp shiv is known to have very good insulative properties. Nanofillers used in this series were None (control), nZnO and nClay along with PVAc. The third series ('C', Table 7.1) was devised to offer strength to the wall hence hemp fibre and PVAc was used with lime and one nanomaterial for this purpose.

Table 7.1 Test Schedule for thermal conductivity

Part*	No	Base material	W/L	Age at test (days)**	Nanofillers (% by wt lime)				
					a	**b**	**c**	**d**	**e**
					Control	nSiO2	nClay	nZnO	nZnO + nClay
R	1	Lime	0.4	14	None	2%	2%	4%	4%+2%
	2	Lime	0.4	150	None	2%	2%	4%	-
	3	Lime	0.4	300	None	2%	2%	4%	4%+2%
I	4	30% Hemp shiv/lime	0.75	14	None	-	-	4%	4%+2%
	5	20% Hemp shiv/lime/12% PVAc	0.75	14	None	-	-	-	-
C	6	10% Hemp fibre/lime/12% PVAc	0.75	14	-	-	-	4%	-

*R = Render; I = Insulator; C = Core, see Figure 7.1, **Specimens demoulded at 5 days, immersed in isopropanol for 7 days, oven dried at 60°C for 2 days (14 days total). Stored beyond 14 days at 20°C/60% RH

Compressive strength testing for the 'C' specimen, Figure 7.1, was done in accordance with the relevant British Standard (BSEN1015, 1999). For compressive strengths, the average of eight specimens was taken. As for thermal conductivity specimens, one sample was tested for thermal conductivity and porosity as is generally the case for these test methods.

7.2.1 Porosity and Bulk Density

Render samples ('R') were tested using the mercury intrusion porosimetry to investigate the porous structure in a quantitative way. The specimens containing hemp shiv ('I') were not tested for porosity due to their highly porous composition meaning porosity data may not be very useful. Porosity of the 'R' samples was conducted at 60 days age i.e. 46 days stored at 20°C/60%RH upon completion of the solvent exchange drying technique at 14 days. It was necessary to conduct the porosity test of the hemp fibre ('C') which was made from 10 wt. % HF/L, 12 wt. % PVAc and 4 wt. % nZnO/L, to determine the porosity of core, due to the significance of core which was designed as load bearing. The porosity specimens of HF/L and PVAc of the same percentages without nZnO were tested too.

The function of pressure is recorded as the volume of mercury that penetrates the specimens (Aligizaki, 2014). Particularly, information on the pore size/volume distribution & specific surface can be provided and bulk density as these properties impact on aspects of material performance such as moisture movement, heat transfer and durability.

PASCAL 140/240 device, a mercury intrusion porosimeter was used which is capable of measuring pore size in the range of 116 μm to 0.0074 μm pore diameter. British Standard BS ISO 15901-1 procedures were followed (BSISO, 2016). Specimen fragments measuring approximately 5 x 5 x 10 mm were used in the porosity test, which were dried in a fan-assisted oven at 60 ºC until constant weight prior to testing. The mercury contact angle was taken to be 140°.

7.3 Results and Discussion

7.3.1 Thermal Conductivity

The thermal conductivity and mean temperature profiles versus time for the specimens of control, nclay, nSiO2 and 4% nZnO are given in Figure 7.2 to Figure 7.5. The thermal conductivity was obtained from the steady state portion of the graph (approximately from 30 mins onwards). This group of graphs is a representative sample and other specimens were also tested for thermal conductivity in the same way. The results of the thermal conductivities are given in Table 7.2. Referring to Table 7.2, the thermal conductivity increased with time (14, 150 and 300 days) but its increase reduced when 4 wt. % nZnO was used. Increasing thermal conductivity is as a result of the hydration process, new materials emerged which partially filled the pores. This may lead to an increase in density which leads to an increase in compressive and flexural strength and shrinkage but may also decrease porosity by decreasing the pore size.

Table 7.2 Thermal conductivity test results

1	2	3	4	5	6
Part*	**ID**	**W/L %**	**Age at test (days)**	**% Nanofiller/Lime**	**Thermal conductivity (W/mK)**
	1a	0.4	14	0% (control)	0.159
	1b	0.4	14	2% nSiO2	0.154
	1c	0.4	14	2% nClay	0.147
	1d	0.4	14	4% nZnO	0.131
	1e	0.4	14	4% nZnO + 2% nClay	0.151
	2a	0.4	150	0% (control)	0.173
R	2b	0.4	150	2% nSiO2	0.160
	2c	0.4	150	2% nClay	0.182
	2d	0.4	150	4% nZnO	0.132
	3a	0.4	300	0% (control)	0.179
	3b	0.4	300	2% nSiO2	0.152
	3c	0.4	300	2% nClay	0.201
	3d	0.4	300	4% nZnO	0.147
	4a	0.75	14	30 % hemp shiv/lime (control)	0.098
	4d	0.9	14	12 % hemp shiv/lime/4% nZnO	0.068
I	4e	0.75	14	12 % hemp shiv/lime/4% nZnO/2%	0.101
	5a	0.75	14	20% Hemp shiv/lime/12% PVAc	0.069
C	6d	0.75	14	10% Hemp fibre/lime/12% PVAc/4% nZnO	0.122

*R = Render; I = Insulator; C = Core, see Figure 7.1, ****** Specimens demoulded at 5 days, immersed in isopropanol for 7 days, oven dried at 60°C for 2 days (14 days total). Stored beyond 14 days at 20°C/60% RH

Referring to Figure 7.2, the wall layers (see Figure 7.1) are given in col. 1. The specimen ID is determined from Figure 7.1 where the Test number (1-6) and nanofiller identifier (a-e) are combined to produce the identity (col. 2). The free water:lime ratio is given in col. 3 and is 0.4 for specimens in Test 1-3 but is either 0.75 or 0.9 for Test IDs 4-6 as hemp shiv or fibre is included in the mixture. The different ages at testing is given in col. 4 and varies between 14 and 300 days. The quantity of nanofiller included as a percentage of the mass of lime is given in col. 5. The thermal conductivities, determined as described in Section 3.4.3 and is given in col. 6, Table 7.2. From the data given in Table 7.2, a number of variables will be considered such as influence of nanofiller on thermal conductivity and porosity.

The thermal conductivity results of 4 wt. % nZnO at 14, 150 and 300 days were 0.131, 0.132 and 0.147 W/mK respectively. These minor increase with time show consistency and repeatability.

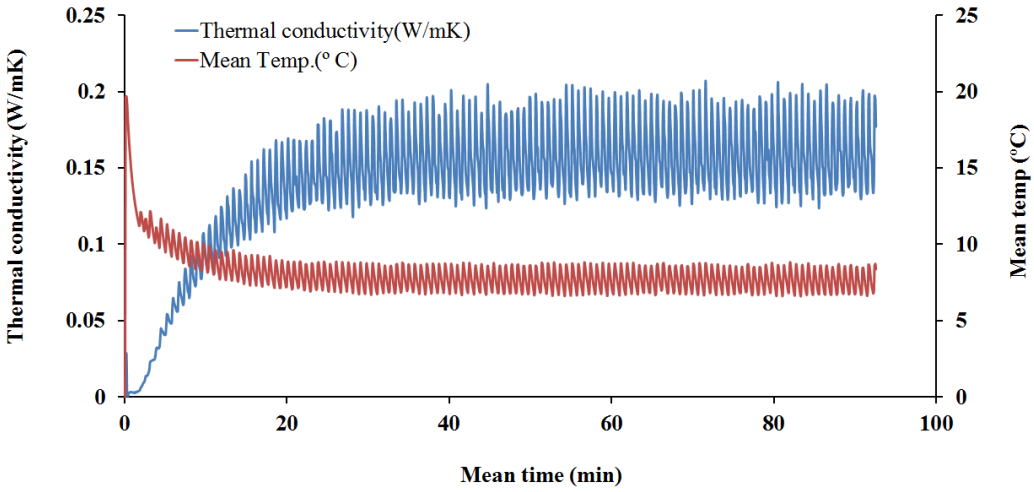

Figure 7.2 Determination of thermal conductivity for a Render specimen (Control, Thermal Conductivity= 0.159 W/ mK)

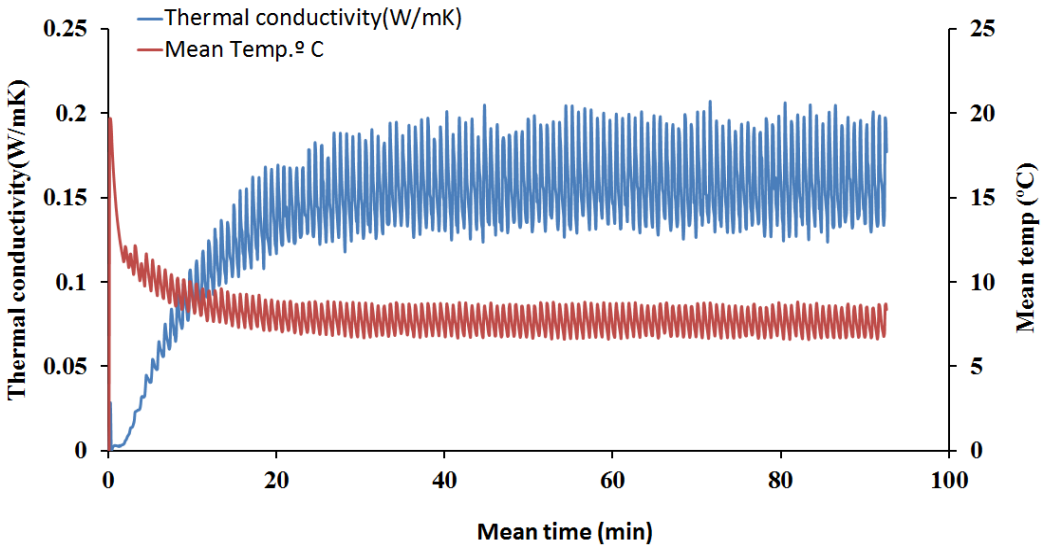

Figure 7.3 Determination of thermal conductivity for a Render specimen (2 % nclay/L, Thermal Conducivity= 0.147 W/ mK)

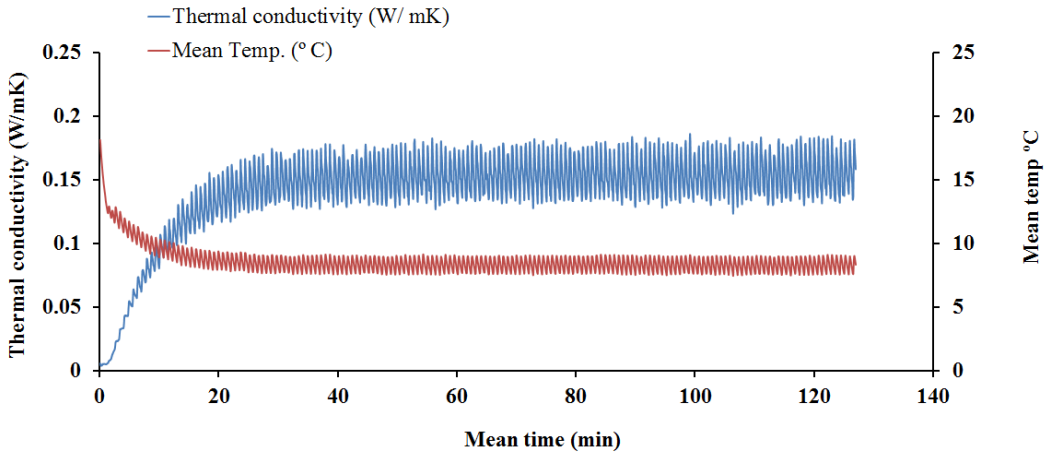

Figure 7.4 Determination of thermal conductivity for a Render specime (2 wt.% $nSiO_2$ Thermal Conductivity= 0.154 W/ mK)

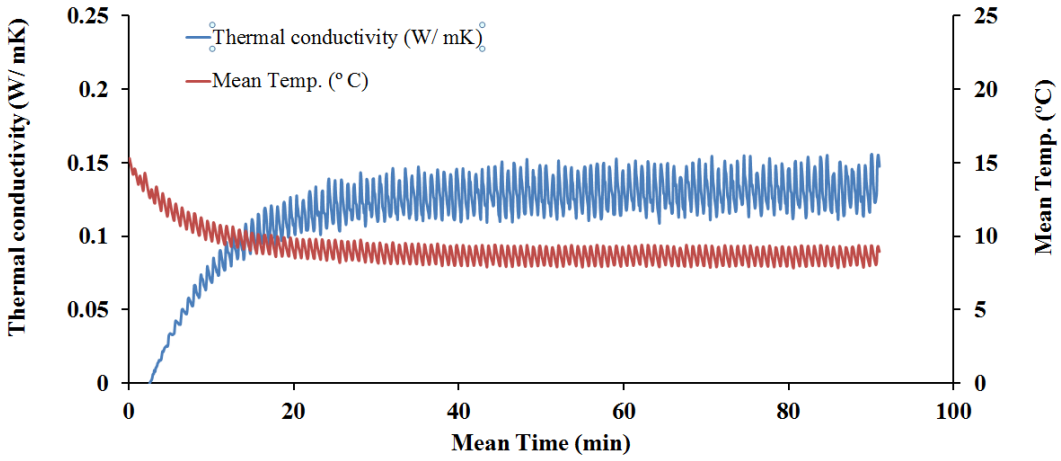

Figure 7.5 Determination of thermal conductivity for a Render specimen (4 % nZnO, Thermal Conductivity= 0.131 W/ mK)

7.3.2 Influence of Nanofiller on Thermal Conductivity

For the 'R' specimens (Table 7.2), the thermal conductivities (λ) are given in Figure 7.6. At 14, 150 and 300 days age, thermal conductivities were determined for the different specimens. The best performing specimen at 14 days age, was Specimen 1d consisting of 4% nZnO, λ being 0.131 W/mK. The Control averaged 0.159 W/mK, hence a reduction of 18%. The performance of the specimens 1b (2% nSiO2), 1c (2% nClay) and 1e (2% nClay+4% nZnO) were performed better than the control (0.154, 0.147 and 0.151 W/mK respectively). High heat absorption capacity property is by nanomaterial nZnO as shown elsewhere (Bhagat & Khanna, 2015) and this was the primary reason for Specimen 1b exhibiting the best performance. However, blending 2% nClay with 4% nZnO, λ was increased to 0.151 W/mK, higher than either Specimens c (2% nClay) and d (4% nZnO). This is likely to be as a result of the higher bulk density due to the addition of nClay (see Section 7.2.1) as previous research (Barbero et al., 2014; Ankita Hazarika et al., 2015; Stacy et al., 2014) linked an increase in thermal conductivity to an increase in density.

At 150 days, the thermal conductivities show an increase for Specimens 2a (Control), 2b (2% nSiO2) and 2c (2% nClay) but Specimen d (4% nZnO) maintains its low λ, now very marginally higher at 0.132 W/mK compared to the 14 days value. A thermal conductivity test at 150 days for Specimen 2e was not conducted as the specimen got damaged prior to the test.

Specimen 3d (4% nZnO) at 300 days exhibited a slight increase in λ to 0.147 W/mK but still the lowest of all specimens. The best thermal stability was exhibited by Specimen b (2% $nSiO_2$) between 14 and 300 days with a relatively low thermal conductivity ranging between 0.152 to 0.160 W/mK. nClay exhibited the highest value at 300 days, λ being 0.201 W/mK. λ increased over time, despite an accelerated drying method being employed for all nanomaterials, the highest increases were evident at 300 days. Further research is required to establish the reason behind this. It is likely that the storage conditions beyond the 14 days solvent exchange procedure had an influence. Specimens were stored under controlled conditions (20° C/60% RH) meaning the moisture content would have increased and likely leading to a higher λ. Furthermore, it possibly is the hydration/carbonation process restarted. It could be due to reactions occurring as a result of certain nanomaterials. For example, a possible reason why the best performing nanorender (nZnO) increased its thermal conductivity is given elsewhere (Venkatesan, Ngo, Khatiwada, Zhang, & Qiao, 2015). Although the research in question investigated the surface passivation of metal oxide for polymer solar cells, surface oxidation over time led to the nanomaterial becoming Zn metal which is higher in thermal conductivity than its oxide. Further research is needed to determine if oxidation is responsible for an increase in thermal conductivity in the lime/ZnO nanorender and establish ways to prevent it. The previous research suggested that surface oxidation can be suppressed by using a surface modifier like polyethyleneimine ethoxylated (PEIE) (Venkatesan et al., 2015).

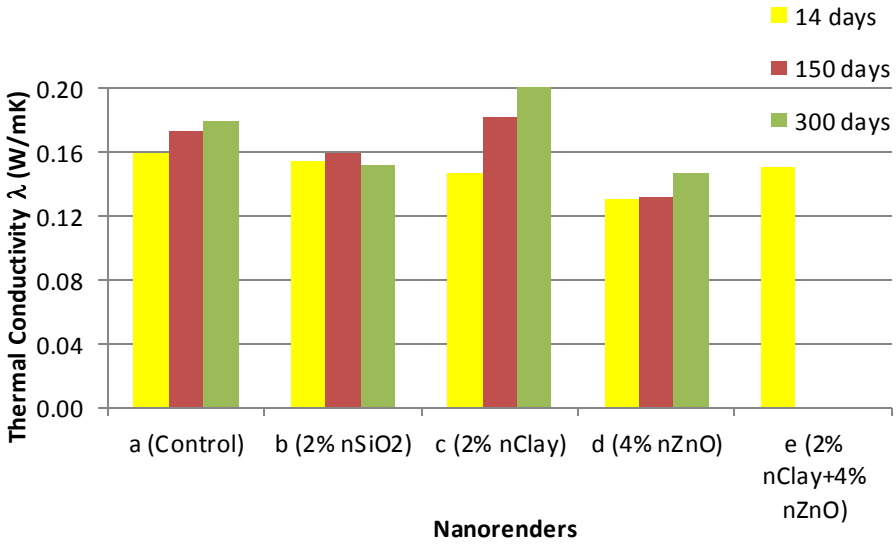

Figure 7.6 Influence on nanofiller and age on thermal conductivity for lime renders

The thermal conductivities for the hemp shiv/lime nanocomposites ('Insulator') and hemp fibre/lime nanocomposite ('Core') are given in Table 7.2. Specimen 4a is a Control sample and yields a λ of 0.098 W/mK. 4% nZnO (Specimen 4d, 0.068 W/mK) again was the best performing sample but as in the case of the renders. Table 7.2, the blended nanofiller of 2% nClay and 4% nZnO produces a higher thermal conductivity (0.101 W/mK), which is marginally higher than the control specimen. Specimen 5a which includes PVAc (30% wt. water) has a very similar λ to specimen 4d which includes the 4% nZnO (0.069 W/mK). Since specimen 4d and 5a both possess similar λ values, other parameters such as strength and cost can be taken into account to establish which material best suits a particular purpose and this is briefly discussed in Section 7.3.5. Thermal conductivity was 0.122 W/mK for the hemp fibre/lime nanocomposite ('Core'), it was higher than the hemp shiv insulators but this is likely to be as a result of hemp fibres being used which have a greater influence on thermal conductivity than hemp shiv (Collet & Prétot, 2014). Samples of insulators for strength testing were not made since the hemp shiv insulators were primarily designed as an insulator, not for strength. It is shown in Table 7.2, Part I that composites containing hemp shiv do not meet minimum strength requirements for load bearing walls (0.6 and 0.4 MPA compressive and flexural strength respectively).

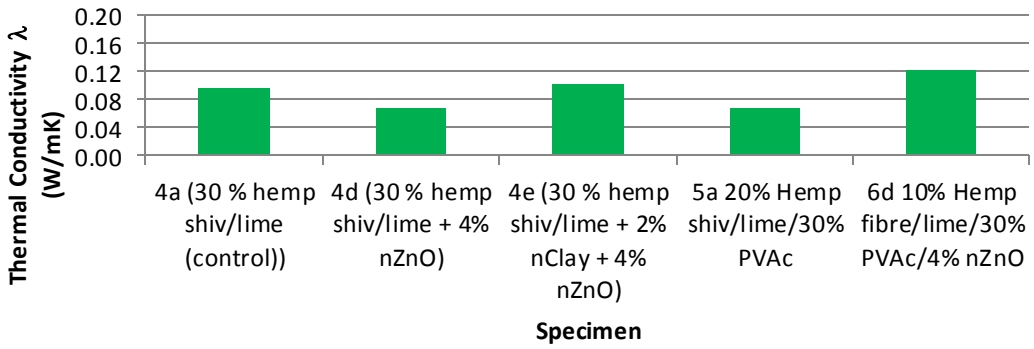

Figure 7.7 Influence on nanofiller on thermal conductivity for hemp shiv/fibre/lime nanocomposite

7.3.3 Influence of Nanofiller on Porosity

A summary of the pore structure properties of the nano modified and Control renders are given in Table 7.3 and Figure 7.9. It is evident that all three nanomaterials affect the pore structure of the mortar by reducing the modal pore diameter d_{cr} and the porosity (Figure 7.8 and Table 7.3). The highest porosity decrease was observed for the mortar modified with 4% nZnO (50.2 % decrease compared to the Control), followed by those modified with 2% nClay (13.2 %) and 2% $nSiO_2$ (5.5%). The use of $nSiO_2$ yielded an increase in the total pore surface area of the mortar (Figure 7.6), which can be attributed to a reduction in the population of pores with diameters between 1 μm and 2 μm and an increase in the population of pores with diameters between 1 μm and 0.01 μm Figure 7.9). A similar pore size distribution can be observed for the mortar modified with 2 % nClay, however, this is characterised by a lower peak in the region of the modal pore diameter (≈ 0.9 μm) and by a smaller number of pores with diameters between 0.1 μm and 0.01 μm (Figure 7.9). This results in the mortar having a lower total pore surface area, close to that of the control. Whilst it yielded the biggest porosity decrease, the use of 4 % nZnO had the lowest impact on the pore size distribution of the mortar, leading to a slight decrease in the modal pore diameter (Figure 7.8 and Figure 7.9). The observed porosity decrease is due to a reduction in the population of pores with diameters between 0.5 μm and 2 μm (Figure 7.9).

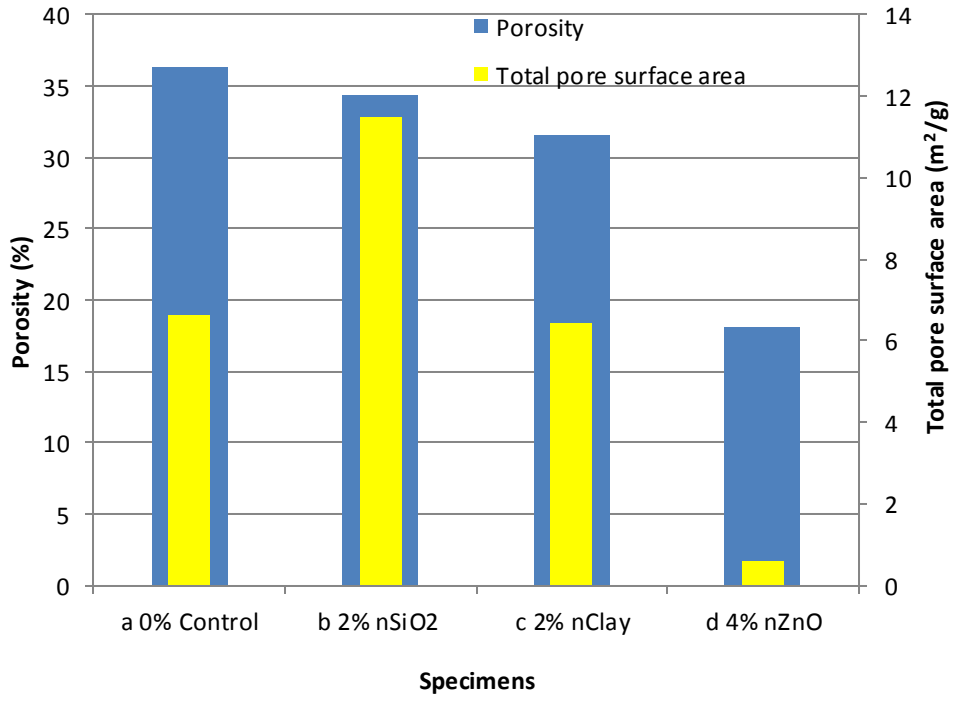

Figure 7.8 Comparison of total porosity and total pore surface area

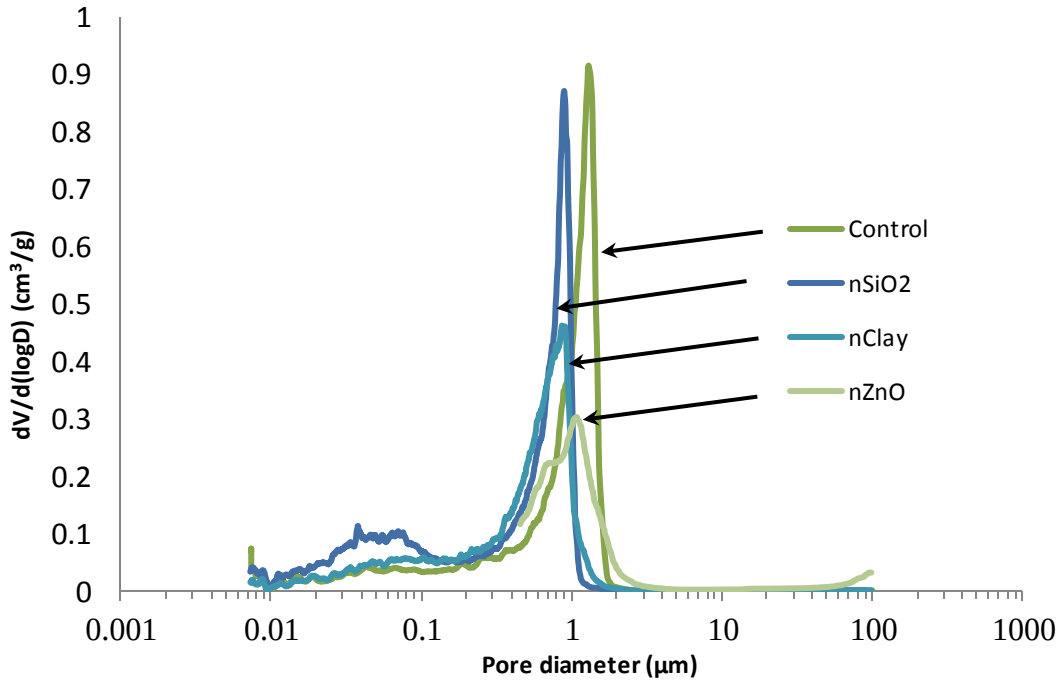

Figure 7.9 Differential volume of intruded mercury versus pore diameter of modified and control nanorender samples

Table 7.3 Pore structure properties

Part	Specimen	Porosity (%)	Porosity decrease (%)	d_{cr} (µm)	Total pore surface area (m^2/g)
	a Control	36.35	-	1.301	6.647
R	**b 2% $nSiO_2$**	34.34	5.5	0.8958	11.482
	c 2% nClay	31.54	13.2	0.8645	6.451
	d 4% nZnO	18.09	50.2	1.088	0.592

7.3.4 Influence of Nanofiller on Density

Bulk densities, ρ, of four of the lime renders are given in Figure 7.10 and were determined during the porosity testing (60 days age). The render with the lowest bulk density is Specimen d (4% nZnO) at 1.232 g/cm^3. Next best in the renders is Specimen b (2% nSiO2) at 1.261 g/cm^3 followed by the Control (1.339 g/cm^3) and Specimen c (2% nClay, 1.409 g/cm^3).

The longer term λ values (300 days age) are also given in Figure 7.9. Specimen d (4% nZnO) exhibits both the lowest density and lowest thermal conductivity. Specimens a and b also follow a similar trend but yield a higher ρ and higher λ compared to Specimen d. The nanorender specimen with the highest density also exhibits the highest λ and this was generally the case with other research findings as described in Section 7.1.3.2 The relationship between both properties for the lime nanocomposite renders in this research is shown in Figure 7.11. Referring to Figure 7.11, a linear relationship exists between λ and ρ which yield the equation

$$\lambda = 0.31\rho - 0.24 \qquad \text{Equation 7.1}$$

Therefore, it is clearly beneficial to design renders with lower bulk densities which will yield lower thermal conductivities.

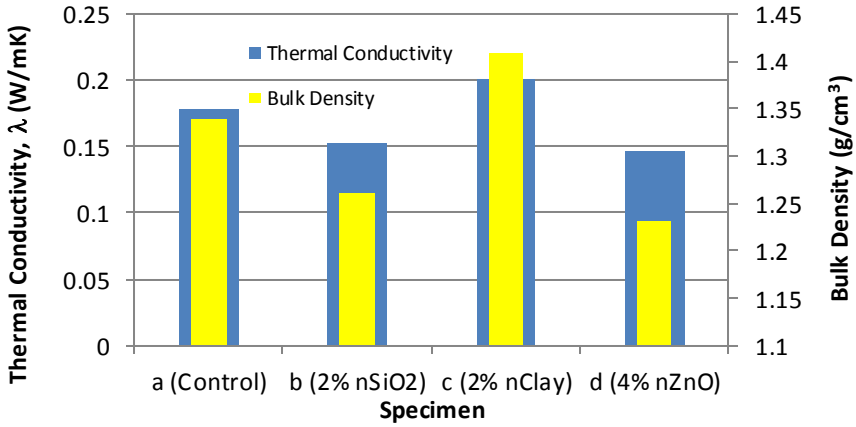

Figure 7.10 Bulk density and thermal conductivity of specimens

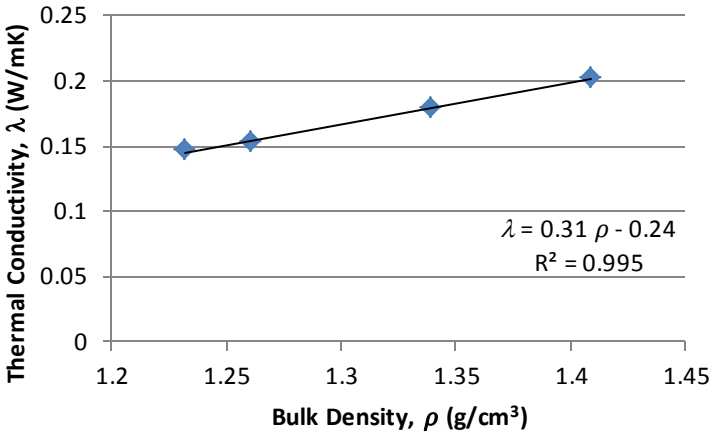

Figure 7.11 Relationship between bulk density and thermal conductivity for lime nanocomposite renders

7.3.5 Compressive Strength

In this research, the compressive strength of the Insulator (No's. 4, 5, Table 7.1) was not obtained as its main purpose is to provide insulative properties for the wall. However, previous research has shown that the compressive strength of lime hemp shiv varied across a number of researchers. The highest compressive strength was 2.78 MPa (de Bruijn et al., 2009) whereas other researchers obtained strengths of 0.4-1.2 MPa (Arnaud et al., 2006) and 0.2-0.5 MPa (Evrard, 2003). A load bearing lime/hemp material would require a compressive strength comparable to that of load-bearing lightweight expanded clay aggregate, i.e. 3-5 MPa (de Bruijn et al., 2009). This is difficult to achieve with lime and hemp shiv alone, hence the reason for adding PVAc to the Core material containing lime and hemp fibres.

The average compressive strength of the Core material was 10.29 N/mm^2, 2-3 times stronger than the required strength to make it load bearing. There is, therefore, room to optimise the quantity of PVAc and other constituents in this material to make it more cost and thermally effective.

7.3.6 Curing Method

The research reported in this thesis showed that although the procedure adopted a water removal technique which stops the hydration process from the age of only 5 days, the tested materials still possessed the required characteristics of strength and thermal performance. More research is required to assess the influence of accelerated drying on

the durability of renders and to investigate the best drying method for site use and the optimum time for implementation due to thickness of the material and possible adverse weather conditions. A possible candidate for site use would be microwave curing, a technique which has recently been developed at Sheffield Hallam University for accelerated curing of concrete patch repairs (Grigoriadis, Mangat, & Abubakri, 2017; Mangat, Abubakri, & Grigoriadis, 2017; P. S. Mangat, Grigoriadis, & Abubakri, 2016) and has the potential to be used for site based accelerated drying.

7.4 Applications of Findings to Wall Design

Figure 7.12 provided a section through the proposed high performance wall to be designed with enhanced material properties from the findings presented in this project. The new design consists of the five material layers as shown in (numbered 2, 3, 4, 3, 2). For the purpose of U value calculations, Layer 1 is the external and internal air resistance. The design of the new eco-friendly wall will be compared to an existing design where conventional lime/hemp based materials are used, Figure 7.12 (right). Referring to Figure 7.12 (right), the wall consists of a lime/hemp mixture as the core of the wall with two layers of render on each face. Therefore, comparing Figure 7.12 (right) with Figure 7.12 (left), the lime/hemp core is extended to compensate for the insulator layers which have been omitted. Overall thickness remains the same. Additionally, the influence of the timber studding in Figure 7.12 (right) has been omitted for simplicity.

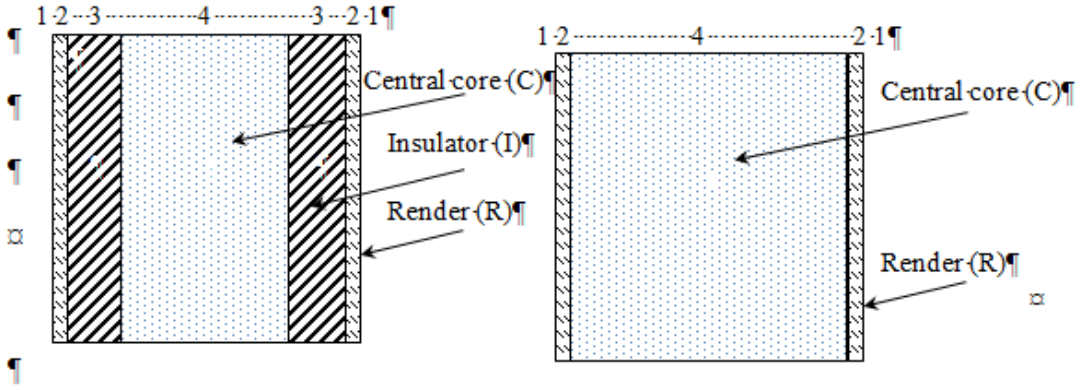

Figure 7.12 Cross section through: (left) eco-friendly wall; (right) lime/hemp wall (right) (timber studding omitted for clarity)

Table 7.4 shows the U value calculation for the new proposed design in Figure 7.12 (left). The Building Regulations (H.M. Government, 2010) state that a U value of 0.18 W/m^{2}K is required for external walls to meet design requirements. Hence, the wall has been designed to comply with this requirement. It was assumed that the Render is 20 mm thick and the insulator layer is 100 mm thick. The thickness of the central core is then selected to achieve an overall U value of 0.18 W/m^{2}K, which for this design is 253 mm. The overall thickness, therefore, is 493 mm. For the purpose of calculations, the long term thermal conductivity for the Render was taken as the 300 day value, Table 7.2. The lowest thermal conductivity for the Insulator was 0.068 W/mK (Materials 4d, Table 7.2) whereas the thermal conductivity of the Core nanomaterial was taken as material 6d in, Table 7.2. Referring to Table 7.4, the total thermal resistance of this wall is 5.55 m^{2}K/W giving the U value of 0.18 W/m^{2}K.

Table 7.4 Design of new wall with nanocomposite materials

Layer	Materials	λ [W/mK]	Thickness (m)	R [m^{2}K/W]	U [W/m^{2}K]
1	External Resistance	-	-	0.13	
2	Render (lime nanocomposite)	0.147	0.02	0.14	
3	Insulator (lime/hemp shiv PVAc)	0.068	0.1	1.47	
4	Core (lime/hemp fibres)	0.122	0.253	2.07	
5	Insulator (lime/hemp shiv PVAc)	0.068	0.1	1.47	
6	Render (lime nanocomposite)	0.147	0.02	0.14	
7	Internal surface resistance	-	-	0.13	
			0.493	5.55	0.180

If material 6d (λ=0.122 W/mK) was replaced with the PVAc modified insulator containing hemp shiv as is commonly used in eco-friendly design (material 5a, Table 7.2, λ=0.069, assuming the minimum strength has been obtained through the addition of the PVAc), then the thickness of the core could reduce to 144 mm and still achieve a U value of 0.18 W/m^{2}K. However, structural calculations would be required to ensure the wall is adequate to carry the applied loads.

A similar calculation was conducted on an existing lime/hemp wall as shown in Table 7.5. The overall wall thickness is assumed as 493 mm to match the thickness of the wall design in Table 7.4. Again, two outer layers of render at 20 mm thickness is assumed, the remaining 453 mm consists of a lime/hemp shiv material (giving the total thickness of 493 mm). For the purpose of calculation, λ is taken as 0.098 as obtained from the control material 4a in Figure 7.2 (30% hemp shiv/lime). A slightly higher U value of 0.196 W/m^{2}K results (the thickness of this core would have to increase to 497 mm to comply with the Building Regulations U value of 0.18 W/m^{2}K). Although there is not a great deal of difference between the new and existing wall design in terms of thermal conductivity and overall thickness, the major difference is the ability of the new wall design to be load bearing, hence eliminating the need to timber framing. However, research is required on the optimum constituents of the core material, either using hemp shiv or hemp fibre, to optimise the strength and thermal conductivities for enhanced performance. In addition, further research is also required on the most efficient method of application, the options being site cast (leading to formwork requirements and drying issues as mentioned earlier) or as prefabricated blocks or panels installed using conventional techniques.

Table 7.5 Design of lime/hemp wall without nanocomposites

Layer	Materials	λ [W/(mK)]	Thickness (m)	R [m^2K/W]	U [W/m^2K]
1	External Resistance	-	-	0.13	
2	Lime render	0.179	0.02	0.11	
3	Lime/hemp shiv	0.098	0.453	4.62	
4	Lime render	0.179	0.02	0.11	
5	Internal Resistance	-	-	0.13	
			0.493	5.08	0.196

7.5 Conclusions

This study is conducted to investigate the influence of nanomaterials on the thermal characteristics of lime and hemp/lime composites for optimal wall design. An accelerated drying process was also trialled to assess its suitability in quickening drying times but without negatively influencing material properties. Based on the results from this experimental research, the following conclusions have been drawn:

- application of 4% nZnO to the lime render led to the lowest thermal conductivity. λ reduced by 18% to 0.131 WmK at 14 days compared to the Control sample (0.159 W/mK). λ increased to 0.147 W/mK at 300 days for this nanomaterial. Application of 2% nSiO2 also helps reduce λ but not to the same extent as nZnO. The storage condition (60% RH) beyond the end of the solvent exchange procedure is likely to have influenced the longer term thermal conductivity.

- application of 4% nZnO to a 30 % wt. hemp shiv/lime nanocomposite reduced the thermal conductivity by 31% compared to the control sample.

- the addition of the nanomaterials to the lime render had an impact on the density and thermal conductivity. Nanomaterial such as nClay led to a higher density than the control but nZnO and nSiO2 both exhibited lower densities and lower thermal conductivities. A linear relationship between thermal conductivity (λ) and bulk density (ρ) was determined where : $\lambda = 0.31\rho - 0.24$

- the render with 4% nZnO exhibited the lowest porosity (18.09%) whereas the renders with 2% nClay and 2% nSiO2 both had porosities at 31.54% and 34.34% respectively. The Control specimen had a porosity of 36.35%. The 4% nZnO render specimen also exhibited the lowest total pore surface area of 0.592 m^2/g.
- Two insulators exhibited similar thermal conductivity values hence selection of the optimum material should be based on not only thermal characteristics but also on cost and whether or not a stronger insulator is required to either share the load carrying the hemp fibre core material or even replace it due to its lower thermal conductivity characteristics
- the core material consisting of 10 % Hemp fibre/lime/12 % PVAc/w and 4% nZnO exhibited an average compressive strength of 10.3 N/mm^2 so further optimisation is required for efficient structural and thermal performance.
- despite the application of the solvent exchange method at five days after casting, all nanocomposites still exhibited usable properties from the point of view of wall design. Further research is required to optimise an accelerated drying technique for site use.
- The present study is based on investigating the influence of nanomaterials on the relevant properties required for hemp/lime construction. The study focused on improving the properties responsible for energy efficiency. The impact of the stronger core nanocomposite and insulator on the quantity of timber studding for strength is beyond the scope of this research and will be considered in the future publication.
- Results showed that the maximum 28 day decrease in λ for the Render was by using 4% nZnO, λ being 18 % compared to the control sample. The same render also exhibited the lowest density. For the Insulator, λ was decreased 31 % when also using 4% nZnO in comparison to the nano-free specimen. Strength of the Core exceeded 10 MPa, much greater than the minimum load bearing requirement.

Chapter 8 - **Conclusions and Future Work**

8.1 208 Introduction

In this thesis, the aim was to develop load bearing, lightweight, high performance construction materials. The material should be durable, have low porosity, low shrinkage, low thermal conductivity and high water vapour permeability. The materials included biomass natural fibres for reinforcement and nanomaterials to give a nanocomposite construction material. Table 8.1, is a comparison of CO_2 emissions between concrete and the proposed lime based wall. Table 8.2 shows a summary of the objectives of the thesis and how these goals were achieved.

8.1.1 Selection of Optimum Materials

Hemp fibres and fibre glass were used for the first time as chopped fibres mixed with lime. Hemp fibres were chosen for their properties, hemp was environmentally friendly, a speedily grown agriculture renewable plant, 4-6 m high within a period of 3-4 months, abundant, durable, biodegradable, energy modest (no need for more energy in its life production). Lime is cheap and lightweight as a construction binder material in comparison to cement concrete mix. It is compatible with the biomass from hemp shives and hemp fibres which were used in the present project. Lime carbonation continues as the lime absorbs CO_2 from the atmosphere and reduces pollution in the environment. This is done through its raw materials releasing CO_2 but absorbing it through its lifetime in use. Table 8.1 show calculations and a comparison between CO_2 emission from 1 m^3 of concrete and 1 m^3 of proposed wall built from Polyvinyl acetate (12 wt. % PVAc), nanozinc oxide (4 wt. % nZnO), Hemp (20 wt. % shives or 10 wt. % fibres)/Lime. Wall emission under self-weight is 354 (585) kg CO_2/m^3 Lime if combustion emission is considered and 934.56 kg CO_2/m^3.Concrete.

Table 8.2, is a summary of the findings from this project.

Table 8.1 A comparison of CO_2 emissions between concrete and the proposed lime based wall

No	CO_2-Emissions			
	Item	Hemp/lime nanocomposites ($1m^3$)		Concrete ($1m^3$)
		Quantities	Notes	Quantities and notes
1	**Volume**	V = t*w*d = $1m^3$ V = 0.493*1*d= $1m^3$ d= 2.03 m	$1m^3$ of material is assumed. The thickness (t) is 0.493 as calculated in Table 7.4 and Figure 8.1. A width (w) of 1 m is assumed, thereby, the depth (d) is calculated to give a volume of 1 m^3	$1m^3$ of concrete
2	**Density kg/m^3**	'R' layers x 2 : ρ_1= 1231 kg/m^3 Mixture (4 % nZnO+12 % PVAc) 'I' layers x 2 : ρ_2= 540 kg/m^3 Mixture (4 % nZnO+12 % PVAc+20 % HS) 'C' layer x 1 : ρ_3= 1260 kg/m^3 Mixture (4 % nZnO+12 PVAc+10 % HF)	See Fig. 8.1 for definition of layers (R, I, C) Density obtained from porosity test, Section 7.3.4	Density assumed as 2,500 kg/m^3 in general
3	**Weight kg**	Total weight of lime (W) = $2*(\rho_1*v_{1)} + 2*(\rho_2)(v_{2)} + (\rho_{3)}(v_3)$ W1 of 'R' layers x 2: ρ_1 = 1231 kg/m^3; v_1 = (0.02*1.0*2.03) = 0.04 m^3 $2*(\rho_{1)}(v_1) - 2*(4+12)\%*(\rho_{1)}(v_{1)}$ =	Weight of individual layers in the wall calculated i.e. 2 x 'R', 2 x 'I', 2 x 'C', Fig. 8.1	2541 kg in 1 m^3 in the reference

No	CO_2-Emissions			
	Item	Hemp/lime nanocomposites ($1m^3$)		Concrete ($1m^3$)
		Quantities	Notes	Quantities and notes
		2*1231*(0.02*1.0*2.03) - 2*0.16*1231*0.04 = 84 kg W2 of 'I' layers x 2: ρ_2 == 540, kg/m^3; v_2 = (0.1*1.0*2.03) = 0.203 m^3 2*(ρ_2)(v_2) - 2*(4+12+20)%*(ρ_2)(v_2) 2*540* (0.1*1.0*2.03) - 2* 0.36*540*0.203= W2=140 kg W3 of 'C' layer x 1: ρ_3 == 1260, kg/m^3; v_3 = (0.253*1.0*2.03)= 0.51 m^3 (ρ_3)(v_3) - (4+12+10)%*(ρ_2)(v_2) = 1260*0.51 - 0.26*1260*0.51 W3= 476 kg Weight of lime= W1+W2+W3 Wt= 84 + 140 + 476= Weight of lime in $1m^3$ = 700 kg		
4	**Emission kg**	Lime emission = 0.77 kg CO_2/kg Lime (EuLA, 2014) [Lime emissions = Process + Electricity + Combustion] = 0.751+0.019+ 0.322 (neglected)	Combustion emission neglected as lime absorbs CO_2 during its strength gain 328 kg/m^3: weight of cement	Average concrete weight (kg/m^3): (cement + fine aggregates + coarse aggregates + water) + 328 +781 + 1242 + 190 = 2541 kg/m^3

No	CO_2-Emissions			
	Item	Hemp/lime nanocomposites ($1m^3$)		Concrete ($1m^3$)
		Quantities	Notes	Quantities and notes
		Water emission = 0.00026 kg CO_2/kg (Florentin, Pearlmutter, Givoni, & Gal, 2017) Hemp emission = 0.085 (intial) - (1.8) sequestered = -1.715 kg CO_2/kg hemp (Florentin, Pearlmutter, Givoni, & Gal, 2017)	269 Kg/m^3 emission of cement If the combustion emission of If lime emission is considered completely not absorbed: Lime emission = 0.751+0.019+ 0.322 =1.092 or ≈ 1.1 kg CO_2/kg Lime	W/C (water cement ratio) = 0.58 (Turner & Collins, 2013; R. Zhao & Sanjayan, 2009)
5	**Emission kg/m^3**	CO_2 emission from 1 m^3 lime: = 700*0.77= 539 kg CO_2 Emission of additives (other than hemp) are < 1 kg CO_2/m^3 (Turner & Collins, 2013) CO_2 emissions of additives - all layers ('R' layers x 2 + 'I' layers *2 + 'C' layer x 1 = 1 kg CO_2 Negative CO_2 emissions of hemp fibres (HF) and hemp shiv (HS) - 'I' layers 'I' layers x 2 HS x CO_2 = 540*2*0.1*1.0*2.03*20%*-1.715 = - 75 kg CO_2 Negative CO_2 emissions of hemp fibres (HF) - 'C'	CO_2 emission from 1 m^3 lime: = 700*1.1 = 770 kg CO_2 Total emission = [770 (lime) + 1 (additives) - 75 (shives) - 111 (hemp fibres)] = 585 kg CO_2/m^3	Weight. of CO_2 emission (kg/m^3): (cement + coarse aggregates + fine aggregates + admixtures + batching + curing + transport + placement) =269 +51 + 11 + 1 +3 + 1 + 9 +9 = 354 kg/m^3 (as derived by a following study below which took into consideration many factories) (Turner & Collins, 2013)

No	CO_2-Emissions			
	Item	Hemp/lime nanocomposites ($1m^3$)		Concrete ($1m^3$)
		Quantities	Notes	Quantities and notes
		layers 'C' layer x 1= ρ_3*v_3 * 0.1*-1.715 = 1260*0.253*1*2.03*0.1*- 1.715 = - 111 kg CO_2 Water CO_2 emission = 0.00026*0.4*703.2 = 0.073 kg CO_2 (very low, therefore neglect) Total emission = [539 (lime) + 1 (additives) - 75 (shives) - 111 (hemp fibres)] = 354 kg CO_2/m^3		
6	**Wall Emission under self-weight**	WL = weight of lime in 1 m^3 = weight of ('R' layers * 2 + 'I' layers * 2 + 'C' layer * 1) WL= (2*0.02*1231 + 2*0.1*540 + 1260*0.253)* 2.03=966 kg Force = 966*10 = 9,660 N Weight ratio concrete/lime = 2541/966= 2.63 Weight of lime = Weight of concrete/2.63 σ = compressive stress in lime wall under self-weight, A = cross sectional area of lime wall = 0.493*1= 0.493	Explanation: The cross section of the wall should be larger for concrete than lime under their self-weight to withstand the access load of concrete in comparison to lime	WC = weight of concrete in 1 m^3= 2541 kg, A = cross section area of concrete wall σ = compressive stress in concrete wall, t = thickness of concrete wall, m σ of concrete wall must = σ of lime wall σ = WC/A= 2.63 WL/A σ = WC/A= 2.63 WL/A σ = 2.63*966/A

No	CO_2-Emissions			
	Item	Hemp/lime nanocomposites ($1m^3$)		Concrete ($1m^3$)
		Quantities	Notes	Quantities and notes
		m^2 ($0.493*10^6$ mm^2) $\sigma = 9660/(0.493*10^6) = 0.02$ N/mm^2 Emission of lime wall constant= 354 kg CO_2/m^3	Emission of lime wall constant (if emission of lime combustion is considered)= 585 kg CO_2/m^3 Anyway, that means emission of lime is 345-585 kg CO_2/m^3 and it is less than wall emission of concrete (934.56 kg CO_2/m^3)	A = 2.63*966/1959= 1.29 ≈ 1.3 m^2 A = 1.3= 1* t t= 1.3/1= 1.3 m Concrete wall dimensions, t= 1.3 m, w= 1 m and d= 2.03m V = volume of concrete wall =1.3*1*2.03= 2.64 m^3 V= 2,64 Emission of new volume of concrete wall= 354 kg/m^3*2.64 m^3 = 934.56 kg CO_2/m^3

It can be said, many notes in this project are remarkable:

1. There was minor enhancement (in relative to construction object) in strength (flexural and compressive) by adding different nano-fillers (nanoclay, nanosilica, nanocellulose fibres, expanded graphite) to lime but the highest improvement was by blending natural and industrial fibres (fibre glass and hemp fibres) to lime which increased the compressive strength of the resulting composite material from non-loadbearing (3-4 MPa compressive strength) to loadbearing by adding 10 wt. % HF/L (compressive and flexural strength were 8.9 MPa and 4.7 MPa respectively). The flexural strength is comparable to the flexural strength of cement mortar which was around 4 MPa in the literature.

2. PVAc adhesive (polyvinyl acetate) was added as a new way to improve the bond between lime mortar and fibres (FG and HF). The specimen 12 % PVAc/L and 10 % HF/L with 4 wt. % nZnO gave compressive and flexural strengths of 10.3 MPa and 4.4 MPa respectively. These were the highest strength for the hemp fibres composite by the oven drying method. In contrast, the same mix by air drying gave 17.7 MPa and 7.3 MPa respectively. The result of 10 % FG and 12 % PVAc by oven drying was a little higher (11.7 and 4.5 MPa compressive and flexural strength respectively) but because FG is not as friendly to the environment as hemp it was not the preferred choice. The compressive strength can be designed to meet the required strength by changing the percentages of HF, the length of fibres and quantity of PVAc to optimise the cost.

Table 8.2 Summary of the results and findings.

No	Objective	What and how the objectives were achieved?
1	Environmentally friendly, lightweight material	Biomass lime nanocomposite from HF, HS and lime were chosen as environmentally friendly materials. Carbon emission for $1m^3$ of the proposed wall of lime (416.9 Kg) is less than $1m^3$ of concrete wall (1850 Kg), Table 8.1.
2	High CS and FS	Oven drying method, 10 % HF/L and 12 % PVAc/L and 4 wt. % nZnO which gave more than 10 MPa and 4.4 MPa, CS and FS respectively
3	Highest CS ad FS	Air curing method, using 10 % HF/L and 12 % PVAc/L and 4 wt. % nZnO which gave 17.8 and 7.3 MPa
3	Low λ for insulator panels	SE method and 20 % HS/L, 12 % PVAc /L and 4% nZnO/L, λ= 0.06 W/ mK
4	Low λ for the core of proposed wall	SE method and 10 % HF/L, 12 % PVAc/L and 4 % nZnO/L, λ= 0.12 W/ mK
5	Low λ for the render	SE method, 12 % PVAc/L and 4 % nZnO/L, λ=0.13 W/ mK
6	Low Porosity for the render	Air curing method, using 4 % nZnO/L, P %= 18.1 %
7	Low Porosity for the core of proposed wall	Air curing method, using 10 % HF/L, 12 % PVAc, 4 % nZnO, P %=20.7 %
8	Low Shrinkage for the Render of proposed wall	Air curing method, 4 wt. % nZnO gave SR = 750.4 μs
9	High WVP for breathability	All nanomaterials used enhanced WVP (breathability), the highest WVP= 1.96×10^{-11} ($kg \cdot m^{-1} \cdot s^{-1} \cdot Pa^{-1}$) was by adding 2 % nclay in comparison to pure lime where WVP = 1.43×10^{-11} ($kg \cdot m^{-1} \cdot s^{-1} \cdot Pa^{-1}$)

Key of Table 8.2 symbols: HF= hemp fibres, HS= hemp shives, CS= Compressive strength, FS= flexural strength, SE = Solvent exchange method, nZnO= nanozinc oxide, PVAc= Polyvinyl acetate, λ= thermal conductivity, P %= porosity %, FG= fibre glass, SR= shrinkage and WVP= water vapour permeability (breathability).

3. The hemp fibre lime composite exhibited high ductility in which the failure was not sudden but gradual. The specimens compressed up to failure without cracking but exhibited a large reduction in the thickness under loading.

4. The porosity decreased when different nanomaterials were mixed with lime e.g. 2 % $nSiO_2$/L; 2 % EG/L; 2 % nclay/L; 4 % nZnO with 12 % PVAc /L with 10 % HF/L; 4 % nZnO/L and 30 % PVAc of W/L, 10 % HF/L. The porosities were 34.3, 28.4, 31.5, 20.7, 18.0 and 16.6 % respectively in comparison pure lime which had a porosity of 36.3 %. The optimum porosity was from the nanozinc oxide/lime nanocomposite (18 %) which can be used as a render. There are two low porosity results from the samples containing 10 % HF/L + 12 % PVAc/L, with and without 4 % nZnO and the porosities were 20.6 % and 16.6 % but 16.6 % was considered the best option, not only for decreasing porosity and thermal conductivity but due the impact of nanozinc oxide which acts as an anti-fungal and anti-bacteria agent. The pore size was limited to 0.01-10 μm and the volume of pores was decreased in comparison to pure lime.

5. 4 wt. % nanozinc oxide and lime was cured using a Solvent exchange drying method. This led to a decrease in thermal conductivity, ƛ being 0.13. W/mK. This will be used as a render for the proposed wall. The optimum ƛ for the insulator panel was 0.06 W/mK by blending 20 % HS/L + 4 % nZnO/L + 12 % PVAc/L. The best ƛ for the core was from the specimen containing 10 wt. % HF/L (0.122 W/mK). This material again included 4 wt. % nZnO/L and Solvent exchange drying method was used.

6. The shrinkage decreased by using the nanomaterials 2 wt. % EG/L and 10 wt. % FG/L giving a shrinkage value of 0.025 % (2500 μs) and 0.012 % (1200 μs) respectively. The result of FG was similar to the shrinkage of lime/ sand (good granulated) according the standard CEN EN 196-1 (its shrinkage was 1200 μs). The lowest value of shrinkage was of 771.8 μs by using 4 wt. % nZnO/L using air dry curing. The goal of decreasing the shrinkage was achieved to levels lower to the lowest shrinkage of lime/sand found in previous studies.

7. The WVP in lime is already good but by using nanomaterials (Control, 1.5 % EG/L, 2 % nclay/L and 2 % $nSiO_2$/L), it was improved (1.43×10^{-11}, 1.71×10^{-11}, 1.96×10^{-11} and 1.902×10^{-11} $kg \cdot m^{-1} \cdot s^{-1} \cdot Pa^{-1}$ respectively). The highest WVP was (1.96×10^{-11} $kg \cdot m^{-1} \cdot s^{-1} \cdot Pa^{-1}$) which was by adding 2 wt. % nclay. The goal of keeping the WVP value of lime or increasing it by using nanocomposite was achieved.

8. The optimum design of the proposed wall, Figure 8.1, is (from left to right):

1- Outdoor render layer, 4 % nZnO/L, 2 cm thick.

2- External insulator layer or panel, 4 % nZnO/L + 20 % HS/L + 12 % PVAc /L, 10 cm thick.

3- Central core panel of the wall, 4 % nZnO/L + 10 % HF/L + 12 % PVAc /L, 25 cm thick.

4- Internal insulator layer or panel, 4 % nZnO/L + 20 % HS/L + 12. % PVAc /L, 10 cm thick.

5- Indoor render layer, 4 % nZnO/L, 2 cm thick.

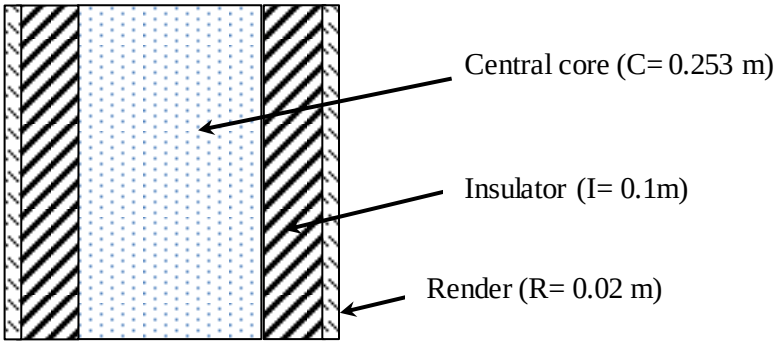

Figure 8.1 Cross section through wall: (R) Lime nanocomposite render; (I) lime/hemp shiv nanocomposite insulator (C); lime/hemp fibres nanocomposite.

8.2 Future Work

The following is a summary of further work which can be considered in the future

1. The length of hemp fibres which have an important impact on the strength of the lime composite could be tested to find the optimised length for enhanced compressive and flexural strength.
2. Study the impact of more than one nanomaterial with hemp fibres in a specimen and investigate their impact on the properties of the fibre reinforced lime nanocomposites. For example, nanoclay with nanosilica or both with expanded graphite.
3. Try other kinds of organic adhesives such as water based acrylic adhesive to increase the strength. Furthermore, add nanoclay or others nanomaterials to PVAc and determine their effect on the properties of the material.
4. Examine further the dry curing method and compare its result to other methods. For example, a microwave curing technique has been developed at Sheffield Hallam University and this has potential benefits as an accelerated curing method on site.
5. Solvent exchange method decreased thermal conductivity and porosity, but due to its effect of stopping hydration, the strength decreased. Further research is required to find a balance between optimum strength, thermal conductivity and porosity.
6. Mix different percentages of gypsum with the main matrix (lime) to study their effect on the setting time, quicker drying and the mechanical properties of the nanocomposite specimens.
7. Investigate ways of controlling the shrinkage of the render, for example by using fine aggregate in the mix or by adding hemp fibres.
8. Determine the effect of removing the timber studding and replacing with load bearing lime nanocomposite materials.

References

459-1, B. (2015). BS EN 459-1:2015 Building lime Part 1: Definitions, specifications and conformity criteria. In BSI (Ed.).

A. Sánchez, J., Barrios, J., Barrios Padura, A., & De Arellano Agudo, A. R. (1997). The shrinkage in lime mortars. *1997*.

Aggarwal, P., Singh, R. P., & Aggarwal, Y. (2015). Use of nano-silica in cement based materials—A review. *Cogent Engineering, 2*(1), 1078018.

Ahmad, Z., Ibrahim, A., & Tahir, P. (2010). Drying shrinkage characteristics of concrete reinforced with oil palm trunk fiber. *Int. J. Eng. Sci. Technol, 2*(5), 1441-1450.

Aho, I., & Ndububa, E. (2015). Compressive and flexural strength of cement mortar stabilized with raffia palm fruit peel (RPEP). *Global Journal of Engineering Research, 14*(1), 1-7.

Alam, M., & O'Flaherty, F. (2017). *Thermal characterisation of Composite Insulation Panels using a vacuum insulated core*. Paper presented at the SOLARIS Conference, London.

Alemán, J., Chadwick, A. V., He, J., Hess, M., Horie, K., Jones, R. G., . . . Moad, G. (2007). Definitions of terms relating to the structure and processing of sols, gels, networks, and inorganic-organic hybrid materials (IUPAC Recommendations 2007). *Pure and Applied Chemistry, 79*(10), 1801-1829.

Ali, M. A., Majumdar, A. J., & Singh, B. (1975). Properties of glass fibre cement — the effect of fibre length and content. *Journal of Materials Science, 10*(10), 1732-1740. doi:10.1007/BF00554935

Aligizaki, K. K. (2014). *Pore structure of cement-based materials: testing, interpretation and requirements*: CRC Press.

Alvarez, J. I., Fernández, J. M., Navarro-Blasco, I., Duran, A., & Sirera, R. (2013). Microstructural consequences of nanosilica addition on aerial lime binding materials: Influence of different drying conditions. *Materials Characterization, 80*, 36-49. doi:http://dx.doi.org/10.1016/j.matchar.2013.03.006

Amziane, S., & Arnaud, L. (2013). *Bio-aggregate-based building materials: applications to hemp concretes*: John Wiley & Sons.

Anderzej K. B., Adam Jaskiewicz, and, M. U., & Walczak, D. S. (2012). Biocomposites in the past and in the future. *Fibres and textiles in Eastern Europe, 20, 6B*(96), 14-22.

Anna J. Svagan, My A. S. Azizi Samir, & Berglund, a. L. A. (2007). Biomimetic Polysaccharide Nanocomposites of High Cellulose. *Biomacromolecules, 8*(8), 2556-2563.

Antonelli, L. (2015). Ireland's 1st hemp-built passive house. *Ireland's 1st hemp-built passive house*. Retrieved from https://passivehouseplus.ie/magazine/new-build/ireland-s-1st-hemp-built-passive-house

Arandigoyen, M., & Alvarez, J. I. (2006). Blended pastes of cement and lime: Pore structure and capillary porosity. *Applied Surface Science, 252*(23), 8077-8085. doi:https://doi.org/10.1016/j.apsusc.2005.10.019

Arandigoyen, M., & Alvarez, J. I. (2007). Pore structure and mechanical properties of cement–lime mortars. *Cement and Concrete Research, 37*(5), 767-775. doi:https://doi.org/10.1016/j.cemconres.2007.02.023

References

Ariadurai, S. A. (2013). *Biocomposites Current Status and Future*. Paper presented at the 5th International technical Conference.

Arizzi, A., Brummer, M., Martin-Sanchez, I., Cultrone, G., & Viles, H. (2015). The influence of the type of lime on the hygric behaviour and bio-receptivity of hemp lime composites used for rendering applications in sustainable new construction and repair works. *PLoS ONE, 10*(5), e0125520. doi:10.1371/journal.pone.0125520

Arizzi, A., & Cultrone, G. (2013). The water transfer properties and drying shrinkage of aerial lime-based mortars: An assessment of their quality as repair rendering materials. *Environmental earth sciences, 71*. doi:10.1007/s12665-013-2574-x

Arnaud, L., Cerezo, V., & Samri, D. (2006). *Global approach for the design of building material containing lime and vegetable particles.* Paper presented at the The 6th International Symposium on Cement and Concrete, Xi'an, China.

Assaedi, H., Shaikh, F. U. A., & Low, I. M. (2016). Effect of nano-clay on mechanical and thermal properties of geopolymer. *Journal of Asian Ceramic Societies, 4*(1), 19-28. doi:https://doi.org/10.1016/j.jascer.2015.10.004

ASTM. (2017). Standard Test Method for Length Change of Hardened Hydraulic-Cement Mortar and Concrete. In *C157/ C157M* (pp. 1-8). US: World Trade Organization Technical Barriers to Trade (TBT) Committee.

Asuka, M., & Sigmund, W. M. (2009). Nanoparticle sol-gel composite hybride transparent coating materials. In: Google Patents.

Atai, M., Pahlavan, A., & Moin, N. (2012). Nano-porous thermally sintered nano silica as novel fillers for dental composites. *Dental Materials, 28*(2), 133-145.

Awad, W. H., Beyer, G., Benderly, D., Ijdo, W. L., Songtipya, P., Jimenez-Gasco, M. d. M., . . . Wilkie, C. A. (2009). Material properties of nanoclay PVC composites. *Polymer, 50*(8), 1857-1867. doi:http://dx.doi.org/10.1016/j.polymer.2009.02.007

Awwad, E., Hamad, B., Mabsout, M., & Khatib, H. (2010). *Sustainable construction material using hemp fibers–preliminary study.* Paper presented at the Proceedings of the Second International Conference on Sustainable Construction Materials and Technologies. Ancona, Italy: Università Politecnica delle.

Aydemir, D., Gündüz, G., Aşık, N., & Wang, A. (2016). The Effects of Poly (vinyl acetate) Filled with Nanoclay and Cellulose Nanofibrils on Adhesion Strength of Poplar and Scots Pine Wood. *Drvna industrija: Znanstveni časopis za pitanja drvne tehnologije, 67*(1), 17-24.

Babak, F., Abolfazl, H., Alimorad, R., & Parviz, G. (2014). Preparation and Mechanical Properties of Graphene Oxide: Cement Nanocomposites. *The Scientific World Journal, 2014*, 10. doi:10.1155/2014/276323

Bagherpour, S. (2012). Fibre Reinforced Polyester Composites. doi:10.5772/48697

Balčiūnas, G., Vėjelis, S., Vaitkus, S., & Kairyte, A. (2013). Physical Properties and Structure of Composite Made by Using Hemp Hurds and Different Binding Materials. *Procedia Engineering, 57*, 159–166. doi:10.1016/j.proeng.2013.04.023

Bandyopadhyay-Ghosh, S., Ghosh, S. B., & Sain, M. (2015a). 19 - The use of biobased nanofibres in composites. In *Biofiber Reinforcements in Composite Materials* (pp. 571-647): Woodhead Publishing.

References

Bandyopadhyay-Ghosh, S., Ghosh, S. B., & Sain, M. (2015b). The use of biobased nanofibres in composites. 571-647. doi:10.1533/9781782421276.5.571

Barbero-Barrera, M. M., Medina, N. F., & Guardia-Martin, C. G. (2017). Influence of the addition of waste graphite powder on the physical and microstructural performance of hydraulic lime pastes. *Construction and Building Materials, 149*, 599-611. doi:10.1016/j.conbuildmat.2017.05.156

Barbero, S., Dutto, M., Ferrua, C., & Pereno, A. (2014). Analysis on existent thermal insulating plasters towards innovative applications: Evaluation methodology for a real cost-performance comparison. *Energy and Buildings, 77*, 40-47. doi:10.1016/j.enbuild.2014.03.037

Barnat-Hunek, D., Smarzewski, P., & Fic, S. (2015). Mechanical and thermal properties of hemp-lime composites. *Composites Theory and Practice, 15*(1), 21-27.

Bederina, M., Marmoret, L., Mezreb, K., Khenfer, M., Bali, A., & Quéneudec, M. (2007). Effect of the addition of wood shavings on thermal conductivity of sand concretes: experimental study and modelling. *Construction and Building Materials, 21*(3), 662-668.

BEIS. (2018). UK Energy Statistics, Energy Consumption in the UK July 2018 [Press release]. Retrieved from https://assets.publishing.service.gov.uk/government/uploads/system/uploads/attachment_data/file/729317/Energy_Consumption_in_the_UK__ECUK__2018.pdf

Benfratello, S., Capitano, C., Peri, G., Rizzo, G., Scaccianoce, G., & Sorrentino, G. (2013). Thermal and structural properties of a hemp–lime biocomposite. *Construction and Building Materials, 48*, 745-754. doi:http://dx.doi.org/10.1016/j.conbuildmat.2013.07.096

Benhaim, P. (2013). Build a house with hemp. Retrieved from http://thehempbuilder.com/build-a-house-with-hemp2

Bhagat, & Khanna, a. (2015). Study of Zinc Oxide Nanofluids for Heat Transfer Application. *SAJ Nanoscience and Nanotechnology, 1*(1), 1-7.

Bhattacharya, M. (2016). Polymer nanocomposites—a comparison between carbon nanotubes, graphene, and clay as nanofillers. *Materials, 9*(4), 262.

Bilodeau, M. A., & Bousfield, D. W. (2015). Composite building products bound with cellulose nanofibers. In: Google Patents.

Bose, A. (2016). Techniques to Convert Particles to Nano Scale *Review of various conventional and noble techniques to convert Particles to Nano Scale* Retrieved from http://www.pharmainfo.net/book/emerging-trends-nanotechnology-pharmacy-1introduction-nanotechnology/techniques-convert

Bouziadi, F., Boulekbache, B., & Hamrat, M. (2016). The effects of fibres on the shrinkage of high-strength concrete under various curing temperatures. *Construction and Building Materials, 114*, 40-48. doi:10.1016/j.conbuildmat.2016.03.164

Bouzourâa, M. B., Naciri, A. E., Moadhen, A., Rinnert, H., Guendouz, M., Battie, Y., . . . Oueslati, M. (2016). Effects of silicon porosity on physical properties of ZnO films. *Materials Chemistry and Physics, 175*, 233-240. doi:https://doi.org/10.1016/j.matchemphys.2016.03.026

Bowley, B. (1994). Historic ceilings. *Structural Survey, 12*(2), 24-28.

Brás, A., Gonçalves, F., & Faustino, P. (2014). Cork-based mortars for thermal bridges correction in a dwelling: Thermal performance and cost evaluation.

Energy and Buildings, 72, 296-308. doi:http://dx.doi.org/10.1016/j.enbuild.2013.12.022

BRE. (2015). *The Cost of poor housing in the European Union*: Simon Nicol, Mikes Roys, David Ormandy and Vironique Ezratty.

Brzyski, P., Barnat-Hunek, D., Suchorab, Z., & Łagód, G. (2017). Composite Materials Based on Hemp and Flax for Low-Energy Buildings. *Materials, 10*(5), 510.

BS-ISO-1920-8. (2009). Testing of concrete. Determination of the drying shrinkage of concrete for samples prepared in the field or in the laboratory.

BSEN1015-19. (1999). Part 19 determination of water vapour prmeability of hardened rendering and plastering mortar. In *Methods of test for mortar for masonary* (pp. 1-10). UK: BSI.

BSEN1015. (1999). Method of test for mortar flexural and compressive strength BS EN 1015-11:1999. In *Part 11: Determination of flexural and compressive strength of hardened mortar* (pp. 1-33). UK.

BSEN1015. (2000). EN 1015 11 2000 flexural and compression test. In *Methods of test for mortar for masonry. Determination of flexural and compressive strength of hardened mortar*. UK: BSI.

BSEN12664. (2001). Thermal performance of building materials and products Determination of thermal resistance by means of guarded hot plate and heat flow meter methods Dry and moist products of medium and low thermal resistance. In. UK: BSI.

BSI. (2005). Methods of testing cement BS EN 196-1. In *Part 1* (pp. 1-36). UK.

BSISO. (2016). BSISO 15901-1-2016--[2018-09-12--02-12-59 PM]. In: British Standard Institution.

Bu, J., & Tian, Z. (2016). Relationship between pore structure and compressive strength of concrete: Experiments and statistical modeling. *Sādhanā, 41*(3), 337-344.

Burgueno, R., Mohanty, A. K., & Quagliata, M. J. (2007). Hybrid natural-fiber composites with cellular skeletal structures. In: Google Patents.

Campbell, F. C. (2010). Introduction to Composite Materials. In A. International (Ed.), *Structural Composite Materials* (pp. 1-2).

Canada, N. R. C. (2009). National Research Council Canada. Retrieved from https://www.bing.com/images/search?view=detailV2&ccid=ZybziKmm&id=403F7AF0C5391C0DA105BD6E000C104CB258FEA8&thid=OIP.ZybziKmmLoQ20o7liB_EnQHaFx&mediaurl=https%3A%2F%2Fwww.nrc-cnrc.gc.ca%2Fobj%2Fimages%2Fachievements-realisations%2Fhighlights-saillants%2F2009-2009%2Fnatural_fibres-fibres_naturel_1.jpg&exph=300&expw=385&q=cross+section+of+hemp+stem&simid=608022782002334341&selectedindex=6&ajaxhist=0

Canut, M. M. C. (2011). *Pore structure in blended cement pastes.* (PhD), Technical University of Denmark, Denmark.

Cao, Y., Zavaterri, P., Youngblood, J., Moon, R., & Weiss, J. (2015). The influence of cellulose nanocrystal additions on the performance of cement paste. *Cement and Concrete Composites, 56*, 73-83. doi:10.1016/j.cemconcomp.2014.11.008

Carrion, F. J., Sanes, J., & Bermudez, M. D. (2007). Influence of ZnO nanoparticle filler on the properties and wear resistance of polycarbonate. *Wear, 262*(11-12), 1504-1510. doi:10.1016/j.wear.2007.01.016

References

Chandra, A., Turng, L.-S., Gopalan, P., Rowell, R. M., & Gong, S. (2008). Study of utilizing thin polymer surface coating on the nanoparticles for melt compounding of polycarbonate/alumina nanocomposites and their optical properties. *Composites Science and Technology, 68*(3–4), 768-776. doi:http://dx.doi.org/10.1016/j.compscitech.2007.08.027

Chari, V. D., Sharma, D. V., Prasad, P. S., & Murthy, S. R. (2013). Dependence of thermal conductivity in micro to nano silica. *Bulletin of Materials Science, 36*(4), 517-520.

Chau, J. L. H., Hsu, S. L.-C., Chen, Y.-M., Yang, C.-C., & Hsu, P. C. F. (2010). A simple route towards polycarbonate–silica nanocomposite. *Advanced Powder Technology, 21*(3), 341-343. doi:10.1016/j.apt.2010.02.005

Chen, P. W., & Chung, D. D. (1993). Carbon Fiber Reinforced Concrete for Smart Structures Capable of Non-Destructive Flaw Detection. *Smart Materials and Structures, 2*(1), 22.

Chen, X., Wu, S., & Zhou, J. (2014). Experimental study and analytical model for pore structure of hydrated cement paste. *Applied Clay Science, 101*, 159-167. doi:https://doi.org/10.1016/j.clay.2014.07.031

Choolaei, M., Rashidi, A. M., Ardjmand, M., Yadegari, A., & Soltanian, H. (2012). The effect of nanosilica on the physical properties of oil well cement. *Materials Science and Engineering: A, 538*, 288-294. doi:https://doi.org/10.1016/j.msea.2012.01.045

Choudalakis, G., & Gotsis, A. D. (2009). Permeability of polymer/clay nanocomposites: A review. *European Polymer Journal, 45*(4), 967-984. doi:http://dx.doi.org/10.1016/j.eurpolymj.2009.01.027

Chrissafis, K., & Bikiaris, D. (2011). Can nanoparticles really enhance thermal stability of polymers? Part I: An overview on thermal decomposition of addition polymers. *Thermochimica Acta, 523*(1–2), 1-24. doi:http://dx.doi.org/10.1016/j.tca.2011.06.010

Chuah, S., Pan, Z., Sanjayan, J. G., Wang, C. M., & Duan, W. H. (2014). Nano reinforced cement and concrete composites and new perspective from graphene oxide. *Construction and Building Materials, 73*, 113-124. doi:http://dx.doi.org/10.1016/j.conbuildmat.2014.09.040

Cigasova, J., Stevulova, N., Terpakova, E., Sicakova, A., & Junak, J. (2013). Modified hemp hurds as a filler in composites. *International Multidisciplinary Scientific GeoConference: SGEM: Surveying Geology & mining Ecology Management*, 385.

Coleman, J. N., Cadek, M., Blake, R., Nicolosi, V., Ryan, K. P., Belton, C., . . . Blau, W. J. (2004). High Performance Nanotube-Reinforced Plastics: Understanding the Mechanism of Strength Increase. *Advanced Functional Materials, 14*(8), 791-798. doi:10.1002/adfm.200305200

Coleman, J. N., Khan, U., Blau, W. J., & Gun'ko, Y. K. (2006). Small but strong: A review of the mechanical properties of carbon nanotube–polymer composites. *Carbon, 44*(9), 1624-1652. doi:http://dx.doi.org/10.1016/j.carbon.2006.02.038

Collet, F., & Prétot, S. (2014). Thermal conductivity of hemp concretes: Variation with formulation, density and water content. *Construction and Building Materials, 65*, 612-619.

Collier, N. C., Sharp, J. H., Milestone, N. B., Hill, J., & Godfrey, I. H. (2008). The influence of water removal techniques on the composition and microstructure

of hardened cement pastes. *Cement and Concrete Research, 38*(6), 737-744. doi:https://doi.org/10.1016/j.cemconres.2008.02.012

CommitteeOnClimateChange. (2008). Climate Change Act 2008, UK regulation. In. UK.

Constantinides, G. (2013). Nanoscience and nanoengineering of cement-based materials. In M. V. Diamanti, A. Nazari, & C. G. Granqvist (Eds.), *Nanotechnology in Eco-Efficient Construction* (pp. 9-37a): Woodhead Publishing.

Cyras, V. P., Manfredi, L. B., Ton-That, M.-T., & Vázquez, A. (2008). Physical and mechanical properties of thermoplastic starch/montmorillonite nanocomposite films. *Carbohydrate Polymers, 73*(1), 55-63. doi:10.1016/j.carbpol.2007.11.014

D.K. HWANG, J.H. MOON, Y.G. SHUL, K.T. JUNG, KIM, D. H., & LEE, A. D. W. (2003). Scratch Resistant and Transparent UV Protective Coating on Polycarbonate. *Journal of Sol-Gel Science and Technology, 26*, 783–787.

Dan, C. H., Lee, M. H., Kim, Y. D., Min, B. H., & Kim, J. H. (2006). Effect of clay modifiers on the morphology and physical properties of thermoplastic polyurethane/clay nanocomposites. *Polymer, 47*(19), 6718-6730. doi:http://dx.doi.org/10.1016/j.polymer.2006.07.052

Dang, W., Song, Y., Wang, Q., & Wang, W. (2008). Improvement in compatibility and mechanical properties of modified wood fiber/polypropylene composites. *Frontiers of Forestry in China, 3*(2), 243-247.

de Bruijn, P. B., Jeppsson, K.-H., Sandin, K., & Nilsson, C. (2009). Mechanical properties of lime–hemp concrete containing shives and fibres. *Biosystems engineering, 103*(4), 474-479. doi:https://doi.org/10.1016/j.biosystemseng.2009.02.005

Deka, B. K., & Maji, T. K. (2011). Effect of TiO2 and nanoclay on the properties of wood polymer nanocomposite. *Composites Part A: Applied Science and Manufacturing, 42*(12), 2117-2125. doi:http://dx.doi.org/10.1016/j.compositesa.2011.09.023

Deka, B. K., & Maji, T. K. (2012). Effect of nanoclay and ZnO on the physical and chemical properties of wood polymer nanocomposite. *Journal of Applied Polymer Science, 124*(4), 2919-2929.

Deka, B. K., Mandal, M., & Maji, T. K. (2012). Effect of nanoparticles on flammability, UV resistance, biodegradability, and chemical resistance of wood polymer nanocomposite. *Industrial & Engineering Chemistry Research, 51*(37), 11881-11891.

Demo, M. (2017). *Study on The Effect of Moisture in The Building*. Paper presented at the 1-st International Scientific Conference on Professional Sciences, Durres, Albania.

Denis Mihaela Panaitescu, Adriana Nicoleta Frone, Marius Ghiurea, Catalin Ilie Spataru, and, C. R., & Iorga, M. D. (2011). Properties of Polymer Composites with cellulose microfibrils. In.

Devi, R. R., & Maji, T. K. (2012). Effect of Nano-ZnO on Thermal, Mechanical, UV Stability, and Other Physical Properties of Wood Polymer Composites. *Industrial & Engineering Chemistry Research, 51*(10), 3870-3880. doi:10.1021/ie2018383

Du, H., & Pang, S. D. (2015). Enhancement of barrier properties of cement mortar with graphene nanoplatelet. *Cement and Concrete Research, 76*, 10-19. doi:http://dx.doi.org/10.1016/j.cemconres.2015.05.007

References

Ebnesajjad, S. (2012). Characteristics of Adhesive Materials. In *Handbook of Adhesives and Surface Preparation* (pp. 168-169).

Edward AJ Hirst, Peter Walker, Kevin A Paine, & Yates, a. T. (2010). *Characterisation of Low Density Hemp Lime Composite*. Paper presented at the 2nd international conference on sustainable construction material and technology, Italy. http://www.claisse.info/Proceedings.htm

Elfordy, S., Lucas, F., Tancret, F., Scudeller, Y., & Goudet, L. (2008). Mechanical and thermal properties of lime and hemp concrete ("hempcrete") manufactured by a projection process. *Construction and Building Materials, 22*(10), 2116-2123. doi:http://dx.doi.org/10.1016/j.conbuildmat.2007.07.016

Energy, U. d. o. (2008). *Energy Efficiency Trends in residential and commercialbuildings*. Retrieved from

ENNF. (2001). Thermal Performance of Building Materials and Products–Determination of Thermal Resistance by Means of Guarded Hot Plate and Heat Flow Meter Methods–Dry and Moist Products of Medium and Low Thermal Resistance.

Erniati, Tjaronge, M. W., Zulharnah, & Irfan, U. R. (2015). Porosity, Pore Size and Compressive Strength of Self Compacting Concrete Using Sea Water. *Procedia Engineering, 125*, 832-837. doi:https://doi.org/10.1016/j.proeng.2015.11.045

Ershadi, V., Ebadi, T., Rabani, A., Ershadi, L., & Soltanian, H. (2011). The effect of nanosilica on cement matrix permeability in oil well to decrease the pollution of receptive environment. *International Journal of Environmental Science and Development, 2*(2), 128.

EuLA. (2014). *A competitive and Efficient Lime Industry*. Retrieved from Belgium: www.eula.eu

Evrard, A. (2003). Hemp concretes-A synthesis of physical properties. *Construire en Chanvre*.

Feldman, D. (2014). Polymer Nanocomposites in Building, Construction. *Journal of Macromolecular Science Part a-Pure and Applied Chemistry, 51*(3), 203-209. doi:10.1080/10601325.2014.871948

Fernandes, E. M., Pires, R. A., Mano, J. F., & Reis, R. L. (2013). Bionanocomposites from lignocellulosic resources: Properties, applications and future trends for their use in the biomedical field. *Progress in Polymer Science, 38*(10-11), 1415-1441. doi:10.1016/j.progpolymsci.2013.05.013

Ferreira, A. M., & Carvalho, A. J. F. (2014). TPS Nanocomposite reinforced with MFC by melting process. *Materials Research, 17*, 807-810.

Feynman, R. P. (1960). There's Plenty of Room at the Bottom. *Caltech Engineering and Science, 23*(5), 22-36.

Fiberlean. *Microfibrillated cellulose a new dimension in paper making*. Retrieved from http://www.fiberlean.com/brochure/FiberLean.pdf

Foley, K. M., VanderHooven, D. I., & Hull, J. D. (1981). Method of Sealing Pores and Lost circulation additives, US Ptent

Fornes, T. D., Baur, J. W., Sabba, Y., & Thomas, E. L. (2006). Morphology and properties of melt-spun polycarbonate fibers containing single- and multi-wall carbon nanotubes. *Polymer, 47*(5), 1704-1714. doi:10.1016/j.polymer.2006.01.003

Gao, K., Lin, K.-L., Wang, D., Hwang, C.-L., Shiu, H.-S., Chang, Y.-M., & Cheng, T.-W. (2014). Effects SiO2/Na2O molar ratio on mechanical properties and the microstructure of nano-SiO2 metakaolin-based geopolymers.

Construction and Building Materials, 53, 503-510. doi:http://dx.doi.org/10.1016/j.conbuildmat.2013.12.003

Gao, T., Sandberg, L. I. C., & Jelle, B. P. (2014). Nano Insulation Materials: Synthesis and Life Cycle Assessment. *Procedia CIRP, 15*, 490-495. doi:https://doi.org/10.1016/j.procir.2014.06.041

Gao, Y., He, P., Lian, J., Wang, L., Qian, D., Zhao, J., . . . Shi, D. (2006). Improving the Mechanical Properties of Polycarbonate Nanocomposites with Plasma‐Modified Carbon Nanofibers. *Journal of Macromolecular Science, Part B, 45*(4), 671-679. doi:10.1080/00222340600770392

Gauvin, F., & Robert, M. (2015). Durability study of vinylester/silicate nanocomposites for civil engineering applications. *Polymer Degradation and Stability, 121*, 359-368. doi:http://dx.doi.org/10.1016/j.polymdegradstab.2015.09.010

Glé, P., Gourdon, E., & Arnaud, L. (2011). Acoustical properties of materials made of vegetable particles with several scales of porosity. *Applied Acoustics, 72*(5), 249-259. doi:https://doi.org/10.1016/j.apacoust.2010.11.003

Goddard, D. M., & Kendall, E. G. (1977). Fibreglass-reinforced lead composites. *Composites, 8*(2), 103-109. doi:https://doi.org/10.1016/0010-4361(77)90067-2

Gómez-Avilés, A., Darder, M., Aranda, P., & Ruiz-Hitzky, E. (2010). Multifunctional materials based on graphene-like/sepiolite nanocomposites. *Applied Clay Science, 47*(3–4), 203-211. doi:http://dx.doi.org/10.1016/j.clay.2009.10.004

Gomez-Ortiz, N., De la Rosa-Garcia, S., Gonzalez-Gomez, W., Soria-Castro, M., Quintana, P., Oskam, G., & Ortega-Morales, B. (2013). Antifungal coatings based on Ca(OH)2 mixed with ZnO/TiO2 nanomaterials for protection of limestone monuments. *ACS Appl Mater Interfaces, 5*(5), 1556-1565. doi:10.1021/am302783h

Gong, K., Pan, Z., Korayem, A., Qiu, L., Li, D., Collins, F., . . . Duan, W. (2014). Reinforcing Effects of Graphene Oxide on Portland Cement Paste. *Journal of Materials in Civil Engineering, 27*(2), A4014010. doi:10.1061/(ASCE)MT.1943-5533.0001125

Gregor, L. (2014). *Performance of Hempcrete Walls Subjected to a Standard Time-temperature Fire Curve*.

Griffiths, R. (2015). The house that doubles as a power station . *Solcer house's low energy construction*. Retrieved from http://www.dailymail.co.uk/sciencetech/article-3162441/The-house-doubles-POWER-STATION-Three-bedroom-positive-energy-home-solar-panels-heat-pump.html

Grigoriadis, K., Mangat, & Abubakri, S. (2017). Bond between microwave cured repair and concrete substrate. *Materials and Structures, 50*(2), 125. doi:ARTN 125

10.1617/s11527-016-0990-6

H. Assaedi, F. U. A. Shaikh, & Low, I. M. (2015a). Characteristics of Nanosilica-Geopolymer nanocomposites and mixing effect. *International Journal of Chemical, Molecular, Nuclear, Materials and Metallurgical Engineering, 9*(12).

H. Assaedi, F. U. A. Shaikh, & Low, I. M. (2015b). Characteristics of Nanosilica-Geopolymer nanocomposites and mixing effect. *International Journal of*

Chemical, Molecular, Nuclear, Materials and Metallurgical Engineering, 9(12).

H.M. Government, R. (2010). The building regulations, Conservation of fuel and power, Approved document L1A: conservation of fuel and power-new dwellings 2010 edition. In: NBS London.

Hakamy, A., Shaikh, F., & Low, I. M. (2015). Characteristics of nanoclay and calcined nanoclay-cement nanocomposites. *Composites Part B: Engineering, 78*, 174-184.

Hakamy, A., Shaikh, F. U. A., & Low, I. M. (2013). Microstructures and mechanical properties of hemp fabric reinforced organoclay–cement nanocomposites. *Construction and Building Materials, 49*, 298-307. doi:http://dx.doi.org/10.1016/j.conbuildmat.2013.08.028

Hakamy, A., Shaikh, F. U. A., & Low, I. M. (2014). Characteristics of hemp fabric reinforced nanoclay–cement nanocomposites. *Cement and Concrete Composites, 50*, 27-35. doi:http://dx.doi.org/10.1016/j.cemconcomp.2014.03.002

Hakamy, A., Shaikh, F. U. A., & Low, I. M. (2014). Thermal and mechanical properties of hemp fabric-reinforced nanoclay–cement nanocomposites. *Journal of Materials Science, 49*(4), 1684-1694. doi:10.1007/s10853-013-7853-0

Hakamy, A., Shaikh, F. U. A., & Low, I. M. (2015). Characteristics of nanoclay and calcined nanoclay-cement nanocomposites. *Composites Part B: Engineering, 78*, 174-184. doi:https://doi.org/10.1016/j.compositesb.2015.03.074

Hakimelahi, H. R., Hu, L., Rupp, B. B., & Coleman, M. R. (2010). Synthesis and characterization of transparent alumina reinforced polycarbonate nanocomposite. *Polymer, 51*(12), 2494-2502.

Hamedi, G. H., Nejad, F. M., & Oveisi, K. (2016). Estimating the moisture damage of asphalt mixture modified with nano zinc oxide. *Materials and Structures, 49*(4), 1165-1174. doi:10.1617/s11527-015-0566-x

Handoko, A. D., Liew, L.-L., Lin, M., Sankar, G., Du, Y., Su, H., . . . Goh, G. K. L. (2018). Elucidation of thermally induced internal porosity in zinc oxide nanorods. *Nano Research, 11*(5), 2412-2423. doi:10.1007/s12274-017-1862-2

Harcourt, H. M. (2016). American Heritage Dictionary of the English Language, Edition. *phonon. (n.d.)*

Fifth. Retrieved from https://www.thefreedictionary.com/phonon

Harlin, A., & Vikman, M. (2010). *Developments in advanced nanocomposite* (1455-0865 (URL: http://www.vtt.fi/publications/index.jsp)). Retrieved from Finland

Hatherngton, S. (2014). Comparative testing of hydraulic lime and OPC mortar mixes. *Journal of Building Survey, Appraisal & Valuation, 3*(3).

Hazarika, A., Baishya, P., & Maji, T. K. (2015). Bio-based Wood Polymer Nanocomposites: A Sustainable High-Performance Material for Future. *75*, 233-257. doi:10.1007/978-81-322-2470-9_8

Hazarika, A., & Maji, T. K. (2014). Modification of Softwood by Monomers and Nanofillers. *Defence Science Journal, 64*(3), 262-272. doi:DOI 10.14429/dsj.64.7325

References

Heisters, S. S. (2008). *Illegally Green Environmental Costs of hemp prohibition*. Retrieved from https://reason.org/wp-content/uploads/files/1030ae0323a3140ecf531bd473632b57.pdf

Henderson, R. M., Reinert, S. A., Dekhtyar, P., & Migdal, A. (2015). Climate Change in 2018: Implications for Business. *risk*, *1*.

Henriksson, M., Berglund, Lars A. (2007). Structure and properties of cellulose nanocomposite films containing melamine formaldehyde. *Journal of Applied Polymer Science*, *106*(4), 2817-2824. doi:10.1002/app.26946

Hollaway, L. C. (2003). The evolution of and the way forward for advanced polymer composites in the civil infrastructure. *Construction and Building Materials*, *17*(6), 365-378. doi:https://doi.org/10.1016/S0950-0618(03)00038-2

Horszczaruk, E., Mijowska, E., Kalenczuk, R. J., Aleksandrzak, M., & Mijowska, S. (2015). Nanocomposite of cement/graphene oxide – Impact on hydration kinetics and Young's modulus. *Construction and Building Materials*, *78*, 234-242. doi:http://dx.doi.org/10.1016/j.conbuildmat.2014.12.009

Hunt, R. (2018). The importance of breathability in old building. *Green Pec*. Retrieved from http://www.greenspec.co.uk/building-design/importance-of-breathability-in-old-buildings/

Hurter, R., & Eng, P. (2001). Nonwood Plant Fiber Characteristics.

IAQ, I. (2013). Moisture Control Guidance for Building Design. *Construction and Maintenance*.

Ilić, V., Šaponjić, Z., Vodnik, V., Potkonjak, B., Jovančić, P., Nedeljković, J., & Radetić, M. (2009). The influence of silver content on antimicrobial activity and color of cotton fabrics functionalized with Ag nanoparticles. *Carbohydrate Polymers*, *78*(3), 564-569. doi:http://dx.doi.org/10.1016/j.carbpol.2009.05.015

Inovatecsystem. (2006-2016). The new energy-efficient, affordable way to build in the 21st century.

.

Jahanmardi, R., Kangarlou, B., & Dibazar, A. R. (2013). Effects of organically modified nanoclay on cellular morphology, tensile properties, and dimensional stability of flexible polyurethane foams. *Journal of Nanostructure in Chemistry*, *3*(1), 1-6. doi:10.1186/2193-8865-3-82

Pharmaceuticall Nanotech, (2007).

Jancar, J., Douglas, J. F., Starr, F. W., Kumar, S. K., Cassagnau, P., Lesser, A. J., . . . Buehler, M. J. (2010). Current issues in research on structure–property relationships in polymer nanocomposites. *Polymer*, *51*(15), 3321-3343. doi:10.1016/j.polymer.2010.04.074

Jennings, H., M.,, Thomas, J. J., Rothstein, D., & Chen, J. J. (2008). Cement as Porous Materials. In *Materials. Handbook of Porous Solids* (pp. 2971–3028).

Jeon, I.-Y., & Baek, J.-B. (2010a). Nanocomposites Derived from Polymers and Inorganic Nanoparticles. *Materials*, *3*(6), 3654.

Jeon, I.-Y., & Baek, J.-B. (2010b). Nanocomposites Derived from Polymers and Inorganic Nanoparticles. *Materials*, *3*(6), 3654-3674. doi:10.3390/ma3063654

Ji, T. (2005). Preliminary study on the water permeability and microstructure of concrete incorporating nano-SiO2. *Cement and Concrete Research*, *35*(10), 1943-1947. doi:http://dx.doi.org/10.1016/j.cemconres.2005.07.004

References

Ji, Z., Jin, X., George, S., Xia, T., Meng, H., Wang, X., . . . Zink, J. I. (2010). Dispersion and Stability Optimization of TiO2 Nanoparticles in Cell Culture Media. *Environmental Science & Technology, 44*(19), 7309-7314. doi:10.1021/es100417s

Jiao, L., Su, M., Chen, L., Wang, Y., Zhu, H., & Dai, H. (2016). Natural cellulose nanofibers as sustainable enhancers in construction cement. *PLoS ONE, 11*(12), e0168422.

Jiaqi Zhu, W. C., Mingli Yue, Ying Hou, Jiecai Han and Ming Yang. (2015). Strong and Stiff Aramid Nanofiber Carbon Nanotube Nanocomposites. *American Chemical Society Nano, 9 No3*, 2489–2501.

Jittabut, P. (2015). Effect of Nanosilica on Mechanical and Thermal Properties of Cement Composites for Thermal Energy Storage Materials. *Energy Procedia, 79*, 10-17. doi:https://doi.org/10.1016/j.egypro.2015.11.454

JOHNSON, H. V. (1926). CEMENT LIME MORTARS. In (pp. 241-174): BUREAU OF STANDARDS.

Jungbluth, N. (2008). *Life Cycle Inventory of Sodium Acetate and Expanded Graphite*. Retrieved from

K.Rajkumar, Prem Ranjan, P.Thavamani, P.Jeyanthi, & P.Pazhanisamy, a. (2013). DISPERSION STUDIES OF NANOSILICA IN NBR BASED on polymer nanocomposites. *Rasaian j. chem., 6*(2), | 122-133 |.

Kaboorani, A., & Riedl, B. (2011). Effects of adding nano-clay on performance of polyvinyl acetate (PVA) as a wood adhesive. *Composites Part A: Applied Science and Manufacturing, 42*(8), 1031-1039. doi:https://doi.org/10.1016/j.compositesa.2011.04.007

Khater, H. M., & Abd el Gawaad, H. A. (2016). Characterization of alkali activated geopolymer mortar doped with MWCNT. *Construction and Building Materials, 102, Part 1*, 329-337. doi:http://dx.doi.org/10.1016/j.conbuildmat.2015.10.121

Khatua, B. B., Maiti, S., Shrivastava, N. K., & Suin, S. (2013). A strategy for achieving low percolation and high electrical conductivity in melt-blended polycarbonate (PC)/multiwall carbon nanotube (MWCNT) nanocomposites: Electrical and thermo-mechanical properties. *Express Polymer Letters*. doi:10.3144/expresspolymlett.2013.47

Kim, H., Miura, Y., & Macosko, C. W. (2010). Graphene/Polyurethane Nanocomposites for Improved Gas Barrier and Electrical Conductivity. *Chemistry of Materials, 22*(11), 3441-3450. doi:10.1021/cm100477v

Kim, S., & Kim, H.-J. (2005). Effect of addition of polyvinyl acetate to melamine-formaldehyde resin on the adhesion and formaldehyde emission in engineered flooring. *International Journal of Adhesion and Adhesives, 25*(5), 456-461. doi:https://doi.org/10.1016/j.ijadhadh.2005.01.001

Kim, Y. Y., Lee, K. M., Bang, J. W., & Kwon, S. J. (2014). Effect of W/C Ratio on Durability and Porosity in Cement Mortar with Constant Cement Amount. *Advances in Materials Science and Engineering*. doi:Artn 27346010.1155/2014/273460

Kinnane, O., McGranaghan, G., Walker, R., Pavia, S., Byrne, G., & Robinson, A. (2015). *Experimental investigation of thermal inertia properties in hemp-lime concrete walls.* Paper presented at the Proceedings of the 10th conference on advanced building skins.

References

Kiran, M., Nandanwar, A., Naidu, M. V., & Rajulu, K. C. V. (2012). Effect of density on thermal conductivity of bamboo mat board. *International Journal of Agriculture and Forestry*, *2*(5), 257-261.

Klemm, D., Heublein, B., Fink, H. P., & Bohn, A. (2005). Cellulose: fascinating biopolymer and sustainable raw material. *Angew Chem Int Ed Engl*, *44*(22), 3358-3393. doi:10.1002/anie.200460587

Konecny, L., & Naqvi, S. J. (1993). The effect of different drying techniques on the pore size distribution of blended cement mortars. *Cement and Concrete Research*, *23*(5), 1223-1228. doi:https://doi.org/10.1016/0008-8846(93)90183-A

Kreyling, W. G., Semmler-Behnke, M., & Chaudhry, Q. (2010). A complementary definition of nanomaterial. *Nano Today*, *5*(3), 165-168. doi:http://dx.doi.org/10.1016/j.nantod.2010.03.004

Laadila, M. A., Hegde, K., Rouissi, T., Brar, S. K., Galvez, R., Sorelli, L., . . . Abokitse, K. (2017). Green synthesis of novel biocomposites from treated cellulosic fibers and recycled bio-plastic polylactic acid. *Journal of Cleaner Production*, *164*, 575-586. doi:10.1016/j.jclepro.2017.06.235

Lam, H. J. (2015). *Investigation on the Usage of Optimum Content of Graphite Oxide for Bitumen Modification*. UTAR,

Lancellotti, I., Kamseu, E., Michelazzi, M., Barbieri, L., Corradi, A., & Leonelli, C. (2010). Chemical stability of geopolymers containing municipal solid waste incinerator fly ash. *Waste Management*, *30*(4), 673-679. doi:http://dx.doi.org/10.1016/j.wasman.2009.09.032

Laustsen, J. (2008). Energy Efficiency Requirements in building codes energy efficiency policies for new building.pdf>. *International Energy Agency*, 1-85.

Lawrence, R. M. H., & & Walker, P. (2008). The impact of the water lime ratio on the structural characteristics of air lime mortar. *Structural Analysis of Historic Construction –BRE Centre for Innovative Construction Materials*, 885-889.

Lee, H. J., Yeo, S. Y., & Jeong, S. H. Antibacterial effect of nanosized silver colloidal solution on textile fabrics. *Journal of Materials Science*, *38*(10), 2199-2204. doi:10.1023/a:1023736416361

Lee, K.-Y., Aitomäki, Y., Berglund, L. A., Oksman, K., & Bismarck, A. (2014). On the use of nanocellulose as reinforcement in polymer matrix composites. *Composites Science and Technology*, *105*, 15-27. doi:10.1016/j.compscitech.2014.08.032

Lee, K. Y., et al. (2009). Green hierarchical composites: The bottom-up approach. . *ICCM International Conferences on Composite Materials*.

Lee, S.-Y., Chun, S.-J., Kang, I.-A., & Park, J.-Y. (2009). Preparation of cellulose nanofibrils by high-pressure homogenizer and cellulose-based composite films. *Journal of Industrial and Engineering Chemistry*, *15*(1), 50-55. doi:10.1016/j.jiec.2008.07.008

Leila Shahraiari, & Athawale, A. A. (2014). Graphene Oxide Synthesized by using Modified Hummers Approach. *International Journal of Renewable Energy and Environmental Engineering*, *2*(1), 58-63.

Li, J., Kim, J.-K., & Lung Sham, M. (2005). Conductive graphite nanoplatelet/epoxy nanocomposites: Effects of exfoliation and UV/ozone treatment of graphite. *Scripta Materialia*, *53*(2), 235-240. doi:https://doi.org/10.1016/j.scriptamat.2005.03.034

References

Liao, Y., Wu, X., Wang, Z., Yue, R., Liu, G., & Chen, Y. (2012). Composite thin film of silica hollow spheres and waterborne polyurethane: Excellent thermal insulation and light transmission performances. *Materials Chemistry and Physics, 133*(2-3), 642-648. doi:10.1016/j.matchemphys.2012.01.041

Lin, C., Wei, W., & Hu, Y. H. (2016). Catalytic behavior of graphene oxide for cement hydration process. *Journal of Physics and Chemistry of Solids, 89*, 128-133. doi:http://dx.doi.org/10.1016/j.jpcs.2015.11.002

Liu, L., Barber, A. H., Nuriel, S., & Wagner, H. D. (2005). Mechanical Properties of Functionalized Single-Walled Carbon-Nanotube/Poly(vinyl alcohol) Nanocomposites. *Advanced Functional Materials, 15*(6), 975-980. doi:10.1002/adfm.200400525

Liu, Y., Kuang, Y., Huang, N., Wu, Z., & Wang, C. (2009). CO2 emission from cement manufacturing and its driving forces in China. *International Journal of Environment and Pollution, 37*(4), 369-382.

London, N. (2017). Turning windows into solar panels. Retrieved from http://www.cpr.org/news/story/turning-windows-into-solar-panels

Low, I. M., Hakamy, A., & Shaikh, F. (2017). *High Performance Natural Fiber-Nanoclay Reinforced Cement Nanocomposites*: Springer International Publishing.

Lowrence, D. T. a., & Fukushina, H. (2009). USA Patent No.: U. S. patent.

Luyt, A. S., Messori, M., Fabbri, P., Mofokeng, J. P., Taurino, R., Zanasi, T., & Pilati, F. (2010). Polycarbonate Reinforced with Silica Nanoparticles. *Polymer Bulletin, 66*(7), 991-1004. doi:10.1007/s00289-010-0408-5

M. E. Ali Mohsin, Agus Arsad, & Alothman, O. Y. (2014). Enhanced thermal mechanical and morphological properties of cnt hdpe nanocomposite using mmt as secondary filler. *International Journal of Chemical, Molecular, Nuclear, Materials and Metallurgical Engineering, 8*(2), 117-120.

Maciel, M. H., Soares, G. S., de Oliveira Romano, R. C., & Cincotto, M. A. (2019). Monitoring of Portland cement chemical reaction and quantification of the hydrated products by XRD and TG in function of the stoppage hydration technique. *Journal of Thermal Analysis and Calorimetry, 136*(3), 1269-1284.

Maddalena, R., & Hamilton, A. (2017). Low-pressure silica injection for porosity reduction in cementitious materials. *Construction and Building Materials, 134*, 610-616. doi:https://doi.org/10.1016/j.conbuildmat.2016.11.016

Madhuri B. M., Prashant S. K., Aravin p. p., & S., a. L. S. (2012). Review of Recent Trends & Developments in Biocomposites. Retrieved from http://www.cottonbangladesh.com/April2014/DevelopmentinBioComposite.htm

Mala, N., Ravichandran, K., Pandiarajan, S., Srinivasan, N., Ravikumar, B., Catherine Siriya Pushpa, K., . . . Arun, T. (2016). Formation of hexagonal plate shaped ZnO microparticles – A study on antibacterial and magnetic properties. *Ceramics International, 42*(6), 7336-7346. doi:https://doi.org/10.1016/j.ceramint.2016.01.132

Mangat, Abubakri, & Grigoriadis. (2017). Bond of steel reinforcement with microwave cured concrete repair mortars. *Materials and Structures, 50*(6), 249. doi:ARTN 24910.1617/s11527-017-1115-6

Mangat, & Ojedokun, O. (2018). Pore size distribution of an alkali activated cementitious (AACM) mortar. *International Journal of Global Advanced Materials & Nanotechnology, 1*(3), 68.

References

Mangat, P. S., Grigoriadis, K., & Abubakri, S. (2016). Microwave curing parameters of in-situ concrete repairs. *Construction and Building Materials, 112*, 856-866. doi:10.1016/j.conbuildmat.2016.03.007

Marchetti, P., Mechelhoff, M., & Livingston, A. G. (2015). Tunable-Porosity Membranes From Discrete Nanoparticles. *Sci Rep, 5*, 17353. doi:10.1038/srep17353

Marczyk, R. (Jul 12, 2013). Fibre for durable cloth. Retrieved from https://tokesignals.com/worth-repeating-humans-discover-hemp-10000-b-c/

Mariano, M., El Kissi, N., & Dufresne, A. (2015). Melt processing of cellulose nanocrystal reinforced polycarbonate from a masterbatch process. *European Polymer Journal, 69*, 208-223. doi:10.1016/j.eurpolymj.2015.06.007

MasterKureER50. (2014). *Concrete Technology in Focus shrinkage of concrete*. Retrieved from www.master-builders-solutions.basf.us

Matias, G., Faria, P., & Torres, I. (2008). *Lime mortars with brick dust and grounded particles for ancient masonry: development and evaluation.* Paper presented at the HMC08-Historical Mortars Conference.

Meng, Q. (2010). *Poly (lactic acid) (PLA)/clay/wood nanocomposites.* (3402103 Ph.D.), Tulane University School of Science and Engineering, Ann Arbor. Retrieved from http://lcproxy.shu.ac.uk/login?url=http://search.proquest.com/docview/305221448?accountid=13827 http://shulinks.shu.ac.uk/?ctx_ver=Z39.88-2004&ctx_enc=info:ofi/enc:UTF-8&rfr_id=info:sid/&rft_val_fmt=info:ofi/fmt:kev:mtx:dissertation&rft.genre=dissertations+%26+theses&rft.jtitle=&rft.atitle=&rft.au=Meng%2C+Qingkai&rft.aulast=Meng&rft.aufirst=Qingkai&rft.date=2010-01-01&rft.volume=&rft.issue=&rft.spage=&rft.isbn=9781109739022&rft.btitle=&rft.title=Poly+%28lactic+acid%29+%28PLA%29%2Fclay%2Fwood+nanocomposites&rft.issn=&rft_id=info:doi/

Meng, Q. K., Hetzer, M., & De Kee, D. (2011). PLA/clay/wood nanocomposites: nanoclay effects on mechanical and thermal properties. *Journal of Composite Materials, 45*(10), 1145-1158. doi:10.1177/0021998310381541

Mi, H.-Y., Jing, X., Peng, J., Salick, M. R., Peng, X.-F., & Turng, L.-S. (2014). Poly(ε-caprolactone) (PCL)/cellulose nano-crystal (CNC) nanocomposites and foams. *Cellulose, 21*(4), 2727-2741. doi:10.1007/s10570-014-0327-y

Mitsunaga, M., Ito, Y., Ray, S. S., Okamoto, M., & Hironaka, K. (2003). Intercalated Polycarbonate/Clay Nanocomposites: Nanostructure Control and Foam Processing. *Macromolecular Materials and Engineering, 288*(7), 543-548. doi:10.1002/mame.200300097

Mohammadkazemi, F., Doosthoseini, K., Ganjian, E., & Azin, M. (2015). Manufacturing of bacterial nano-cellulose reinforced fiber–cement composites. *Construction and Building Materials, 101, Part 1*, 958-964. doi:http://dx.doi.org/10.1016/j.conbuildmat.2015.10.093

Mohammed, A., Sanjayan, J. G., Duan, W. H., & Nazari, A. (2015). Incorporating graphene oxide in cement composites: A study of transport properties. *Construction and Building Materials, 84*, 341-347. doi:http://dx.doi.org/10.1016/j.conbuildmat.2015.01.083

Mohandas, A., Pt, S. K., Raja, B., Lakshmanan, V.-K., & Jayakumar, R. (2015). Exploration of alginate hydrogel/nano zinc oxide composite bandages for infected wounds. *International journal of nanomedicine, 10*(Suppl 1), 53-66. doi:10.2147/IJN.S79981

References

Mokarem, D. W., Weyers, R. E., & Lane, D. S. (2005). Development of a shrinkage performance specifications and prediction model analysis for supplemental cementitious material concrete mixtures. *Cement and Concrete Research, 35*(5), 918-925. doi:https://doi.org/10.1016/j.cemconres.2004.09.013

Mondal, S., & Hu, J. L. (2007). A novel approach to excellent UV protecting cotton fabric with functionalized MWNT containing water vapor permeable PU coating. *Journal of Applied Polymer Science, 103*(5), 3370-3376. doi:10.1002/app.25437

Mònica Ardanuy, Josep Claramunt, Raquel Arévalo, Ferran Parés, Elisabetta Aracri, & Vidal, a. T. (2012). Nanofibrillated cellulose NFC as potential reinforcement for high performance cement mortar composites. *Bioresources, 7*(3), 3883-3894.

Morsy, F. A., El-Sheikh, S. M., & Barhoum, A. Nano-silica and SiO2/CaCO3 nanocomposite prepared from semi-burned rice straw ash as modified papermaking fillers. *Arabian Journal of Chemistry*. doi:http://dx.doi.org/10.1016/j.arabjc.2014.11.032

Morsy, M., Alsayed, S., & Aqel, M. (2010). Effect of nano-clay on mechanical properties and microstructure of ordinary Portland cement mortar. *International Journal of Civil & Environmental Engineering IJCEE-IJENS, 10*(01), 23-27.

Muphy, F., Pavia, S., & Walker, R. (2010). An Assessment of the Physical Properties of Lime-Hemp. *Proc. of BRI/CRI. Ní Nualláin, Walsh, West, Cannon, Caprani, McCabe eds. Cork*, 431-439.

Nakagaito, A. N., Iwamoto, S., & Yano, H. (2004). Bacterial cellulose: the ultimate nano-scalar cellulose morphology for the production of high-strength composites. *Applied Physics A, 80*(1), 93-97. doi:10.1007/s00339-004-2932-3

Nakagaito, A. N., & Yano, H. (2004). The effect of morphological changes from pulp fiber towards nano-scale fibrillated cellulose on the mechanical properties of high-strength plant fiber based composites. *Applied Physics A, 78*(4), 547-552. doi:10.1007/s00339-003-2453-5

Narender Kumar, & Dahiya, J. B. (2013). Polypropylene nanoclay composites containing flame retardant additive Thermal stability and kinetic study in inert atmosphere. *Adv. Mat. Lett., 4*(9), 708-713. doi:10.5185/amlett.2013.1412

Nawla, H. S. (2004 (vol. 1-10) and 2011 (10-25)). Encyclopedia of Nanoscience and Nanotechnology, 25-Volume Set *Surfactant Factor*. Retrieved from www.aspbs.com/jnn

Nazari, A., & Riahi, S. (2011). The Effects of ZnO2 Nanoparticles on Strength Assessments and Water Permeability of Concrete in Different Curing Media. *Materials Research-Ibero-American Journal of Materials, 14*(2), 178-188. doi:10.1590/S1516-14392011005000030

Nezeraud, E. (2012). Vertical wind power plant design and production. *Demain dès aujourd'hui*. Retrieved from https://www.pinterest.fr/pin/755901118676825022/?lp=true

Nguyen, V. S., Rouxel, D., & Vincent, B. (2014). Dispersion of nanoparticles: From organic solvents to polymer solutions. *Ultrasonics Sonochemistry, 21*(1), 149-153. doi:http://dx.doi.org/10.1016/j.ultsonch.2013.07.015

Nikalje, A. P. (2015). Nanotechnology and its Applications in Medicine. *Medicinal Chemistry, 5*(2). doi:10.4172/2161-0444.1000247

References

Niyigena, C., Amziane, S., Chateauneuf, A., Arnaud, L., Collet, F., Lawrence, M., . . . Sonebi, M. (2015, 2015-06-22). *RRT3: Statistical analysis of hemp concrete mechanical properties variability*. Paper presented at the First International Conference on Bio-Based Building Materials, Clermont-Ferrand, France.

Nokken. (2003). Water Transport in Brick, Stone and Concrete. *Cement Concrete and Aggregates - CEMENT CONCRETE AGGREGATES, 25*. doi:10.1520/CCA10518J

O'Flaherty, F., & Alam, M. (2018). Thermal and sound insulation performance assessment of vacuum insulated composite insulation panels for building façades. *Advances in Building Energy Research*, 1-21. doi:10.1080/17512549.2018.1520645

Ohannessian, K. (2015). Transparent solar panel. *Environment*. Retrieved from https://www.slideshare.net/IvonnePortilla/transparent-solar-panels

Origin: http://www.techtimes.com/articles/13575/20140820/tra nsparent-solar-panel-cell-michigan-state-university.htm Tech Times, Go solar with a view using newly developed transparent cells by Jim Algar, August 20 2014

Oja, P. K., & Nanosiliko, A. (2013). Nanosilica-reinforced polymer composites. *Material in Technologies, 47*, 285-293.

Ojijo, V., & Sinha Ray, S. (2013). Processing strategies in bionanocomposites. *Progress in Polymer Science, 38*(10–11), 1543-1589. doi:http://dx.doi.org/10.1016/j.progpolymsci.2013.05.011

OkenWa O. I. Okoli, Tallahassee, F. U., Myungsoo Kim, & Tallahassee, F. U. (2010). US Patent No.: T. Florida State University Research Foundation, FL (US).

Oksman, K., Aitomäki, Y., Mathew, A. P., Siqueira, G., Zhou, Q., Butylina, S., . . . Hooshmand, S. (2016). Review of the recent developments in cellulose nanocomposite processing. *Composites Part A: Applied Science and Manufacturing, 83*, 2-18. doi:http://dx.doi.org/10.1016/j.compositesa.2015.10.041

Olad, A. (2011). Polymer/Clay Nanocomposites, Advances in Diverse Industrial Applications of Nanocomposites. In D. B. Reddy (Ed.): InTech.

Osorio, M. A., Restrepo, D., Velásquez-Cock, J. A., Zuluaga, R. O., Montoya, U., Rojas, O., . . . Castro, C. I. (2014). Synthesis of thermoplastic starch-bacterial cellulose nanocomposites via in situ fermentation. *Journal of the Brazilian Chemical Society, 25*, 1607-1613.

Pan, Z., DUAN, W., Li, D., & Collins, F. (2013). Graphene oxide reinforced cement and concrete. In: Google Patents.

Pan, Z., Wenhui, D., Li, D., & Collins, F. (2013). Graphene oxide reinforced cement and concrete. In: Google Patents.

Panthapulakkal, S., & Sain, M. (2012a). Preparation and Characterization of Cellulose Nanofibril Films from Wood Fibre and Their Thermoplastic Polycarbonate Composites. *International Journal of Polymer Science, 2012*, 6. doi:10.1155/2012/381342

Panthapulakkal, S., & Sain, M. (2012b). Preparation and Characterization of Cellulose Nanofibril Films from Wood Fibre and Their Thermoplastic Polycarbonate Composites. *International Journal of Polymer Science, 2012*, 1-6. doi:10.1155/2012/381342

Parveen, S., Rana, S., & Fangueiro, R. (2013). A Review on Nanomaterial Dispersion, Microstructure, and Mechanical Properties of Carbon Nanotube

and Nanofiber Reinforced Cementitious Composites. *Journal of Nanomaterials, 2013*, 1-19. doi:Artn 71017510.1155/2013/710175

Passuello, A., Moriconi, G., & Shah, S. P. (2009). Cracking behavior of concrete with shrinkage reducing admixtures and PVA fibers. *Cement and Concrete Composites, 31*(10), 699-704.

Pattanayak, A., & Jana, S. C. (2005). Properties of bulk-polymerized thermoplastic polyurethane nanocomposites. *Polymer, 46*(10), 3394-3406. doi:http://dx.doi.org/10.1016/j.polymer.2005.03.021

Peev, P. I. (2012). Is industrial hemp a sustainable construction material? *Bachelor of Architectural Technology and Construction Management, Via University College, Horsens, Denmark*.

Peled, A., Bentur, A., & Yankelevsky, D. (1999). Flexural Performance of Cementitious Composites Reinforced with Woven Fabrics. *Journal of Materials in Civil Engineering, 11*(4), 325-330. doi:10.1061/(ASCE)0899-1561(1999)11:4(325)

Peponi, L., Puglia, D., Torre, L., Valentini, L., & Kenny, J. M. (2014). Processing of nanostructured polymers and advanced polymeric based nanocomposites. *Materials Science and Engineering: R: Reports, 85*, 1-46. doi:http://dx.doi.org/10.1016/j.mser.2014.08.002

Pizzatto, L., Lizot, A., Fiorio, R., Amorim, C. L., Machado, G., Giovanela, M., . . . Crespo, J. S. (2009). Synthesis and characterization of thermoplastic polyurethane/nanoclay composites. *Materials Science and Engineering: C, 29*(2), 474-478. doi:http://dx.doi.org/10.1016/j.msec.2008.08.035

Ponni, M., & Baskar, R. (2015). A study on indoor temperature and comfort temperature. *International Journal of Engineering and Science Invention, 4*, 7-14.

Potts, J. R., Dreyer, D. R., Bielawski, C. W., & Ruoff, R. S. (2011). Graphene-based polymer nanocomposites. *Polymer, 52*(1), 5-25. doi:http://dx.doi.org/10.1016/j.polymer.2010.11.042

Pourrahimi, A. M., Liu, D., Ström, V., Hedenqvist, M., Olsson, R. T., & Gedde, U. W. (2015). Heat treatment of ZnO nanoparticles: new methods to achieve high-purity nanoparticles for high-voltage applications. *Journal of Materials Chemistry A, 3*(33), 17190-17200.

Qi, K., Chen, X., Liu, Y., Xin, J. H., Mak, C. L., & Daoud, W. A. (2007). Facile preparation of anatase/SiO2 spherical nanocomposites and their application in self-cleaning textiles. *Journal of Materials Chemistry, 17*(33), 3504-3508. doi:10.1039/B702887C

Qijie Xu1, Fangfei Chen1, Xiaohong Li1, & Zhang1, Z. (2013). The effect of surface functional groups of nanosilica on the properties of polamide 6 SiO2 nanocomposites. *Polish Journal of Chemical Technology,,, 15*(3), 20 — 24.

Quercia Bianchi, G., & J H Brouwers, H. (0002). *Application of nano-silica (nS) in concrete mixtures*.

Radhika Pavgi, Dr. Osman Ozbulut, & Daghash, S. (2015). MECHANICAL AND ELECTRICAL PROPERTIES OF GRAPHENE NANOPLATELET REINFORCED CEMENTITIOUS COMPOSITES.

Rafał Poręba1, Milena Špírková, & Hrdlička, Z. (2011). Mechanical and thermomechanical properties of polycarbonate based polyurethane silica nanocomposites. *Processing and Application of Ceramics composites, 5*(3), 155–159.

References

Raheel, M., Yao, K., Gong, J., Chen, X.-c., Liu, D.-t., Lin, Y.-c., . . . Tang, T. (2015). Poly(vinyl alcohol)/GO-MMT nanocomposites: Preparation, structure and properties. *Chinese Journal of Polymer Science, 33*(2), 329-338. doi:10.1007/s10118-015-1586-2

Rai, S., & Tiwari, S. (2018). Nano Silica in Cement Hydration. *Materials Today: Proceedings, 5*(3, Part 1), 9196-9202. doi:https://doi.org/10.1016/j.matpr.2017.10.044

Raju, B. N., Ramji, K., & Prasad, V. S. R. K. (2015). Mechanical Properties of Glass Fiber Reinforced Polyester ZnO NanoComposites. *Materials Today-Proceedings, 2*(4-5), 2817-2825. doi:10.1016/j.matpr.2015.07.294

Ranjbar, N., Mehrali, M., Mehrali, M., Alengaram, U. J., & Jumaat, M. Z. (2015). Graphene nanoplatelet-fly ash based geopolymer composites. *Cement and Concrete Research, 76*, 222-231. doi:10.1016/j.cemconres.2015.06.003

Rauwendaal, C. (2002). New directions for extrusion: compounding with single screw extruders. *Plastics, Additives and Compounding, 4*(6), 24-27. doi:http://dx.doi.org/10.1016/S1464-391X(02)80090-3

Rhydwen, R. (2015). Building with Hempand Lime *MSE architecture*.

Rifkin, J. (2011). *The third industrial revolution: how lateral power is transforming energy, the economy, and the world*: Macmillan.

Rollins, A., Collet, P., & Andres, V. (2018). *Concrete Porosity Reduction by Colloidal Silica Nano Technology*.

Roth, L. (2014). Glas Fibre reinforced Polyvinyle Acetate. *Educational programmes.* Retrieved from http://www.iaacblog.com/programs/glass-fiber-reinforced-polyvinyl-acetate-2/

Saba, N., Tahir, P. M., & Jawaid, M. (2014). A review on potentiality of nano filler/natural fiber filled polymer hybrid composites. *Polymers, 6*(8), 2247-2273.

Saberian, M., Jahandari, S., Li, J., & Zivari, F. (2017). Effect of curing, capillary action, and groundwater level increment on geotechnical properties of lime concrete: Experimental and prediction studies. *Journal of Rock Mechanics and Geotechnical Engineering, 9*(4), 638-647. doi:10.1016/j.jrmge.2017.01.004

Sanchez, F., & Sobolev, K. (2010). Nanotechnology in concrete – A review. *Construction and Building Materials, 24*(11), 2060-2071. doi:http://dx.doi.org/10.1016/j.conbuildmat.2010.03.014

Saraya, M. (2010). *Stopping of cement hydration by various methods* (Vol. 6).

Sarika, S. P., Rao S., Sekhar, S. T., & Apparao.G. (2013). Studies on Relationship Between Water Binder Ratio And compressive strength. *American Journal of Engineering Research (AJER), 02*(08), 115-122.

Saxena, A. (2013). *Nanocomposites based on nanocellulose whiskers.* (PhD), Georgia Institute of Technology,

Scarfato, P., Di Maio, L., Fariello, M. L., Russo, P., & Incarnato, L. (2012). Preparation and evaluation of polymer/clay nanocomposite surface treatments for concrete durability enhancement. *Cement and Concrete Composites, 34*(3), 297-305. doi:http://dx.doi.org/10.1016/j.cemconcomp.2011.11.006

Scheer, A. M., & Hoppner, C. (2010). The public consultation to the UK Climate Change Act 2008: a critical analysis. *Climate Policy, 10*(3), 261-276. doi:10.3763/cpol.2009.0029

References

Schuster, M. B., Becker, D., & Coelho, L. A. F. (2015). The processing of polycarbonate nanocomposites generated with various nanofillers. 87-101. doi:10.1016/b978-1-78242-308-9.00005-7

Sedaghat, A., Ram, M. K., Zayed, A., Kamal, R., & Shanahan, N. (2014). Investigation of Physical Properties of Graphene-Cement Composite for Structural Applications. *Open Journal of Composite Materials, 04*(01), 12-21. doi:10.4236/ojcm.2014.41002

Sen, P., Suresh, K., Vinoth Kumar, R., Kumar, M., & Pugazhenthi, G. (2016). A simple solvent blending coupled sonication technique for synthesis of polystyrene (PS)/multi-walled carbon nanotube (MWCNT) nanocomposites: Effect of modified MWCNT content. *Journal of Science: Advanced Materials and Devices, 1*(3), 311-323. doi:https://doi.org/10.1016/j.jsamd.2016.06.016

Shahzad, A. (2013). A Study in Physical and Mechanical Properties of Hemp Fibres. *Advances in Materials Science and Engineering, 2013*, 1-9. doi:10.1155/2013/325085

Sharma, B., Chhibber, R., & Mehta, R. (2016). Effect of surface treatment of nanoclay on the mechanical properties of epoxy/glass fiber/clay nanocomposites. *Composite Interfaces, 23*(7), 623-640. doi:10.1080/09276440.2016.1165522

Shenoy, V., Joshi, S., & Dange, M. (2019). *Effect of Nanocellulose as an Additive in Cement*. Paper presented at the Proceedings of the Fourth International Conference in Ocean Engineering (ICOE2018).

Shrinkage of concrete. (2018). Retrieved from http://keu92.org/uploads/Search%20engineering/Shrinkage%20of%20concrete.pdf.

Shuai, C., Liu, T., Gao, C., Feng, P., Xiao, T., Yu, K., & Peng, S. (2016). Mechanical and structural characterization of diopside scaffolds reinforced with graphene. *Journal of Alloys and Compounds, 655*, 86-92. doi:http://dx.doi.org/10.1016/j.jallcom.2015.09.134

Sičáková, A. (2015). Basics of Building Materials. 1-127.

Sikora, P., Horszczaruk, E., Skoczylas, K., & Rucińska, T. (2017). *Thermal properties of cement mortars containing waste glass aggregate and nanosilica*.

Singh, A. K., & Prakash, R. (2014). Effect of Organoclay on Compatibilization, Thermal and Mechanical Properties of Polycarbonate/Polystyrene Blends.

Singh, A. P. a., & Tiwari, A. (2017). Effect of Zinc Oxide Nanoparticle on Compressive strength and durability of cement mortar. *International Journal for Research in Applied Science & Engineering Technology (IJRASET), 45.98*(VII, July 2017), 1668-1674.

Singh, M., & Garg, M. (1992). Glass fibre reinforced water-resistant gypsum-based composites. *Cement and Concrete Composites, 14*(1), 23-32. doi:https://doi.org/10.1016/0958-9465(92)90036-U

Singh, T. (2012). Venger Wind Unveils World's Largest Rooftop Wind Farm in Oklahoma City. *environment*. Retrieved from https://inhabitat.com/venger-wind-unveils-worlds-largest-rooftop-wind-farm-in-oklahoma-city/

Sinha Ray, S. (2013). Environmentally friendly nanofillers as reinforcements for composites. In *Environmentally Friendly Polymer Nanocomposites* (pp. 41-73): Woodhead Publishing.

References

Siró, I., & Plackett, D. (2010). Microfibrillated cellulose and new nanocomposite materials: a review. *Cellulose, 17*(3), 459-494. doi:10.1007/s10570-010-9405-y

Slosarczyk, A., & Krawczyk, P. (2016). Influence of expanded graphite coming from the electrochemical oxidation of phenol on cement-polymer matrix. *Polish Journal of Chemical Technology, 18*(4), 5-8. doi:10.1515/pjct-2016-0063

Soundararajah, Q. Y., Karunaratne, B. S. B., & Rajapakse, R. M. G. (2009). Mechanical Properties of Poly(vinyl alcohol) Montmorillonite Nanocomposites. *Journal of Composite Materials, 44*(3), 303-311. doi:10.1177/0021998309347040

Souza Aguiar, A., Tanomaru, J., Faria, G., Leonardo, R., & Tanomaru-Filho, M. (2015). *Antimicrobial Activity and pH of Calcium Hydroxide and Zinc Oxide Nanoparticles Intracanal Medication and Association with Chlorhexidine* (Vol. 16).

Spitalsky, Z., Tasis, D., Papagelis, K., & Galiotis, C. (2010). Carbon nanotube–polymer composites: Chemistry, processing, mechanical and electrical properties. *Progress in Polymer Science, 35*(3), 357-401. doi:10.1016/j.progpolymsci.2009.09.003

Stacy, S. C., Zhang, X., Pantoya, M., & Weeks, B. (2014). The effects of density on thermal conductivity and absorption coefficient for consolidated aluminum nanoparticles. *International Journal of Heat and Mass Transfer, 73*, 595-599. doi:http://dx.doi.org/10.1016/j.ijheatmasstransfer.2014.02.050

Stevulova, N., Cigasova, J., Schwarzova, I., Sicakova, A., & Junak, J. (2018). Sustainable Bio-Aggregate-Based Composites Containing Hemp Hurds and Alternative Binder. *Buildings, 8*(2), 25.

Stevulova, N., Kidalova, L., Cigasova, J., Junak, J., Sicakova, A., & Terpakova, E. (2013). Lightweight Composites Containing Hemp Hurds. *Procedia Engineering, 65*, 69-74. doi:https://doi.org/10.1016/j.proeng.2013.09.013

Stevulova, N., & Schwarzova, I. (2014). Changes in the properties of composites caused by chemical treatment of hemp hurds. *Int. J. Chem. Nucl. Metall. Mater. Eng, 8*(5), 409-413.

Suhara Panthapulakkal, & Sain, M. (2013). Isolation of Nano Fibres from Hemp and Flax and Their Thermoplastic Composites. *Plastic and Polymer Technology, 2*(1).

Suzuki, K., Sato, A., Okumura, H., Hashimoto, T., Nakagaito, A. N., & Yano, H. (2013). Novel high-strength, micro fibrillated cellulose-reinforced polypropylene composites using a cationic polymer as compatibilizer. *Cellulose, 21*(1), 507-518. doi:10.1007/s10570-013-0143-9

Swan, C. w., & and Bonora, A. M. (2017). *Compressive, flexural and tensile strength of various mortar mixex containing synthetic lightweght aggregate*. Paper presented at the 2017 World of Cool Ash, Lexington, KY. HTTP://WWW.flyash.info/

Tahereh Ghaffari, Ali Barzegar, Fahimeh Hamedi Rad, & Moslehifard, a. E. (2016). Effect of Nanoclay on Thermal Conductivity and Flexural Strength of Polymethyl Methacrylate Acrylic Resin. *J Dent Shiraz Univ Med Sci., 2016 June, 17(2)*, 121-127.

Tanpichai, S., Sampson, W. W., & Eichhorn, S. J. (2013). *Microfibrillated cellulose reinforced poly (vinyl alcohol) composites.* Paper presented at the Advanced Materials Research.

References

Tassew, S. T., & Lubell, A. S. (2014). Mechanical properties of glass fiber reinforced ceramic concrete. *Construction and Building Materials, 51*, 215-224. doi:https://doi.org/10.1016/j.conbuildmat.2013.10.046

Tavassoli Hojati, S., Alaghemand, H., Hamze, F., Ahmadian Babaki, F., Rajab-Nia, R., Rezvani, M. B., . . . Atai, M. (2013). Antibacterial, physical and mechanical properties of flowable resin composites containing zinc oxide nanoparticles. *Dental Materials, 29*(5), 495-505. doi:https://doi.org/10.1016/j.dental.2013.03.011

Thomas, J. A. G. (1972). Fibre composites as construction materials. *Composites, 3*(2), 62-64. doi:https://doi.org/10.1016/0010-4361(72)90376-X

Tran, L. Q. N., Fuentes, C. A., Dupont-Gillain, C., Van Vuure, A. W., & Verpoest, I. (2013). Understanding the interfacial compatibility and adhesion of natural coir fibre thermoplastic composites. *Composites Science and Technology, 80*, 23-30. doi:https://doi.org/10.1016/j.compscitech.2013.03.004

Turner, L. K., & Collins, F. G. (2013). Carbon dioxide equivalent (CO2-e) emissions: A comparison between geopolymer and OPC cement concrete. *Construction and Building Materials, 43*, 125-130. doi:https://doi.org/10.1016/j.conbuildmat.2013.01.023

Ulbikas, J. (2017). Solar facades of any shape and color. *Glass on web*. Retrieved from https://www.glassonweb.com/news/solar-facades-any-shape-and-color, http://www.smartflex-solarfacades.eu/fileadmin/user_upload/download-seite/SmartFlex-Broschuere.pdf

Umeda, T., Hashimoto, K., Satou, K., Furukawa, H., & Nishi, Y. (1994).

Venkatesan, S., Ngo, E., Khatiwada, D., Zhang, C., & Qiao, Q. (2015). Enhanced Lifetime of Polymer Solar Cells by Surface Passivation of Metal Oxide Buffer Layers. *ACS Applied Materials & Interfaces, 7*(29), 16093-16100. doi:10.1021/acsami.5b04687

Walker, R., & Pavía, S. (2014). Moisture transfer and thermal properties of hemp–lime concretes. *Construction and Building Materials, 64*, 270-276. doi:10.1016/j.conbuildmat.2014.04.081

Wang, P., Zhang, J., Dong, L., Sun, C., Zhao, X., Ruan, Y., & Lu, H. (2017). Interlayer Polymerization in Chemically Expanded Graphite for Preparation of Highly Conductive, Mechanically Strong Polymer Composites. *Chemistry of Materials, 29*(8), 3412-3422. doi:10.1021/acs.chemmater.6b04734

Wang, R. H., Xin, J. H., & Tao, X. M. (2005). UV-Blocking Property of Dumbbell-Shaped ZnO Crystallites on Cotton Fabrics. *Inorganic Chemistry, 44*(11), 3926-3930. doi:10.1021/ic0503176

Wang, W. C. (2017). Compressive strength and thermal conductivity of concrete with nanoclay under Various High-Temperatures. *Construction and Building Materials, 147*, 305-311. doi:10.1016/j.conbuildmat.2017.04.141

Wikimedia. (2017). Hemp shives.jpg. Retrieved from https://commons.wikimedia.org/w/index.php?title=File:Hemp_shives.jpg&oldid=256091207

Yan, S., He, P., Jia, D., Yang, Z., Duan, X., Wang, S., & Zhou, Y. (2015). In situ fabrication and characterization of graphene/geopolymer composites. *Ceramics International, 41*(9, Part A), 11242-11250. doi:http://dx.doi.org/10.1016/j.ceramint.2015.05.075

Yan, S., He, P., Jia, D., Yang, Z., Duan, X., Wang, S., & Zhou, Y. (2016). Effect of reduced graphene oxide content on the microstructure and mechanical

properties of graphene–geopolymer nanocomposites. *Ceramics International, 42*(1, Part A), 752-758. doi:http://dx.doi.org/10.1016/j.ceramint.2015.08.176

Yehia, S., A Khattab, E., S Khalil, I., & El-Baky, S. (2013). Effect of Nano-Clay on The Mechanical Properties of Fresh and Hardened Cement Mortar Comparing with Nano-Silica.

Yoon, P. J., Hunter, D. L., & Paul, D. R. (2003). Polycarbonate nanocomposites: Part 2. Degradation and color formation. *Polymer, 44*(18), 5341-5354. doi:http://dx.doi.org/10.1016/S0032-3861(03)00523-8

Yu, M., Gu, G., Meng, W.-D., & Qing, F.-L. (2007). Superhydrophobic cotton fabric coating based on a complex layer of silica nanoparticles and perfluorooctylated quaternary ammonium silane coupling agent. *Applied Surface Science, 253*(7), 3669-3673. doi:http://dx.doi.org/10.1016/j.apsusc.2006.07.086

Yusak, M., Ibrahim, M., Putra Jaya, R., Hainin, M. R., Ibrahim, W., & Haziman, M. (2014). A review of microstructure properties of porous concrete pavement incorporating nano silica.

Z. Duan, and, N. L. T., & Huang, W. (2013). Water vapour permeability of polylactic acid nanocomposites. *membrane science, 445*, 112-118.

Zaman, A., Gutub, S. A., & Wafa, M. A. (2013). A review on FRP composites applications and durability concerns in the construction sector. *Journal of Reinforced Plastics and Composites, 32*(24), 1966-1988. doi:10.1177/0731684413492868

Zara, M. (2016). What is wood glue made of and how is it made? *Glue and Adhesives*. Retrieved from https://www.quora.com/What-is-wood-glue-made-of-and-how-is-it-made

Zeng, Q., Li, K., Fen-chong, T., & Dangla, P. (2012). Pore structure characterization of cement pastes blended with high-volume fly-ash. *Cement and Concrete Research, 42*(1), 194-204. doi:http://dx.doi.org/10.1016/j.cemconres.2011.09.012

Zhang, B., Tian, Y., Jin, X., Lo, T., & Cui, H. (2018). Thermal and mechanical properties of expanded graphite/paraffin gypsum-based composite material reinforced by carbon fiber. *Materials, 11*(11), 2205.

Zhang, J., Hong, S., Dong, B., Tang, L., Lin, C., Liu, Z., & Xing, F. (2019). Water distribution modelling of capillary absorption in cementitious materials. *Construction and Building Materials, 216*, 468-475. doi:https://doi.org/10.1016/j.conbuildmat.2019.05.023

Zhang, M.-h., Jiang, M.-q., & Chen, J.-k. (2008). Variation of flexural strength of cement mortar attacked by sulfate ions. *Engineering Fracture Mechanics, 75*(17), 4948-4957. doi:10.1016/j.engfracmech.2008.06.023

Zhao, H., Xiao, Q., Huang, D., & Zhang, S. (2014). Influence of pore structure on compressive strength of cement mortar. *ScientificWorldJournal, 2014*, 247058. doi:10.1155/2014/247058

Zhao, R., & Sanjayan, J. (2009). Test method for concrete spalling using small electric furnace. *Fire and Materials, 34*, 189-201. doi:10.1002/fam.1020

Zhao, Y., Yan, Y., Kumar, A., Wang, H., Porter, W. D., & Priya, S. (2012). Thermal conductivity of self-assembled nano-structured ZnO bulk ceramics. *Journal of Applied Physics, 112*(3), 034313.

Zhou, R.-J., & Burkhart, T. (2010). Mechanical and optical properties of nanosilica-filled polycarbonate composites. *Journal of Thermoplastic Composite Materials, 23*(4), 487-500.

References

Zhou, R. J., & Burkhart, T. (2009). Mechanical and Optical Properties of Nanosilica-filled Polycarbonate Composites. *Journal of Thermoplastic Composite Materials, 23*(4), 487-500. doi:10.1177/0892705709353720

Zhou, R. J., & Burkhart, T. (2010). Mechanical and Optical Properties of Nanosilica-filled Polycarbonate Composites. *Journal of Thermoplastic Composite Materials, 23*(4), 487-500. doi:10.1177/0892705709353720

Zhu, A., Cai, A., Zhou, W., & Shi, Z. (2008). Effect of flexibility of grafted polymer on the morphology and property of nanosilica/PVC composites. *Applied Surface Science, 254*(13), 3745-3752. doi:http://dx.doi.org/10.1016/j.apsusc.2007.11.042

Chapter 9 - **Appendix**

9.1 Introduction

This Appendix is for definitions, terms and tables which are no necessary to be in the context of the research.

9.2 Terminology

Many terms are encountered in the literature studies and the following is an attempt to give a simple definition for the terms that may be repeated in the literature review.

9.2.1 Composite

Two or more materials that can be considered as composite materials that have beneficial chemical and physical properties when connected together, an example is cement with fillers such as the fibre glass or carbon fibres, silica fly ash etc. (Schuster, Becker, & Coelho, 2015; Zaman et al., 2013). The fibres (woven and non-woven) reinforced polymer composites (FRPC) are used in advanced applications such as automotive, civil structure, aeroplanes and military applications. These advanced applications use fibres such as carbon or glass fibres, which are added to reinforce polymers to achieve the required polymer fibre reinforcement composite (OkenWa O. I. Okoli, Tallahassee, Myungsoo Kim, & Tallahassee, 2010).

9.2.2 Biomass Composite

The main materials are called the matrix and biomass blended with fillers. It is bio-based consisting of one or more material or fibre (H. Assaedi, F. U. A. Shaikh, & Low, 2015a; A. Hakamy, F. U. A. Shaikh, & I. M. Low, 2015; Peponi, Puglia, Torre, Valentini, & Kenny, 2014).

9.2.3 Nanomaterials

Materials at the nanosize level are made by applying one of two main methods: top-down or bottom-up which decompose or divide the original materials to make small pieces in the nanoscale, one dimension or more, or assemble the materials at the

atom scale to nanostructure. There is another new definition that depends on the volume or the specific surface area (VSSA). Nanomaterial is defined as a material that has VSSA value 60 m^2/ cm^3 or more (Kreyling, Semmler-Behnke, & Chaudhry, 2010).

Nanomaterials are used for enhancing mechanical properties like flexural, compressive or tensile strength in some matrices like cement or polymers. Another choice involves nanozinc oxide which is mainly used for Ultra Violet resistance and at the same time as a heat isolator when used as a coating, but it was found from lab tests in the present project that it decreased the porosity more than any other nanomaterial used.

9.2.4 Bio-nano-Composite

The main matrix is a biomass or a natural material such as lime and the fillers (natural fibres and shives or nanocellulose) are biomass blended with one or more nanomaterials like $nSiO_2$, nClay, nZnO, etc. (Fernandes, Pires, Mano, & Reis, 2013; Ojijo & Sinha Ray, 2013).

9.2.5 Dispersion

Dispersion means a homogeneous distribution of the nanoparticles in the matrix but it can be called bad dispersion when the particles are assembled as conglomerates, or in other words, in microscale not in nanoscale and the factors affecting the dispersion are the aspect volume ratios of particles; the ratio between the shortest dimension and the longest dimension of the particles. The second factor involves the interaction of the large surface area of the particle between the particles themselves and in the other direction between the nanoparticles and the polymer (Gauvin & Robert, 2015; Jancar et al., 2010; Nguyen, Rouxel, & Vincent, 2014; Ojijo & Sinha Ray, 2013)

9.2.5.1 Method of Dispersion

There are many methods to achieve dispersion for the nanofiller in the matrix, then are summarised as follows.

9.2.5.2 Melt Mixing

Melt mixing is done by a compounding extruder especially for polymer matrices. This has a single or two screws that are rotated in any required revolution/min within certain limits and with different heat degrees as the matrix melting point of the polymer and the nanofillers are fed through the extruding process (Rauwendaal, 2002).

9.2.5.3 Solution Mixing

The second method is solution mixing by a solvent to dissolve the matrix; the nanofillers are suspended in the solvent and mixed with the polymer by various methods such as stirring of the polymer using a magnetic heating plate with different heat degrees and different revolution / minute and a PTEF stirrer is put inside the mixture to circulate the components according to the need of the polymer and fillers for heating and circulating to gain homogeneous dispersion.

9.2.5.4 Dispersion by Mixer

Dispersion is achieved for some matrices by using a mixer for lime or cement matrix with water solvent (Jancar et al., 2010; Z. Ji et al., 2010; Sen, Suresh, Vinoth Kumar, Kumar, & Pugazhenthi, 2016).

9.2.5.5 Dispersion of Nanomaterials

In the Cement Matrix, a study on cement blended with carbon nanotube and nanofibres mentioned that the major factors that strongly influence the properties of nanocomposites is the dispersion of nanomaterials such as CNTs and CNFs. Due to presence of attractive forces (Van der Waals) of these nanomaterials, they have a strong tendency to agglomerate and this belongs to the polarizable of their electron

systems. It is very difficult to disperse or infiltrate the agglomerates with matrices, and it represents the source of probable defects in nanocomposites. Dispersion is the method of decomposition of the agglomerates and distribution of nanomaterials within matrices or solvents (Parveen et al., 2013).

9.3 Compatibility

Compatibility is the ability of the matrix material to mix with another one or more matrices, fillers or nanofillers without the separation or segregation of some of the components (Alemán et al., 2007). Compatibility is mostly related to the reaction routes like the acyl chloride route which shows compatibility with certain polymers. Adding a coupling agent is a good method to achieve compatibility in addition to the physical and chemical methods. For example wood fibre surfaces are usually treated by physical or chemical methods to improve the quality of surfaces, or by adding a coupling agent to improve interfacial compatibility (Dang, Song, Wang, & Wang, 2008; Tran, Fuentes, Dupont-Gillain, Van Vuure, & Verpoest, 2013).

Appendix A

Table 9.1 Summary of Matrices, Filler processing and Property Enhancement.

No	Matrix	Filler	Improved property	Processing	Ref
1	PVA polyvinyl alcohol	< wt.1% CNT	3.7, 4.3 and 1.7 times modulus of elasticity, tensile strength and toughness was improved	Solution in water	(J. N Coleman et al., 2004)
2	PP poly-propylene	< wt. 1% CNT	3.1, 3.9 and 4.4 times modulus of elasticity, tensile strength and toughness improved	Chlorinated solution	(J. N Coleman et al., 2004)
3	Film or aramid and CNT layer by layer	CNT+ ANF Aramid nanofibers (the nanoscale version of polyparaphenylene terephthal amide)	Tensile strength =361.2 MPa increased 101.7% E=34.4GPa increased 170.8%	Solution DMSO / KOH layer by layer assembly	[(Jiaqi Zhu, 2015)
4	PC	5wt% CNT	Tensile strength 43 MPa for neat PC and 63.9 for nanocomposite	Melt extrusion and by solution	(Fornes, Baur, Sabba, & Thomas, 2006)
5	PC	1-2 wt. % CNT	10% increase in tensile strength.	Solution by chloroform and the CNT modified by stirring in vacuum with plasma	(Y. Gao et al., 2006)
6	Polylactic acid PLA	5wt% MCC Microcrystalline cellulose	12% tensile strength increase		(Bandyopadhyay-Ghosh et al., 2015b)
7	Wood pulp-based	5wt% MFC micro-fibrillated cellulose degree of fibrillation 30 passes	300 MPa tensile strength	Solution	(Saxena, 2013)
8	PP Polypropylene	30wt% MFC	60% tensile strength higher than neat PP	Twin screw extruder	(Suzuki et al., 2013)
9	Xylan from	Aqueous suspension of	141% tensile strength increase	Solution + Deionized	(Saxena, 2013)

Appendix A

Table 9.1 Summary of Matrices, Filler processing and Property Enhancement.

No	Matrix	Filler	Improved property	Processing	Ref
	Oat spelt	sulfonated whisker		water and stirring 95ºC 15 min. and dried in room temp.	
10	PVA polyvinyl alcohol	5wt%MCC ultrasonic treated	50% tensile strength increase	Aqueous solution stirring 500/min 80ºC 3hrs	(Denis Mihaela Panaitescu et al., 2011)
11	Hydroxy-propyl cellulose HPC as a matrix	5wt% Micro-cellulose fibres 20µm to prepare nano-fibrillated cellulose	57.4% tensile strength of comp. film higher than 1wt% loading and 52.2%higher than neat HPC film	Solution aqueous and high pressure homogenizer	(S.-Y. Lee, Chun, Kang, & Park, 2009)
12	PF	2.2wt% BC Bacterial cellulose	Tensile strength. improved to 370 MPa	Solution by methanol several layers	(A. N. Nakagaito et al., 2004; Oksman et al., 2016)
13	PCL polycaprolactone	5wt% CNC Cellulose nanocrystal	Tensile strength improved from 185 MPa to 220 MPa	Melt mix by twin screw extruder	(Mi et al., 2014)
14	Amylopectin Glycerol	70WT% MFC micro-fibrillated cellulose	Tensile strength improved from 2MPa to 130 MPa	Solution in deionized water and stirring	(Anna J. Svagan, My A. S. Azizi Samir, & Berglund, 2007)
15	PC	4vol.% nSiO2	Stiffness and toughness were improved	Direct melt compounding Brabender mixer and then compression moulded	(Zhou & Burkhart, 2009)
16	Epoxy	49vol% BC bacterial cellulose	Tensile strength improved to 102 MPa	Solution	(K.-Y. Lee, Aitomäki, Berglund, Oksman, & Bismarck, 2014)
17	HPE high	MWNT Multi wall carbon	Tensile strength from <50 MPa to	Hot drawing 60-70 ratio	(Jonathan N. Coleman,

Appendix A

Table 9.1 Summary of Matrices, Filler processing and Property Enhancement.

No	Matrix	Filler	Improved property	Processing	Ref
	density polyethylene	nanotubes	150MPa		Khan, Blau, & Gun'ko, 2006)
18	PVA	0.8wt% SWNT hydroxyl functionalize	Tensile strength improved 70MPa to 107MPa	Solution	(L. Liu, Barber, Nuriel, & Wagner, 2005)
19	PC	0.11wt% MWNT	Thermal conductivity increased	Melt mixing and hot press moulded	(Khatua, Maiti, Shrivastava, & Suin, 2013)
20	PC	0.5wt%nZnO	0.5% Highly improved in tensile strength and decrease at 1wt%	By miller the dry mix 18000rpm injection moulded at 280°C	(Carrion et al., 2007)
21	PC	5wt% AL2O3 mixed by hand with PC pellets alumina before grafted with coupling agent	Transparency at (1-2)wt. %alumina	Compounding with alumina 5000 rpm 249ºC for 30-45 s the molten press into plates before mix alumina sonicated with THF	(Chandra, Turng, Gopalan, Rowell, & Gong, 2008)
22	PC	Functionalize Alumina nano-whisker with PC	Tensile strength enhanced from 32MPa to 66MPa and E. Good transparency no effect decrease	Polymerization in situ	(Hakimelahi, Hu, Rupp, & Coleman, 2010)
23	PC	0.5WT%TiO2	Impact 85 on Izod test 91.4% whiteness	Solution resin in situ polymerization	(Umeda, Hashimoto, Satou, Furukawa, & Nishi, 1994)
24	PC	2vol% nSiO2	Hardness shore D improved from 521N neat PC to 1330 N nanocomposite	Melt processing by mixer 60rpm, 240°C for 30 min. compress moulding sheets	(Luyt et al., 2010)

Appendix A

Table 9.1 Summary of Matrices, Filler processing and Property Enhancement.

No	Matrix	Filler	Improved property	Processing	Ref
25	PC	nSiO2 sol gel	270% increase E, 25% hardness, 20% fracture toughness excellent barrier	Sol gel processing	(Asuka & Sigmund, 2009)
26	PC	10% MFC	Modulus of elasticity enhanced 100% tensile strength 24% by layers on PC and layers of MFC	Solving of MFC and making film layer of MFC then by hot press on pc	(Panthapulakkal & Sain, 2012a)
27	PC	4wt% nSiO2 aerogel	Tensile strength from neat PC 63.41 MPa to 66.14 comp. Stiffness and toughness 43% improved, transmission didn't change	Melt mix compounding	(R. J. Zhou & T. Burkhart, 2010)
28	PC	5wt% nSiO2 modified MPS methacryloxyr-opyl tri-metho-xysilane	Hardness neat PC= B pencil hardness PC/5wt% nSiO2/ MPS=HB	Solution method by THF solvent separately and mixed, dried and then by melt extruder	(Chau, Hsu, Chen, Yang, & Hsu, 2010)
29	PC	13% Hemp or Flax	Tensile strength PC/ Hemp fibres increase 1.7% and 2.7% PC/n Flax nano-cellulose to neat PC	Hot press film of nano-cellulose on sheet of polycarbonate between two steel plates 210ºC 800lb load	(Suhara Panthapulakkal & Sain, 2013)
30	PC	TiO2, TiO2 modified	5wt %TiO2, 5wt% TiO2 modified good clearance, adhesion 100% modified, 80% unmodified. Hardness pencil unmodified 5H, modified 6H UV protector 20 week test under radiation without losing their	By sol gel technique and spray coating dried at 130°C	(D.K. HWANG et al., 2003)

Appendix A

Table 9.1 Summary of Matrices, Filler processing and Property Enhancement.

No	Matrix	Filler	Improved property	Processing	Ref
			properties		
31	PC	CNT	1wt% tensile strength increased 20%,E 20% 0.5wt% MWNT/P3HT-G-PcL compatibilist and by solution blending tensile strength and modulus of elasticity (47, 46) % respectively.	By three methods: melt, solution and in situ + melt mixing	(Spitalsky, Tasis, Papagelis, & Galiotis, 2010)
32	PC/15wt% SMA styrene co-maleic anhydride	nClay(SFH) flurohectorite or C185 SFH [Optimimum mixing is 82wt%PC 10wt%SMA 0wt%SFH 8wt%C185 SFH or 5% after burning]	Thermal stability; HDT PC= 129ºC nClay=136ºC HDTPC/ nClay=116°C Tensile strength.PC = 91MPa for PC/ nClay = 111MPa	Melt mixing	(Mitsunaga, Ito, Ray, Okamoto, & Hironaka, 2003)
33	PC	nSiO2 or (PU+0.5wt%nClay 40)	Tensile strength.=36.5 MPa PC/nSiO2 50.9MPa (PU+0.5wt%nClay40)	Synthesis in situ	(Rafał Poręba1, Milena Špírková, & Hrdlička, 2011)
34	PC	0.02-0.03 wt. % (Na^+ MMT) with difference amine. Better improvement is for high Mw PC	Tensile strength PC neat= 50.9 MPa, PC/MMT (4.4-4.5) wt. %= 70.5MPa and 83.9MPa for PC/ 2.4wt. % MMT	Melt mixing twin screw extruder	(Yoon, Hunter, & Paul, 2003)
35	PC/PS polystyrene	Organoclay	Tensile strength neat PC=59.5 MPa, PS neat=36.5 MPa, PC/PS=61.5 MPa PC=PS=3wt%nClay=66.8 MPa , tensile strength decreased more than 3wt%	Melt mixing technique	(A. K. Singh & Prakash, 2014)
36	PU	MMT Montmorillonite	Tensile strength physical, thermal stability properties were improved	Melt processing	(Dan, Lee, Kim, Min, & Kim, 2006)

Appendix A

Table 9.1 Summary of Matrices, Filler processing and Property Enhancement.

No	Matrix	Filler	Improved property	Processing	Ref
37	PU water borne	nSiO2+3 aminpropyl-triethox-silane + HCl (for good compatibility with PU)	Thermal insulation is 0.05 w/ mK and light transmission is above 80%	Solution in methanol solvent	(Liao et al., 2012)
38	PU	3wt%nClay	110% modulus of elasticity increased 170% tensile strength increased and 110% tear strength increased if nClay is fully exfoliated	Solution method	(Jeon & Baek, 2010b; Pattanayak & Jana, 2005)
39	PU	5wt%nClay	Tensile strength increased and good thermal stability	Solution method	(Pattanayak & Jana, 2005)
41	PVC	nClay	Good for fire retardancy and thermal stability	Melt mixing by Brabender device	(Awad et al., 2009)
43	Polypropylene	nClay	Enhanced fire retardant and thermal stability by 20ºC	Melt mixing by Twin screw extruder	(Narender Kumar & Dahiya, 2013)
44	HDPE High density poly-ethyl	1wt% CNT+ 3wt%MMT	Tensile strength and flexural strength increased thermal stability, improved decomposition temp. increased from 382-431 at 20wt loss% dispersion of CNT due to MMT was very well and its larger aggregates were disappeared	Melt mix rotating Twin screw extruder	(M. E. Ali Mohsin, Agus Arsad, & Alothman, 2014)
45	TPU thermoplastic polyurethane	nClay (Cloisite®30B)	TPU3WT5nClay was the best improvement in tensile strength 28% increase and increase in tear strengths	Twin screw extruder and bulk polymerization of polysterpolyol and diphenylmethanedi-isosyanate with 1,4-butanediol	(Pizzatto et al., 2009)

Appendix A

Table 9.1 Summary of Matrices, Filler processing and Property Enhancement.

No	Matrix	Filler	Improved property	Processing	Ref
46	PU WATER BORNE	Silica hollow spheres treated by 3-amino-propyl-triethoxy-silane (KH55) and hydro-chloric acid	excellent thermal isolation 0.05 w/mk and light transmission above 80%	Solution mix ethanol solvent 1:1 with WPU emulsion. Then dried on glass sheet as a film after evaporation of ethanol and water	(Liao et al., 2012)
48	PC 1/8 pyridine	3wt%CNC1/4 PC	Mechanical properties was improved thermal stability was improved for PC coated CNC but decreasing in thermal stability due to degradation	Firstly, by dissolving with pyridine and water with magnetic stirring and precipitating and then diluted by melt extrusion	(Mariano, El Kissi, & Dufresne, 2015)
49	PC	18wt%CNC	T. modulus increased 100% tensile strength increased 30% Good thermal stability at high temp.	Fibre CNC press moulding 205°C sheets in between polycarbonate sheets	(Panthapulakkal & Sain, 2012a)
50	PC	nClay	Thermal stability controlled by surfactants and remarkable improvements of mechanical properties tensile strength from (91-116)MPa	Melt method	(Mitsunaga et al., 2003)
51	PU	2wt%nClay	Modulus of elasticity was improved but dimension stability was deteriorated	Solution mix foam	(Jahanmardi, Kangarlou, & Dibazar, 2013)
52	Geopolymer (cement)	3wt%very fine nano-silica 20nm and W/C 0.6	Porosity and permeability declined 33.3% and 99% respectively and	Cement with nanosilica dry mixed and then the	(Ershadi et al., 2011)

Appendix A

Table 9.1 Summary of Matrices, Filler processing and Property Enhancement.

No	Matrix	Filler	Improved property	Processing	Ref
			compressive strength jumped from 10.24 MPa to 26.21 MPa	water and admixture were added at propeller 4000 rpm	
53	Bis-GMA and TEGDMA	nSiO2 porous thermally sintered 12nm	Improvement in flexural modulus and fracture toughness.	The fume silica was sintered at different temperatures of 1200◦C, 1300◦C, and 1400◦C using an electric furnace 20°C/min. and then ground by ball mill passed 500 mesh ASTM sieve. The micro-filler and sintered nano-filler silanised with 1 and 3wt% γ-MPS prehydrolyzed 1hr in an aquious solution of 70wt% ethanol and 30wt% deionized water 3-4 PH adjusted by droplets of acetic acid	(Atai et al., 2012)
54	Geopolymer cement	nSiO2	Enhance resistance of chloride strength and durability	4wt% with water and mix with high speed	(Aggarwal et al., 2015)
55	Gepolymer cement and porous concrete	nSiO2	Strength enhancement, reduce Ca leaching, refine pore structure increase durability and accelerate hydration rate	Mixed by a propeller mixer	(Yusak et al., 2014)

Appendix A

Table 9.1 Summary of Matrices, Filler processing and Property Enhancement.

No	Matrix	Filler	Improved property	Processing	Ref
	pavement [(15-30)% of fine aggregates are removed] high permeability and weak strength				
56	Acrylonitrile butadiene rubber(NBR)	Nano-silica	Greatly increased in modulus of elasticity, tensile strength and thermal resistance also was increased	Solution by using liquid NBR polymer	(K.Rajkumar, Prem Ranjan, P.Thavamani, P.Jeyanthi, & P.Pazhanisamy, 2013)
57	Concrete substrates and plain resin separately	4wt% n Clay	1-Barrier as coating and sealer film on the surface of concrete such as polyurethane, acrylic and epoxy resin. 2-Pore liners that line concrete surface pores like silane, siloxane and fluorinated polymers 3-Pore blockers which penetrate concrete and block pores as liquid silicates and liquid silico-fluorides. These nanomaterials enhanced mechanical and barrier properties, thermal stability, fire retarding ability, wear resistance and others	By solution with solution polymers and solvents and water	(Scarfato et al., 2012)
58	Geopolymer	CNT, nTiO2, nAl2O3,	CNT, nSiO2, and copolymers reduced	Solution method	(Feldman, 2014)

Appendix A

Table 9.1 Summary of Matrices, Filler processing and Property Enhancement.

No	Matrix	Filler	Improved property	Processing	Ref
	cement	nSiO2and nClay with different copolymers based on acrylic acid, acrylic amide incorporating colloidal nano-silica PVA with MMT	porosity increased mechanical properties pollutant resisted and self-cleaning property (TiO2). Resistance to fungal effect Ca(OH)2 and ZnO/TiO2		
59	Starch and calcium carbonate	CNF50/50	The result of fracture of toughness ten time more the plain board	Solution method	(Bilodeau & Bousfield, 2015)
60	Fly ash based geopolymer	1wt% nSiO2 with or not with alkaline solutions	27% Flexural and 28% compression strength of geopolymer were enhanced	Dry mix and wet mixing but dry mix give better results	(H. Assaedi, F. U. A. Shaikh, & Low, 2015b)
61	Slag geopolymeric mortar with 6% NaOH as alkaline activation	0.1wt% MWCNT superplasticizer Gelenium Ace-30 was used (1.4-2.2)% at 40°C	Compression strength was enhanced and the water absorption value and drying shrinkage decreased	Solution mix (0.34-0.39)% w/binder	(Khater & Abd el Gawaad, 2016)
62	Geopolymer incinator fly ash 20wt%	Si/Al 1:3 ratio (1.8-1.9) and 1.0<Na/Al <1.29 ratio it can be(1.0) with Alkali activation it is available commercially as kaolinite for ceramic tiles industry	Compressive strength increases only for Si/Al ratio (1.15-1.9) the chemical stability is very high and low release of heavy metals	Alkaline solution by dissolving Sodium Hydroxide pellets in a Sodium silicate solution(SiO2/Na2O3:1) Gepolymer IFA was added to alkaline solution separately from meta-kaolin and the meta-kaolin was added with stirring and the paste	(Lancellotti et al., 2010)

Appendix A

Table 9.1 Summary of Matrices, Filler processing and Property Enhancement.

No	Matrix	Filler	Improved property	Processing	Ref
				poured into mould and the cast stays for 24 hrs at room temp and 24hrs at 50ºC	
63	Geopolymer (fly ash)	2wt%nClay (Cloisite30B) platelets	Mechanical properties were improved. The highest flexural increased 20% and compressive strength 23% also high flexural modulus and hardness at 2wt% and better thermal stability not only these but the porosity decreased and the resistance to water absorption was increased at last lower moisture content	Adding alkaline solution to fly ash Geopolymer ratio 0.75 Sodium silicate/Sodium Hydroxide =2.5. The materials were mixed in a Hobart mixer 10 min., low speed 10 min. high speed and adding nano-clay. The mix was poured in wooden mould under vibration 2 min. and covered by plastic film and 80°C in oven24 hrs	(Assaedi, Shaikh, & Low, 2016)
64	Geopolymer	rGO reduction of graphene oxide with alkaline solution. GO powder/ Geopolymeric slurry ratio was tested. rGO/ geopolymeric composite was prepared by adding meta-kaolin powders	Fracture toughness was increased 61.5% at 0.5wt% of rGO Maximum value is 17.9 MPa at rGO 0.3wt%. Flexural strength was improved	Silica solution with KOH 3days BY magnetic stirring to make Geopolymeric solution. GO powder dispersed by ultrasonic in distilled water 3hrs at the end 100 ml of GO solution was	(Yan et al., 2016)

Appendix A

Table 9.1 Summary of Matrices, Filler processing and Property Enhancement.

No	Matrix	Filler	Improved property	Processing	Ref
		and mixing 45 min using a high shear mixer and ultra-sonication		added to mol Geopolymeric solution and stirring 15 min. and obtain Rgo/ Geopolymeric mixture at 25º and meta-kaolin was added and mixed and casted in plastic mould cured at 60°C 7 days	
65	Cement	Polyethylene woven fabric 5,7, or 10 fills/cm and 22 warps /cm	Flexural strength was improved from about 9 MPa to 18MPa for fabrics and 20 for crimped yarns.	w/c=.3 of paste matrix with 8 layers of fabrics moulded at intensive vibration 21 days in water to test after demoulding for 1 day	(Peled, Bentur, & Yankelevsky, 1999)
67	Cement	GO Graphene Oxide	Accelerate the hydration rate of cement as a catalyst behaviour and enhance the intensity due to the oxygen containing which provides adsorption sites for water and cement and the water on GO constitute water reservoir and water transport channels for further hydration of cement. This means novel factor to promote the hydration of cement.	40g cement 120g sand 12g water and 4g polycarboxylate super plasticizer solution. GO was suspended in distilled water and sonicated 3hrs at last, the cement and sand were added	(Lin, Wei, & Hu, 2016)
68	Portland cement	(0.03wt %) Graphene (GO) **Graphene:** Is a one-atom thick, honeycomb like sheet	- Tensile strength 50% and comp. strength 46% was increased. -Porosity decreased from 32.8% plain	1-GO synthesized by modified Hummer's method (chemical	(Gong et al., 2014)

Appendix A

Table 9.1 Summary of Matrices, Filler processing and Property Enhancement.

No	Matrix	Filler	Improved property	Processing	Ref
		3-D conjugated system	cement to 28.2%. - Degree of Hydration increased: a- Non-evaporable water by 9%. b- Calcium hydroxide 6%.	oxidation) was diluted in distilled water 30min. using Branson digital sonicator (VCX 750, 750W, 30%Amplitude). ASTM TYPE1 (ASTM C 150) (ASTM 2012) were used. 2- The resultant stable GO (0.002) g/mol was diluted in further tap water to produce GO/cement composite w/c 0.5(GO/water) included and a high speed shear mixer (CTE 7000) used within ASTM C1738-11a,) (ASTM 2011). 3- The steps are the go solution in mixer at low speed (100-200) rpm 15 min. cement powder added 30 s then 4000rpm for 60 s. 4 - The mixer was stopped and the collected cement paste on the sides was scraped down. The mixer was operated	

Appendix A

Table 9.1 Summary of Matrices, Filler processing and Property Enhancement.

No	Matrix	Filler	Improved property	Processing	Ref
				12000 rpm for 30 s, and stopped 15 s, then operated 30 s.	
69	Cement	1.5wt% GO 0.5wt%Polycarboxylate as a superplasticiser for dispersion	Tensile strength 48% increase at 1.5wt% SEM Field emission scanning electron microscopy showed well dispersion and no aggregates observed. -Also showed growth of the (C-S-H) gel	1-G powder were oxidized to graphite oxide by modified Hummers method 1g G powder, 0.5g sodium nitrate, added to70 ml H_2SO_4 in an ice bath 3g $KMnO_4$ added gradually and stirred 2h then diluted in deionized water and re-dispersed in (DI) water and sonication (S450D, 35% amplitude). The mixture was filtered and washed with diluted HCl to remove metal ions. Finally washed with (DI) to remove the acid. 2-[1:3] C/S and w/c 0.4 c=146.86 g water=59.62g GO=2.2g sand=440.58 g additive=.73g Total=650g GO gradually added to water containing	(Babak et al., 2014; Leila Shahraiari & Athawale, 2014)

Appendix A

Table 9.1 Summary of Matrices, Filler processing and Property Enhancement.

No	Matrix	Filler	Improved property	Processing	Ref
				polycarboxylate ether PCE as super plasticizer in sonicated mixer 5 min after each addition to be 40 min. sonication total time, cement powder. Sonication (amplitude=50%, frequency=20Hz, power=500W, titanium alloy probe width 13 mm and constant applied energy=1900J/min.). cement added to dispersion GO and w/c 0.4 mixed 30s(rotary mixer)	
70	Cement	3wt%GO	Mechanical properties strongly increased, for example modulus of elasticity increased from 10 to 29 GPa. GO is enlarge microstructure of CSH.	reference is Portland cement water and sand in contrast cement with 3wt% GO. The steps are GO suspended in distilled water and sonicated 3h then cement was added w/c ratio still 0.6 at the end the sand was added, The mortar was placed on glass plate and the	(Horszczaruk, Mijowska, Kalenczuk, Aleksandrzak, & Mijowska, 2015)

Appendix A

Table 9.1 Summary of Matrices, Filler processing and Property Enhancement.

No	Matrix	Filler	Improved property	Processing	Ref
				ripening samples after they were stored in a humidity chamber at constant temperature of 20°C.	
71	Cement	GO 0.05wt%	Increases comp. str. 15-33% and Flexural strength. 41-59%	Dispersion by stirring, or lime saturated water followed by sonication is the best way than stirring and sometimes needs surface modification with sonication or stirring	(Chuah et al., 2014)
72	Geopolymer	rGO	Fracture toughness increased 61.5% rGO 0.5wt% and the flexural strength of Rgo/GP Geopolymer increased to 17.9MPa at 0.3wt%	The geopolymeric solutions were prepared by mixing silica sol with KOH for 3 d with the help of magnetic stirring. Dispersions were prepared ultrasonically dispersing GO powders in distilled water for 3 h. GO dispersion 100 mL was added to 1 mol geopolymeric solution and stir for 15 min to accomplish the simple in situ reduced process and obtain rGO/geopolymeric	(Yan et al., 2016)

Appendix A

Table 9.1 Summary of Matrices, Filler processing and Property Enhancement.

No	Matrix	Filler	Improved property	Processing	Ref
				mixture at 25°C. rGO/ geopolymer composite slurry was prepared by adding the meta-kaolin powders and mixing for 45min using a high-shear mixer and ultra-sonication. Finally, the slurry was cast into a plastic container and cured at 60 1C for 7 d.	
73	Fly ash based geopolymer	1%GNP-Graphene nano Platelets	Compressive and flexural stress were increased 44% and 116%	Alkali activator solution was prepared by mixing 16 M NaOH with theNa2SiO3 solution at a NaOH ratio of 2.5. The activator to binder ratio of 0.5 and additional water to fly ash ratio of 0.1weremaintained for all mixes. GNP fly ash based geopolymer composites were produced in two separate stages of preparation of the geo- polymer matrix and sonicated GNPs, which were ultimately	(Ranjbar, Mehrali, Mehrali, Alengaram, & Jumaat, 2015)

Appendix A

Table 9.1 Summary of Matrices, Filler processing and Property Enhancement.

No	Matrix	Filler	Improved property	Processing	Ref
				mixed together. The GNPs were sonicated in the mixing water with a geo-polymer using a Branson B3210 Ultrasonic for 5 mins to separate the bundles into individual flakes, producing a uniform suspension. Alkali activators were gradually added to the fly ash and mixed for 7 mins. The graphene suspension was added to the fresh geopolymer and mixed for 3 mins to produce a homogenous and workable mixture. The material was poured into moulds and vibrated for 30 s and maintained outside for 1 h. Afterward, the samples were maintained in a 65 °C oven for 24 h.	
74	Geopolymer	1wt% rGO	Fracture toughness improved 17%	The geopolymeric solution was prepared by mixing silica sol With	(Yan et al., 2015)

Appendix A

Table 9.1 Summary of Matrices, Filler processing and Property Enhancement.

No	Matrix	Filler	Improved property	Processing	Ref
				KOH for 3 days with magnetic stirring. GO powders (1000 mg) were ultrasonically dispersed in 60 mL of distilled water for 6 h. Then, the obtained GO solution was divided into 4 parts. Each part was added into 0.1 mol geopolymeric solution and stirred for 15 min to obtain the mixed solution, the mixture was cured at 60ºC (according to the best cured temperature of geopolymers) for 0.25, 3, 6 and 72 h. In this step, GO is reduced in situ. The obtained metakaolin powders were added to the GO/geopolymeric solutions and using both ultrasonic and mechanical stirrer mixed for 45 mins to get rGO /geopolymer slurry. The slurry was poured in a plastic container, removed pores in	

Appendix A

Table 9.1 Summary of Matrices, Filler processing and Property Enhancement.

No	Matrix	Filler	Improved property	Processing	Ref
				vacuum oven and cured at 60 1C for 7 days to realize the in situ synthesis of rGO/ geopolymer composites.	
75	Graphene-like(G-sepiolite) clay mineral sepolite is white rocks (Mg4Si6O15 (OH)2 6(H2O)) or Si12O30Mg8 (OH,F)4(H2 O)4·8H2O	This product grafted with Organo-alcoxy-silane	It is new approach preparing carbon clay nanocomposite	Sepiolite Si12O30Mg8 (OH,F)4(H2O)4·8H2O from Vallecas-Vicálvaro clay deposits (Madrid, Spain) commercially named Pangel S9. The present results show a new approach for the preparation of carbon–clay nanocomposites from natural and cheap resources such as sucrose and sepiolite. The process implied formation of intermediate caramel sepiolite nanocomposites. Resulting carbon sepiolite materials showed good electrical conductivity (around 10−2 Scm−1 at room temperature) and were directly used as	(Gómez-Avilés, Darder, Aranda, & Ruiz-Hitzky, 2010)

Appendix A

Table 9.1 Summary of Matrices, Filler processing and Property Enhancement.

No	Matrix	Filler	Improved property	Processing	Ref
				electrode of rechargeable lithium batteries without addition of conducting carbons The presence of sepiolite fibers in the nanocomposites instead of montmorillonite, also had the advantage to functionalize the nanocomposite by reaction with different organosilanes. In this way, new properties associated to the functional groups of the silanes can be designed.	
76	Diposide (Di) as scffolds (Ca-SiO2-MgO). It was candidated as bone repair as perfect biocompatib-ile	1wt% GPN's graphene nanoplatelet	Compressive and fracture strength improved 102% and 34% respectively.	GNP's and Di powder were separately added to DMF and their solutions sonicated using Ultrasonic cleaning instrument (Kudos, SK3300H,59 kHz) for 1h. The dispersion solutions were combined and sonicated 30 min more before ball milling. The composite drying	(Shuai et al., 2016)

Appendix A

Table 9.1 Summary of Matrices, Filler processing and Property Enhancement.

No	Matrix	Filler	Improved property	Processing	Ref
				100°C 1 day	
77	Bitumen	(0.3-0.4) wt% GO	Strength, consistency, deformation and softening point of bitumen were improved	80/100 pen virgin bitumen in oven 160ºC 2h, 500g of virgin bitumen was blended 20mins at 2000rpm high shear mixer. GO is blended with virgin bitumen or sheared in the same rate and time [3.5G g +80 ml Phosphoric acid +18g K Permanganate slowly added +100ml hydrogen peroxide(10%)+100 ml distilled water. Vacuum filtered 0.2 Micro cellulose acetate membrane. Wash the residual cake by 5% HCl, then centrifuge 10000rpm for 29 min. Centrifuge was continued until PH is within 4-5 then dry in 70°C if PH is not within this range repeat centrifuge.	(Lam, 2015)

Appendix A

Table 9.1 Summary of Matrices, Filler processing and Property Enhancement.

No	Matrix	Filler	Improved property	Processing	Ref
78	Cement	2.5wt% Graphene naoplatelets GNP'S	Water penetration depth, chloride diffusion coefficient and chloride migration coefficient were significantly decreased 64%, 70% and 31% respectively, GNP work as a barrier.	Water/cement/sand were 0.485:1:2.75 by weight (ASTM C109). GNP was added to naphthalene sulfonate based superplasticizer (SP) in aqueous solution. The uniformly dispersed aqueous solution of GNP and SP was added and mixed with cement and sand. SP is 50% of GNP. Here in this study 1500 ml SP added for every 2.5% GNP. GNP+SP+WATER hand stirred 1 min. then ultra-sonicated 1 h in a water bath to cool down. Then added to the mixer of cement and sand in a Hobart mixer. Specimens: 3 of 50*50*50 mm cubes,8 of 40*40*160 mm prisms,3 of diam. 100*50 disk and 3of d 100*200mm cylinders at 28 days tested for ASTM C109 compressive strength and	(Du & Pang, 2015)

Appendix A

Table 9.1 Summary of Matrices, Filler processing and Property Enhancement.

No	Matrix	Filler	Improved property	Processing	Ref
				ASTM C348 for flexural strength and two cylinders were tested for water permeability according BS EN 12390-8	
79	Cement	0.05wt% GO	Improved flexural strength of cement (41-59)%, compressive strength (15-33)% patent mentioned that 46% higher than neat cement, decrease total porosity from (32.6)% to(28.2)%, improve the ductility and degree of hydration	By solution method	(Chuah et al., 2014; Z. Pan, DUAN, Li, & Collins, 2013)
80	Cement	0.01wt% GO	0.01wt% GO Hinder effectively the ingress of chloride ions, 0.03wt% GO significantly enhanced the asorbtivity to resist permeability	Water dispersion solution	(Mohammed, Sanjayan, Duan, & Nazari, 2015)
81	Cement	G platelets	Enhanced thermal properties or reduction in early age thermal cracking and durability improvement of the concrete structures	Solution mix by commercial mixer w/c 0.5	(Sedaghat, Ram, Zayed, Kamal, & Shanahan, 2014)
82	Cement	0.1, 0.3, 0.5wt% G platelets	No significant improvement in compressive and flexural strength happened due to the difficulty in dispersion of GP in mortar mix	Direct mix of GP in cement mortar	(Radhika Pavgi, Dr. Osman Ozbulut, & Daghash, 2015)
83	Cement	0, 0.5, 1.5. 2.5wt%GO	Remarkably was accelerated the hydration rate of cement due to its catalytic behaviour.	Cement/ sand 1:3 and w/c= 0.3 super plasticizer solution (polycarboxylate PC) 0.1wt% for cement.	(Lin et al., 2016)

Appendix A

Table 9.1 Summary of Matrices, Filler processing and Property Enhancement.

No	Matrix	Filler	Improved property	Processing	Ref
				GO was suspended and sonicated 3h in distilled water, then PC solution was added, cement and sand were added.	
84	Fly-ash (geopolymer)	0.5, 1, 2, 3wt% Nano-silica	Enhanced microstructure, improved compressive and flexural strength	Alkaline solution to fly ash ratio of 0.75 was used and the ratio of sodium silicate solution to sodium hydroxide solution was fixed at 2.5. The concentration of sodium hydroxide solution was 8 M, and was prepared and combined with the sodium silicate solution one day dry before mixing. A dry and wet process. For dry-mix process, the nanosilica was added first to the fly-ash at the dosages of 0%, 0.5%, 1.0%, 2.0% and 3.0% by weight. The fly-ash and nanosilica were dry-mixed for 5 min in a covered mixer at a low speed and then mixed for another 10 min at high	(H. Assaedi et al., 2015b)

Appendix A

Table 9.1 Summary of Matrices, Filler processing and Property Enhancement.

No	Matrix	Filler	Improved property	Processing	Ref
				speed until homogeneity was achieved. The alkaline solution was then added slowly to the fly-ash/nanosilica powders in the Hobart mixer at a low speed until the mixes became homogeneous, then further mixed for another 10 min on high speed.	
85	Concrete (cement and fly ash + fine agg. + coarse agg.)	Nano-silica	Nano-SiO2 can improve the resistance of water penetration of concrete.	The superplasticizer TW-7 is naphthalene-type with a solid content of 40%. The coarse aggregates used are the continuous grading crushed gravels, with the maximum 2 mins. Though nano-SiO2 cannot be dissolved in water, a smaller amount of nano-SiO2 can be dispersed evenly by the superplasticizer TW-7. The cement, fine aggregates, coarse aggregates and fly ash were mixed in a rotary mixer for 30 s. The	(T. Ji, 2005)

Appendix A

Table 9.1 Summary of Matrices, Filler processing and Property Enhancement.

No	Matrix	Filler	Improved property	Processing	Ref
				ready-mixed liquid including water, TW-7 and nano-SiO2 was poured into the rotary mixer slowly. The concrete mixture was mixed for another 1.5 min.	
86	Geopolymer	1wt% nano-silica and 1.5 silica/Na2O	Compressive strength of nano-silica increased more with 1.5 SiO2/Na2O , microstructure early become dense, less porosity	Na2SiO3solution mixed with NaOH in distilled water, stirring and nano-silica was added to the alkali activator. Mechanical mixer was used to mix 1000 g meta-kaolin solution few min.	(K. Gao et al., 2014)
87	Cement (ordinary Portland cement OPC)	nano-clay (NC) and calcined nano-clay(CNC). Calcined nclay is prepared by heating nclay (cloisite 30B) platelets 900ºC 2h	1wt% calcined nclay was reduced 31.2% porosity and 34% water absorption, increased 9.7% density, 40% compressive strength, 42.9% flexural strength, 40% fracture toughness and 33.6% impact strength, 31.1% Rockwell hardness and 3.3% thermal stability of cement nanocomposite	Ordinary Portland cement (OPC) is partially substituted by nano-clay (NC) or calcined nano-clay (CNC) of 1, 2 and 3% by weight of OPC. The OPC and NC or CNC were first dry mixed for 5 min in a Hobart mixer at a low speed and then mixed for another 10 min at high speed until homogeneity	(A. Hakamy et al., 2015)

Appendix A

Table 9.1 Summary of Matrices, Filler processing and Property Enhancement.

No	Matrix	Filler	Improved property	Processing	Ref
				was achieved. The binder is either nano-clay-cement dry powder or calcined nano-clay-cement dry powder. The cement nanocomposite paste was prepared through adding water with a water/binder ratio of 0.485. The cement nanocomposite containing 1, 2 and 3 wt. % NC is termed as NCC1, NCC2 and NCC3, respectively. And also the cement nanocomposite containing 1, 2 and 3 wt. % CNC is termed as CNCC1, CNCC2 and CNCC3, respectively. The cement paste (C) was considered as a control.	
88	Geopolymer (solid aluminosilicate + alkaline solution from sodium	2wt%nClay	2.0 wt. % of nano-clay decreases the porosity and increases the nano composite's resistance to water absorption significantly. The optimum 2.0 wt. % nano-clay addition exhibited the highest flexural and compressive	Alkaline solution to fly ash ratio of 0.75 was used and the ratio of sodium silicate solution to sodium hydroxide solution was fixed at 2.5.	(Assaedi et al., 2016)

Appendix A

Table 9.1 Summary of Matrices, Filler processing and Property Enhancement.

No	Matrix	Filler	Improved property	Processing	Ref
	hydroxide s and sodium silicate grade D solution) and fly ash		strengths, flexural modulus and hardness. Nano-clay behaves not only as a filler to improve the microstructure, but also as an activator to facilitate the geopolymeric reaction, also better thermal stability than its counterpart pure geopolymer.	The concentration of sodium hydroxide solution was 8 M, which is prepared and combined with the sodium silicate solution one day before mixing.The nano-clay was added to the fly-ash at the loadings of 1.0%, 2.0% and 3.0% by weight. The fly-ash and nano-clay were first dry mixed for 5 min in a Hobart mixer at a low speed and then mixed for another 10 min at high speed until a uniform mixture was achieved.	
89	Cement	fly ash	(i) w/b ratios=water/binder have determinant impact on all characteristics of pore structure; (ii) fly-ash replacement ratio can influence the pore structure significantly at early age but this influence becomes less important with sample age by fly-ash hydration process; (iii) the total porosity and specific surface area are well correlated with the chemical kinetics of hydration through hydration degree	Cement paste samples were prepared with two water to binder (w/b) ratios (0.3, 0.5), and four fly-ash contents. The fly-ash content, ff, is noted as the mass ratio between fly-ash and binder (fly-ash and cement). After mixing, cement pastes of different mixtures were cast into cylinder tubes	(Zeng et al., 2012)

Appendix A

Table 9.1 Summary of Matrices, Filler processing and Property Enhancement.

No	Matrix	Filler	Improved property	Processing	Ref
			or the formed gel/space ratio but the critical pore size is rather independent on the chemical kinetics.	of 10mm diameter and placed in room condition with temperature controlled at 20 °C. After that, the hardened specimens were demoulded from the tubes at the age of 3 d, then immersed into water. To avoid the possible leaching, the ratio of specimen to water is kept at roughly 1:1 in volume or 2:1 in weight. At the ages of 7 d, 28 d and 90 d, specimens were taken out of water and crushed to particle samples of size 1mm–2mm for later experiments. The crushed particles were selected deliberately from the middle part of cylinder specimens to avoid the in homogeneity of material. The crushed samples were then vacuum dried immediately to stop the hydration and control the	

Appendix A

Table 9.1 Summary of Matrices, Filler processing and Property Enhancement.

No	Matrix	Filler	Improved property	Processing	Ref
				possible carbonation extent as low as possible.	
90	Cement	0.2vol%Nanocellulose	30% increase flexural strength , the degree of hydration was increased	Mixing CNC suspensions, water and cement powder to obtain mixtures with different concentrations of CNC. After preparing the CNC–cement paste mixture, three main aspects of the resulting material were investigated: (1) the curing process, (2) the mechanical properties and (3) the microstructure. While isothermal calorimetry (IC) and thermogravimetric analysis (TGA) were used to determine the DOH of cement pastes; zeta potential, water adsorption and rheological measurements were used to investigate the interaction and affinity of CNCs with cement	(Cao, Zavaterri, Youngblood, Moon, & Weiss, 2015)

Appendix A

Table 9.1 Summary of Matrices, Filler processing and Property Enhancement.

No	Matrix	Filler	Improved property	Processing	Ref
				particles. Additionally, ball-on-three-ball (B3B) flexural testing was performed to measure the flexural strength of the cement pastes at four different age	
91	Cement	6wt% bacterial nano-cellulose	Bacterial nano-cellulose (BNC) as powder (P), gel (G), and coated onto the fibres (C) on the mechanical and micro-structural properties of bagasse fibre cement composites(FCCs) was explored. Results indicated that FCCs containing 6 wt.% fibre content manufactured with BNC-coated fibres and BNC gel enhanced mechanical properties and maximum hydration temperature (MHT). However, P FCCs exhibited inferior properties compared to C and G FCCs.	Unbleached Bagasse pulp fibres were provided by a papermaking factory. The average length, diameter, and lignin content of fibres were 1.13 mm, 29.5 lm and 2.7%, respectively. Type II Portland cement (PC) used had a specific surface area of 2600 cm2 g1 and specific gravity of 3–3.25 ton m3. Calcium chloride (5% by dry weight of cement) and polycarboxylate based superplasticizer (0.5% by dry weight of cement) were also used. For BNC production, the bacterial strain Gluconacetobacter xylinus was cultured in a	(Mohammadkazemi, Doosthoseini, Ganjian, & Azin, 2015)

Appendix A

Table 9.1 Summary of Matrices, Filler processing and Property Enhancement.

No	Matrix	Filler	Improved property	Processing	Ref
				selected medium. The harvested gel-like BNC was washed with 1% NaOH solution at 80°C for 1 h and then washed with distilled water repeatedly until a neutral pH was reached. BNC was prepared in two forms of gel and powder. For the preparation of the gel, BNC was blended using a blender to produce a uniform dispersion. To prepare BNC powder, BNC was freeze-dried using a freeze-drier (SCANVAC, cool safe) at 92 C and 0.02 hPa for 2 days. Next, it was milled to the same size of BNC gel using a rotary mill. A dispersion of 0.1 wt.% BNC was prepared in deionized water in which bagasse fibres were added and left at 30ºC overnight. In this study, 50 wt. % of fibres was	

Appendix A

Table 9.1 Summary of Matrices, Filler processing and Property Enhancement.

No	Matrix	Filler	Improved property	Processing	Ref
				coated with BNC. Thereafter, coated fibres were vacuum filtered to remove additional water. Superplasticizer as a water reducer was used. CaCl2 as a catalyst agent was dissolved in water and added to the composition. The mortar was mixed using an electric mixer for 5 min (3 min mixing with two one-minute pauses). The target density and thickness of FCCs were 1.2 g Cm3 and 12 mm, respectively. The mixture was uniformly poured and distributed on a metal plate inside a frame-like mould (100, 250, 40, mm3); next, another plate was placed on the top of the mat. Two sides of the mat were covered with cellophane in order to prevent sticking. Thereafter, the mat was	

Appendix A

Table 9.1 Summary of Matrices, Filler processing and Property Enhancement.

No	Matrix	Filler	Improved property	Processing	Ref
				cold pressed until it reached to the required thickness after 24 h curing time. Afterward, the composite was released from the mould and conditioned at 95% relative humidity (RH) for 28 days at room temperature (20 ± 1ºC). The cured FCCs were then conditioned and dried at 65 ± 2% RH and 20 ± 1 °C for 1 month	
92	Cement	NFC nano-fibrillated cellulose	Flexural strength increased	Direct mix with cement matrix. My opinion of the results was not very good due to the direct mix which was no good for better dispersion. NFC must be stirred in DI water or sonicated.	(Mònica Ardanuy et al., 2012)
93	Paste of cellulose wood	20wt.% NCC	2 times fracture toughness or (10-20) times of any conversion and wood particles board. tensile strength more than ¼ times other ordinary wood particles board.	solution method	(Bilodeau & Bousfield, 2015)
94	Thermoplastic starch TPS	10wt. % MFC	Tensile strength increased 60%	Melt mixing by single screw extruder	(Ferreira & Carvalho, 2014)

Appendix A

Table 9.1 Summary of Matrices, Filler processing and Property Enhancement.

No	Matrix	Filler	Improved property	Processing	Ref
95	Starch and poly-vinyl-pyrrolidone	nZnO (19-30)nm	Reduced effectively the temp. propagation, the heat absorption capacity was increased (30-40) % and good optical properties.	Solution method with solvents for starch with sodium hydroxide at PH8.	(Pourrahimi et al., 2015)
96	Wood polymer nanocomposite WPNC composed[HDPE,LDPE, PP,PVC, PE-CO-Glycidyl methacrylate + Wood flour WF]	[nCla,nSiO2, nZnO]	UV resistance was improved; bacterial degradation of WPC was increased with nClay increased and nanoparticles. Flame retarding, chemical resistance and water vapour resistance were become max with 3phr each of clay , SiO2and ZnO	Solution by methanol and water 1:1 for SiO2 and ZnO and stirred each separately and dried homogeneous solution of HDPE, LDPE, PP (1:1:1) and 5phr PE-CO-GMA, also PVC in THF and PVC IN 70:30 Xylene and THF and stirred at 120ºC then oven dry WF 40 phr was added the composite sheets were done by hot press moulding at 150°C 80 MPa.	(Biplab K Deka et al., 2012)
97	Potato starch	MMT	Thermal resistance was improved the water absorbed at 75% humidity was reduced and E improved 500% at 5wt% MMT, it raised to 170MPa.	Solution method starch in water and 30wt% glycerol at 70ºC and MMT was dispersed in distilled water and sonicated the film was casted in mould at 45°C.	(Cyras et al., 2008)
98	Wood pulp-based	5wt% MFC micro-fibrillated cellulose degree of fibrillation 30 passes	300 MPa tensile strength	Solution	(Saxena, 2013)

Appendix A

Table 9.1 Summary of Matrices, Filler processing and Property Enhancement.

No	Matrix	Filler	Improved property	Processing	Ref
99	Xylan from Oat spel	Aqueous suspension of sulfonated whisker	141% tensile strength increased	Solution + Deionized water and stirring 95ºC 15 min. and dried in room temp.	(Saxena, 2013)
100	Hydroxy-propyl cellulose HPC as a matrix	5wt% Micro-cellulose fibres 20µm to prepare nano-fibrillated cellulose	57.4% tensile strength of comp. Film higher than 1wt% loading and 52.2%higher than neat HPC film	Solution aqueous and high pressure homogenizer	(S.-Y. Lee et al., 2009)
101	Starch and calcium carbonate	CNF50/50	The result of fracture of toughness ten time more the plain board	Solution method	(Bilodeau & Bousfield, 2015)
102	Thermoplasti c Starch	Bacterial Cellulose (BC) 15wt%	Strong interfacial adhesion, thermal behaviour was improved, mechanical properties enhanced.	In situ polymerization	(Osorio et al., 2014)
103	Soluble Starch	NCT's with clay Palygorskite and catalysts	The nanomaterial NCT's prepared in this way 17 times greater specific area to the same ordinary NCT's and the starch nanocomposite resulted is environmental remediation used in situ immobilisation of organic pollutants in soil.	Solution starch and NCT's grafted with polypropylene.	(Osorio et al., 2014)
104	Wood flour (WF)+PE -co-glycidyl methacrylate + HDPE+LDP E+PP+ PVC	3vol% nClay + nTiO2	Improvement in thermal stability, mechanical, UV resistance and flame retarding properties. Decrease in water vapour and water absorption	Solution blending method	(Biplab K. Deka & Maji, 2011)

Appendix A

Table 9.1 Summary of Matrices, Filler processing and Property Enhancement.

No	Matrix	Filler	Improved property	Processing	Ref
105	Hemp and sisal fibres with PLLA poly lactic acid	5WT %BC	Increase tensile strength about 14%	Solution method solvents	(K. Y. Lee, et al., 2009)
106	cellulose fibre	nano-cellulose nano-silver	Antibacterial efficacy after laundering many times	Cotton fabric wt. 109 g/m2, Polyester fabric wt. 89 g/m2, polyester/cotton blended fabric (ratio of 65/35) weighting 80 g/m2, and polyester/spandex mixed fabric (ratio of 92/8) wt 85 g/m2 were bleached. Experiments were performed on samples with maximum dimensions 97cm×97 cm. The ethanol based nano-silver colloids was supplied from Nano EnC. Co. Ltd., at the concentration of 2,000 ppm. This colloidal solution was diluted with distilled water by 50 ppm and 25 ppm at RT for our experimentation. Padding was performed at the	(H. J. Lee, Yeo, & Jeong)

Appendix A

Table 9.1 Summary of Matrices, Filler processing and Property Enhancement.

No	Matrix	Filler	Improved property	Processing	Ref
				constant pressure for all samples after wet pickup of 83% through of colloids bath. Cotton and polyester. Cotton and polyester fabrics were padded through 25 ppm and 50 ppm silver colloids. First eight pieces of cotton and polyester samples were padded before dying, respectively. Thereafter, other eight pieces of cotton and polyester fabrics were padded after dyeing, respectively. Some samples were rinsed in water after padding at 25◦C and the others were not.	
107	Cotton fabrics	Colloidal silver nanoparticle	Anti-microbial efficiency after laundering many times	AgNO3 (Kemika) and reducing agent NaBH4 (Fluka) of p.a. grade were used for the synthesis of colloidal Ag NPs. 1.7 mg of AgNO3 was dissolved in 100 mL of water purged by argon for 30 min.	(Ilić et al., 2009)

Appendix A

Table 9.1 Summary of Matrices, Filler processing and Property Enhancement.

No	Matrix	Filler	Improved property	Processing	Ref
				Under vigorous stirring, 10 mg of NaBH4 was added to the solution and left for 1 h in argon atmosphere. The concentration of silver colloid was 10 ppm. The silver colloids of higher concentration (50 ppm) were synthesized in the same manner. One gram of cotton fabric was immersed in 45 mL of colloid of Ag NPs for 5 min and dried at room temperature.	
108	Cotton fabrics	TiO2 (anatase)/ SiO2 prepared by sol-gel. TiO2 nanoparticles were deposited on the surface of SiO2 spheres.	Better self-cleaning	The SiO2 powder was added to TiO2 sol and dispersed in an ultrasonic bath for 15 min. The TiO2/SiO2 mixture was kept for 12 h to form SiO2 supported TiO2 spherical nanocomposites with a core–shell structure (pH = 3–5). The suspension was used to prepare TiO2/SiO2 nanocomposites on woven white cotton	(Qi et al., 2007)

Appendix A

Table 9.1 Summary of Matrices, Filler processing and Property Enhancement.

No	Matrix	Filler	Improved property	Processing	Ref
				fabrics.	
109	Cotton fabrics	3wt% nZnO	Significant advance in UV protect	Solution method by solvent	(R. H. Wang, Xin, & Tao, 2005)
110	Cotton Fabric as a substrate	nSiO2 + perfluorooctylated quaternary ammonium silane coupling agent (PFSC)	Excellent water repellent property and the oil repellency was improved, the contact angle to oil (CH2I2) was 125 degree for cotton with (PFSC) only and become 131 degree by adding SiO2 with them	By sol gel method for silica via alkaline hydrolysis of tetraethoxysilane (TEOS) 11.5 ml in a mixture of ethanol and water and stirring with 25 ml ethanol (C2H5OH), water 3.6 ml and NH3. Fabric samples were first immersed in the silica sol, then padded with two dips and two nips to reach a wet	(Yu, Gu, Meng, & Qing, 2007)

Appendix A

Table 9.1 Summary of Matrices, Filler processing and Property Enhancement.

No	Matrix	Filler	Improved property	Processing	Ref
				pickup of 70%. The samples were dried at 808ºC for 3 min, and then immersed in the methanol solution of PFSC (3 wt.%), padded with two dips and two nips to reach a wet pickup of 70% and dried at 80 8C for 3 min, cured at 160 8C for 3 min	
111	Cotton fabric	Water vapour permeable coating containing MWNT with solution polymer of hydrophilic polyurethane	Excellent protection to UV	solution method	(Mondal & Hu,]2007)
112	Hemp fibre with cement	1wt% Calcined nano-clay	Reduced Porosity and increased fracture toughness	The ordinary Portland cement (OPC) is partially substituted by calcined nano-clay (CNC) of 1, 2 and 3 % by weight of OPC. The OPC and CNC were first dry mixed for 15 minutes in Hobart mixer. The binder is CNC -cement powder. The cement nanocomposite matrix	(A. Hakamy et al., 2015)

Appendix A

Table 9.1 Summary of Matrices, Filler processing and Property Enhancement.

No	Matrix	Filler	Improved property	Processing	Ref
				was prepared with a water / binder ratio of 0.485.	
113	Cement and 2.5wt% hemp fabric	1wt% Nanoclay platelets (cloisite 30 B)	Mechanical properties generally increased; Porosity decreased, significantly flexural strength and fracture toughness increased. Also, the hemp fabric-matrix adhesion was improved	Cement is partially substituted by nano-clay. Cement and nano-clay were first dry mixed for 5 min in Hobart mixer at a low speed and then mixed for another 10 min at high speed until homogeneity was achieved. The cement–nano-composite paste was prepared through adding water with a water/binder (nano-clay–cement) ratio of 0.48. The cement paste without nano-clay was considered as a control.	(Hakamy, Shaikh, & Low, 2013)

Appendix A

Table 9.1 Summary of Matrices, Filler processing and Property Enhancement.

No	Matrix	Filler	Improved property	Processing	Ref
114	Wood flour + PLA (polylactic acid)	5WT% Nano-clay	30% flexural and tensile moduli was increased	Twin screw extruder	(Q. Meng, 2010)

Appendix A

Table 9.2 Flexural and compressive strength test results for pure lime, Part A- Air cured.

1 Part	2 No	3 % wt. nano-filler/ lime	4 W/L	5 Age at test days	6 Storage condition to 5 days % RH/ºC	7 Curing up to 28 days % RH/ºC	8 Compressive strength MPa	9 Flexural strength MPa
A	1	0 wt. % control	0.5	28	60 /20	60/20	2.7	2.9
A	2	0 wt. % control	0.5	28	60/20	60/20	2.8	3.0
A	3	0 wt. % control	0.5	28	60/20	60/ 20	2.8	0.8
A	4	0 wt. % control	0.5	28	60/20	60/20	2.6	0.7
A	5	0 wt. % control	0.5	28	60/20	60/20	3.9	0.2
A	6	0 wt. % control	0.5	28	60/20	60/20	4.2	0.2
A	7	0 wt. % control	0.5	28	60/20	60/20	1.8	2.0
A	8	0 wt. % control	0.5	28	60/20	60/20	2.1	1.5
A	9	0 wt. % control	0.5	28	60/20	60/20	2.8	-
A	10	0 wt. % control	0.5	28	60/20	60/20	2.9	-
Av.		-	-	-	-	-	2.9	1.4

Appendix A

Table 9.3 Flexural and compressive strength test results for nSiO2/ lime nanocomposite, Part A-Air-cured

1	2	3	4	5	6	7	8	9
Part	**No**	**% wt. nano-filler/ lime**	**W/L**	**Age at test days**	**Storage condition to 5 days % RH/ºC**	**Curing up to 28 days % RH/ºC**	**Compressive strength MPa**	**Flexural strength MPa**
A	1	2 wt. % $nSiO_2$	0.5	28	60/20	60/20	1.9	0.2
A	2	2 wt. % $nSiO_2$	0.5	28	60/20	60/20	2.3	0.3
A	3	2 wt. % $nSiO_2$	0.5	28	60/20	60/20	3.2	0.8
A	4	2 wt. % $nSiO_2$	0.5	28	60/20	60/20	3.7	
Av.							2.8	0.4
A	1	4 wt. % $nSiO_2$	0.5	28	60/20	60/20	2.6	0.2
A	2	4 wt. % $nSiO_2$	0.5	28	60/20	60/20	2.5	0.2
A	3	4 wt. % $nSiO_2$	0.5	28	60/20	60/20	2.8	2.1
A	4	4 wt. % $nSiO_2$	0.5	28	60/20	60/20	2.9	
Av.							2.7	0.8

Appendix A

Table 9.4 Flexural and compressive strength test results for nclay/ lime nanocomposite, Part A-Air cured

1	2	3	4	5	6	7	8	9
Part	**No**	**% wt. nano-filler/ lime**	**W/L**	**Age at test days**	**Storage condition to 5 days % RH/ ºC**	**Curing up to 28 days**	**Compressive strength MPa**	**Flexural strength MPa**
A	1	0.5 wt. % nclay	0.5	28	60/20	60/20	2.8	0.3
A	2	0.5 wt. % nclay	0.5	28	60/20	60/20	2.6	0.3
A	3	0.5 wt. % nclay	0.5	28	60/20	60/20	3.4	-
A	4	0.5 wt. % nclay	0.5	28	60/20	60/20	3.0	-
Av.							3.0	0.3
A	1	1 wt. % nclay	0.5	28	60/20	60/20	2.8	0.5
A	2	1 wt. % nclay	0.5	28	60/20	60/20	2.7	0.7
A	3	1 wt. % nclay	0.5	28	60/20	60/20	2.6	-
A	4	1 wt. % nclay	0.5	28	60/20	60/20	3.3	-
Av.							2.9	0.6
A	1	2 wt. % nclay	0.5	28	60/20	60/20	3.3	0.6
A	2	2 wt. % nclay	0.5	28	60/20	60/20	3.8	0.7
A	3	2 wt. % nclay	0.5	28	60/20	60/20	3.5	-
A	4	2 wt. % nclay	0.5	28	60/20	60/20	3.6	-
Av.							3.6	0.7

Appendix A

Table 9.5 Nanofibrillated cellulose nFc/ lime nanocomposites, Part A-Air cured

1	2	3	4	5	6	7	8	9
Part	**No**	**% wt. nano-filler/ lime**	**W/L**	**Age at test days**	**Storage condition to 5 days % RH/ºC**	**Curing up to 28 days % RH/ºC**	**Compressive strength MPa**	**Flexural strength MPa**
A	1	5 wt. % nFc	0.5	28	60/20	60/20	2.2	0.3
A	2	5 wt. % nFc	0.5	28	60/20	60/20	2.3	0.4
A	3	5 wt. % nFc	0.5	28	60/20	60/20	2.5	-
A	4	5 wt. % nFc	0.5	28	60/20	60/20	2.3	-
Av.							2.3	0.4
A	1	7 wt. % nFc	0.5	28	60/20	60/20	2.2	0.8
A	2	7 wt. % nFc	0.5	28	60/20	60/20	2.3	0.8
A	3	7 wt. % nFc	0.5	28	60/20	60/20	2.5	0.8
Av.							2.3	0.8

Table 9.6 Fibre glass (FG)/Lime composite specimens, Part A-Air-cured

1	2	3	4	5	6	7	8	9
Part	**No**	**% wt. nano-filler/ lime**	**W/L**	**Age at test days**	**Storage condition to 5 days % RH/ºC**	**Curing up to 28 days % RH/ºC**	**Compressive strength MPa**	**Flexural strength MPa**
A	1	5 wt.% FG	0.5	28	60/20	60/20	4.4	2.2
A	2	5 wt.% FG	0.5	28	60/20	60/20	3.3	1.9
A	3	5 wt.% FG	0.5	28	60/20	60/20	3.1	2.2
A	4	5 wt.% FG	0.5	28	60/20	60/20	4.9	1.5
A	5	5 wt.% FG	0.5		60/20	60/20	1.9	3.1
A	6	5 wt.% FG	0.5	28	60/20	60/20	2.9	-
Av.	-	-	-	-			3.4	2.2
A	1	10 wt.% FG	0.5	28	60/20	60/20	10.5	3.1
A	2	10 wt.% FG	0.5	28	60/20	60/20	11.5	4.6
A	3	10 wt.% FG	0.5	28	60/20	60/20	10.2	-
Av.	-	-	-	-	-		10.7	3.9
A	1	15 wt.% FG	0.5	28	60/20	60/20	5.6	1.6
A	2	15 wt.% FG	0.5	28	60/20	60/20	7.3	1.6
A	3	15 wt.% FG	0.5	28	60/20	60/20	7.2	2.5
Av.							6.7	1.9

Table 9.7 Hemp fibres (HF), PVAc and nZnO/Lime nanocomposite specimens, Part A-Air- cured

1	2	3	4	5	6	7	8	9
Part	**No**	**% wt. nano-filler/ lime**	**W/L**	**Age test day**	**Storage condition to 5 days % RH/ºC**	**Curing up to 28 days % RH/ºC**	**Compressive strength MPa**	**Flexural strength MPa**
A	1	10 wt.% HF, 4wt.% nZnO, 12 % wt. PVAc/L	0.4	28	60/20	60/20	19.7	7.5
A	2	10 wt.% HF, 4wt.% nZnO, 12 % wt. PVAc/L	0.4	28	60/20	60/20	16.6	6.7
A	3	10wt.% HF, 4wt.% nZnO, 12 % wt. PVAc/L	0.4	28	60/20	60/20	17.6	7.7
A	4	10wt.% HF, 4wt.% nZnO, 12 % wt. PVAc/L	0.4	28	60/20	60/20	19.7	-
A	5	10wt.% HF, 4wt.% nZnO, 12 % wt. PVAc/L	0.4	28	60/20	60/20	18.4	-
A	6	10wt.% HF, 4wt.% nZnO, 12 % wt. PVAc/L	0.4	28	60/20	60/20	14.4	-
Av.	-	-	-	-			17.7	7.3
A	1	4 wt. % nZnO/L	0.4	28	60/20	60/20	0.9	0.7
A	2	4 wt. % nZnO/L	0.4	28	60/20	60/20	0.6	0.6
A	3	4 wt. % nZnO/L	0.4	28	60/20	60/20	0.6	
A	4	4 wt. % nZnO/L	0.4	28	60/20	60/20	0.7	
Av.	-	-	-	-	-		0.7	0.6

Table 9.8 Water absorption test and capillary porosity calculation

No	Item	Time (min.)	Control (g)	2% nclay (g)	10% FG (g)	2% nSiO2 (g)	2% EG (g)	Sec^0.5
1	2	3	4	5	6	7	8	9
1	Dry weight	0	396.96	367.5	377.8	323	301.1	
2	1st hour wet weight	5	409.8	398.4	417.7	339.2	318.3	2.23607
3	1st hour wet weight	10	426.7	410	436.3	344.4	325.6	3.16228
4	1st hour wet weight	15	444.2	420.2	442.7	349.2	330.9	3.87298
5	1st hour wet weight	20	457	428	442.7	352.3	334.3	4.47214
6	1st hour wet weight	25	467.3	434.6	442.4	355.7	337.7	5.00000
7	1st hour wet weight	30	470.7	434.7	442.5	358.5	340.4	5.47723
8	1st hour wet weight	45	478.6	434.6	442.2	366.2	341.4	6.7082
9	1st hour wet weight	60	481.2	434.3	442.5	373.5	342.4	7.74597
10	2nd hour wet weight	90	482.1	434.1	442.7	379.2	343.1	9.48683
11	2nd hour wet weight	120	482.3	434	443	383.4	345.2	10.9545
12	3rd hour wet weight	150	482.7	434.3	442.8	388.2	345.4	12.2474
13	3rd hour wet weight	180	482.8	434.1	442.8	394.07	348.3	13.4164
14	4th hour wet weight	240	483.2	433.9	442.6	396.6	349.4	15.4919
15	5th hour wet weight	300	483.2	433.9	442.6	396.6	349.4	17.3205
16	24 hours wet weight	1440	483.2	433.9	442.6	396.6	349.4	37.9473

Table 9.8 (Continued) water absorption test and capillary porosity calculation

No	Item	Time (min.)	Control (g)	2% nclay (g)	10% FG (g)	2% nSiO2 (g)	2% EG (g)	Sec^0.5
1	2	3	4	5	6	7	8	9
1.	U_t= (wet - dry) weight	-	12.84	30.9	39.9	16.2	17.2	-
2.	U_t= (wet - dry) weight	-	29.74	42.5	58.5	21.4	24.5	-
3.	U_t= (wet - dry) weight	-	47.24	52.7	64.9	26.2	29.8	-
4.	U_t= (wet - dry) weight	-	60.04	60.5	64.9	29.3	33.2	-
5.	U_t= (wet - dry) weight	-	70.34	67.1	64.6	32.7	36.6	-
6.	U_t= (wet - dry) weight	-	73.74	67.2	64.7	35.5	39.3	-
7.	U_t= (wet - dry) weight	-	81.64	67.1	64.4	43.2	40.3	-
8.	U_t= (wet - dry) weight	-	84.24	66.8	64.7	50.5	41.3	-
9.	U_t= (wet - dry) weight	-	85.14	66.6	64.9	56.2	42	-
10.	U_t= (wet - dry) weight	-	85.34	66.5	65.2	60.4	44.1	-
11.	U_t= (wet - dry) weight	-	85.74	66.8	65	65.2	44.3	-
12.	U_t= (wet - dry) weight	-	85.84	66.6	65	71.07	47.2	-
13.	U_t= (wet - dry) weight	-	86.24	66.4	64.8	73.6	48.3	-
14.	U_t= (wet - dry) weight	-	86.24	66.4	64.8	73.6	48.3	-
15.	U_t= (wet - dry) weight	-	86.24	66.4	64.8	73.6	48.3	-

Table 9.8 (Continued) water absorption test and capillary porosity calculation

No	Item	Time (min.)	Control (g)	2% nclay (g)	10% FG (g)	2% nSiO2 (g)	2% EG (g)	Sec^0.5
1	2	3	4	5	6	7	8	9
1.	U_o= Wmax-Wdry	-	86.24	66.4	64.8	73.6	48.3	-
2.	U_o= Wmax-Wdry	-	86.24	66.4	64.8	73.6	48.3	-
3.	U_o= Wmax-Wdry	-	86.24	66.4	64.8	73.6	48.3	-
4.	U_o= Wmax-Wdry	-	86.24	66.4	64.8	73.6	48.3	-
5.	U_o= Wmax-Wdry	-	86.24	66.4	64.8	73.6	48.3	-
6.	U_o= Wmax-Wdry	-	86.24	66.4	64.8	73.6	48.3	-
7.	U_o= Wmax-Wdry	-	86.24	66.4	64.8	73.6	48.3	-
8.	U_o= Wmax-Wdry	-	86.24	66.4	64.8	73.6	48.3	-
9.	U_o= Wmax-Wdry	-	86.24	66.4	64.8	73.6	48.3	-
10.	U_o= Wmax-Wdry	-	86.24	66.4	64.8	73.6	48.3	-
11.	U_o= Wmax-Wdry	-	86.24	66.4	64.8	73.6	48.3	-
12.	U_o= Wmax-Wdry	-	86.24	66.4	64.8	73.6	48.3	-
13.	U_o= Wmax-Wdry	-	86.24	66.4	64.8	73.6	48.3	-
14.	U_o= Wmax-Wdry	-	86.24	66.4	64.8	73.6	48.3	-
15.	U_o= Wmax-Wdry	-	86.24	66.4	64.8	73.6	48.3	-

Table 9.8 (Continued) water absorption test and capillary porosity calculation

No	Item	Time (min.)	Control (g)	2% nclay (g)	10% FG (g)	2% nSiO2 (g)	2% EG (g)	Sec^0.5
1	2	3	4	5	6	7	8	9
1.	IC= U_o/ W_d	-	0.217251	0.1806803	0.171519	0.2278638	0.160412	-
2.	IC= U_o/ W_d	-	0.217251	0.1806803	0.171519	0.2278638	0.160412	-
3.	IC= U_o/ W_d	-	0.217251	0.1806803	0.171519	0.2278638	0.160412	-
4.	IC= U_o/ W_d	-	0.217251	0.1806803	0.171519	0.2278638	0.160412	-
5.	IC= U_o/ W_d	-	0.217251	0.1806803	0.171519	0.2278638	0.160412	-
6.	IC= U_o/ W_d	-	0.217251	0.1806803	0.171519	0.2278638	0.160412	-
7.	IC= U_o/ W_d	-	0.217251	0.1806803	0.171519	0.2278638	0.160412	-
8.	IC= U_o/ W_d	-	0.217251	0.1806803	0.171519	0.2278638	0.160412	-
9.	IC= U_o/ W_d	-	0.217251	0.1806803	0.171519	0.2278638	0.160412	-
10.	IC= U_o/ W_d	-	0.217251	0.1806803	0.171519	0.2278638	0.160412	-
11.	IC= U_o/ W_d	-	0.217251	0.1806803	0.171519	0.2278638	0.160412	-
12.	IC= U_o/ W_d	-	0.217251	0.1806803	0.171519	0.2278638	0.160412	-
13.	IC= U_o/ W_d	-	0.217251	0.1806803	0.171519	0.2278638	0.160412	-
14.	IC= U_o/ W_d	-	0.217251	0.1806803	0.171519	0.2278638	0.160412	-
15.	IC= U_o/ W_d	-	0.217251	0.1806803	0.171519	0.2278638	0.160412	-
16.	IC= U_o/ W_d	-	0.217251	0.1806803	0.171519	0.2278638	0.160412	-

Table 9.8 (Continued) water absorption test and capillary porosity calculation

No	Item	Time (min.)	Control (g)	2% nclay (g)	10% FG (g)	2% nSiO2 (g)	2% EG (g)	Sec^0.5
1	2	3	4	5	6	7	8	9
1.	ABS= IC X 100	-	21.72511084	18.06802721	17.15193224	22.78637771	16.04118233	-
2.	ABS= IC X 100	-	21.72511084	18.06802721	17.15193224	22.78637771	16.04118233	-
3.	ABS= IC X 100	-	21.72511084	18.06802721	17.15193224	22.78637771	16.04118233	-
4.	ABS= IC X 100	-	21.72511084	18.06802721	17.15193224	22.78637771	16.04118233	-
5.	ABS= IC X 100	-	21.72511084	18.06802721	17.15193224	22.78637771	16.04118233	-
6.	ABS= IC X 100	-	21.72511084	18.06802721	17.15193224	22.78637771	16.04118233	-
7.	ABS= IC X 100	-	21.72511084	18.06802721	17.15193224	22.78637771	16.04118233	-
8.	ABS= IC X 100	-	21.72511084	18.06802721	17.15193224	22.78637771	16.04118233	-
9.	ABS= IC X 100	-	21.72511084	18.06802721	17.15193224	22.78637771	16.04118233	-
10.	ABS= IC X 100	-	21.72511084	18.06802721	17.15193224	22.78637771	16.04118233	-
11.	ABS= IC X 100	-	21.72511084	18.06802721	17.15193224	22.78637771	16.04118233	-
12.	ABS= IC X 100	-	21.72511084	18.06802721	17.15193224	22.78637771	16.04118233	-
13.	ABS= IC X 100	-	21.72511084	18.06802721	17.15193224	22.78637771	16.04118233	-
14.	ABS= IC X 100	-	21.72511084	18.06802721	17.15193224	22.78637771	16.04118233	-
15.	ABS= IC X 100	-	21.72511084	18.06802721	17.15193224	22.78637771	16.04118233	-
16.	ABS= IC X 100	-	21.72511084	18.06802721	17.15193224	22.78637771	16.04118233	-

Table 9.8 (Continued) water absorption test and capillary porosity calculation

No	Item	Time (min.)	Control (g)	2% nclay (g)	10% FG (g)	2% nSiO2 (g)	2% EG (g)	Sec^0.5
1	2	3	4	5	6	7	8	9
1.	OP%= V_{op}/V_{sp*} 100	-	33.6875	25.9375	25.3125	28.75	18.8671875	-
2.	OP%= V_{op}/V_{sp}	-	33.6875	25.9375	25.3125	28.75	18.8671875	-
3.	OP%= V_{op}/V_{sp}	-	33.6875	25.9375	25.3125	28.75	18.8671875	-
4.	OP%= V_{op}/V_{sp}	-	33.6875	25.9375	25.3125	28.75	18.8671875	-
5.	OP%= V_{op}/V_{sp}	-	33.6875	25.9375	25.3125	28.75	18.8671875	-
6.	OP%= V_{op}/V_{sp}	-	33.6875	25.9375	25.3125	28.75	18.8671875	-
7.	OP%= V_{op}/V_{sp}	-	33.6875	25.9375	25.3125	28.75	18.8671875	-
8.	OP%= V_{op}/V_{sp}	-	33.6875	25.9375	25.3125	28.75	18.8671875	-
9.	OP%= V_{op}/V_{sp}	-	33.6875	25.9375	25.3125	28.75	18.8671875	-
10.	OP%= V_{op}/V_{sp}	-	33.6875	25.9375	25.3125	28.75	18.8671875	-
11.	OP%= V_{op}/V_{sp}	-	33.6875	25.9375	25.3125	28.75	18.8671875	-
12.	OP%= V_{op}/V_{sp}	-	33.6875	25.9375	25.3125	28.75	18.8671875	-
13.	OP%= V_{op}/V_{sp}	-	33.6875	25.9375	25.3125	28.75	18.8671875	-
14.	OP%= V_{op}/V_{sp}	-	33.6875	25.9375	25.3125	28.75	18.8671875	-
15.	OP%= V_{op}/V_{sp}	-	33.6875	25.9375	25.3125	28.75	18.8671875	-
16.	OP%= V_{op}/V_{sp}	-	33.6875	25.9375	25.3125	28.75	18.8671875	-

Table 9.8 (Continued) water absorption test and capillary porosity calculation

No	Item	Time (min.)	Control (g)	2% nclay (g)	10% FG (g)	2% nSiO2 (g)	2% EG (g)	Sec^0.5
1	2	3	4	5	6	7	8	9
1	M_i= Ut/ 64 cm^3	-	0.200625	0.482813	0.623438	0.253125	0.26875	-
2	M_i= Ut/ 64 cm^3	-	0.4646875	0.664063	0.914063	0.334375	0.382813	-
3	M_i= Ut/ 64 cm^3	-	0.7381250	0.823438	1.014063	0.409375	0.465625	-
4	M_i= Ut/ 64 cm^3	-	0.9381250	0.945313	1.014063	0.457813	0.518750	-
5	M_i= Ut/ 64 cm^3	-	1.0990625	1.048438	1.009375	0.510938	0.571875	-
6	M_i= Ut/ 64 cm^3	-	1.1521875	1.050000	1.010938	0.554688	0.614062	-
7	M_i= Ut/ 64 cm^3	-	1.2756250	1.048438	1.00625	0.675000	0.629687	-
8	M_i= Ut/ 64 cm^3	-	1.3162500	1.043750	1.010938	0.789063	0.645312	-
9	M_i= Ut/ 64 cm^3	-	1.3303125	1.040625	1.014063	0.878125	0.65625	-
10	M_i= Ut/ 64 cm^3	-	1.3334375	1.039063	1.018750	0.94375	0.689062	-
11	M_i= Ut/ 64 cm^3	-	1.3396875	1.04375	1.015625	1.01875	0.692187	-
12	M_i= Ut/ 64 cm^3	-	1.3412500	1.040625	1.015625	1.110469	0.737500	-
13	M_i= Ut/ 64 cm^3	-	1.3475000	1.037500	1.012500	1.150000	0.754687	-
14	M_i= Ut/ 64 cm^3	-	1.3475000	1.037500	1.012500	1.150000	0.754687	-
15	M_i= Ut/ 64 cm^3	-	1.3475000	1.037500	1.012500	1.15000	0.754687	-
16	M_i= Ut/ 64 cm^3	-	1.4115625	1.612500	1.745313	1.592188	1.382813	-

Appendix A